Università degli Studi di Milano Bicocca
Facoltà di Scienze Matematiche, Fisiche e Naturali

Corso di Dottorato in

Fisica e Astronomia - Ciclo XXIV

Neutron and gamma-ray emission spectroscopy as fast ion diagnostics in fusion plasmas

Massimo Nocente
Matricola 055848

Supervisor:

Prof. Giuseppe Gorini

Coordinator of PhD School:

Prof. Giberto Chirico

Anno Accademico 2010/2011

We live at a time when emotions and feelings
count more than truth,
and there is a vast ignorance of science
– James Lovelock

Alla mia famiglia

Summary

Understanding the physics of fast ions in a fusion plasma is widely considered as one of the crucial tasks for the reliable operation of a fusion reactor. In a future fusion reactor, energy will be released via the $d + t \rightarrow n + \alpha$ reaction, that occurs in a tokamak between deuterium and tritium in a plasma state at typical temperatures of 10-20 keV. Each reaction releases about 17.5 MeV of energy that is shared in unequal parts between the α particle ($E_\alpha = 3.5$ MeV) and the neutron ($E_n = 14$ MeV). Having no charge, the neutrons are unaffected by the magnetic fields that confine the plasma and leave the tokamak. Their kinetic energy can be converted to thermal energy by an ad-hoc designed mantle surrounding the tokamak. On the other hand, the α particles remain confined in the plasma. Their role is vital for the self-sustainment of fusion reactions. α particles, that are produced at an energy much higher than the average deuterium and tritium temperatures, need to transfer their energy to the reacting ions by slowing down in the bulk plasma through multiple small-angle Coulomb collisions. Slowing down happens on a finite time scale (up to about 1 s in a fusion reactor), unless other events impede this process. It is a common observation on present day devices that fast ions drive instabilities, which in turn affect their confinement and are a severe threat for the reliable operation of a fusion reactor.

Nowadays, experiments are performed in deuterium plasmas where the source of fast ions is external; i.e. energetic ions are produced on purpose by auxiliary heating, such as radio frequency acceleration or neutral beam injection. A number of dedicated diagnostic measurements has been conceived and operated for the task of studying fast ion physics. A large amount of information has been collected and explained, although several fundamental questions on the confinement of α particles in a fusion reactor still remain unanswered and might find a solution only in experiments on a burning deuterium-tritium plasma. From the diagnostic point of view, a high power, large volume deuterium-tritium plasma represents a harsh operation environment where most of the fast ion diagnostics used in present-day devices are exposed to severe technical and principle limitations. New processes therefore need to be sought. Neutron and γ-ray emission fluxes will be significantly high in a burning plasma machine. Neutrons are produced by the d+t reaction itself, while γ-ray emission results from interaction between α particles (or other energetic ions) and impurities. Both processes can in principle be used to provide information on fast ions in a burning plasma device, as the associated detection techniques overcome most of the technical and principle problems encountered

by present-day fast ion diagnostics.

This thesis work addresses neutron and γ-ray emission spectroscopy as fast ion diagnostics for fusion plasmas. Two main topics are considered. The first one is the determination of the fast ion energy distribution from measured neutron and γ-ray emission spectra. Neutron spectroscopy has been used at the JET tokamak since 1984. Advanced spectrometers have been built and several features of the neutron emission spectrum have been measured and interpreted in terms of the reaction kinematics. This thesis adds to this knowledge base by inspecting the role of nuclear elastic scattering in producing high energy components in the spectrum from fusion neutrons. The analysis focuses on the possibility to determine the energy distribution tail temperature of radio-frequency heated ^{3}He ions in deuterium plasmas with an admixture of ^{3}He. The RF generation of fast ^{3}He ions is described and the knock-on components are determined with the help of newly derived ^{3}He +d scattering cross sections. Results are presented on the neutron emission spectrum and its contributions from different deuteron velocity components. It is shown that knock-on leaves an observable feature in the spectrum with a clear dependence on absorbed RF power. The investigation is then generalized to D, (^{3}He)D, DT and (^{3}He)DT plasmas, where the relative magnitude of nuclear elastic scattering from different fusion products is determined. The resulting signatures in the neutron emission spectrum are calculated and their relevance for fast ions diagnosis in a burning plasma experiment is discussed.

Gamma-ray spectroscopy is a relatively new technique compared to neutron spectroscopy. The Doppler broadening of characteristic γ-ray emission peaks from ^{12}C(^{3}He, pγ)^{14}N reactions in fusion plasmas was measured for the first time in 2008 at the JET tokamak thanks to the installation of a High Purity Germanium detector. In this thesis, intensities and detailed spectral shapes of γ-ray emission peaks are successfully reproduced using a physics model combining the kinetics of the reacting ions with a detailed description of the nuclear reaction differential cross sections for populating the L1-L8 ^{14}N excitation levels yielding the observed γ-ray emission. A Monte Carlo code, named GENESIS, was written for the purpose of interpreting γ-ray emission from fusion plasmas and is used here to determine the tail temperature of fast ^{3}He ions from the observed peak shapes. Experiments performed in ^{4}He plasmas of the JET tokamak are also presented. ^{4}He ions were accelerated to the MeV range by coupling third harmonic radio frequency heating to an injected ^{4}He beam. For the first time, Doppler broadening of γ-ray peaks from the ^{12}C(d, pγ)^{13}C and ^{9}Be(α, nγ)^{12}C reactions was observed and is here interpreted

with the GENESIS code. Acceleration of ^{4}He particles at energies as high as 6 MeV is demonstrated; implications of these results for α particle observations through γ-ray emission spectroscopy in next step deuterium-tritium plasmas are discussed.
A second topic addressed by this work is the study of fast ion driven instabilities through γ-ray emission spectroscopy, with emphasis on the development of instrumentation. A high efficiency, high resolution, fast γ-ray spectrometer based on the $LaBr_3$ scintillator and designed for measurements in the MHz range was developed and is here presented. An algorithm based on pulse shape fitting was written to reconstruct γ-ray spectra from digitized data and is shown to provide an energy resolution equivalent to a traditional analog spectrometry chain at low counting rates. The same system was used to perform γ-ray spectroscopy in the MHz range, as demonstrated in experiments performed at nuclear accelerators. γ-ray emission spectra at rates as high as 4 MHz from p + ^{27}Al reactions collected at the Tandem Van der Graaf accelerator of the Nuclear Institute "Horia Hulubei" (Magurele, RO) are presented and show little or no degradation of the energy resolution. The developed system was also employed to study instabilities driven by fast protons in the ASDEX Upgrade tokamak. The observed γ-ray emission level induced by energetic protons is used to determine an effective tail temperature of the proton distribution function that can be compared with Neutral Particle Analyzer measurements. More generally the measured emission rate is used to assess the confinement of protons with energies less than 400 keV in discharges affected by Toroidal Alfvén Eigenmode instabilities. The derived information on confined ions is combined with observations made with the ASDEX Upgrade Fast Ion Loss Detector.
The results presented in this thesis represent a step forward in the development of nuclear radiation based methods for burning plasma diagnostics. In particular, they demonstrate that quantitative information on the energy distribution of fast ions and their interaction with plasma instabilities can be inferred from neutron and γ-ray measurements by taking into account in detail the reaction processes contributing to the emission of nuclear radiation from the plasma.

List of papers

This thesis is based on the following papers, which are referred to in the text by their Roman numerals:

I) M. Nocente, G. Gorini , J. Källne and M. Tardocchi,
Calculated neutron emission spectrum with knock-on effects for RF heated (^{3}He)D plasmas
Nucl. Fusion **51**, 063011 (2011)[1]

II) M. Nocente, G. Gorini , J. Källne and M. Tardocchi,
Cross section of the $d + {}^3He \rightarrow \alpha + p$ reaction of relevance for fusion plasma applications
Nucl. Fusion **50**, 055001 (2010)[2]

III) M. Nocente, J. Källne, G. Grosso, M. Tardocchi and G. Gorini
Nuclear scattering effects and neutron emission spectrum from fusion plasmas, submitted to Nucl. Fusion

IV) I. Proverbio, M. Nocente, V. G. Kiptily, M. Tardocchi, G. Gorini,
The $^{12}C(^3He, p\gamma)^{14}N$ reaction cross section for γ-ray spectroscopy simulation of fusion plasmas
Rev. Sci. Instrum. **81**, 10D320 (2010)[3]

V) M. Tardocchi, M. Nocente, I. Proverbio, V. G. Kiptily, P. Blanchard, S. Conroy, M. Fontanesi, G. Grosso, K. Kneupner, E. Lerche, A. Murari, E. Perelli Cippo, A. Pietropaolo, B. Syme, D. Van Eester, and G. Gorini,
Spectral Broadening of Characteristic γ-Ray Emission Peaks from $^{12}C(^3He, p\gamma)^{14}N$ Reactions in Fusion Plasmas
Phys. Rev. Lett. **107**, 205002 (2011)[4]

---

[1]Paper reprinted with permission from the Institute of Physics;

[2]Paper reprinted with permission from the Institute of Physics;

[3]Paper reprinted with permission from the American Institute of Physics;

[4]Paper reprinted with permission from the American Physical Society;

VI) M. Nocente, M. Tardocchi, V.G. Kiptily, P.Blanchard, I. Chugunov, S. Conroy, T. Edlington, A.M. Fernandes, G. Ericsson, M. Gatu Johnson, D. Gin, G. Grosso, C. Hellesen, K. Kneupner, E. Lerche, A. Murari, A. Neto, R.C. Pereira, E. Perelli Cippo, S. Sharapov, A. Shevelev, J. Sousa, D.B. Syme, D. Van Eester, G. Gorini and JET-EFDA contributors,
High resolution gamma ray spectroscopy measurements of the fast ion energy distribution in JET ^{4}He plasmas
submitted to Nucl. Fusion

VII) M. Nocente, M. Tardocchi, I. Chugunov, R. C. Pereira, T. Edlington, A. M. Fernandes, D. Gin, G. Grosso, V. Kiptily, A. Murari, A. Neto, E. Perelli Cippo, A. Pietropaolo, I. Proverbio, A. Shevelev, J. Sousa, B. Syme, G. Gorini,
Energy resolution of gamma-ray spectroscopy of JET plasmas with a $LaBr_3$ scintillator detector and digital data acquisition
Rev. Sci. Instrum. **81**, 10D321 (2010)[5]

VIII) M. Nocente, M. Tardocchi, A. Olariu, S. Olariu, I.N. Chugunov, A. Fernandes, D.B. Gin, G. Grosso, V.G. Kiptily, A. Neto, R. C. Pereira, A.E. Shevelev, M. Silva, J. Sousa and G. Gorini,
High Resolution Gamma Ray Spectroscopy at MHz Counting Rates with $LaBr_3$ Scintillators
submitted to IEEE Trans. Nucl. Sci.

IX) M. Nocente, M. Garcia-Munoz, G. Gorini, M. Tardocchi, A. Weller, S. Akaslompolo, R. Bilato, V. Bobkov, C. Cazzaniga, B. Geiger, G. Grosso, A. Herrmann, V.G. Kiptily, M. Maraschek, R. McDermott, J.M. Noterdaeme, Y. Podoba, G. Tardini and the ASDEX Upgrade Team,
Gamma-ray spectroscopy measurements of fast ions on ASDEX Upgrade
submitted to Nucl. Fusion

[5]Paper reprinted with permission from the American Institute of Physics;

Papers published on peer-reviewed journals that were not included in this thesis

- E. Lerche, D. Van Eester, J. Ongena, M.-L. Mayoral, M. Laxaback, F. Rimini, A. Argouarch, P. Beaumont, T. Blackman, V. Bobkov, D. Brennan, A. Brett, G. Calabro, M. Cecconello, I. Coffey, L. Colas, A. Coyne, K. Crombe, A. Czarnecka, R Dumont, F. Durodie, R. Felton, D. Frigione, M. Gatu Johnson, C. Giroud, G. Gorini, M. Graham, C. Hellesen, T. Hellsten, S. Huygen, P. Jacquet, T. Johnson, V. Kiptily, S. Knipe, A. Krasilnikov, P. Lamalle, M. Lennholm, A. Loarte, R. Maggiora, M. Maslov, A. Messiaen, D. Milanesio, I. Monakhov, M. Nightingale, C. Noble, **M. Nocente**, L. Pangioni, I. Proverbio, C. Sozzi, M. Stamp, W. Studholme, M. Tardocchi, T.W. Versloot, V. Vdovin, M. Vrancken, A. Whitehurst, E. Wooldridge, V. Zoita and JET EFDA contributors
  Optimizing ion-cyclotron resonance frequency heating for ITER: dedicated JET experiments
  Plasma Phys. Control. Fusion 53, 124019 (2011)

- R.C. Pereira, A.M. Fernandes, A. Neto, J. Sousa, C.A.F. Varandas, J. Cardoso, C.M.B.A. Correia, M. Tardocchi, **M. Nocente**, G. Gorini, V. Kiptily,B. Syme, M. Jennison
  Pulse Analysis for Gamma-Ray Diagnostics ATCA Sub-Systems of JET Tokamak
  IEEE Trans. on Nucl. Sci. 58, 1531 (2011)

- I N Chugunov, A E Shevelev, D B Gin, V G Kiptily, G Gorini, **M Nocente**, M Tardocchi, D N Doinikov, V O Naidenov and E M Khilkevitch
  Development of Gamma-Ray Diagnostics for ITER
  Nucl. Fusion 51, 083010 (2011)

- F. Ognissanto, G. Gorini, J. Kallne, L. Ballabio, **M. Nocente**, M. Tardocchi
  The elastic ^{3}He+d cross section of relevance for knock-on effects in radio frequency heated (^{3}He)D plasmas
  Nucl. Instrum. Meth. B, 786 (2011)

- D. B. Gin, V. G. Kiptily, A. A. Pasternak, I. N. Chugunov, A. E. Shevelev, G. Gorini, M. Tardocchi, **M. Nocente** and JET-EFDA contributors
  Doppler shapes of the γ line in the $\alpha(^9Be, n)^{12}C$ reaction in plasma at temperatures

$T_\alpha < 0.6\ MeV$
Bulletin of the Russian Academy of Sciences: Physics 75, 931 (2011)

- M. Gatu Johnson , C. Hellesen , E. Andersson Sunden , M. Cecconello , S. Conroy , G. Ericsson , G. Gorini , V. Kiptily, **M. Nocente**, S. Pinches , E. Ronchi , S. Sharapov , H. Sjostrand , M. Tardocchi , M. Weiszflog and JET-EFDA contributors
Neutron emission from beryllium reactions in JET deuterium plasmas with ^3He minority
Nucl. Fusion 50, 045005 (2010)

- C. Hellesen, M. Gatu Johnson, E. Andersson Sunden, S. Conroy, G. Ericsson, J. Eriksson, G. Gorini, T. Johnson, V. Kiptily, S. Pinches, S. Sharapov, H. Sjostrand, **M. Nocente**, M. Tardocchi, M. Weiszflog and JET EFDA contributors
Measurements of fast ions and their interactions with MHD activity using neutron emission spectroscopy
Nucl. Fus. 50, 084006 (2010)

- M. Gatu Johnson, C. Hellesen, E. Andersson Sunden, M. Cecconello, S. Conroy, G. Ericsson, G. Gorini, **M. Nocente**, E. Ronchi, M. Tardocchi, M. Weiszflog and JET EFDA contributors
Neutron emission levels during the ITER zero activation phase
Nucl. Fus. 50, 084020 (2010)

- M. Gatu Johnson, E. Andersson Sunden, M. Cecconello, S. Conroy, G. Ericsson, J. Eriksson, G. Gorini, C. Hellesen, V. Kiptily, **M. Nocente**, S. Sangaroon, S.E. Sharapov, M. Tardocchi, D. van Eester, M. Weiszflog and JET EFDA contributors
Neutron Spectrometry of JET Discharges with ICRH-acceleration of Helium Beam Ions
Rev. Sci. Instrum. 81, 10D336 (2010)

- V. Kiptily, G. Gorini, M. Tardocchi, P. de Vries, F. Cecil, I. Chugunov, T. Craciunescu, M. Gatu Johnson, D. Gin, V. Goloborodâko, C. Hellesen, T. Johnson, K. Kneupner, A. Murari, **M. Nocente**, E. Perelli Cippo, A. Pietropaolo, S. Pinches, I. Proverbio, P. Sanchez, S. Sharapov, A. Shevelev, B. Syme, V. Yavorskij, V. Zoita and JET EFDA contributors
Doppler broadening of gamma ray lines and fast ion distribution in JET plasmas
Nucl. Fusion 50, 084001 (2010)

Papers published as Conference Proceedings that were not included in this thesis

- **M. Nocente**, M. Tardocchi, A. Olariu, S. Olariu, I.N. Chugunov, A. Fernandes, D.B. Gin, G. Grosso, V.G. Kiptily, A. Neto, R. C. Pereira, A.E. Shevelev, M. Silva, J. Sousa and G. Gorini
  High Resolution Gamma Ray Spectroscopy at MHz Counting Rates with $LaBr_3$ Scintillators
  Proceedings of the 2011 IEEE Nuclear Science Symposium and Medical Imaging Conference, Valencia

- **M. Nocente**, M. Garcia-Munoz, G. Gorini, M. Tardocchi, A. Weller, S. Akaslompolo, R. Bilato, V. Bobkov, C. Cazzaniga, B. Geiger, G. Grosso, A. Herrmann, V. Kiptily, M. Maraschek, R. McDermott, J.M. Noterdaeme, Y. Podoba, G. Tardini and the ASDEX Upgrade Team
  Gamma-ray spectroscopy measurements of fast ions on ASDEX Upgrade
  Proceedings of the 12th IAEA Technical Meeting on Energetic Particles in Magnetic Confinement Systems, Austin, 2011

- **M. Nocente**, M. Angelone, C. Cazzaniga, I. Chugunov, R.C. Pereira, G. Croci, D. Gin, G. Grosso, A. Neto, A. Olariu, S. Olariu, M. Pillon, A. Shevelev, J. Sousa, M. Tardocchi and G. Gorini
  γ-ray measurements and neutron sensitivity in a fusion environment
  Proceedings of the 1st International Conference on "Fusion for Neutrons and Subcritical Nuclear Fission", Varenna, 2011

- M. Tardocchi, **M. Nocente**, A. Bruschi, D. Marocco, G. Calabrò, A. Cardinali, F. Crisanti, B. Esposito, L. Figini, G. Gorini, G. Grossetti, G. Grosso, M. Lontano, S. Nowak, F. Orsitto, U. Tartari and O. Tudisco
  Production and Diagnosis of Energetic Particles in FAST
  Proceedings of the 23rd IAEA Fusion Energy Conference, Daejon, 2010

- Pereira, R.C.; Fernandes, A.M.; Neto, A.; Sousa, J.; Varandas, C.A.F.; Cardoso, J.; Correia, C.M.B.A.; Tardocchi, M.; **Nocente, M.**; Gorini, G.; Kiptily, V.; Syme, B.; Jennison, M.
  Pulse analysis for gamma-ray diagnostics ATCA sub-systems of JET tokamak

17th Real-Time Conference - IEEE-NPSS Technical Committee on Computer Applications in Nuclear and Plasma Sciences (RT 2010)

- M. Tardocchi, V.G. Kiptily, **M. Nocente**, I. Proverbio, I. Chugunov, R. Costa Pereira, T. Edlington, A. M. Fernandes, G. Ericsson, M. Gatu Johnson, D. Gin, G. Grosso, C. Hellesen, K. Kneupner, A. Murari, A. Neto, E.Â Perelli Cippo, A. Pietropaolo, S. Sharapov, A. Shevelev, J. Sousa, B. Syme, G. Gorini and JET-EFDA contributors
  High resolution gamma-ray spectroscopy observations in JET ^{4}He plasmas with ICRH
  Proceedings of the 37th Conference on Plasma Physics of the European Physical Society, Dublin, 2010

- E. Lerche, D. Van Eester, T. Johnson, T. Hellsten, J. Ongena, M.-L. Mayoral, D. Frigione, C. Sozzi, G. Calabro, M. Lennholm, P. Beaumont, T. Blackman, D. Brennan, A. Brett, M. Cecconello, I. Coffey, A. Coyne, K. Crombe1, A. Czarnecka, R. Felton, M. Gatu, C. Giroud, G. Gorini, C. Hellesen, P. Jacquet, V. Kiptily, S. Knipe, A. Krasilnikov, M. Maslov, I. Monakhov, C. Noble, **M. Nocente**, L. Pangioni, I. Proverbio, M. Stamp, W. Studholme, M. Tardocchi, T. Versloot, V. Vdovin, A. Whitehurst, E. Wooldridge, V. Zoita and JET EFDA Contributors
  Experimental investigation of ICRF heating scenarios for ITERâs half-field Hydrogen phase performed in JET
  Proceedings of the 37th Conference on Plasma Physics of the European Physical Society, Dublin, 2010

- D. Van Eester, E. Lerche, T. Johnson, T. Hellsten, J. Ongena, M.-L. Mayoral, D. Frigione, C. Sozzi, G. Calabro, M. Lennholm, P. Beaumont, T. Blackman, D. Brennan, A. Brett, M. Cecconello, I. Coffey, A. Coyne, K. Crombe, A. Czarnecka, R. Felton, M. Gatu Johnson, C. Giroud, G. Gorini, C. Hellesen, P. Jacquet, Y. Kazakov, V. Kiptily, S. Knipe, A. Krasilnikov, Y. Lin, M. Maslov, I. Monakhov, C. Noble, **M. Nocente**, L. Pangioni, I. Proverbio, M. Stamp, W. Studholme, M. Tardocchi, T.W. Versloot1, V. Vdovin, A. Whitehurst, E. Wooldridge, V. Zoita and JET EFDA Contributors
  Mode conversion heating in JET plasmas with multiple mode conversion layers
  Proceedings of the 37th Conference on Plasma Physics of the European Physical Society, Dublin, 2010

Paper accepted for publication on peer-reviewed journals that were not included in this thesis

- M. Tardocchi, A. Bruschi, L. Figini, G. Grossetti, D. Marocco, **M. Nocente**, G. Calabrò, A. Cardinali, F. Crisanti, B. Esposito, G. Gorini, G. Grosso, M. Lontano, S. Nowak, F. Orsitto, U. Tartari and O. Tudisco
  Production and Diagnosis of Energetic Particles in FAST
  accepted for publication on Nucl. Fusion

- D. Van Eester, E. Lerche, T. Johnson, T. Hellsten, J. Ongena, M.-L. Mayoral, D. Frigione, C. Sozzi, G. Calabro, M. Lennholm, P. Beaumont, T. Blackman, D. Brennan, A. Brett, M. Cecconello, I. Coffey, A. Coyne, K. Crombe, A. Czarnecka, R. Felton, M. Gatu Johnson, C. Giroud, G. Gorini, C. Hellesen, P. Jacquet, Ye. Kazakov, V. Kiptily, S. Knipe, A. Krasilnikov, Y. Lin, M. Maslov, I. Monakhov, C. Noble, **M. Nocente**, L. Pangioni, I. Proverbio, M. Stamp, W. Studholme, M. Tardocchi, T.W. Versloot,V. Vdovin, A. Whitehurst, E. Wooldridge, V. Zoita and JET EFDA contributors
  Minority and mode conversion heating in (^{3}He)-H JET plasmas
  accepted for publication on Plasma Phys. Control. Fusion

- V.G. Kiptily, D. Van Eester, E. Lerche, T. Hellsten, M.-L. Mayoral, J. Ongena, F.E. Cecil, D. Darrow, M. Gatu Johnson, V. Goloborodâko, G. Gorini, C. Hellesen, T. Johnson, Y. Lin, M. Maslov, **M. Nocente**, M. Tardocchi, I. Voitsekhovitch and JET EFDA contributors
  Fast ions in mode conversion heating (^{3}He)-H plasmas in JET
  accepted for publication on Plasma Phys. Control. Fusion

Contents

Chapter 1

Introduction

We say that we will put the sun into a box.
The idea is pretty.
The problem is,
we don't know how to make the box.
– Sebastien Balibar

1.1 Thermonuclear fusion

The increasing energy demand urges modern society to find new ways of producing energy. Several methods are being developed, but, at present, all have limitations that are difficult to overcome. Controlled thermonuclear fusion could be the unlimited energy source the world is dreaming of. Nuclear fusion makes our Sun burn and powers the Universe. In the Sun, the fusion reaction between two protons, that creates a deuteron, a positron and a neutrino, releases 1.44 MeV of energy and initiates the supply of energy and matter for the cosmic cauldron where all elements are created. The dream of reproducing a similar process on Earth has been around probably since the fusion mechanism was recognized as the one powering the sun. On Earth, the hopes for fusion energy are posed on a different reaction, d + t $\rightarrow \alpha$ + n , that releases about 17.5 MeV, i.e 10 times the energy of the p+p reaction. The d+t reaction uses deuterium and tritium as fuels and produces an α particle and a neutron. Deuterium is abundant on the Earth and can be extracted from water. Tritium is rare, but it can be bred from lithium when irradiated with neutrons produced by the d+t reaction itself. Lithium is found in sea water and in the Earth crust. Assuming to feed the present world energy demand with thermonuclear fusion only, the natural deuterium and tritium reservoirs

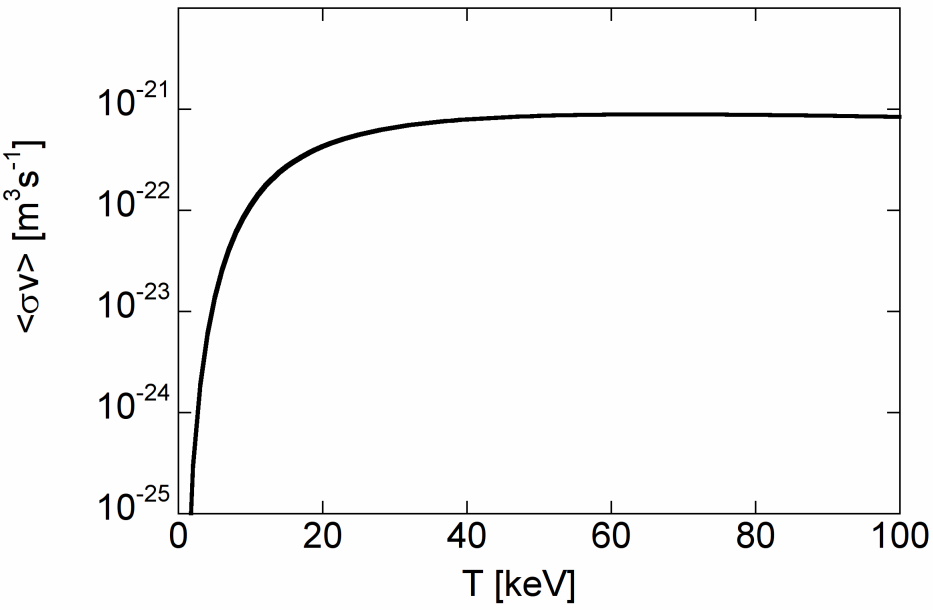

Figure 1.1: Reactivity of the d + t $\rightarrow \alpha$ + n reaction evaluated for deuterium and tritium ions assumed to be in thermal equilibrium at a temperature T.

on the Earth would last for about 1 million years [1].

Unfortunately thermonuclear fusion has been found quite hard to obtain on Earth. Dedicated researches have started in the '50s and, although significant scientific and technological progress has been made, a commercial nuclear fusion powered reactor is still a long time to come. For fusion power to be useful, a certain number of d+t reactions must occur per unit time. In physics, the likelihood for a reaction to happen is expressed by the reactivity $< \sigma v >$ in $\mathrm{m^3 s^{-1}}$. Figure 1.1 shows the reactivity of the d+t reaction as a function of the temperature T of the reactants, assumed to be in thermal equilibrium. The reactivity is maximum for $T \approx 70$ keV and drops by orders of magnitude for $T <$1 keV. Temperatures in the keV range are necessary for producing fusion energy on the Earth. At these temperatures, matter is completely ionized and it is said to be in a "plasma" state. A plasma is a quasi-neutral mass of ionized gas at high temperatures, where electromagnetic interactions are dominant. A high temperature plasma is hard to confine, much harder than a gas at room temperature. The confinement device that has shown better results so far is called the tokamak (figure 1.2). This is a toroidal device where the plasma is confined by magnetic fields. A toroidal magnetic field is generated by external coils; a poloidal magnetic field is produced by the current that flows in the plasma. The resulting field follows a helical trajectory around the torus and assures a

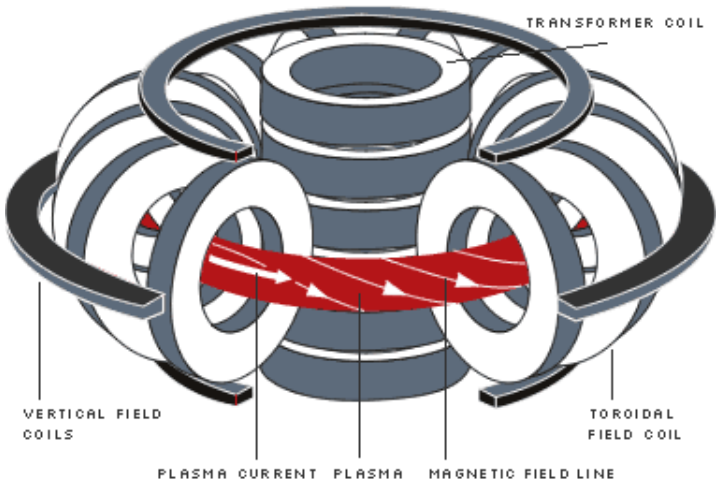

Figure 1.2: Sketch of a tokamak. Reproduced from [2]

certain degree of confinement. A comprehensive review of tokamak properties is given in [1].

In a d + t $\rightarrow \alpha$ + n reaction occurring in a 50:50 DT plasma confined by a tokamak, the released 17.5 MeV energy per reaction are shared between the neutron and the α particle in inverse proportion to their mass: the lighter neutron carries 14 MeV, while the four times more massive α particle has the remaining 3.5 MeV. Having no charge, the neutron is unaffected by the magnetic fields that confine the plasma and leaves the tokamak. Its kinetic energy can be converted to thermal energy by an ad-hoc designed mantle surrounding the tokamak. On the other hand, the α particle remains confined in the plasma. Its role is vital for the self-sustainment of fusion reactions. α particles, that are produced at an energy much higher than the average deuterium and tritium temperatures, need to transfer their energy to the reacting ions by slowing down in the bulk plasma to get the reaction going. This self heating has to be high enough to compensate for inevitable power losses.

In more detail, an energy balance can be written down to account for all different sources of input and output power in a tokamak reactor. For net fusion power production, the useful output power P_{out} must exceed the input power P_{in}, supplied by external heating systems. P_{out} is only a fraction of the released power P_{rel}, due to losses in converting the energy of the neutrons into useful electric energy. In a tokamak reactor some power, P_{loss}, is always lost, for example by radiative emission, in the form of visible light, x-rays and γ-rays. However, this can be compensated by the self heating power delivered from α particle through slowing down, P_{self}. Two favorable energetic scenarios are possible.

In the first one, the externally applied heating system helps self-heating to overcome the lost power, $P_{in} + P_{self} = P_{loss}$, with net power production, $P_{out} \geq P_{in}$. In the second one, self heating power only is sufficient to overcome lost power, without the need of an external input power, i.e. $P_{self} \geq P_{loss}$. This is called *ignition*. An economically feasible commercial thermonuclear power reactor does not need to reach ignition, provided that $P_{rel}/P_{in} \approx 30$. Ignition remains however a fundamental scientific goal. In both scenarios, P_{self} should be as close as possible to the full power delivered to α particles, P_α, by the $\mathrm{d} + \mathrm{t} \rightarrow \alpha + \mathrm{n}$ reactions. This in turn require that 3.5 MeV α particles release as much energy as possible to the bulk plasma by slowing down. α particles are therefore a key player of a thermonuclear fusion reactor.
Slowing down of α particles happens on a finite time scale τ_α, that can reach up to about 1 s in a fusion reactor. If an instability arises while the α particle is slowing down, it could be that, on a global scale, $P_{self} << P_\alpha$, as slowing down is interrupted before the α particle can deliver its full 3.5 MeV energy to the bulk plasma. If instabilities were not under control, power losses would soon predominate and the reaction would burn out. Clearly, this situation must be avoided.
Unfortunately, it is common observation on present day devices that ions which are suprathermal, like α particles in a DT plasma, drive instabilities.

1.2 Fast ions in fusion plasmas

A fusion plasma can support a large number of waves, each one with its own dispersion relation [3, 4]. The landscape is so broad that the term "wave zoo" is sometimes adopted. Waves are typically employed for heating purposes. External antennas excite modes that propagate in the plasma and are damped on the fuel ions or electron at a resonance location. Energy is thus transferred from the wave to the particles in the plasma. In unfavorable cases, a wave can be excited but not damped and lead to an instability. Uncontrolled instabilities are a major threat for a thermonuclear reactor, as they can limit the fusion performance or even cause abrupt losses of the plasma itself, called disruptions, which can cause damage to the first wall due to high power deposition.
The interest in fast ions studies comes from the observation that energetic ions (such as α particles) can drive the shear Alfvén wave unstable in magnetically confined plasma. The shear Alfvén wave is a transverse low frequency magnetic wave that propagates

along the magnetic field. In a uniform, cold plasma its dispersion relation is simply [4]

$$\omega_A = k_{\|} v_A \tag{1.1}$$

where $k_{\|}$ is the component of the wave vector along the magnetic field and v_A is the Alfvén speed. The latter depends on the magnetic field B and the ion mass m and density n through

$$v_A = \frac{B}{\sqrt{\mu_0 \sum_s n_s m_s}} \tag{1.2}$$

Here μ_0 indicates the vacuum diamagnetic constant and summation is carried over all ion species s. The wave dispersion relation implies that, in a uniform plasma, the group velocity $\partial\omega/\partial\mathbf{k}$ coincides with the phase velocity. A shear Alfvén wave is thus non dispersive in a uniform plasma. In a cylindrical plasma, measurements reveal that the dispersion relation agrees well with equation 1.1 provided that kinetic effects are taken into account [5].

In the general case the confinement geometry of the plasma affects the dispersion relation significantly [6]. The reason is that periodic geometrical boundary conditions produce a discretization of the wave number, that can only be a multiple of $1/\lambda$, where λ is a characteristic wavelength of the system. In solid state theory, a common example is the solution of the Schrödinger equation in the Sommerfeld model, where the periodicity of the crystal lattice requires the wave number to be multiple of the inverse of the lattice step. In a tokamak, there are two periodicity constraints, one along the toroidal direction, the other one along the poloidal direction, that are linked due to the peculiar geometry of this confinement device. For the shear Alfvén wave, the periodicity results in $k_{\|}$ being discretized as $k_{\|} = (n - mq)/R$, where R is the tokamak major radius and (m, n) are integers associated to the poloidal and toroidal periodicity respectively. q is called the safety factor and has a profile along the minor radius of the plasma cross section, being minimum in the centre and maximum at the plasma edge. Its name derives from the fact that, in fusion plasma theory [7], magneto-hydro-dynamic (MHD) instabilities can arise when q falls below specific values.

A sketch of the typical dispersion relation for the shear Alfvén wave in a tokamak is shown in figure 1.3 for $n = 4$. As q depends on the radius, so does the frequency ω. Waves following the dashed line in figure 1.3 are said to be part of the *Alfvén continuum.* It is very hard to excite waves in the Alfvén continuum. The reason is that the damping rate γ of the Alfvén wave is proportional to the radial gradient of the phase velocity, i.e. $\gamma \propto d/dr(k_{\|} v_A)$. As the phase velocity of waves in the continuum significantly varies

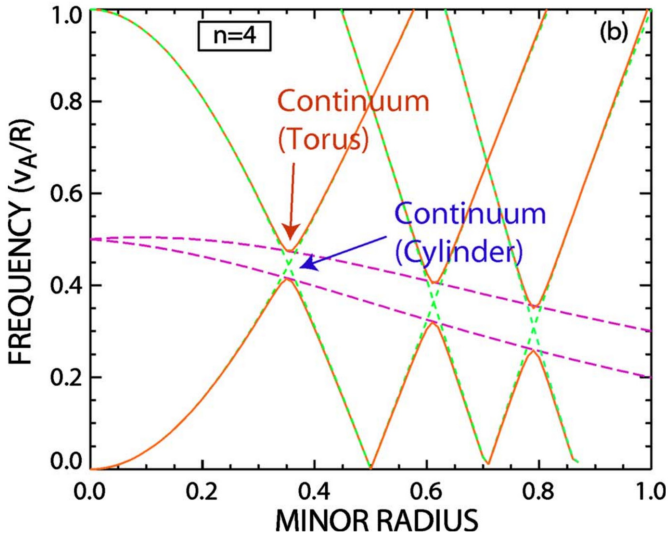

Figure 1.3: Sketch of the dispersion relation of a $n = 4$ shear Alfvén wave in a tokamak plasma. The dashed line represents the dispersion relation without toroidal coupling effects. The latter are taken into account by the solid line. Figure reproduced from reference [6]

with the plasma minor radius (see figure 1.3), waves excited in the continuum are soon damped.

In a toroidal device, however, a gap is produced in the continuum (figure 1.3, solid line). This arises from the periodic modulation of the refraction index associated to Alfvén waves. A wave that propagates along the sheared field lines of a tokamak moves from regions of higher magnetic field to regions of lower magnetic field, as $B \propto 1/R$. This in turn corresponds to a modulation of the Alfvén speed, that is proportional to B (see equation 1.2), and therefore to a periodic change in the refraction index, that produces a gap in the dispersion relation. The appearance of gaps when the refraction index is modulated is again a generic wave phenomenon, that has a counterpart for example in solid state physics, with the appearance of the well-known gap between the conduction and valence bands in insulators and semiconductors.

The Alfvén gap is not empty. Discrete modes can reside within the gaps and can be thought of as to originate from "defects" [6]. Here the similarity is with discrete energy levels that can appear between the conduction and valence bands in doped semiconductors and originate from an injected dopant (a defect). In tokamak plasmas, the defects that produce discrete modes are more complicated and can be the toroidal coupling of the m and $m + 1$ poloidal harmonics (for Toroidal Alfvén eigenmodes, TAE), the absence of magnetic shear at certain minor radius locations (for reverse shear Alfvén

eigenmodes, RSAE) or many others (BAE, EAE, MAE...) [6]. In all cases, the phase velocity for discrete modes within the gap show little radial variations, which implies that discrete modes are weakly damped and thus potentially unstable.

The interest in fast ions as drivers of unstable modes of the Alfvén type comes from the theoretical prediction [8], and subsequent observation [9], that fast ions can excite discrete modes in the gap when the toroidal and poloidal frequencies associated to their orbital motion around the tokamak match that of the wave. As the damping of the wave depends on the energy distribution of fast ions, the evolution of an excited unstable mode is hard to predict. In fact, the wave can exchange energy with the fast ions, which changes their energy distribution and/or can lead to a spatial redistribution (or even loss) of the energetic ions. The distribution function of fast ions in turns affect the subsequent evolution of the wave, producing a non linear chain of wave-particle interactions. The situation is even more complicated when the ratio of the fast ion kinetic pressure to total plasma pressure (kinetic + magnetic) becomes significant (say, a few percent). In this case, besides those modes that reside in the gap and come from the *topology* of the magnetic configuration (such as the RSAE and TAE), new modes, termed the energetic particle modes (EPM), are observed. These have a dispersion relation that depends on details of the fast ion energy distribution in a much stronger way. Indeed, besides influencing the damping of the mode, the fast ion energy distribution also determines the frequency of EPMs, that is observed to vary in time, reflecting changes in the distribution function of energetic ions.

Excitation of discrete modes in the Alfvén gap is a major threat for the performance of a fusion reactor. In a burning device, E=3.5 MeV α particles are originated at a velocity higher than v_A. As they slow down in the bulk plasma, the orbital frequencies associated to their motion cross the Alfvén gap and unstable discrete modes may be excited. Moreover, for high performance fusion plasmas, the α particle kinetic pressure will be significantly high to also excite EPMs. α particles could be redistributed or even expelled from the plasma by the simultaneous excitation of many unstable modes, before they can deliver their full energy to the bulk plasma by slowing down. This concern motivates the research on fast ion physics in fusion plasmas.

The vast majority of present day experiments on fast ions, as well as experiments addressed to investigate other aspects of plasma physics, is performed in deuterium plasmas. The reason is purely practical. Deuterium is cheaper than tritium but, especially, its use avoids many of the technical complications related to handling a radioactive gas

like tritium. The source of fast ions is external. Energetic ions are produced on purpose by auxiliary heating, such as radio frequency acceleration or neutral beam injection. The assumption behind experiments in a deuterium plasma is that results on fast ion properties understood in deuterium can be extrapolated to deuterium-tritium. For example, it is sufficient for fast ions to have a velocity comparable with v_A to excite discrete modes residing in the Alfvén gap, no matter the type of ions, being that an α particle or something else. Clearly, there are issues that are specific to a deuterium-tritium plasma, for example the observation of the effect of the excitation of many discrete modes on the slowing down of α particles. So far, only two machines have operated in deuterium-tritium, TFTR in the US and JET in the United Kingdom, at a ratio between the thermonuclear power to input power never exceeding unity. Their results are certainly of relevance for predicting the α particle behavior in a high performance burning plasma, but are definitively insufficient. α particle studies in a burning plasma are one of the key goals of the next step device ITER, that is currently under construction in Cadarache (France).

From the experimental point of view, knowledge on fast ions in deuterium plasmas is obtained through a dedicated set of diagnostics, that have delivered information at an impressive detail level. Each diagnostic is generally based on a different physics principles and has its own theoretical and experimental foundations. Some diagnostics are designed to derive information on the *structure* of weakly damped discrete modes. Diagnostics belonging to this group are, for example, Mirnov Coils [10] and, more recently, Electron Cyclotron Emission Imaging (ECEI) [11]. Mirnov coils provide information on the mode frequency and on the (m, n) poloidal and toroidal mode numbers; ECEI is a recent development of Electron Cyclotron Emission based techniques and is capable to derive information on the spatial structure of the mode for direct comparison with calculations using magneto-hydro-dynamic computer codes (figure 1.4).

A second set of diagnostics is instead devoted to the characterization of the *fast ion properties*, such as measurement of their energy distribution and characterization of their profile, spatial redistribution and losses. Diagnostics belonging to this second category are for example Neutral Particle Analyzers and Collective Thomson Scattering [10], that measure the energy distribution of confined ions; Fast Ion Loss Detectors (FILD) [12], which characterize the phase space of lost ions; Fast Ion D-Alpha (FIDA) [13] measurements that have been used, for example, to measure the spatial redistribution of fast ions during wave-mode interaction (figure 1.5), by detecting the light produced in the

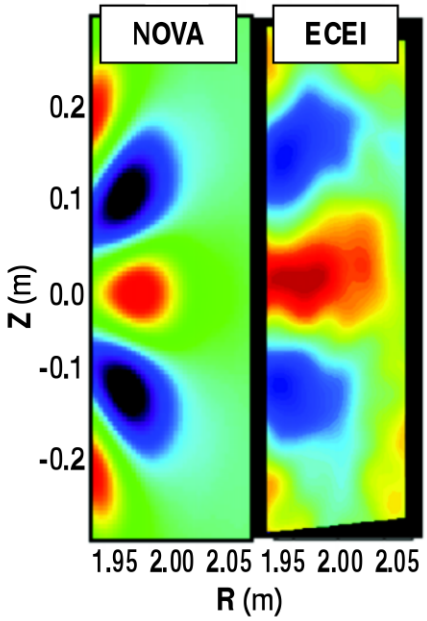

Figure 1.4: Mode structure in the poloidal plane for a RSAE of the DIII-D tokamak. The figure compares the results of a simulation with the MHD code NOVA and measurements with ECEI. Figure taken from reference [11].

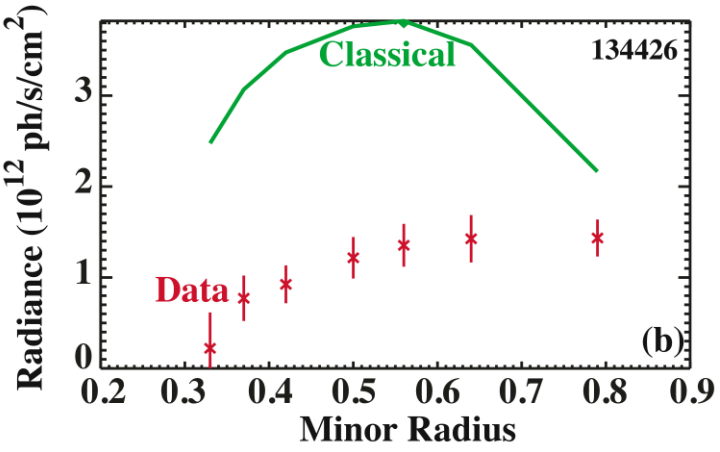

Figure 1.5: FIDA measurements of the fast ion density (proportional to the radiance of the measured Balmer D_α emission line) as a function of the plasma minor radius. The solid line shows the expected fast ion profile if no spatial redistribution due to mode excitation had occurred. Figure reproduced from reference [13].

Balmer D_α transition excited by energetic ions in the plasma.

1.3 Fast ion diagnostics in a burning plasma

Unlike a deuterium plasma, a high power, large volume deuterium-tritium plasma represents a harsh environment for diagnostic operation. Most of the diagnostics designed to derive *properties* of fast ions are faced with severe technical and principle limitations. The high density of a deuterium-tritium plasma might significantly limit diffusion of neutrals from the plasma core to the edge, which limits the use of Neutral Particle Analyzers. The small scattering signal of interest for Collective Thomson Scattering could be overwhelmed by a much stronger radiation coming from electron cyclotron emission. Moreover, the only successful implementation of the Collective Thomson Scattering technique has been performed on the TEXTOR tokamak [14] so far, i.e. on a small-size tokamak; Collective Thomson Scattering is currently being explored on mid-size devices such as ASDEX Upgrade, but other attempts to use this technique on bigger machines such as JET and TFTR have failed. FILD detectors require probes to be put at the plasma edge, where the significant heat fluxes of a high performance reactor might limit their use. As the ratio of the Larmor radius to the tokamak minor radius is decreased by the increased size of the tokamak, fast ions might be mostly spatially redistributed, without necessarily being lost. The FIDA technique, instead, is strongly limited by the cross sections of the Balmer D_α emission, that decreases by orders of magnitude as the relative energy between fast ions and neutral beams (required by this diagnostic) exceeds about 100 keV. The small FIDA signal has to be extracted from a much larger background on a burning plasma device and it is still unclear whether the FIDA signature will be distinguishable.

On the other hand, a burning plasma is a strong source of nuclear radiation, that include neutron and γ-ray emission. Neutrons are produced by the main fusion reactions, d + d $\rightarrow$ ^{3}He + n and d + t $\rightarrow$ α + n . γ-rays are produced by nuclear reactions between fast ions and impurities. Both neutron and γ-ray emission measurements are much less affected by the technical problems faced by other fast ion diagnostic techniques. Neutron and γ-ray fluxes increase as the ratio of the reactor output power to input power is raised. This is in contrast with the signals used by most of present day diagnostic techniques. Moreover, both kind of radiations escape the plasma volume, as they are not affected by the tokamak magnetic field. No probes need to be put near the plasma. Detectors can be placed far from the machine, in shielded areas if necessary.

There are certainly drawbacks that motivate why, in deuterium plasmas of mid-size devices, other diagnostics are preferred. The first one is that neutron and γ-ray fluxes are

not high enough in present devices to deliver information with a time resolution comparable to that of other techniques. A second drawback is that the relation between the measured radiation and fast ions is less direct and, especially for γ-ray measurements, still needs to be further studied and explored. On the other hand, for the reasons stated above, neutron and γ-ray measurements might be the only working fast ion diagnostics in a high power burning plasma device. This motivates the efforts in developing detectors and interpretation frameworks for neutron and γ-ray measurements, that are the topics addressed by this thesis.

The present status of development of neutron and γ-ray emission diagnostics is different. Neutron measurements have been used for about 30 years [15], with particular progress at the JET tokamak. Advanced detectors have been designed, built and operated there [16]. This allowed, for the first time, a precise determination of the fusion neutron energy spectrum. On the interpretation side, a break-through was made possible by Monte Carlo predictions of the neutron spectra [17]. Spectral components related to features of the fast ion energy distribution were identified and measured. A camera system, which allows determination of spatially resolved neutron fluxes, was installed at JET and provided information on fast ion redistribution produced by the so-called sawtooth MHD instability [18]. Upgraded camera systems are being installed on present day devices and will be used to extract information on the spatial redistribution of fast ions produced by weakly damped modes of the Alfvén type [19].

γ-ray emission is being proposed as diagnostic for fast ions on next step tokamaks [20]. In a burning plasma, for example, α particles could be studied by measuring the E_γ=4.44 MeV peak from the ^{9}Be(α, nγ)^{12}C reaction [21]. γ-ray measurements on a tokamak are relatively new with respect to neutron measurements. Peaks from several γ-ray emitting reactions involving different fast ions have been measured and identified with high efficiency, low resolution scintillators. Studies of the interaction between fast particles and Alfvén waves using γ-ray emission measurements have been initiated [20].

This thesis work provides contributions to both neutron and γ-ray emission spectroscopy studies for diagnosis of energetic ions. The role of nuclear elastic collisions in producing high energy components in the spectrum from fusion neutrons is examined using a Monte Carlo model that takes into account details of the relevant cross sections and kinematics. The analysis focuses on the possibility to determine the energy distribution tail temperature of radio-frequency heated ^{3}He ions in deuterium plasmas with an admixture of ^{3}He from the neutron spectrum. The investigation is then extended to D,

(^{3}He)D, DT and (^{3}He)DT plasmas and is focused on the determination of the fast ion energy distribution.

In 2008, the installation of a High Purity Germanium detector at JET provided the first measurement of Doppler broadening of characteristic γ-ray emission peaks from ^{12}C(^{3}He, pγ)^{14}N reactions in fusion plasmas. A theoretical framework to interpret the measurements was required. In this thesis, a Monte Carlo code, named GENESIS, was written for the purpose of interpreting the measured data and, more generally, to study the dependence of the fast ion energy distribution on the shapes of γ-ray emission lines from fast ion induced reactions in fusion plasmas. The code follows the detailed nuclear physics of γ-ray emitting reactions, that is implemented through simulation of the related kinematics. Details of the cross sections and nuclear structure of the emitting nuclei are taken into consideration. Results obtained with the code are presented and compared with measurements from several experiments.

Contribution to studies on fast particle driven instabilities with γ-ray emission spectroscopy are made with the development of a $LaBr_3$ detector equipped with digital data acquisition and designed for measurements in the MHz range (i.e. on a time scale comparable to that of fast ion driven instabilities). The detector performance at JET is presented and γ-ray spectroscopy measurements at nuclear accelerators at counting rates in the MHz range are demonstrated for the first time. The detector was employed to study, for the first time using γ-ray spectroscopy, instabilities driven by fast protons in the ASDEX Upgrade tokamak. The measurements are here presented and interpreted in terms of the nuclear physics of the d(p, γ)^{3}He reaction.

The thesis is organized as follows. The kinematics of two body nuclear reactions, as well as aspects of nuclear physics that are of relevance to predict shapes of γ-ray emission peaks, are presented in chapter 2 and in the Appendix. Chapter 3 presents the core of results of the thesis project, that are more extensively reported in the attached nine papers. Some conclusions are drawn at the end in chapter 4.

Chapter 2

Nuclear reaction kinematics and gamma ray emission from fusion plasmas

"The Answer to the Great Question...
Of Life, the Universe and Everything... Is...
Forty-two", said Deep Thought,
with infinite majesty and calm.
– Douglas Adams

The neutron and gamma-ray emission spectrum can be calculated with kinematics from the reactants energy distribution. The peculiar kinematics of γ-ray emission reactions results in a non-trivial relationship between the broadening of γ-ray emission peaks and the mean energy of the reactants. This is illustrated in this chapter after a brief overview of the relevant two body nuclear reaction kinematics. GENESIS[1], a Monte Carlo code that extends a pre-existing code for neutron spectra calculations, was written to determine the shape of characteristic γ-ray emission peaks and is presented at the end of this chapter.

2.1 Kinematics of two body nuclear reactions

Neutron and γ-ray producing reactions, such as d(t,n)^{4}He or ^{9}Be(α ,nγ)^{12}C, are classified as two body nuclear reactions. A two body nuclear reaction is defined as a reaction of

[1]Gamma Emission and Neutron Emission Simulation and Interpretation Software

the type

$$\mathrm{A} \ + \ \mathrm{B} \ \rightarrow \mathrm{C} \ + \ \mathrm{D} \tag{2.1}$$

where A, B are called the *reactants* and C, D the *reaction products*. A parameter that is often associated to nuclear reactions is the energy release $Q = (m_A + m_B - m_C - m_D) \cdot c^2$, that distinguishes between processes producing energy (exothermic; $Q > 0$) and those requiring energy to occur (endothermic; $Q < 0$). The d(d,n)^{3}He and d(t,n)^{4}He reactions, that are central for the production of fusion energy, are clearly an example of exothermic two body nuclear reactions.

The energy of the product, say C, is related to that of the reactants through classical kinematics. The detailed relation is expressed by [22]

$$E_C = \frac{m_D}{m_C + m_D}(Q + K) + V_{c.m.} \cos\theta \left[\frac{2 m_C m_D}{m_C + m_D}(Q + K) \right]^{1/2} + \frac{1}{2} m_C V_{c.m.}^2 \tag{2.2}$$

Here $Q = (m_A + m_B - m_C - m_D) \cdot c^2$ is the energy release, $K = 1/2 \mu v_{rel}^2$ the relative kinetic energy ($\vec{v}_{rel} = \vec{v}_A - \vec{v}_B$ indicates the relative reactant velocity; $\mu = \frac{m_A m_B}{m_A + m_B}$ is the reduced mass) and $\vec{V}_{c.m.} = \frac{m_A \vec{v}_A + m_B \vec{v}_B}{m_A + m_B}$ the centre of mass (c.m.) velocity. $\cos\theta$ is the cosine of the angle between the velocity of product C in the c.m. frame and $\vec{V}_{c.m.}$.

If the reactants had no velocity (i.e. $K = 0$, $V_{c.m.} = 0$ in equation 2.2), the energy of the product would be constant and equal to $E_0 = \frac{m_D}{m_C + m_D} Q$. The relative motion of the reactants modifies the energy of the products, which is no more constant, but it is shifted by the reactant energy dependent quantity $\Delta E_C = E_C - E_0$. The shift ΔE_C, besides depending on the reactant state of motion, in general depends also on the emission direction of the product, through the $\cos\theta$ term. In other words, the products are described by an *energy spectrum*, that comes from the fact that the reactants are not at rest. One can therefore try to determine the reactant energy distribution from the measured product spectrum. In fusion plasmas, for instance, equation 2.2 is often used to interpret neutron spectroscopy data (see figure 2.1).

Neutron spectra produced by fusion plasmas have been extensively studied at JET since 1984. Several features of the neutron spectrum have been identified and explained in terms of the energy distribution of the reacting ions. When neutrons are produced by ions described by a Maxwellian distribution at a certain temperature T_i, the neutron spectrum has approximately a Gaussian shape. Its width w scales with the square root of the ion temperature, i.e. $w \propto \sqrt{T_i}$ and can be used to measure T_i [22]. In present day tokamaks, a significant amount of auxiliary heating is generally employed to sustain the discharge. This typically results into a fuel ion energy distribution that, besides a

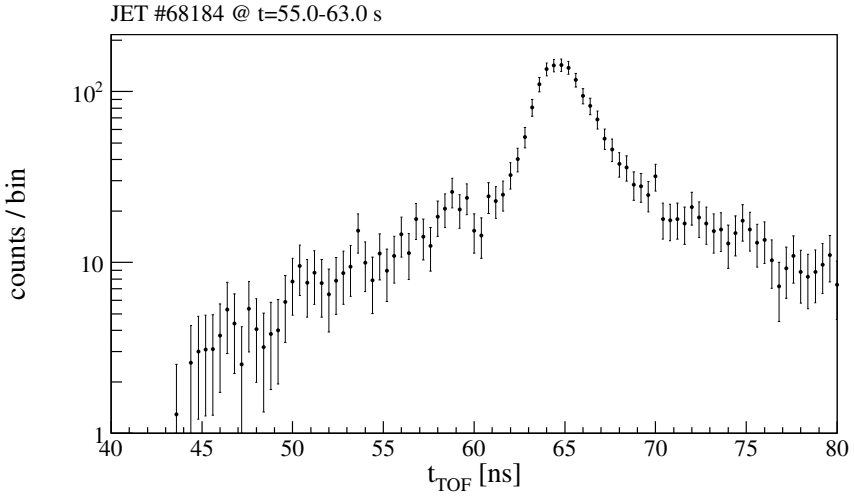

Figure 2.1: Example of a neutron spectrum from the d + d $\rightarrow$ n + ^{3}He reaction (E_0=2.45 MeV) measured at JET with the TOFOR time-of-flight spectrometer [24]. The neutron time-of-flight t_n is related to the neutron energy E_n through $t_n = C/\sqrt{E_n}$, where C is a constant that depends on the detector geometry. Neutrons are described by a spectrum which includes events at energies (time-of-flights) much different than E_0 = 2.45 MeV (t_0= 62.5 ns), due to the fact that the reactants are not at rest. The intense Gaussian peak centred at t_n = 62.5 ns comes from thermal ions. Events at higher energies, lower time of flights (say $t_n < 55$ ns) are due to fast ions.

thermal component at temperature T_i, develops tails at energies higher than the plasma temperature. These are in turn mirrored into high energy components in the neutron spectrum, that add to the Gaussian peak from thermal ions and whose intensity is often weaker than the thermal peak (see figure 2.1). The interpretation of high energy components in the neutron spectrum and its relation to fast component in the fuel ion energy distribution has been the subject of recent works on neutron spectroscopy [23, 24].

In some two body nuclear reactions the product, say C in the reaction 2.1, can be generated in one of its excited states and de-excites to the ground state on a time scale of some pico-seconds or less. When this occurs, γ-rays are emitted. An example is the ^{3}He + ^{12}C $\rightarrow^{14}$ N* + p reaction that is observed in plasmas when a population of fast ^{3}He ions interact with ^{12}C impurities. The ^{14}N nucleus is produced first, either in the ground state or in one of its excited states. When the latter situation happens, γ-rays with different peak energies are emitted, depending on which excited state is populated (see figure 2.2).

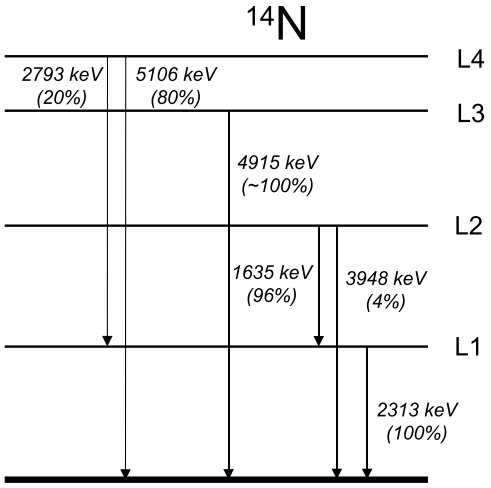

Figure 2.2: Level scheme of the first four ^{14}N excited states. γ-rays of different energies can be emitted depending on the excited state that is populated

From the kinematics point of view, the energy spectrum of the excited nucleus is still described by equation 2.2. As the excited nucleus is not at rest, its state of motion is reflected into an energy spectrum also for the emitted γ-rays. The energy E_γ of each γ-ray is linked to the velocity $\vec{v}_C$ of the excited nucleus through the equation

$$E_\gamma = E_{\gamma 0}(1 + \frac{1}{c}\vec{v}_C \cdot \vec{u}_\gamma) \tag{2.3}$$

where the scalar product between $\vec{v}_C$ and the versor indicating the γ-ray emission direction $\vec{u}_\gamma$ appears. $E_{\gamma 0}$ is the energy the γ-ray has when emitted by a nucleus at rest (for example, $E_{\gamma 0} = 2313$ keV for emission from the first excited state of ^{14}N in figure 2.2). In scientific jargon, it is said that the emitted γ-ray peak is Doppler broadened. As v_C/c is typically of the order of some percents, a Doppler broadening of some tenths of keV can be expected for γ-ray peaks in the MeV range and can be measured with semiconductor detectors, such as Germanium (see chapter 3). As done for neutron spectroscopy, it is worthwhile to measure the detailed peak shape of characteristic γ-ray emission peaks, as the reactant energy distribution might be inferred through the reaction kinematics. However, complications arise as the connection between the reactants state of motion and the γ-ray emission spectrum is mediated by a two-step process, that involves the creation of the emitting nucleus first (equation 2.2) and the emission of a γ-ray afterwards (equation 2.3).

The two step kinematic relationship between the γ-ray emission spectrum and the en-

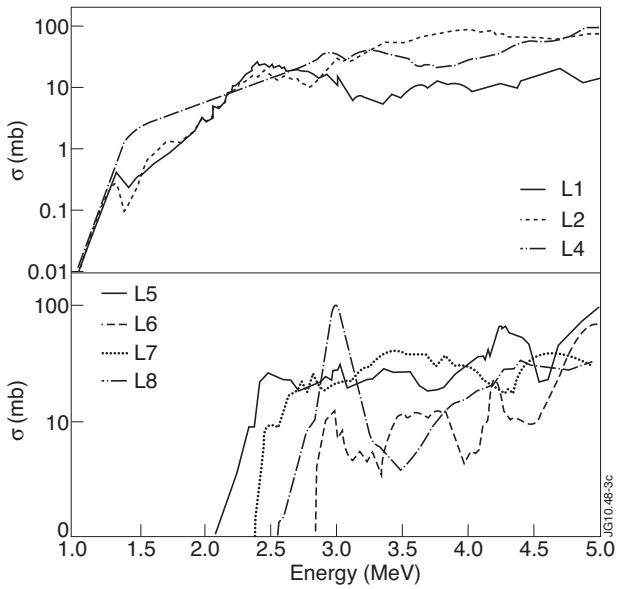

Figure 2.3: Cross sections for the first to the eight ^{14}N* states (L1 - L8) populated in the ^{3}He + ^{12}C $\rightarrow^{14}$ N* + p reaction. The x axis represents the energy of the incoming ^{3}He ions.

ergy of the reactants, as well as the complex nuclear structure of the γ-ray emitting nucleus, introduce new phenomena that are not observed in one step reactions, described by equation 2.2 only. These result in a non-trivial dependence of the peak shape on the reactants energy distribution and are illustrated in the following paragraphs by several examples. Technical details on a semi-analytical derivation to explain some of the observed features are addressed in the appendix.

2.2 Nuclear physics and gamma-ray peak shapes

The complexity of nuclear reactions involving the production of a γ-ray emitting nucleus is revealed by the cross section σ for the ^{3}He + ^{12}C $\rightarrow^{14}$ N* + p reaction shown in figure 2.3. Several curves are shown in the figure. These represent the cross section for populating ^{14}N in one of its first eight excited states. The probability to populate excited states higher than the first is, in general, not negligible and becomes higher and higher as the ^{3}He energy is raised. Higher excited states can also contribute to a transition from a lower excited level. Suppose, for instance, that the peak shape of the γ-ray peak at E_{γ}=2313 keV from de-excitation of the first ^{14}N level has to be simulated. If the fourth ^{14}N excited state is populated, it also contributes to the peak at E_{γ}=2313

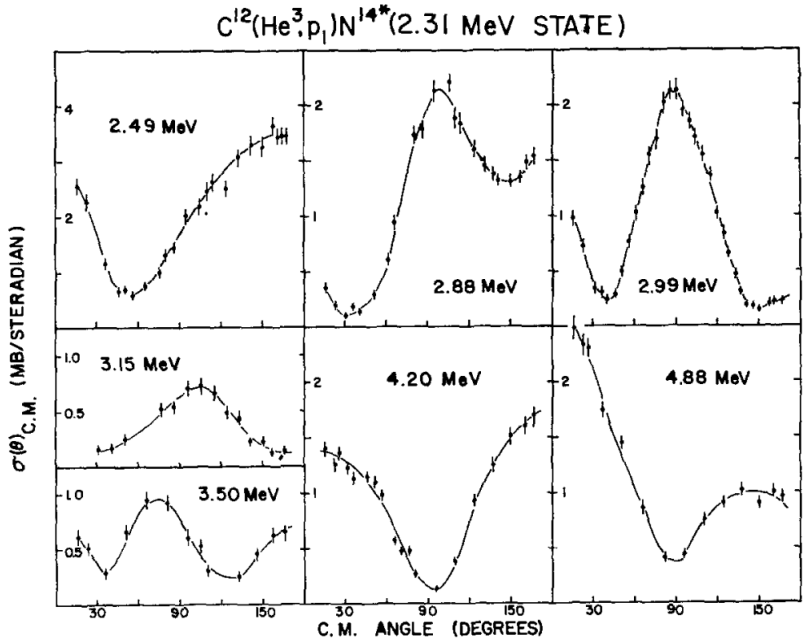

Figure 2.4: Differential cross section for the production of the first ^{14}N* excited state in the ^{3}He + ^{12}C $\rightarrow^{14}$ N* + p reaction. The figure has been reproduced from reference [25].

keV through a cascade transition $L4 \rightarrow L1$, $L1 \rightarrow$ ground state. The branching ratio for this transition amounts to only 20%. However, by inspecting figure 2.3 it is seen that the cross section for populating L4 is higher than that for populating L1 when the ^{3}He energy, E_{3He}, falls in the range 1.5 - 2 MeV for instance. This substantially increases the relative importance of L4 to simulate the E_{γ}=2313 keV peak shape and applies to several ^{14}N* excited states higher than the first.

Most of cross sections for two-step γ-ray emitting reactions show resonances as the energy of the reactant is increased (see figure 2.3). Resonances are reflected in two ways in the final peak shape. As fast ions are described by an energy distribution, the final peak shape can be thought of as a superposition of the forms produced by each single energy value in the distribution. The appearance of a resonance at a given energy E_{res} can enhance the contribution of E_{res} to the peak shape, at the expense of those energy values far from E_{res}. There is a second, more subtle way, in which a resonance affects the resulting peak shape. When a resonance is encountered, the angular distribution of the excited nucleus, expressed by the differential cross section $d\sigma/d\Omega$, profoundly changes. Figure 2.4 shows the differential cross section for the production of the first ^{14}N* excited state in the ^{3}He + ^{12}C $\rightarrow^{14}$ N* + p reaction at several ^{3}He energies. $d\sigma/d\Omega$ has continuous changes in shape that can be related to the many resonances appearing

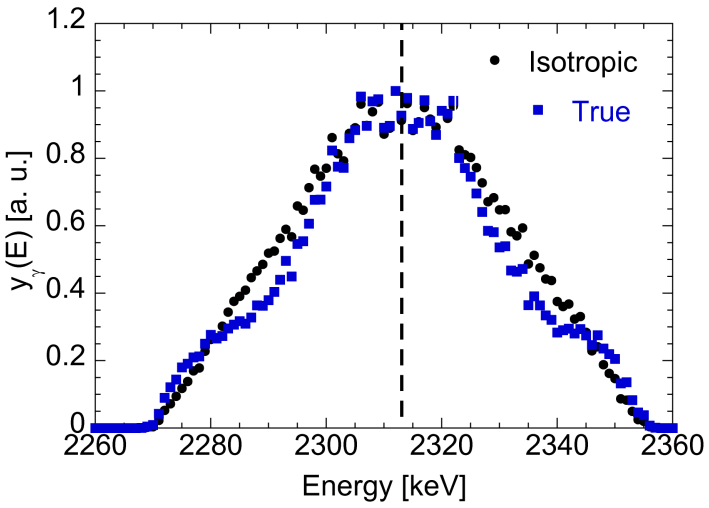

Figure 2.5: Simulated E_γ = 2313 keV peak shape from the ^{3}He + ^{12}C $\rightarrow^{14}$ N* + p for ^{3}He ions having energy E = 4 MeV. The velocity of the ions is assumed to be isotropically distributed. The two curves compare results when the anisotropy of the cross section is taken (blu squares) or is not taken (black circles) into account

in the cross section σ. Each change is manifested in the peak shape, that depends on details of $d\sigma/d\Omega$. Figure 2.5 illustrates this statement. The E_γ=2313 keV peak from the ^{3}He + ^{12}C $\rightarrow^{14}$ N* + p reaction is simulated assuming mono-energetic ^{3}He ions at E_{3He}= 4 MeV. The velocity of the ion is isotropically distributed.The result of the simulation assuming $d\sigma/d\Omega$ to be isotropic is compared to that obtained adopting the real angular distribution of the cross section at E_{3He}= 4 MeV for populating the first ^{14}N* excited state. If the cross section were isotropic, the peak shape would be *exactly* a trapezoid. When anisotropy is taken into account, the trapezoid is deformed and features that are distinctive of $d\sigma/d\Omega$ are reflected in the simulated shape (details are given in the Appendix).

Unfavorable angular distributions of the excited nuclei can even lock the γ-ray peak shapes, which remain almost unchanged even when the reactant energy is raised. This is shown with the results of figure 2.6. The E_γ= 2313 keV peak shape is simulated for two isotropic, mono-energetic ^{3}He ions with energies E_{3He} = 4 and 6 MeV respectively. It is assumed that $d\sigma/d\Omega$ becomes narrower as the energy of the ^{3}He ions is increased. Remarkably, the peak shape remains almost unchanged although the ^{3}He energy is increased by 50%. The result of figure 2.6, although obtained with an artificial $d\sigma/d\Omega$, is of relevance for the behavior of γ-ray peak shapes at high fast ion energies.

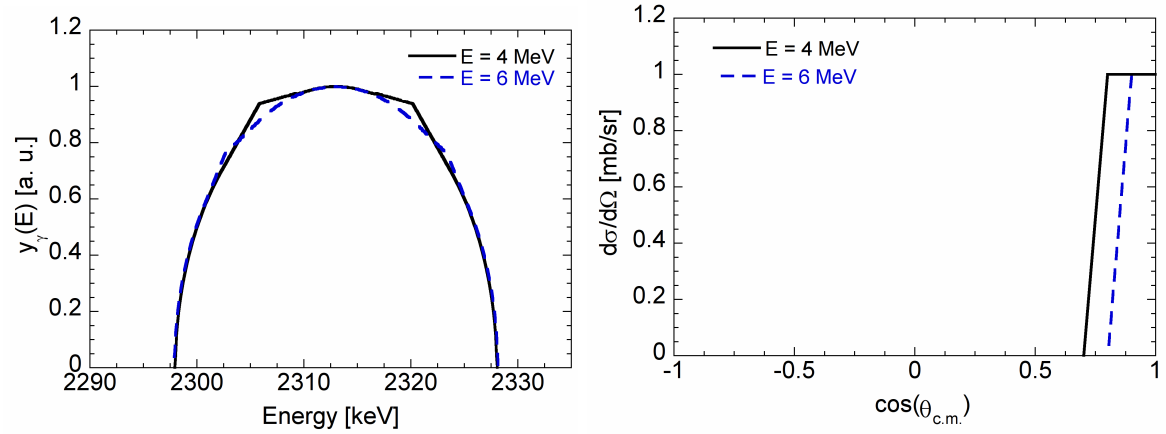

(a) (b)

Figure 2.6: (a) E_γ= 2313 keV peak shape from the ^{3}He + ^{12}C $\rightarrow^{14}$ N* + p reaction calculated for isotropic, mono-energetic ^{3}He ions at energies E_{3He}=4 and 6 MeV. The differential cross section shown in (b) is assumed in the calculations.

When the energy of the reacting ions is sufficiently high, cross sections for all nuclear reactions exhibit forward peaking, that increases as the energy is raised. This is shown, for examples, in figure 2.4 or by cross section measurements for other γ-ray emitting reactions, such as the ^{9}Be(α, nγ)^{12}C or the ^{9}Be(^{3}He, pγ)^{11}B reactions [26, 27, 28]. An increasing forward peaking is almost equivalent to a $d\sigma/d\Omega$ that gets narrower as in figure 2.6. One can therefore expect peak shapes to show no variations when the energy of the reactants is significantly high, which sets a limit to the use of γ-ray Doppler broadening for very high reactant energies. Where the limit is manifested depends on each individual reaction and needs to be studied case by case.
There are further factors that add to the phenomenology of γ-ray peak shapes. One derives, for example, from kinematics only and can lead to peak shrinking in a certain reactant energy range. Further details are given in the Appendix.

2.3 Monte Carlo calculations

The phenomenology of the relation between γ-ray peak shapes and the reactant energy distribution is so varied and complex that an analytic approach is ruled out[2]. A

[2]An analytical derivation of γ-ray peak shapes was carried out in reference [29] for reactions of the type $A + B \rightarrow C + \gamma$, i.e. not a two-step reaction. Moreover, the derivation is based on simplified assumptions on the cross sections and is limited to a prediction of the expected width of the γ-ray peak

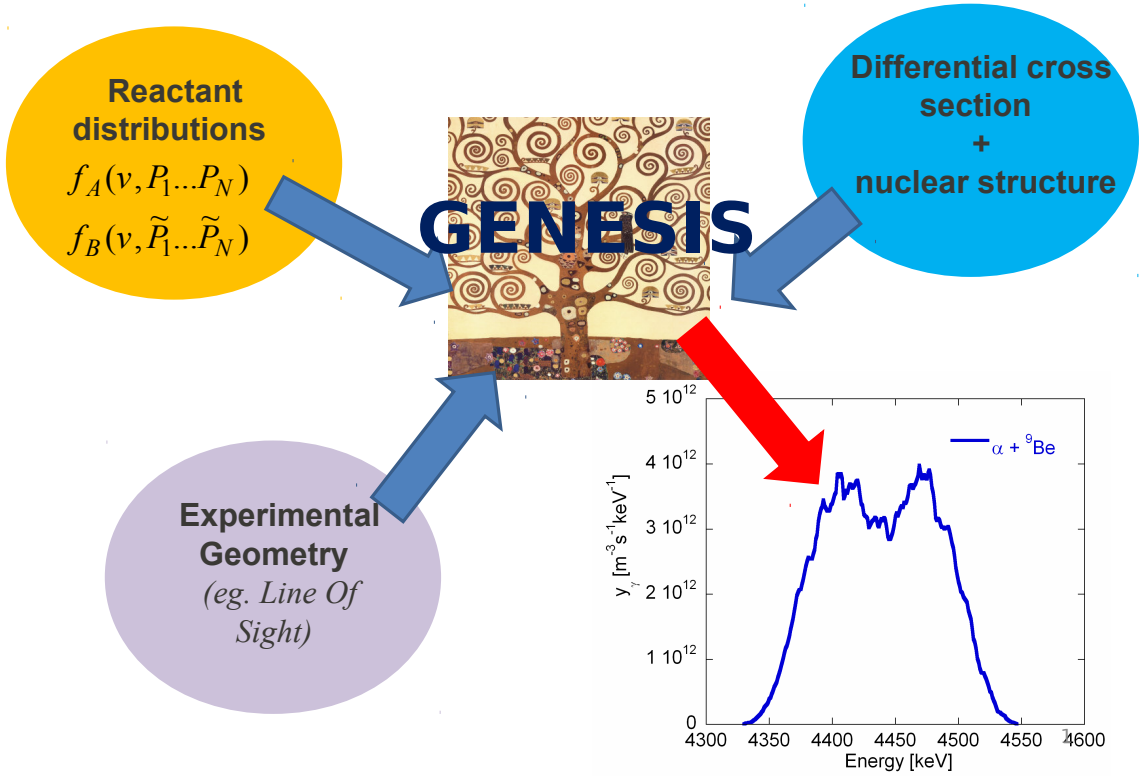

Figure 2.7: Data flow behind the GENESIS code. Input parameters are the reactant energy distributions, the reaction cross section, the nuclear structure of the γ-ray emitting nucleus and the experimental geometry (eg. line of observation). The output is the expected γ-ray peak shape.

Monte Carlo code, that extends a previous code [17] for neutron spectra calculations and is named GENESIS[3], was written for the purpose of calculating γ-ray peak shapes produced by several nuclear reactions occurring in thermonuclear plasmas. The energy spectrum of the excited nucleus is determined through classical kinematics (equation 2.2) by sampling the reactant energy distributions. In a second stage, the resulting gamma ray emission spectrum is evaluated along a specified line of sight (equation 2.3). Isotropic γ-ray emission with respect to the excited nucleus direction in the laboratory frame is assumed and branching ratios are taken into account so as to simulate cas-

shape as a function of the temperature of the reactants, assumed to be in thermal equilibrium

[3]See footnote 1

cade transitions when necessary (see figure 2.2). Figure 2.7 shows the data-flow behind the GENESIS code. The input required by the code is the energy distribution of the reactants, that can depend on parameters (eg. the tail temperature of the fast ion energy distribution) to be determined by multiple simulations and best fit to measured data. Nuclear physics information is summarized in the differential cross sections for the population of excited states of the γ-ray emitting nucleus, besides its level scheme. The experimental geometry is expressed through the viewing angle between the magnetic field and the γ-ray emission direction or, in a future implementation of the code, through the detailed specification of the detector line of sight and fast ion profiles in the plasma.

The GENESIS code has been used to interpret the first measurements of γ-ray Doppler broadening from a tokamak plasma and to calculate the effect of fast ion nuclear elastic scattering on the neutron emission spectrum from fusion plasmas. Results obtained with the code and comparison with measurements are presented in the next chapter.

Chapter 3

Fast ions observations and nuclear radiation from thermonuclear plasmas

Do or do not.
There is no try.
– Jedi Master Yoda

The results obtained in this thesis are here summarized. Two topics are addressed: the determination of the fast ion energy distribution from measured neutron and γ-ray emission spectra and the study of fast ion driven instabilities with γ-ray emission spectroscopy. Fast ion energy distributions are derived from simulated neutron spectra by considering the role of nuclear elastic scattering for specific plasma scenarios. Simulations of γ-ray spectra with the GENESIS code are compared with measurements of γ-ray Doppler broadening from fusion plasmas in several experiments at the JET tokamak. Parameters of the fast ion energy distribution are derived from detailed analysis of spectral shapes and ratios of characteristic emission peaks.
Instrumentation to study fast ion driven instabilities with γ-ray spectroscopy is presented. A $LaBr_3$ detector was developed for high resolution γ-ray spectroscopy at MHz counting rates and was used to demonstrate high rate γ-ray spectroscopy at nuclear accelerators. The same detector was used for γ-ray emission spectroscopy at the tokamak ASDEX Upgrade where it contributed to the study of confined fast protons.

3.1 Fast ion energy distribution and neutron emission spectrum

As discussed in chapter 2, the neutron spectrum from d + d → ^{3}He + n reactions carries information on the deuteron energy distribution (see figure 2.1). The reason is that the state of motion of deuterium (the reactant of the d + d → ^{3}He + n reaction) is reflected in the neutron spectrum through the kinematic relation expressed by equation 2.2. In particular, high energy components of the deuterium energy distribution are reflected into high energy components in the neutron spectrum (figure 2.1). This relation was investigated in detail in the works [23, 24], where a clear correspondence between the neutron spectrum and the fuel ion energy distribution was measured and interpreted in several scenarios of direct interest for fusion plasma studies.
The d+d neutron spectrum can also carry information on fast ions that are *not* reactants. A common technique adopted at JET to study fast ion physics is to accelerate ^{3}He ions in a bulk deuterium plasma. ^{3}He is puffed by external valves, at typical concentration levels of 1%. Radio frequency (RF) heating, tuned to the fundamental ^{3}He cyclotron frequency, is used to heat ^{3}He ions, that develop a high energy tail in their energy distribution. In Paper I it is shown that the temperature of the ^{3}He tail is manifested in a high energy component in the neutron spectrum. On the basis of equation 2.2, this can only happen if a fast *deuterium* population is generated in a (^{3}He)D plasma, although deuterium is not directly heated by RF. The link between fast ^{3}He ions and energetic deuterium is given by *nuclear elastic collisions*. ^{3}He ions, that are continuously accelerated by RF heating and slow down in the bulk plasma, can encounter thermal deuterons. Although rare, in some cases a frontal collision (knock on) occurs between ^{3}He ions and deuterium. Knock on collisions are an effective energy transfer mechanism and produce a distortion of the deuterium energy distribution, that develops high energy tails reflecting the kinematic properties of ^{3}He ions (figure 3.1). When looked from the deuterium phase space, ^{3}He + d nuclear elastic collisions are equivalent to a source of fast deuterons per unit time. The stationary shape of the deuteron energy distribution is given by the balance between fast deuteron generation due to ^{3}He+d collisions and slowing down on bulk plasma due to small angle Coulomb collisions, and is described by a proper Fokker-Planck equation. Suprathermal deuterons generated by d+^{3}He knock on produce a high energy tail in the neutron spectrum (see figure 3.2); its slope depends on the ^{3}He ion tail temperature and can be used for diagnostic purposes (see Paper I).

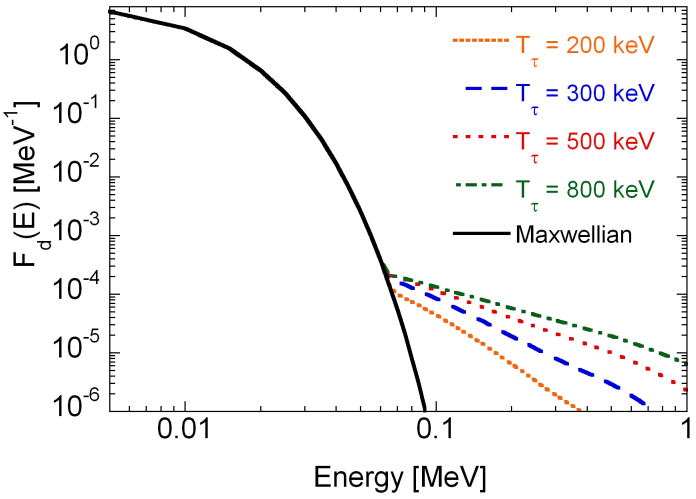

Figure 3.1: Calculated deuterium energy distribution after d+^{3}He knock for different tail temperatures T_τ of the ^{3}He ions. d+^{3}He collisions result in a high energy component in the deuterium energy distribution that appears at energies $>$ 100 keV. A T_d=5 keV Maxwellian distribution describing thermal deuterium, is also shown for comparison

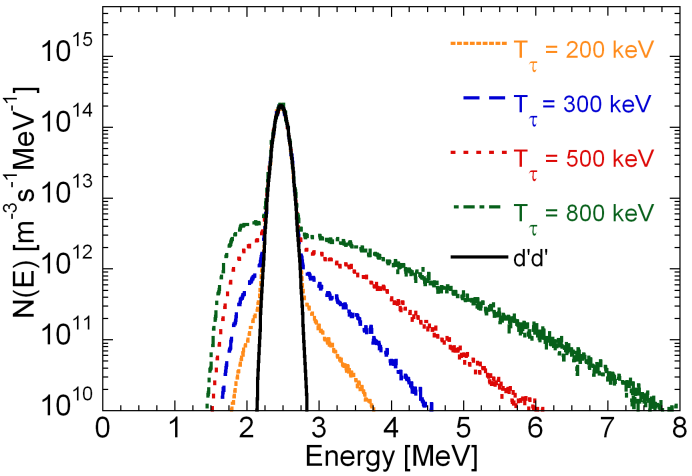

Figure 3.2: Calculated neutron spectrum with d+^{3}He scattering effects for several tail temperatures of the ^{3}He ions. The magnitude and slope of the high energy component ($E_n > 3$ MeV) due to d+^{3}He scattering in the neutron spectrum depends on the ^{3}He tail temperature T_τ. The result of the calculation for a thermal deuterium plasma (T_d=5 keV) is shown by a solid black line.

Energy transfer from fast ^{3}He ions to bulk deuterons is mostly a nuclear physics effect. Figure 3.3 compares the full cross section for d + ^{3}He scattering with that due to Coulomb scattering only. The full cross section takes into account contributions from

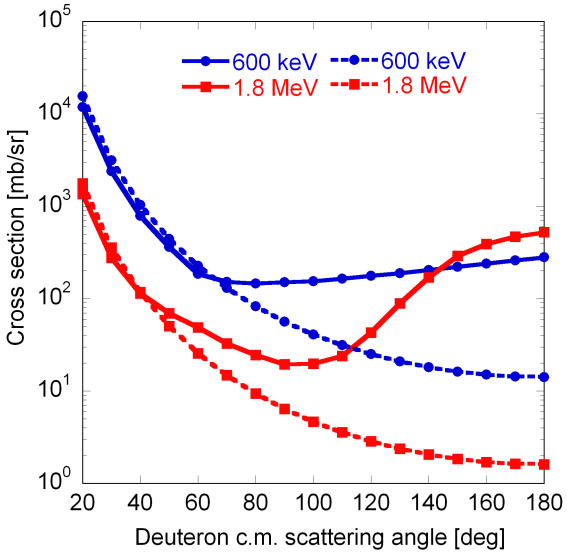

Figure 3.3: Cross section of elastic d+^{3}He scattering for different c.m. energies. The solid line shows the full cross section, that takes into account contributions from nuclear and Coulomb scattering, as well as interference between the two. The dashed line shows the cross section for Coulomb scattering only.

nuclear and Coulomb scattering, as well as interference between the two. The maximum energy transfer between a fast ^{3}He ion and a thermal deuteron occurs for scattering angles in the c.m. frame around 180°. Here the Coulomb cross section is minimum, which implies that the full cross has a significant contribution from nuclear+interference processes [30].

When the ^{3}He tail temperature is raised, the reactivity of the d + ^{3}He $\rightarrow$ α + p fusion reaction is also increased. This is demonstrated by the cross section for the d + ^{3}He $\rightarrow$ α + p reaction shown in figure 3.4. For c.m. energies above 100 keV, the cross section for the d+^{3}He fusion cross section is as high as that for the d + t $\rightarrow$ α + n reaction, which results in a significant production of the fusion products α and p, with an angular distribution that is in general anisotropic (Paper II). Fusion born α particles and protons are also suprathermal and can transfer their energy to bulk deuterium through nuclear elastic collisions. When seen in the deuteron phase space, new fast deuteron source terms are generated due to α + d and p + d elastic scattering (Paper III). The stationary deuteron distribution is modified and features further high energy components that result from competition between elastic scattering from energetic fusion products and slowing down on bulk plasma. This is in turn reflected in additional high

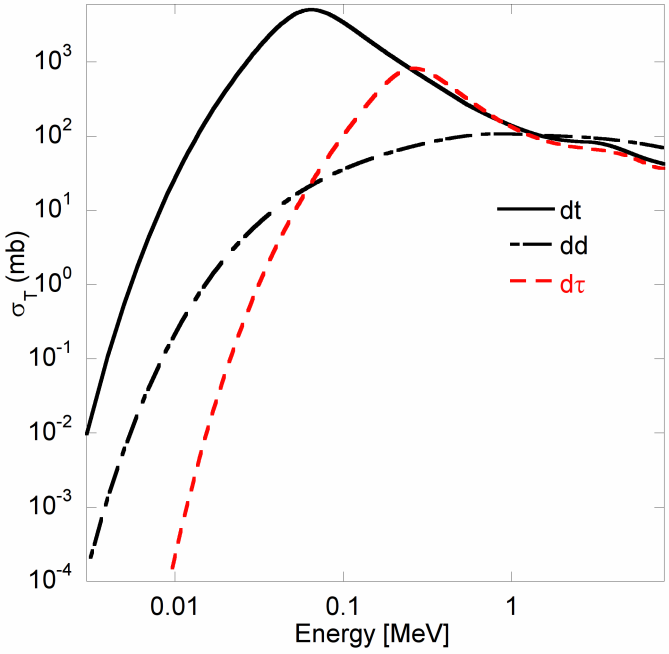

Figure 3.4: Comparison of the cross section for the d + d → ^{3}He + n , d + t → α + n and d + ^{3}He → α + p reaction as a function of the energy in the c.m. frame

energy components in the neutron spectrum from the d + d reaction (figure 3.5).

The rationale behind the search for high energy components in the neutron spectrum is the possibility to track time changes of the fast ion energy distribution by measuring the corresponding components in the neutron emission spectrum. In some cases, however, knock on collisions are not strong enough to produce a detectable component. This is the case of α and proton fusion products in (^{3}He)D plasmas, as shown in figure 3.5. α particle knock on is always dominated by ^{3}He and proton knock on. The latter is only detectable for neutron energies $E_n > 5$ MeV, but its magnitude is too low compared to the sensitivity of current spectrometers for d+d neutrons. In general, fusion products knock on is found to be typically very weak, as discussed in Paper III, where knock on effects in D, (^{3}He)D, DT and (^{3}He)DT plasmas are examined with the aim of completing the map on nuclear elastic scattering effects from energetic light ions in the neutron emission spectrum. An important exception is α particle knock on (AKN) in DT plasmas. α particles, that originate from the d + t → α + n reaction, produce a detectable component in the neutron spectrum, that has been observed at JET with advanced magnetic proton recoil neutron spectrometers (figure 3.6). Its observation is extremely useful in DT plasmas of a burning device, as measured changes in the AKN

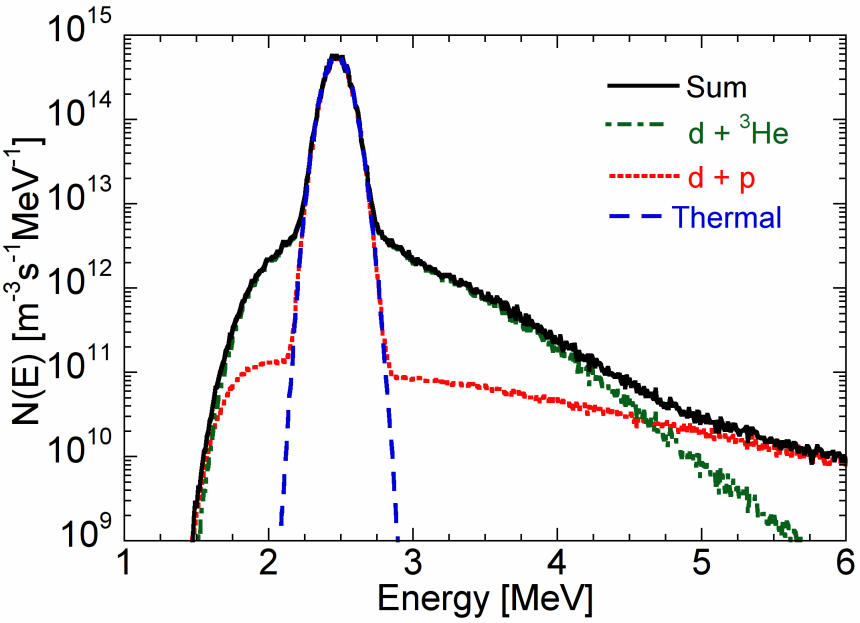

Figure 3.5: Neutron spectrum from the d+d reaction in a (^{3}He)D plasmas with RF including scattering effects from d+^{3}He reactions, as well as that from α and p fusion products from the d + ^{3}He $\rightarrow$ α + p reaction. The α+d component is not shown, as it always falls below the $p + d$ component. A tail temperature of 300 keV is assumed. The neutron spectrum from a thermal deuterium plasma (T_d=5 keV) is also shown for comparison.

component would reflect modifications in the α particle energy distribution. This could be used, for example, to study the effect of the excitation of weakly damped discrete Alfvén eigenmodes (section 1.2) on α particle slowing down in a burning plasma device. Paper III extends the results of [17] by examining the magnitude of the AKN component in a (^{3}He)DT plasma with RF coupled to ^{3}He ions. Knock on arising from d+^{3}He nuclear elastic scattering dominates over α+d, due to the much higher cross section for d+^{3}He. Information on α particles through the AKN components is lost. On the other hand, the ^{3}He knock on component is above, by about two order of magnitude, the sensitivity of current neutron spectrometers for DT plasmas and can be used to diagnose changes in the energy distribution of RF heated ^{3}He ions at very high temporal resolution in a burning (^{3}He)DT plasma (Paper III).

To summarize, the energy distribution of fast, non fuel ions is manifested as weak high energy components in the neutron emission spectrum in several cases of experimental interest in fusion plasmas. Measurements of such components can be used to determine parameters of the fast ion energy distribution, such as the tail temperature of RF heated

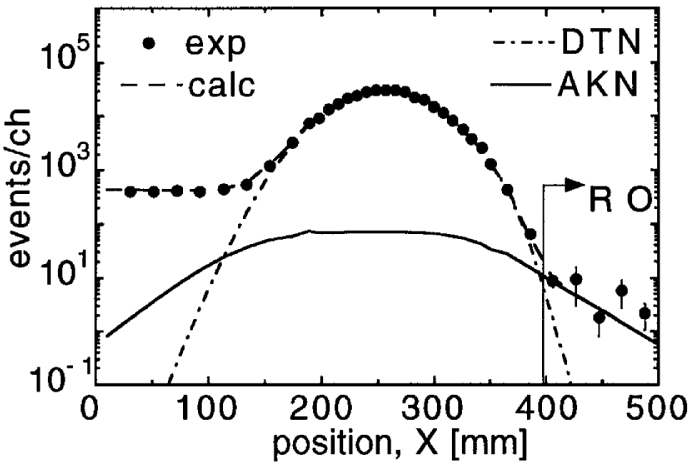

Figure 3.6: Measured neutron spectrum in a DT plasma of the JET tokamak. The signal intensity is plotted vs the X coordinate representing position along a hodoscope. X varies linearly with the neutron energy (see [16] for details). Besides thermal emission (DTN), the simulated α knock on (AKN) component is shown and matches measured data at high neutron energies. Figure reproduced from reference [31].

^{3}He ions. The results of the calculations here summarized (and presented in full details in Papers I to III) are of relevance for diagnostics of the fast ion energy distribution from the neutron emission spectrum at JET and in burning plasmas of next step devices.

3.2 Fast ion energy distribution and γ-ray emission spectrum

Similarly to neutron emission spectroscopy, analysis of γ-ray emission spectra can provide information on the fast ion energy distribution.
In 2008 a High Purity Germanium (HpGe) detector was installed above the JET tokamak. The detector, which features an energy resolution of 2.4 keV at E_γ=1.33 MeV, was used to measure γ-ray emission spectra in a (^{3}He)D plasma with RF tuned to the fundamental ^{3}He harmonic (see Paper V). Measurements were made possible by choosing N-type germanium, which is more resilient to neutron damage, and by equipping the detector with an electromechanical cooling system instead of liquid nitrogen cooling to facilitate operation in restricted areas. The detector was placed in a shielded location 23 m above the tokamak viewing the plasma along a vertically collimated line of sight orthogonal to the toroidal magnetic field. HpGe are commonly used in nuclear radiation

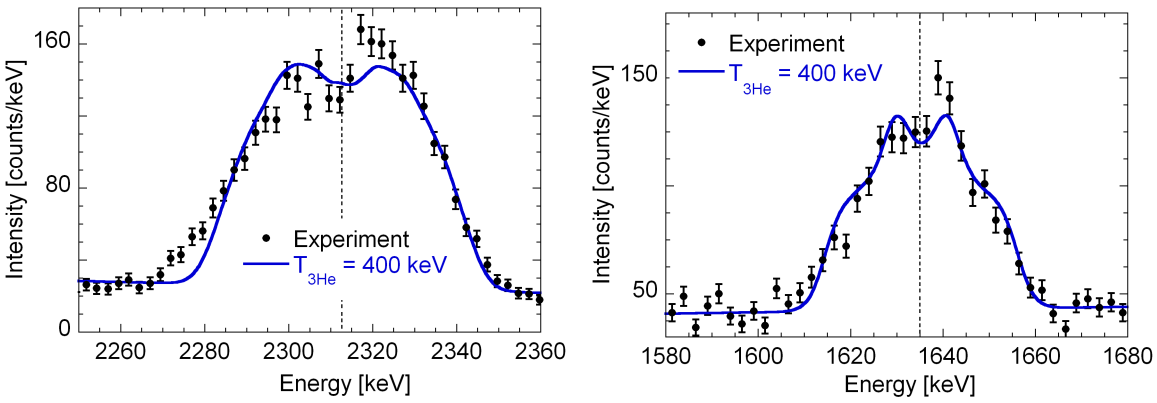

(a) (b)

Figure 3.7: Experimental and fitted (solid line) peak shapes for the $E_{\gamma 1}$=2313 keV (a) and $E_{\gamma 2}$=1635 keV (b) γ-ray emission peaks. The unshifted $E_{\gamma 1}$ and $E_{\gamma 2}$ values are marked with vertical dashed lines.

facilities, but no measurements with these detectors were ever performed on a tokamak. Fast ^{3}He ions produce γ-rays through the ^{12}C(^{3}He, pγ)^{14}N reaction. ^{12}C is available as an impurity at typical concentration levels of 1% at JET due to the composition of the first tokamak wall. The expected energies of the emitted γ-rays depend on which excited state of ^{14}N is populated (see figure 2.2 in chapter 2). In the 2008 experiment, characteristic emission peaks at energies $E_{\gamma 1}$=2313 keV and $E_{\gamma 2}$=1635 keV were detected (figure 3.7). $E_{\gamma 1}$ and $E_{\gamma 2}$ come from de-excitation of the first and second ^{14}N* excited states (see figure 2.2). Peaks due to emission from higher excited states were also observed, but their limited statistics did not allow for a quantitative study.

There are two parameters related to the measured emission peaks that may yield information on the ^{3}He energy distribution. As the relative probability to populate different ^{14}N excited states depends on the mean energy of the ^{3}He ions, the first parameter is the ratio r of the observed $E_{\gamma 1}$ and $E_{\gamma 2}$ emission peaks. The second one, which motivates the need for a HpGe detector, is the width of characteristic emission peaks. The comparison is here with measurements of the temperature of a star in astrophysics. As the Doppler broadening of characteristic emission lines in the light spectrum from a star has information on the star temperature, the same could hold for γ-ray emission from a thermonuclear plasma.

The ratio r can be calculated once the cross section for populating the 1st to 8th ^{14}N* states is known, by taking into account nuclear transition branching ratios of relevance for production of γ-rays at energy $E_{\gamma 1}$ and $E_{\gamma 2}$ (see Paper IV). As discussed in chapter 2,

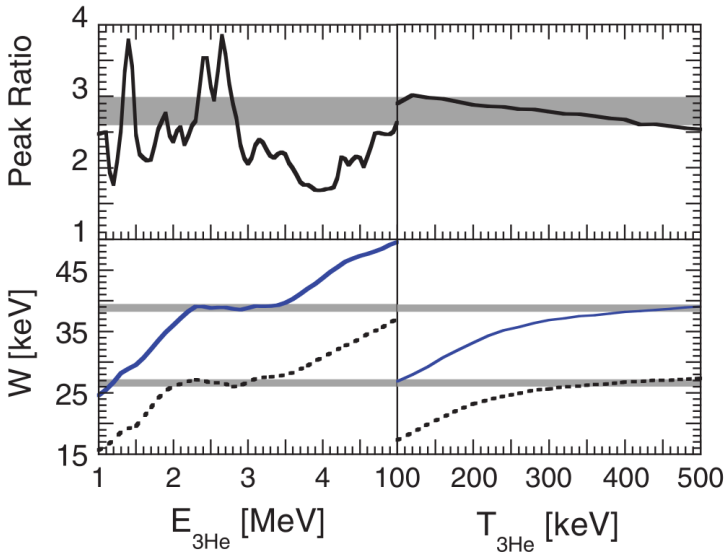

Figure 3.8: Peak ratio (top) and width (bottom) of the simulated $E_{\gamma 1}$ and $E_{\gamma 2}$ γ-ray emission peaks for monoenergetic ^{3}He ions of different energies (left) and Maxwellian ^{3}He ions of different temperatures (right). The horizontal bands are the experimental values with error bars.

excited states higher than the second contribute to the observed ratio, which motivates the need to consider cross section data for populating the 1^{st} to 8^{th} ^{14}N excited states, as done in Paper IV.

The measured ratio was compared to that predicted by Monte Carlo simulations with the GENESIS code (figure 3.8). The peak ratio r calculated for mono-energetic ^{3}He ions lies in the range 2.8 ± 0.2 and suggests that most of the γ-emitting ^{3}He ions in the plasma must have an energy below 3 MeV. When the expected energy distribution for ^{3}He ions is taken into account, it is found that the peak ratio r is rather independent on the ^{3}He tail temperature (T_{3He}) for values in the interval $100 < T_{3He} < 500$ keV (paper V). This can be ascribed to an unfavorable combination of cross sections and branching ratios for γ-ray emission from the ^{12}C(^{3}He, pγ)^{14}N reaction and depends on nuclear physics details of this specific reaction.

Figure 3.8 also compares the measured width of the $E_{\gamma 1}$ and $E_{\gamma 2}$ γ-ray emission peaks with that simulated with the GENESIS code for different tail temperatures of the ^{3}He ions. As for the peak ratio, the width is found to be only slightly dependent on the ^{3}He tail temperature for $T_{3He} > 300$ keV. In other words, the measured width is comparable with that simulated for any T_{3He} value in the range $300 < T_{3He} < 500$ keV. This is further illustrated in figure 3.9, where the expected peak shapes of the $E_{\gamma 1}$ and $E_{\gamma 2}$

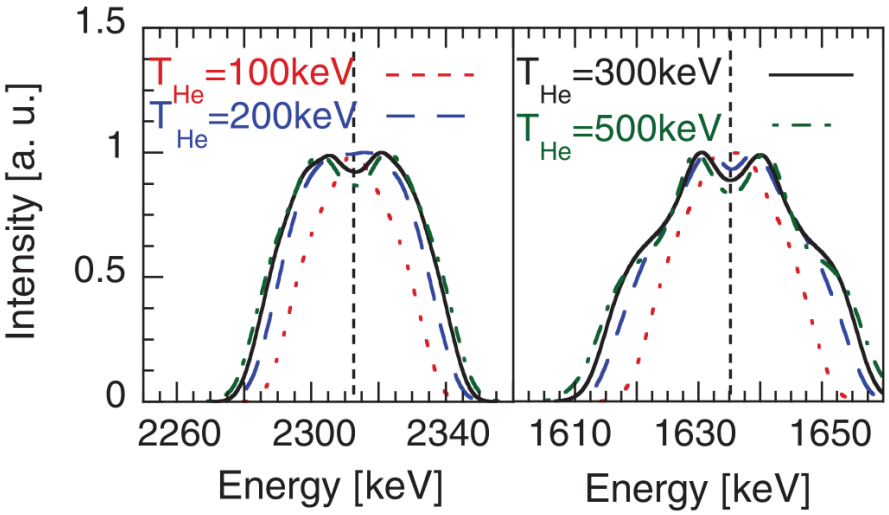

Figure 3.9: Simulated $E_{\gamma 1}$ (left) and $E_{\gamma 2}$ (right) γ-ray emission peak shapes normalized to unit height for ^{3}He ions described by a Stix distribution [3] for several asymptotic tail temperatures $T_{^3He}$. The unshifted $E_{\gamma 1}$ = 2313 keV and $E_{\gamma 2}$ = 1635 keV values are marked with vertical dashed lines.

peaks are simulated with the GENESIS code. Only little variations are seen in the peak shapes for temperature values in the range 300 < T_{3He} < 500 keV. This is an example of the limitations to γ-ray Doppler broadening diagnostics due to peculiarities of two step reactions and nuclear cross sections discussed in chapter 2.

A value for the ^{3}He temperature was finally determined by combining information obtained from the peak shapes and ratios with that extracted from the absolute level of observed counts under the $E_{\gamma 1}$ and $E_{\gamma 2}$ peaks. The absolute level of counts under a peak is in general a function of many parameters, such as the γ-ray emission volume, that depends on the profile of RF power deposition in the plasma; the reactant densities, that are measured with poor accuracy; details of γ-ray transport from the plasma to the detector along the line of sight, that are hard to simulate. For these reasons, the expected absolute number of counts can only be calculated with a typical systematic uncertainty of a factor 2. On the other hand, as shown in figure 3.10, the reactivity for the ^{12}C(^{3}He, pγ)^{14}N reaction varies significantly, i.e. by order of magnitudes, for T_{3He} in the range 300-500 keV and only a value $T_{3He} \approx 400$ keV is able to match the observed absolute count level for realistic ^{12}C concentrations (Paper V), besides reproducing the measured peak shapes and ratios.

Measurements of γ-ray Doppler broadening were carried out again at JET in a different

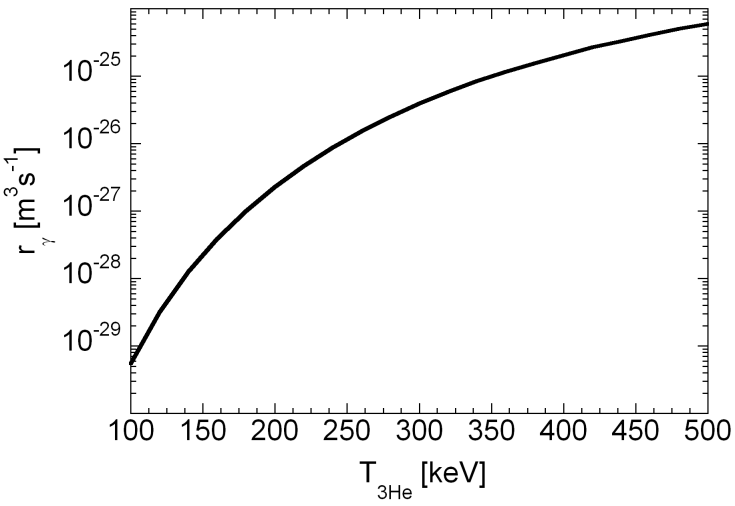

Figure 3.10: Reactivity for the ^{12}C(^{3}He, pγ)^{14}N reaction as a function of the tail temperature of ^{3}He ions.

experiment. A beam of ^{4}He ions was injected perpendicularly to the magnetic field in a (D)^{4}He plasma. The beam was accelerated by coupling RF at the third harmonic with the aim of studying MHD activity induced by energetic ^{4}He ions. The energy distribution that is created in this case is highly non Maxwellian. A rather flat tail is developed in phase space extending to high energies from the neutral beam injection energy up to a certain cut value E^*_α. Correspondingly, a sharp drop is seen in the alpha particle energy distribution and almost no particles have energies extending above E^*_α (figure 3.11). When ^{4}He is accelerated, part of the energy of the incoming RF wave is also damped on bulk deuterium, but with less efficiency, due to peculiarities of RF heating at the III harmonic (see Paper VI). The deuterium energy distribution has qualitative features that resemble those of ^{4}He ions, as also illustrated in figure 3.11. No deuterons are found at energies higher than E^*_d , where the relation $E^*_d = 0.5 \cdot E^*_\alpha$ holds between the cut energies of ^{4}He and deuterium ions (Paper VI).

^{4}He ions can be diagnosed with γ-ray emission spectroscopy via the ^{9}Be(α, nγ)^{12}C reaction, by detecting the E_γ=4.44 MeV peak produced by emission from the first excited state of ^{12}C*. The ^{9}Be(α, nγ)^{12}C reaction is particularly important, as it is the proposed process for α particle diagnosis on ITER [20]. Measurements with both the HpGe detector and a $LaBr_3$ detector (see next section) were performed during the experiment and are reported in detail in Paper VI. Figure 3.12 shows the measured peak shape of the E_γ=4.44 MeV line. The peak displays a clear asymmetry around the E_γ=4439 keV

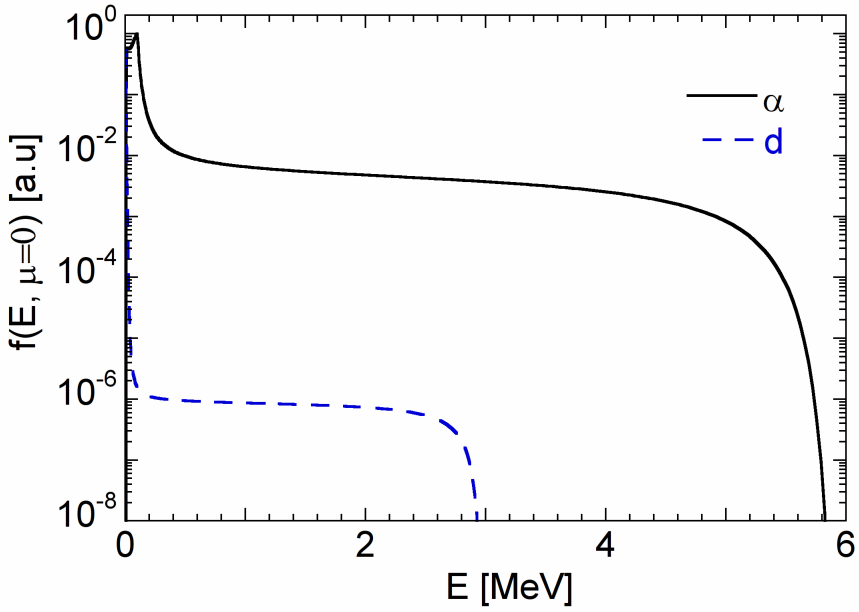

Figure 3.11: Energy distribution for deuterons and ^{4}He ions accelerated at the third harmonic by radio-frequency heating

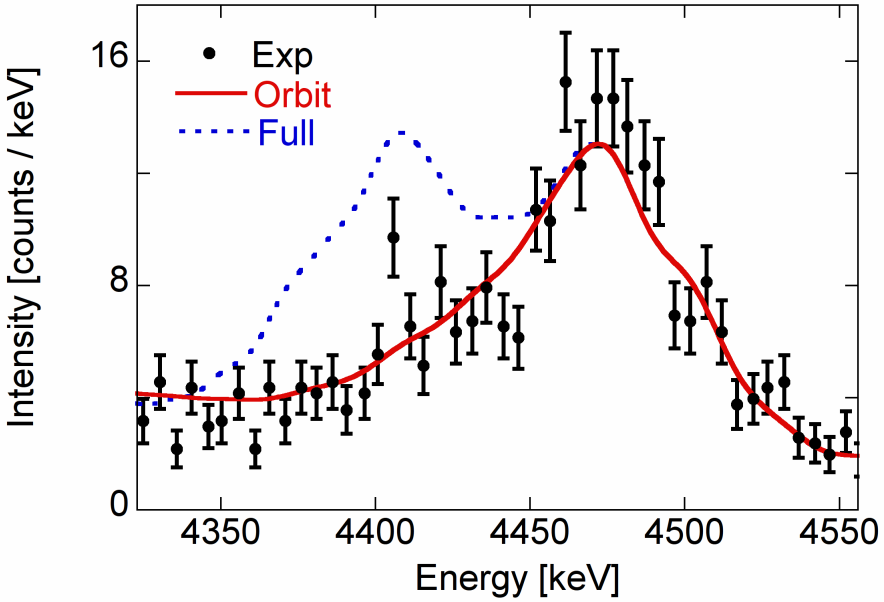

Figure 3.12: Doppler broadened E_γ=4.44 MeV peak from the ^{9}Be(α, nγ)^{12}C reaction as measured with the HpGe detector. The curves are the result of Monte Carlo simulations with the GENESIS code with (solid line) and without (dashed line) correlation between the α particle gyro-radius and the width of the line of sight.

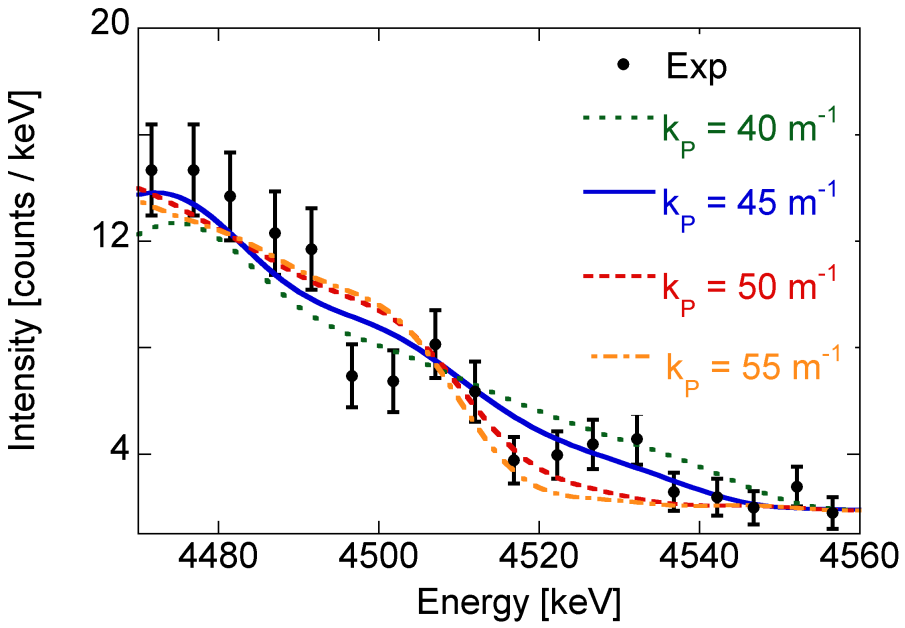

Figure 3.13: Upper half of the E_γ=4.44 MeV peak from the ^{9}Be(α, nγ)^{12}C reaction and simulations with the GENESIS Monte Carlo code for several values of the perpendicular wave number k_p (that depends on E^*_α).

channel, which is confirmed by comparison with a simulation using the GENESIS code. As discussed in Paper VI and in the Appendix, the asymmetry comes from the fact that only part of the ion gyromotion fell into the spectrometer line of sight and is reproduced by the GENESIS code when this effect is included in the simulation.

The upper half of the E_γ=4.44 MeV peak is not affected by the orbit effect and can be used to determine E^*_α . Figure 3.13 shows details of the peak together with simulations with the GENESIS code for several values of k_p. The latter, which represents the perpendicular wave number of the RF wave, is the parameter appearing in the theory describing the propagation of a wave in a plasma and is related to E^*_α (see Paper VI). Clear differences are seen in the simulated peak shape as k_p is varied, in contrast with figure 3.9. The best match with the data is obtained for k_p=45 m^{-1} (which corresponds to $E^*_\alpha = 6$ MeV), although k_p values between 40 m^{-1} and 50 m^{-1} would also describe the data, given the limited statistics. The value k_p=45 m^{-1} is compatible with that independently inferred from the ratio of characteristic emission peaks from the ^{12}C(d, pγ)^{13}C reaction and agrees with observations of other diagnostics (see Paper VI for details). It is noteworthy to observe that, in this measurement, the possibility to infer parameters of the fast ion energy distribution from the Doppler broadened peak shape is limited

only by poor statistics of this particular measurement,*not* by intrinsic limitations of the reaction as for ^{12}C(^{3}He, pγ)^{14}N . In other words, a measurement at increased γ-ray fluxes would allow to determine E^*_α with good accuracy from the Doppler broadening of the E_γ=4.44 MeV peak *only*, in contrast with the ^{12}C(^{3}He, pγ)^{14}N reaction, for which different pieces of information had to be combined. The reason is that the combination of reactant energy distribution, reaction cross section and nuclear structure of the emitting nucleus is favorable for Doppler broadening measurements of the ^{9}Be(α, nγ)^{12}C reaction with acceleration of ^{4}He ions at the third harmonic. These results, combined with those on the ^{12}C(^{3}He, pγ)^{14}N reaction, in general demonstrate that high-resolution γ-ray spectroscopy can be used as a probe of energetic ions in fusion plasmas. However, a careful simulation of the underlying nuclear physics is in general required for determination of the fast ion energy distribution due to the complexity of γ-ray emission nuclear reactions.

3.3 High rate γ-ray spectroscopy and fast ion driven instabilities

This thesis has so far focused on the determination of the fast ion energy distribution from the measured neutron and γ-ray emission spectra. We here address the question of studying wave-particle interaction with γ-ray emission spectroscopy.
The typical frequency of an Alfvén eigenmode is of the order of 100 kHz. In order to study phenomena on this time scale with high temporal resolution, capability to perform measurements of the γ-ray emission spectrum at MHz counting rates is required. γ-ray spectroscopy in the MHz counting rate has never been performed before and dedicated instruments have to be developed. In this thesis, a solution based on a $LaBr_3$ detector is presented. $LaBr_3$ is a new scintillating material [32] delivering a very high light yield and hence energy resolution. It is also fast (see pulse shape in figure 3.14) and it is not significantly damaged by neutrons, in contrast with HpGe, that however features a higher energy resolution.

A conventional analog shaping chain, in which the signal coming from the Photo Multiplier Tube (PMT) is fed into a pre-amplifier followed by an amplifier, is not suitable for γ-ray spectroscopy in the MHz range: the fast scintillation time of the $LaBr_3$ crystal would be dominated by a much longer time due to pulse shaping, that is typically of the order of 1 μs and compares with the inverse of the counting rate at 1 MHz. A

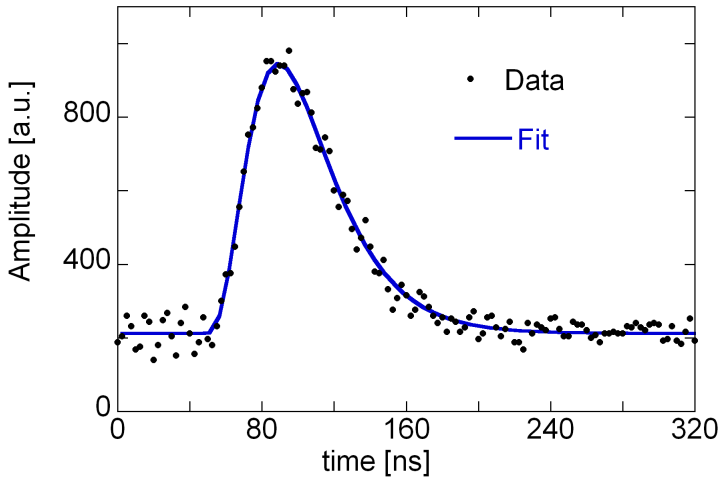

Figure 3.14: Example of $LaBr_3$ digitized pulse from a 1.5 MeV γ-ray. The solid line is the best fit to the data using equation (1) of paper VII

solution based on digitization of the signal at the PMT level (figure 3.15) was instead implemented (Paper VII). A data acquisition system based on the ATCA platform with a sampling rate of 400 MSPS and a nominal 14-bit resolution was used to digitize the PMT signal. The latter is first amplified by a fast, non-shaping pre-amplifier. The acquisition board is operated in the so called "segmented mode". A threshold is set on the signal coming from the detector. When a pulse exceeds the preset threshold, a segment

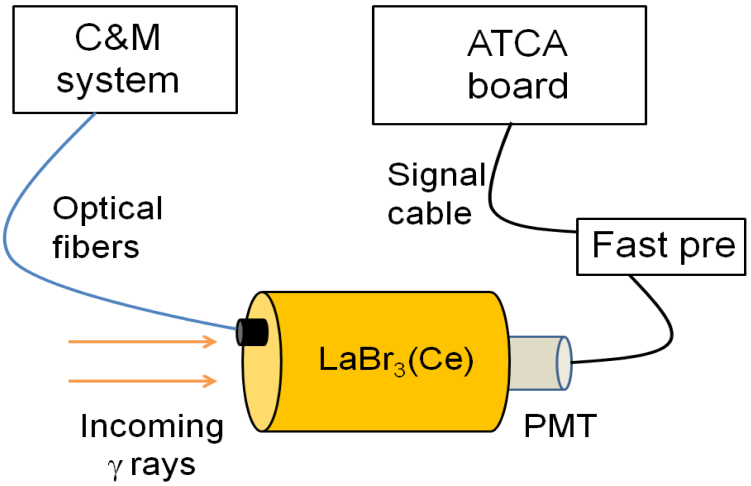

Figure 3.15: Sketch of the acquisition scheme based on digitization for high rate γ-ray spectroscopy with a $LaBr_3$ detector.

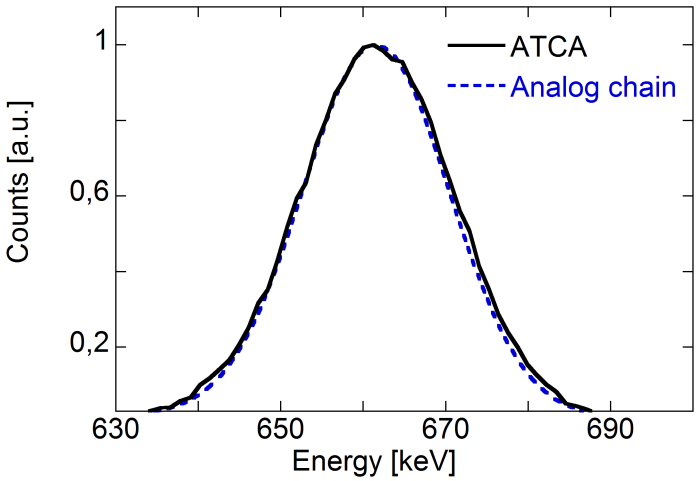

Figure 3.16: Comparison between a reconstructed ^{137}Cs peak at 661.66 keV using the digitized data processed with an algorithm based on pulse fitting (solid line) and the result obtained with an analog spectrometry chain (dashed line). Measurements were performed in low noise laboratory conditions.

is stored. A time stamp is associated to each segment for time resolved analysis of the collected data. A C&M system [33] is also used to monitor changes of the PMT gain. Digitization of the signal can degrade the energy resolution of the system, as the filtering stage provided by a conventional analog shaping chain is not present. Energy resolution was however recovered by a dedicated spectrum reconstruction algorithm, named ORSA and based on pulse fitting, that was applied off-line to the recorded data (see Paper VII for details). An example of a measurement at low counting rate is shown in figure 3.16, where the γ-ray peak at E_γ =662 keV from a laboratory ^{137}Cs source is presented. The figure compares the results of a measurement, in low noise laboratory conditions, performed with a conventional analog shaping chain and with the ATCA platform. Almost no difference is seen in the two cases. This demonstrates that the system, combined with the ORSA algorithm, does not introduce any further degradation of the energy resolution with respect to a conventional analog spectroscopy chain (Paper VII).

High rate capability of the developed γ-ray spectroscopy system was tested in experiments at nuclear accelerators. There are two further challenges that need to be faced to allow for high resolution γ-ray spectroscopy at MHz counting rates. The first one is the stability of the PMT gain, that was however guaranteed up to a few MHz by using an active voltage divider [33]. The second one is pile up. At counting rates in the MHz range more than one pulses can be superimposed and result in a degradation

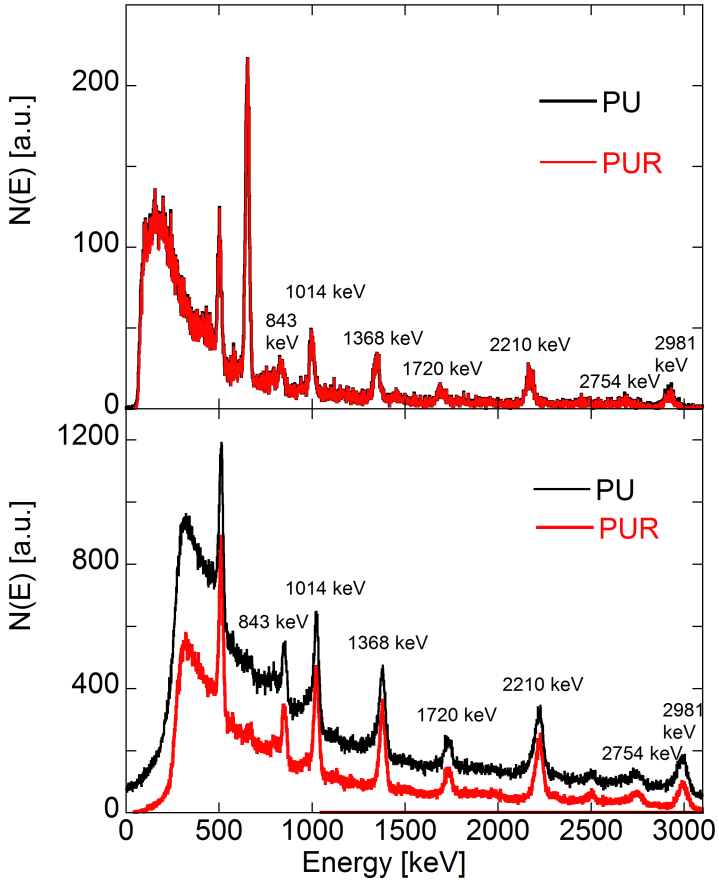

Figure 3.17: γ-ray emission spectrum measured at the "Horia Hulubei" Tandem Van der Graaf accelerator at 80 kHz (top) and 2.6 MHz (bottom) counting rates. The red curve is the spectrum obtained with PUR. The spectrum obtained without PUR is also shown (black line). The E_γ=662 keV peak from a ^{137}Cs calibration source is visible in the measurement at 80 kHz. The sharp peak at E_γ=511 keV originates from background radiation.

of the energy spectrum. For this reason, the ORSA algorithm was equipped with a pile up rejection (PUR) routine (Paper VIII): pulses affected by pile up are discarded and the γ-ray emission spectrum is reconstructed considering only non superimposed pulses. The overall performance of the system was tested in dedicated experiments at the Tandem Van der Graaf accelerator of the Nuclear Institute "Horia Hulubei" in Magurele (RO). A 10 MeV beam of protons was accelerated onto an aluminum target. γ-rays of several energies were emitted and were recorded, at different counting rates, with the $LaBr_3$ based system (Paper VIII). Figure 3.17 compares the γ-ray spectrum recorded at counting rates of 80 kHz and 2.6 MHz. No difference in seen between the

two measurements, but for the fraction of pile up events, which is higher in the 2.6 MHz case as expected. The energy resolution, evaluated at E_γ= 3 MeV, is 2% and is almost unchanged with respect to the value obtained at 80 kHz (1.8%). This demonstrated, for the first time, high resolution, high rate γ-ray spectroscopy with $LaBr_3$ scintillators and provides the instrumental basis for studies of wave-particle interaction with γ-ray spectroscopy in a burning plasma. Further details are presented in paper VIII.

The system developed, based on the $LaBr_3$ detector, was used for γ-ray spectroscopy measurements on the ASDEX Upgrade (AUG) tokamak in Garching (DE). ASDEX Upgrade is a mid-size fusion device. No γ-ray emission spectroscopy measurements had ever been performed on AUG before this thesis project. The reason is that developing a plasma scenario for γ-ray emission spectroscopy is itself a challenge on AUG because of the lower plasma current and magnetic field with respect to JET.

Two plasma scenarios, based on different heating schemes, were designed for γ-ray emission observation on AUG and are discussed in detail in Paper IX. The scenario, that was found to be successful, was based on the acceleration of protons with fundamental radio-frequency heating on hydrogen. Hydrogen is found in AUG deuterium plasmas at typical concentration values of 5% and can be accelerated by RF.

The experiment performed showed clear evidence of MHD activity of the Alfvén type driven by fast protons. Figure 3.18 shows a spectrogram of the signal detected by Mirnov coils (see chapter 1) placed around the tokamak. There are clear frequencies excited from 1 s, i.e. when the RF power is applied to protons. These correspond to excitation of Toroidal Alfvén Eigenmodes (TAEs, see chapter 1) with mode number n between 3 and 6. The frequency evolved in time, until about 2.5 s. The observed TAEs were particularly effective at expelling fast protons. Measurements with fast ion loss detectors (FILD, see chapter 1) revealed a complex loss pattern in phase space. Losses of protons from energy E_p=400 keV up to about 2 MeV were detected (Paper IX).

γ-ray emission from the d(p, γ)^{3}He reaction was detected in this experiment. Figure 3.19(a) shows the measured spectrum. The latter can be divided in two regions. At low energies (say, $E_\gamma < 3$ MeV) there is a significant amount of events, corresponding to a counting rate of about 70 kHz: these correspond to interaction of neutrons with the crystal, as well as background radiation from the plasma. At energies $E_\gamma > 3$ MeV the background radiation is significantly lower and a peak at $E_\gamma \approx 5.5$ MeV due to the d(p, γ)^{3}He reaction emerges. The counting rate detected below the peak is shown in figure 3.19(b) and increases with time, from 1 s to about 2.5 s.

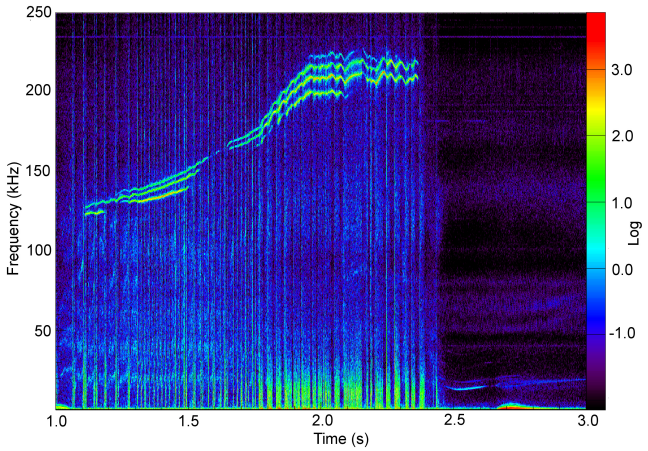

Figure 3.18: Frequency spectrogram from Mirnov coils showing characteristic frequencies of TAEs driven by fast protons on ASDEX Upgrade.

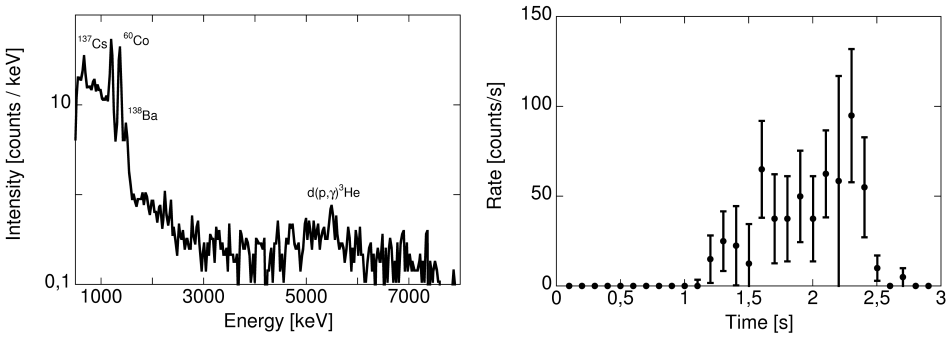

(a) (b)

Figure 3.19: (a) Measured γ-ray emission spectrum on AUG in a experiment with proton acceleration by RF heating. The peak from the d(p, γ)^{3}He reaction is visible at E_γ=5.5 MeV. (b) Counting rate as a function of time measured below the E_γ=5.5 MeV peak, after background subtraction.

The observed increasing counting rate apparently contradicts measurement of lost particles by the FILD. The cross section for the d(p, γ)^{3}He reaction continuously increases as a function of energy up to the MeV range. Thus, the higher the proton energy, the higher is the γ-ray emission level. As protons at energies E_p >400 keV were lost in the discharge, from 1 s, drops in the measured counting rate were correspondingly expected, instead of the increasing rate of figure 3.19(b).

As discussed in Paper IX, the apparent contradiction between γ-ray observations and FILD measurements was solved by considering the differential reactivity for the d(p, γ)^{3}He reaction, i.e. the probability that a proton of given energy emits a γ-ray (see

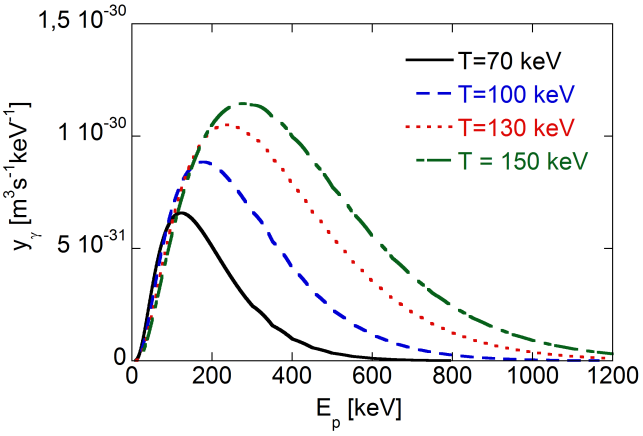

Figure 3.20: Differential reactivity of the d(p, γ)^{3}He reaction for several tail temperatures of the proton energy distribution.

figure 3.20). For temperature values in the range 70-100 keV, measured during the discharge with proton acceleration, γ-ray emission is mostly due to protons with energies $E_p < 400$ keV, i.e. protons that were *not* affected by the TAEs. In other words, the observed increasing counting rate is assessing the *confinement* of protons at $E_p < 400$ keV and is *benchmarking*, not contradicting, the FILD result. Higher temperatures, in the range 130-150 keV at least (figure 3.20), would have been required to observe γ-ray emission from $E_p > 400$ keV protons and thus drops in the counting rate. In paper IX, further details on mode-particle interaction on AUG are derived from the measurements.

Besides the experimental details, the results obtained at AUG provide an example of wave-mode interaction studies using γ-ray spectroscopy with advanced detectors. Although far from providing comprehensive answers to this challenging area of investigation, they restate a fundamental property of fast ion studies with γ-ray spectroscopy: information can be derived from the measured γ-ray emission spectrum, but nuclear physics details of each reaction need to be taken into account. Nuclear physics was here manifested in terms of the d(p, γ)^{3}He differential reactivity, that allowed γ-ray spectroscopy to diagnose protons at $E_p < 400$ keV at the temperatures obtained in the experiments, but not protons at higher energies.

Chapter 4

Conclusions and outlook

End?
No, the journey doesn't end here
– Gandalf the White

A high performance fusion plasma is a harsh environment for diagnostic operation, where severe constraints are met. This is true for a number of measurements that are to be carried out in next generation fusion machines and in particular applies to fast ion diagnostics. The instruments used in present day experiments have so far provided a vast amount of information on the physics of energetic ions, but their use is less promising in future tokamaks, due to intrinsic limitations. On the other hand, the intense neutron and γ-ray emission fluxes produced by high performance plasmas can be used for diagnostic purposes, partially replacing present-day systems. This thesis has contributed to the advancement of neutron and γ-ray emission diagnostics, with focus on fast ion measurements. Neutron emission spectroscopy is an established diagnostic at the JET tokamak: advanced spectrometers have been built and interpretation tools are available and have been used to interpret measurements. The operational domain of neutron spectroscopy has been extended in this thesis by considering the role of nuclear elastic collisions. In particular, in many relevant plasma scenarios, high energy components in the neutron emission spectrum have been shown to carry information on the energy distribution of fast, non-fuel ions. The latter can be fusion products, such as α particles in DT plasmas, or externally heated ions, such as ^{3}He accelerated by radio-frequency in a (^{3}He)D or (^{3}He)DT plasma.
γ-ray emission diagnostics are still in a early stage compared to neutron spectroscopy. In 2008 the first proof-of-principle measurement of Doppler broadening of γ-ray emission

peaks from reactions induced by fast ions was performed with a High Purity Germanium detector at the JET tokamak. In this thesis, a Monte Carlo code, named GENESIS, was developed for the interpretation of γ-ray emission spectra and successfully reproduced the measured data. It was found that information on the fast ion energy distribution is contained in the ratios and shapes of γ-ray emission peaks, but a detailed modeling of the underlying nuclear physics was required to obtain information at a quantitative level, due to the complexity of γ-ray emission reactions. A similar experiment was later carried out at JET, where the γ-ray emission spectrum produced by the interaction of a beam of ^{4}He ions with ^{9}Be impurities was measured and interpreted with the GENESIS code.

On the instrumentation side, an advanced acquisition system based on a $LaBr_3$ scintillator and fast digitization was developed for γ-ray spectroscopy measurements in the MHz range. The system was shown to have no disadvantages in terms of energy resolution when compared to a conventional analog spectroscopy chain. Moreover, for the first time, the system allowed us to demonstrate γ-ray spectroscopy measurements at MHz counting rates at nuclear accelerators, without significant loss of the energy resolution. This result is of relevance for studies of fast ion driven instabilities through γ-ray emission spectroscopy in high performance fusion plasmas, on a time scale close to the alfvénic one. The system was used to perform, for the first time, γ-ray spectroscopy measurements on the ASDEX Upgrade tokamak, where γ-ray emission from the d(p, γ)^{3}He reaction was used to study instabilities driven by protons accelerated by radio-frequency.

As the time distance between present day and next step, high performance fusion devices becomes shorter, a quantitative assessment of fast diagnostic capabilities has to be made. The planned progressive increase of input heating power at the JET tokamak, culminating with a high performance deuterium-tritium plasma, will provide excellent opportunities for testing or further developing the instruments and interpretation models presented in this thesis. The GENESIS code will be the platform to gain unique information on the fast ion energy distribution from the γ-ray emission spectrum. Predictions on high energy components in the neutron spectrum from nuclear elastic scattering will find their test bed. The $LaBr_3$ detector will be the only instrument capable to perform measurements of the γ-ray emission spectrum at the high counting rates expected in the JET deuterium-tritium phase and will be used to study instabilities driven by fusion born α particles or externally heated fast ions. The forthcoming high power JET cam-

paigns are the learning base for fast ion diagnostics on next step fusion devices, such as ITER, where nuclear radiation based methods for plasma diagnostics will have a prominent role. This thesis presents advancements in this field and provides experimental and simulation tools that can be used for future developments.

Chapter 5

Synopsis of attached papers

- **Paper I**

  M. Nocente, G. Gorini , J. Källne and M. Tardocchi,

  Calculated neutron emission spectrum with knock-on effects for RF heated (^{3}He)D plasmas

  Nucl. Fusion **51**, 063011 (2011)

  In this paper the neutron emission from (^{3}He)D plasmas with RF heating is calculated using a model that includes supra-thermal (knock-on) components of the deuteron population. The RF generation of fast ^{3}He ions is described and the knock-on components are determined with the help of newly derived ^{3}He +d scattering cross sections. Results are presented on the neutron emission spectrum and its contributions from different deuteron velocity components. It is shown that knock-on leaves an observable feature in the spectrum with a clear dependence on absorbed RF power. The importance of the nuclear interaction in the elastic cross section is demonstrated. The results represent a step forward in the use of neutron emission spectroscopy to diagnose fusion plasmas with minority supra-thermal components in their fuel ion composition.

- **Paper II**

  M. Nocente, G. Gorini , J. Källne and M. Tardocchi,

  Cross section of the $d + {}^3He \rightarrow \alpha + p$ reaction of relevance for fusion plasma applications

  Nucl. Fusion **50**, 055001 (2010)

  The paper presents the cross section of the d + ^{3}He $\rightarrow \alpha$ + p fusion reaction, that has been determined with regard to its systematic variation with energy (E_{cm})

based on available experimental data. Information is provided on the angular distribution $d\sigma/d\Omega$ at energies up to E_{cm}=8.0 MeV and the total cross section $\sigma(E_{cm})$ for the range E_{cm}=3.0-8.0 MeV. The relevance of the presented results for fusion plasmas heated with RF heating of ^{3}He minority in D and DT plasmas is discussed.

- **Paper III**

  M. Nocente, J. Källne, G. Grosso, M. Tardocchi and G. Gorini

  Nuclear scattering effects and neutron emission spectrum from fusion plasmas, submitted to Nucl. Fusion

  In this paper the effects of nuclear elastic scattering from energetic light ions on the neutron emission spectrum in fusion plasmas are studied. Each elastic scattering process leaves a distinctive signature in the neutron spectrum that is manifested as a high energy component. The relative magnitude of knock on spectral features in D and DT plasmas without and with radio-frequency heating on a ^{3}He minority component is determined through Monte Carlo simulations. The results complete the map on nuclear elastic scattering effects induced by energetic ions in the neutron emission spectrum from D and DT plasmas, besides (^{3}He)D and (^{3}He)DT with radio-frequency heating, and are of relevance for diagnostics of fusion born α particles and fast ^{3}He ions through neutron emission spectroscopy in fusion plasmas.

- **Paper IV**

  I. Proverbio, **M. Nocente**, V. G. Kiptily, M. Tardocchi, G. Gorini,

  The $^{12}C(^3He, p\gamma)^{14}N$ reaction cross section for γ-ray spectroscopy simulation of fusion plasmas

  Rev. Sci. Instrum. **81**, 10D320 (2010)

  The paper presents the cross section of the ^{12}C(^{3}He, pγ)^{14}N reaction of interest for γ-ray spectroscopy observations of fast ^{3}He ions. High resolution γ-ray spectroscopy measurements were performed in JET (^{3}He)D plasmas with high energy ion populations driven by radio-frequency (RF) heating. One of the first reactions investigated was ^{12}C(^{3}He, pγ)^{14}N which was observed at low ^{3}He concentrations. In order to interpret the measurements in this work cross section data for the ^{12}C(^{3}He, pγ)^{14}N reaction are evaluated. Available data for the population of excited states in ^{14}N up to the 8th level are assessed in the range E_{3He}=0-5 MeV.

Discrepancies and gaps in the database have been solved by means of interpolations and consistency analysis. The evaluated cross section data are used to predict the intensity ratio of characteristic 2.31-MeV and 1.63-MeV γ-rays.

- **Paper V**

  M. Tardocchi, **M. Nocente**, I. Proverbio, V. G. Kiptily, P. Blanchard, S. Conroy, M. Fontanesi, G. Grosso, K. Kneupner, E. Lerche, A. Murari, E. Perelli Cippo, A. Pietropaolo, B. Syme, D. Van Eester, and G. Gorini,

  Spectral Broadening of Characteristic γ-Ray Emission Peaks from $^{12}C(^3He, p\gamma)^{14}N$ Reactions in Fusion Plasmas

  Phys. Rev. Lett. **107**, 205002 (2011)

  The paper presents the first observation of spectral broadening of characteristic γ-ray emission peaks from the reaction $^{12}C(^3He, p\gamma)^{14}N$. The measurements were performed in D(^{3}He) plasmas of the JET tokamak with ion cyclotron resonance heating tuned to the fundamental harmonic of ^{3}He. Intensities and detailed spectral shapes of γ-ray emission peaks were successfully reproduced using a physics model combining the kinetics of the reacting ions with a detailed description of the nuclear reaction differential cross sections for populating the L1-L8 ^{14}N excitation levels yielding the observed γ-ray emission. The results provide a paradigm, which leverages knowledge from areas of physics outside traditional plasma physics, for the development of nuclear radiation based methods for understanding and controlling fusion burning plasmas.

- **Paper VI**

  M. Nocente, M. Tardocchi, V.G. Kiptily, P.Blanchard, I. Chugunov, S. Conroy, T. Edlington, A.M. Fernandes, G. Ericsson, M. Gatu Johnson, D. Gin, G. Grosso, C. Hellesen, K. Kneupner, E. Lerche, A. Murari, A. Neto, R.C. Pereira, E. Perelli Cippo, S. Sharapov, A. Shevelev, J. Sousa, D.B. Syme, D. Van Eester, G. Gorini and JET-EFDA contributors,

  High resolution gamma ray spectroscopy measurements of the fast ion energy distribution in JET ^{4}He plasmas

  submitted to Nucl. Fusion

  This paper reports the first observation of γ-ray Doppler broadening from ^{4}He ions in a fusion plasma. High resolution γ-ray measurements were carried out on the Joint European Torus (JET) in an experiment aimed at accelerating ^{4}He particles

in the MeV range by coupling third harmonic radio frequency heating to an injected ^{4}He beam. For the first time, Doppler broadening of γ-ray peaks from the ^{12}C(d, pγ)^{13}C and ^{9}Be(α , nγ)^{12}C reactions was observed and interpreted with dedicated Monte Carlo codes based on the detailed nuclear physics of the processes. Information on the confined ^{4}He and deuteron energy distribution was inferred and confined ^{4}He particles with energies as high as 6 MeV were assessed. A signature of MHD activity in γ-ray traces was also detected. The results have a bearing on diagnostics for fast ions in the MeV range in next step fusion devices.

- **Paper VII**

  M. Nocente, M. Tardocchi, I. Chugunov, R. C. Pereira, T. Edlington, A. M. Fernandes, D. Gin, G. Grosso, V. Kiptily, A. Murari, A. Neto, E. Perelli Cippo, A. Pietropaolo, I. Proverbio, A. Shevelev, J. Sousa, B. Syme, G. Gorini,

  Energy resolution of gamma-ray spectroscopy of JET plasmas with a $LaBr_3$ scintillator detector and digital data acquisition

  Rev. Sci. Instrum. **81**, 10D321 (2010)

  The paper presents a new high efficiency, high resolution, fast γ-ray spectrometer installed at the JET tokamak. The spectrometer is based on a $LaBr_3$(Ce) scintillator coupled to a photo multiplier tube. A digital data acquisition system is used to allow for spectrometry with event rates in excess of 1 MHz expected in future JET DT plasmas. However at the lower rates typical of present day experiments digitization can degrade the energy resolution of the system depending on the algorithms used for extracting pulse height information from the digitized pulses. The paper compares digital and analog spectrometry methods for different experimental conditions. An algorithm based on pulse shape fitting was developed and is here shown to provide an energy resolution equivalent to the traditional analog spectrometry method.

- **Paper VIII**

  M. Nocente, M. Tardocchi, A. Olariu, S. Olariu, I.N. Chugunov, A. Fernandes, D.B. Gin, G. Grosso, V.G. Kiptily, A. Neto, R. C. Pereira, A.E. Shevelev, M. Silva, J. Sousa and G. Gorini,

  High Resolution Gamma Ray Spectroscopy at MHz Counting Rates with $LaBr_3$ Scintillators

  submitted to IEEE Trans. Nucl. Sci.

High resolution γ-ray spectroscopy measurements at MHz counting rates are demonstrated in this paper. The measurements were carried out at nuclear accelerators, combining a $LaBr_3(Ce)$ detector with dedicated hardware and software solutions based on digitization and post-mortem analysis. Spectra were reconstructed at counting rates up to 4 MHz, with little or no degradation of the energy resolution. The reported results represent a step forward towards the final goal of γ-ray spectroscopy measurements on a burning plasma device.

- **Paper IX**

  M. Nocente, M. Garcia-Munoz, G. Gorini, M. Tardocchi, A. Weller, S. Akaslompolo, R. Bilato, V. Bobkov, C. Cazzaniga, B. Geiger, G. Grosso, A. Herrmann, V.G. Kiptily, M. Maraschek, R. McDermott, J.M. Noterdaeme, Y. Podoba, G. Tardini and the ASDEX Upgrade Team,

  Gamma-ray spectroscopy measurements of fast ions on ASDEX Upgrade

  submitted to Nucl. Fusion

  Evidence of γ-ray emission from fast ions in ASDEX Upgrade (AUG) is presented in this paper. The plasma scenarios developed for the experiments involve deuteron or proton acceleration. The observed γ-ray emission level induced by energetic protons is used to determine an effective tail temperature of the proton distribution function that can be compared with Neutral Particle Analyzer measurements. More generally the measured emission rate is used to assess the confinement of protons with energies less than 400 keV in discharges affected by Toroidal Alfvén Eigenmode instabilities. The derived information on confined ions is combined with observations made with the AUG Fast Ion Loss Detector.

Appendix A

Semi-analytical calculations of γ-ray peak shapes

Harry,
I owe you an explanation
– Albus Dumbledore

Semi-analytical calculations of γ-ray emission peaks are performed using simplified assumptions on the fast ion energy distribution. The aim is to elucidate how different features of the observed γ-ray emission peak shape are related to properties of the distribution of energetic ions.

A.1 Notation

We refer to the general reaction

$$\mathrm{A} \ + \ \mathrm{B} \ \rightarrow \mathrm{C}^* \ + \ \mathrm{D}$$

where A is the fast ion and C^* the excited nucleus emitting γ-rays. The B target is assumed at rest. Velocities in the laboratory frame are denoted with the letter $\vec{v}$, while $\vec{w}$ indicates velocities in the c.m. frame. The c.m. frame moves at the $\vec{V}_{c.m.} = \frac{m_A}{m_A+m_B}\vec{v}_A$ velocity. $\vec{u}_\gamma$ is a versor indicating the fixed emission direction of the γ-ray in the laboratory frame. With reference to figure A.1, the following notation is also used

- θ_C is the angle between $\vec{V}_{c.m.}$ and $\vec{w}_C$.
- θ'_C is the angle between $\vec{w}_C$ and $\vec{u}_\gamma$. Note that θ_C and θ'_C are different quantities.

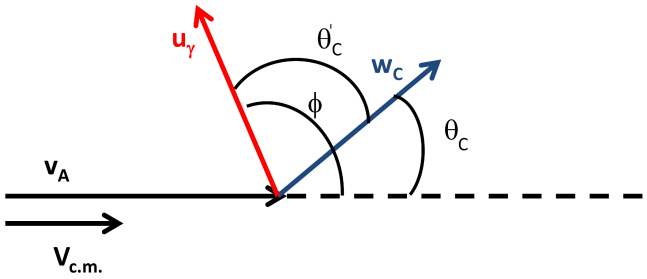

Figure A.1: Sketch of the kinematics for the A + B $\rightarrow$ C* + D reaction

- ϕ is the angle between $\vec{V}_{c.m.}$ and $\vec{u}_\gamma$.

A.2 Peak shape for isotropic cross sections

The γ-ray energy in the laboratory frame is given by

$$E_\gamma = E_{\gamma 0}(1 + \frac{1}{c}\vec{v}_C \cdot \vec{u}_\gamma) \tag{A.1}$$

where $E_{\gamma 0}$ is the energy for $v_C = 0$. In the classical approximation, $\vec{v}_C$ is connected to $\vec{w}_C$ through the Galileo transformation $\vec{v_c} = \vec{w_c} + \vec{V}_{c.m.}$, which gives

$$E_\gamma = E_{\gamma 0}(1 + \frac{w_C}{c}\cos\theta'_C + \frac{V_{c.m.}}{c}\cos\phi) \tag{A.2}$$

In the following we will assume that the cross section for γ-ray production is isotropic in the c.m. frame. Consider a beam-target reaction, where the fast ion vectorial velocity is assigned (i.e. its magnitude, direction and orientation have a fixed value). $\cos\phi$ is constant as $\vec{V}_{c.m.}$ is fully specified and $\vec{u}_\gamma$ is also chosen. As a result of the cross section isotropy, $\cos\theta_C$ is uniformly distributed, and so is $\cos\theta'_C$. The number number of γ-rays per unit energy $dN_\gamma/dE_\gamma \propto dE_\gamma/d\cos\theta'_C \propto$ const. The γ-ray emission spectrum has a rectangular shape, with center at $E_{\gamma 0}(1 + \frac{V_{c.m.}}{c}\cos\phi)$ and width $2E_{\gamma 0}\frac{w_C}{c}$ (independent of $\cos\phi$), as shown in figure A.2.

Let's now assume that the fast ions are mono-energetic, but not a beam. In other words, the magnitude of $\vec{V}_{c.m.}$ is fixed, but $\cos\phi$ can vary uniformly. The resulting spectrum can be thought of as a superposition of the rectangular shape spectra of figure A.2. All spectra have the same width, but the centre, at energy $E_{\gamma 0}(1 + \frac{V_{c.m.}}{c}\cos\phi)$, uniformly shifts as $\cos\phi$ varies in the range -1 to 1. Some rectangles superimpose with each other,

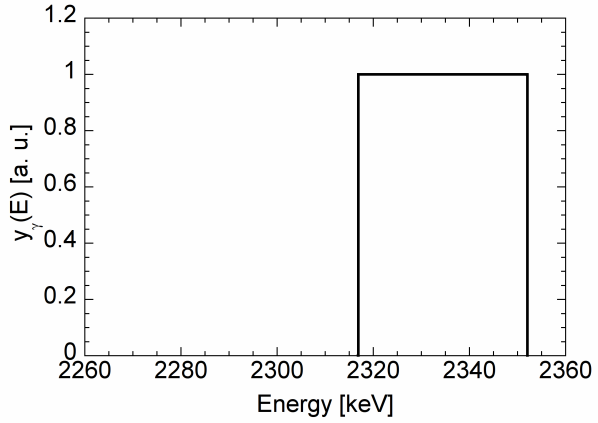

Figure A.2: Shape of the E_γ=2313 keV γ-ray emission peak from the ^{12}C(^{3}He, pγ)^{14}N reaction assuming isotropic cross section. The ^{3}He ions are beam at 4 MeV. ϕ =30°.

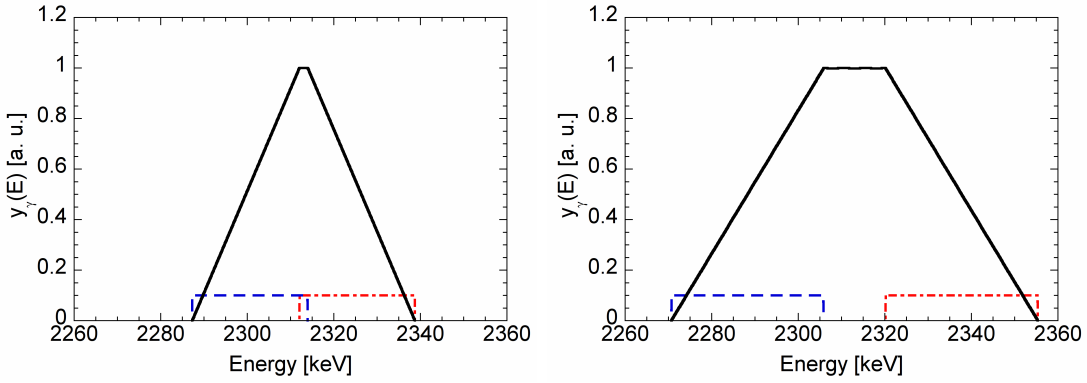

(a) (b)

Figure A.3: Shape of the E_γ=2313 keV γ-ray emission peak from the ^{12}C(^{3}He, pγ)^{14}N reaction assuming isotropic cross section. In the figures, the ^{3}He ions are mono-energetic at 1 MeV (a; $V_{c.m.} < w_C$) and 4 MeV (b; $V_{c.m.} > w_C$) and isotropically distributed. The dashed and dash-dotted lines show the shapes of the leftmost and rightmost rectangles that determine the edges of the minor and major base of the overall γ-ray peak shape (see text for details).

some others do not. The final shape is *exactly* a trapezoid, as shown in figure A.3.

The major base of the trapezoid is determined by the rightmost and leftmost rectangles, i.e. those with centre at $E_{\gamma 0}(1 + \frac{V_{c.m.}}{c})$ and $E_{\gamma 0}(1 - \frac{V_{c.m.}}{c})$. The right and left edges of the major base are given by $E_{\gamma 0}(1 + \frac{V_{c.m.}}{c} + \frac{w_C}{c})$ and $E_{\gamma 0}(1 - \frac{V_{c.m.}}{c} - \frac{w_C}{c})$, respectively. The minor base is the energy region where the majority of rectangles superimpose. The edges of the minor base are given by $E_{\gamma 0}(1 \pm \frac{|V_{c.m.} - w_C|}{c})$. Two situations can occur, depending on the energy of the fast ions. At low reactant energies, $V_{c.m.} < w_C$, as

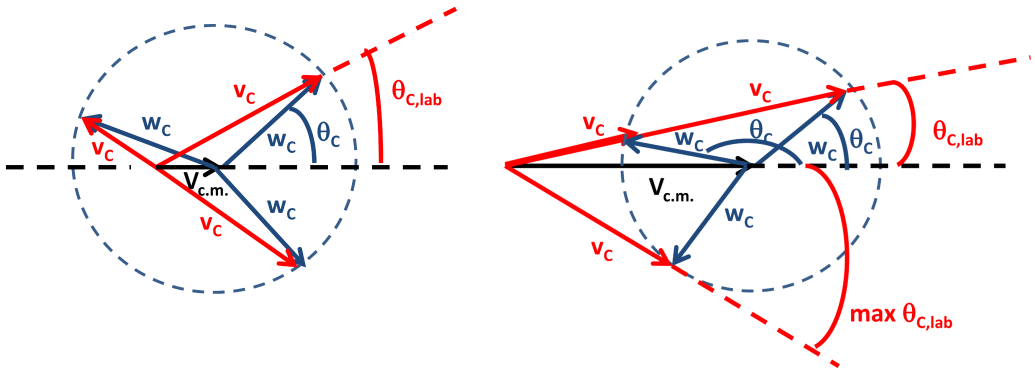

Figure A.4: Graphical representation of the Galilean trasformation $\vec{v}_C = \vec{w}_C + \vec{V}_{c.m.}$ for the cases $V_{c.m.} < w_C$ (a) and $V_{c.m.} > w_C$ (b). $\vec{w}_C$ describes a spherical surface (dashed circle) as the angle θ_C is varied.

$w_C = \sqrt{\frac{2m_D}{m_C(m_C+m_D)}(Q^* + K)}$. $K = \frac{1}{2}\frac{m_B}{m_A}(m_A + m_B)V_{c.m.}^2$ is the relative kinetic energy and $Q^* = Q - E_{\text{state}}$ is the effective Q-value, assumed positive[1], for populating a certain excited state at energy E_{state}. At high reactant energies, the relation $V_{c.m.} > w_C$ can hold instead. As $V_{c.m.}$ moves from low to high values, the minor base in the trapezoid of figure A.3 first shrinks, becoming null when $V_{c.m.} = w_C$, at then broadens again. The major base, instead, always broadens. The regions $V_{c.m.} < w_C$ and $V_{c.m.} > w_C$ have a specific kinematic interpretation. As discussed in [34], the Galilean relation $\vec{v}_C = \vec{w}_C + \vec{V}_{c.m.}$, connecting the velocity of product C in the laboratory and c.m. frame, can be represented as in figure A.4.

If the cross section is isotropic, the tip of $\vec{w}_C$ describes a spherical surface and any angle θ_C is possible. The picture in the laboratory frame is different. The angle between $\vec{v}_C$ and $\vec{V}_{c.m.}$ is $\theta_{C,lab}$. When $V_{c.m.} < w_C$, the excited nucleus C can be emitted at any angle in the laboratory frame $\theta_{C,lab}$ (figure A.4a). When $V_{c.m.} > w_C$, instead, not all angles in the laboratory frame are allowed for the excited nucleus C and a maximum value for $\theta_{C,lab}$ exists (although any angle is allowed in the c.m. frame; figure A.4b); note also that, in this case, there are two c.m. angles θ_C corresponding to the *same* $\theta_{C,lab}$, which corresponds to *two different* energies for the product C for the same emission angle in the laboratory frame (see equation 2.2). The transition between allowed and non-allowed angles in the c.m. frame corresponds to the transition between shrinking and broaden-

[1] In some cases Q^* can also be negative. In those cases, the relation $V_{c.m.} > w_C$ always holds

ing of the minor base in the trapezoidal γ-ray peak shape of figure A.3. Clearly, the higher is the reaction Q value, the higher is the reactant energy that is necessary to enter the kinematic region $V_{c.m.} > w_C$. Besides, for some reactions the condition $V_{c.m.} > w_C$ is never satified. This is the case of the main neutron producing fusion reactions, d + d $\rightarrow$ ^{3}He + n and d + t $\rightarrow$ α + n , whose kinematics always falls in the region $V_{c.m.} < w_C$.

A.3 Peak shape for anisotropic cross sections

In the previous section, the cross section for γ-ray emission was assumed to be isotropic. As discussed in chapter 2, nuclear reaction data show that anisotropy can be significant, instead, and needs to be taken into account. This is done in the following.
Let's consider again the beam-on-target case discussed in the beginning of section A.2. The number of emitted γ-rays per unit energy dN_γ/dE_γ is

$$\frac{dN_\gamma}{dE_\gamma} = \frac{dN_\gamma}{d\cos\theta'_C} \cdot \frac{d\cos\theta'_C}{dE_\gamma} \tag{A.3}$$

The quantity $\frac{d\cos\theta'_C}{dE_\gamma}$ can be evaluated from equation A.2, which gives $\frac{dE_\gamma}{d\cos\theta'_C} = \frac{w_C}{c}E_{\gamma 0}$. We now want to express $\frac{dN_\gamma}{d\cos\theta'_C}$ in terms of $\frac{dN_\gamma}{d\cos\theta_C}$. The reason in that the latter is proportional to the differential cross section $\frac{d\sigma}{d\Omega_C}$ for producing an excited nucleus at an angle θ_C, which is a measured quantity, through

$$\frac{dN_\gamma}{d\cos\theta_C} = \frac{1}{2\pi} n_A n_T v_A \frac{d\sigma}{d\Omega_C}(\cos\theta_C) \tag{A.4}$$

where the product of the beam and target densities, n_A and n_T respectively, appears.
From figure A.5, it can be noted that there are *two different* θ_C angles, named $\theta_{C,1}$ and $\theta_{C,2}$ in the figure, that correspond to the *same* θ'_C value. Therefore

$$\frac{dN_\gamma}{d\cos\theta'_C} = \frac{1}{2}\left(\frac{dN_\gamma}{d\cos\theta_{C,1}} P_\gamma(\cos\theta_{C,1}, \cos\theta'_C) + \frac{dN_\gamma}{d\cos\theta_{C,2}} P_\gamma(\cos\theta_{C,2}, \cos\theta'_C)\right) \tag{A.5}$$

where $P_\gamma(\cos\theta_C, \cos\theta'_C)$ indicates the probability that a γ-ray is emitted along $\vec{u}_\gamma$ by an excited nucleus moving in the θ_C direction. $P_\gamma(\cos\theta_C, \cos\theta'_C) = 1/4\pi$ in the assumption of isotropic γ-ray emission. The factor 1/2 is introduced to avoid double–counting.
From figure A.5 it is seen that $\theta_{C,1} = \phi - \theta'_C$ and $\theta_{C,2} = \phi + \theta'_C$. Therefore, from equations A.4 and A.5

$$\frac{dN_\gamma}{dE_\gamma} = \frac{1}{16\pi^2}\frac{c}{w_C E_{\gamma 0}} n_A n_T v_A \left(\frac{d\sigma}{d\Omega}(\cos(\phi - \theta'_C)) + \frac{d\sigma}{d\Omega}(\cos(\phi + \theta'_C))\right) \tag{A.6}$$

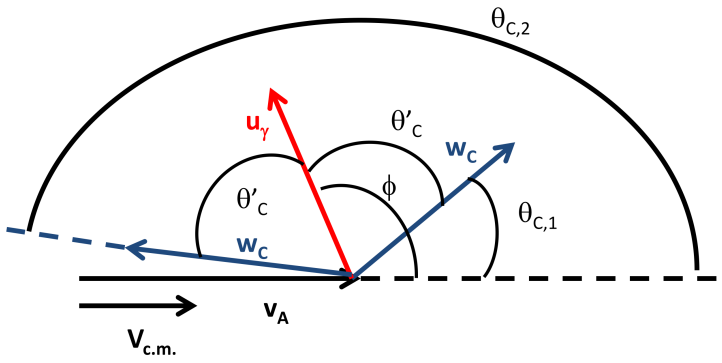

Figure A.5: Sketch of the kinematics for the A + B $\rightarrow$ C* + D reaction showing that two angles, named $\theta_{C,1}$ and $\theta_{C,2}$ in the figure, correspond to the *same* value of the angle θ'_C between $\vec{w}_C$ and $\vec{u}_\gamma$.

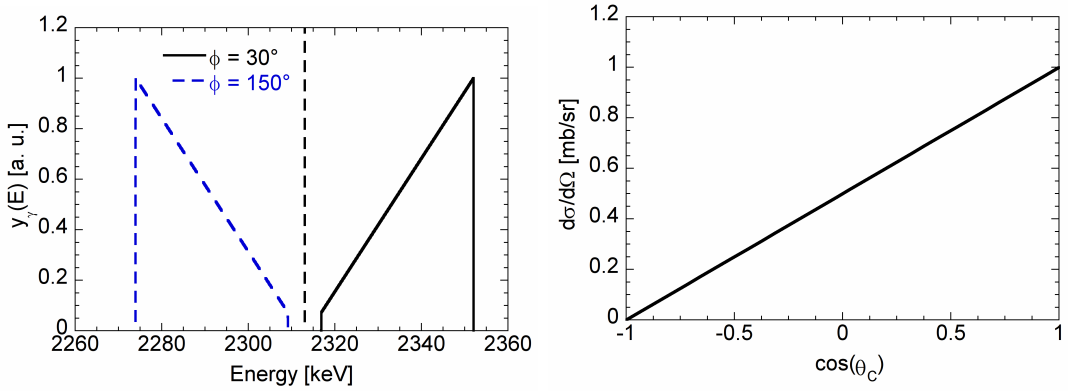

(a) (b)

Figure A.6: (a) Shape of the E_γ=2313 keV γ-ray emission peak from the ^{12}C(^{3}He, pγ)^{14}N reaction assuming the anisotropic cross section shown in figure (b) and calculated with equation A.6. The ^{3}He ions are beam at 4 MeV. γ-rays are observed at ϕ =30°and 150°. The vertical dashed line indicates the energy $E_{\gamma 0}$.

The relation between θ'_C and E_γ is obtained by inversion of equation A.2, i.e. $\theta'_C = \arccos\left(\left(\frac{E}{E_{\gamma 0}} - 1 - \frac{V_{c.m.}}{c}\cos\phi\right)\frac{c}{w_C}\right)$ in the energy region $E_{\gamma 0}\left(1 + \frac{V_{c.m.}}{c}\cos\phi - \frac{w_C}{c}\right) < E_\gamma < E_{\gamma 0}\left(1 + \frac{V_{c.m.}}{c}\cos\phi + \frac{w_C}{c}\right)$. $\frac{dN_\gamma}{dE_\gamma} = 0$ otherwise. ϕ is assigned by the direction where γ-rays are detected.

An example of the peak shape produced by an anisotropic cross section is shown in figure A.6. The rectangular shape that characterizes figure A.2 is now substituted by a triangle that closely mirrors the angular dependence of the cross section. The peak shape produced when ϕ = 30°is symmetric to that obtained for ϕ = 150°with re-

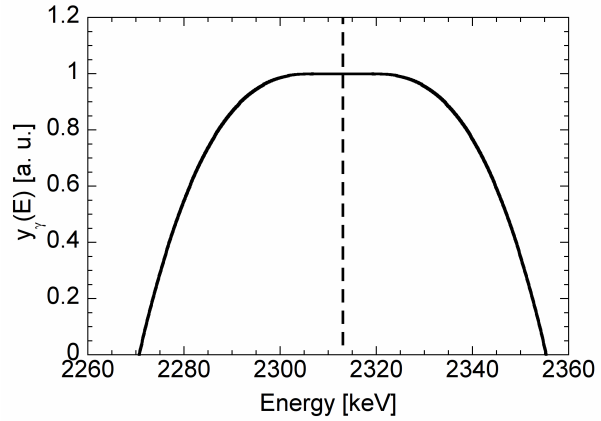

Figure A.7: Shape of the E_γ=2313 keV γ-ray emission peak from the ^{12}C(^{3}He, pγ)^{14}N reaction assuming the anisotropic cross section shown in figure A.6 (b). The ^{3}He ions are isotropically distributed and mono-energetic at 4 MeV. The peak shape is symmetric although the cross section is anisotropic. The vertical dashed line indicates the energy $E_{\gamma 0}$.

spect to a vertical line passing by $E_{\gamma 0}$. The symmetry of the peak shapes obtained for supplementary viewing angles ϕ is a general property and can be demonstrated from equation A.6. Consider the couple of angles (θ'_C, ϕ) and the corresponding energy $E_\gamma = E_{\gamma 0}(1 + \frac{w_C}{c}\cos\theta'_C + \frac{V_{c.m.}}{c}\cos\phi)$ given by equation A.2. Now suppose to change the viewing angle to $\pi - \phi$ and consider the couple $(\pi - \theta'_C, \pi - \phi)$. The energy that corresponds to this couple is $E'_\gamma = E_{\gamma 0}(1 - \frac{w_C}{c}\cos\theta'_C - \frac{V_{c.m.}}{c}\cos\phi)$, which is symmetric to E_γ with respect to a vertical line passing by $E_{\gamma 0}$. The invariance of dN_γ/dE_γ for E_γ and E'_γ follows from the fact that $\cos((\pi - \phi) - (\pi - \theta'_C)) = \cos(\phi - \theta'_C)$ and $\cos((\pi - \phi) + (\pi - \theta'_C)) = \cos(\phi + \theta'_C)$, which makes equation A.6 unchanged when evaluated using (θ'_C, ϕ) or $(\pi - \theta'_C, \pi - \phi)$.

The peak shape produced by a mono-energetic distribution at $E = 4$ MeV is shown in figure A.7. The peak shape is symmetric, although the cross section is anisotropic. Symmetry of the peak shape for isotropic, mono-energetic reactants follows from symmetry of peak shapes produced in the beam-target case at supplementary viewing angles. The reason is that, as stated in section A.2, the γ-ray peak shape produced by mono-energetic ions can be thought of as the superposition of the peak shapes at each viewing angle ϕ. The latter are symmetric with respect to $E_{\gamma 0}$ for each couple of viewing angles $(\phi, \pi - \phi)$.

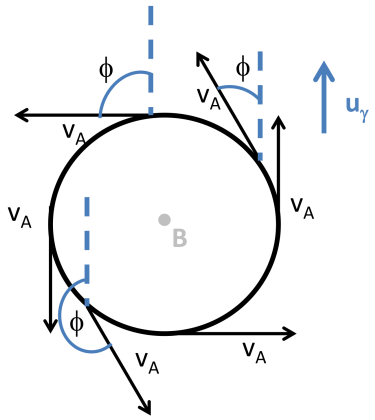

Figure A.8: Gyromotion of a fast ion around the magnetic field $\vec{B}$. γ-rays are emitted perpendicularly to the magnetic field, along $\vec{u}_\gamma$. The angle ϕ between the fast ion velocity $\vec{v}_A$ and $\vec{u}_\gamma$ is uniformly distributed between 0 and 2π.

A.4 Double hump and orbit effects

So far it was assumed that fast ions were mono-energetic and isotropically distributed. An important practical situation in which the energy distribution of fast ions is *not* isotropic is obtained when radio-frequency heating is applied. In this case, the energy of the incoming wave is mainly transferred to the fast ion perpendicular motion. To zeroth-order, the velocity of fast ions is fully perpendicular, with no component along the magnetic field. In other words, fast ions gyrate perpendicularly to the magnetic field, but do not move along the field lines, as in figure A.8. The angle ϕ between the fast ion velocity $\vec{v}_A$ and the γ-ray emission direction $\vec{u}_\gamma$ is uniformly distributed between 0 and 2π. Assuming that the cross section is isotropic, the resulting γ-ray peak shape can still be obtained by superposition of the rectangular shapes discussed in section A.2[2]. In this case, however, as ϕ is isotropic, $\mu = \cos\phi$ is not. Denoting with the letters Φ and M the probability distributions of ϕ and μ respectively, the following relation holds

$$M(\mu) = \Phi(\phi)\left|\frac{d\phi}{d\mu}\right| = \frac{1}{2\pi}\frac{1}{\sqrt{1-\mu^2}} \tag{A.7}$$

Therefore, each rectangular shape with center at $E_{\gamma 0}(1 + \frac{V_{c.m.}}{c}\mu)$ has a weight $M(\mu)$ in the superposition. The resulting peak shape is shown in figure A.9. The ^{3}He ion is rotating counterclockwise around the magnetic field line. A double hump shape, that

[2]If the cross section is anisotropic, the resulting peak shape can be obtained by superposition of the (non rectangular) peak shapes evaluated with equation A.6 for each value of ϕ in the range $[0, 2\pi]$.

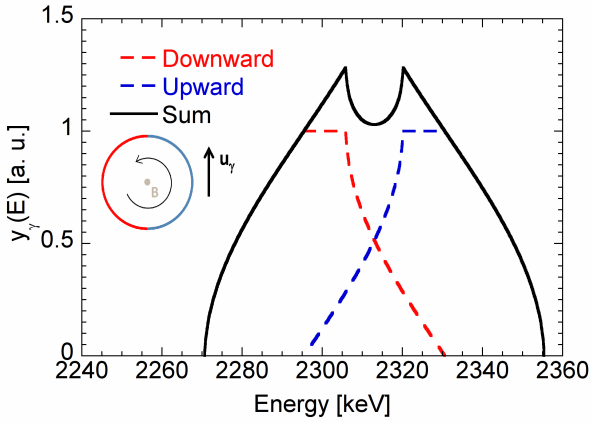

Figure A.9: Shape of the E_γ=2313 keV γ-ray emission peak from the ^{12}C(^{3}He, pγ)^{14}N reaction assuming isotropic cross section. In the figure, the ^{3}He ion velocity is fully perpendicular and ions are gyrating counterclockwise around the magnetic field line as in figure A.8. The separate contribution to the peak shape from the upward and downward ion gyromotion is shown by the blu and red dashed lines.

reflects the anisotropy of the energy distribution and is similarly found also in neutron spectra from fusion plasmas [16], appears, instead of a trapezoid.

The double hump is separated into contributions arising from the upward gyromotion, i.e. when the ion is moving towards the γ-ray emission direction $\vec{u}_\gamma$, and downward, which are reflected by events falling mostly in the energy region $E_\gamma > E_{\gamma 0}$ (upward motion) and $E_\gamma < E_{\gamma 0}$ (downward motion). The two contributions were technically obtained by superimposing the rectangular peak shapes at center $E_{\gamma 0}(1 + \frac{V_{c.m.}}{c}\mu)$, with weight $M(\mu)$ and letting μ vary in the ranges $[0, 1]$ (upward motion) and $[-1, 0]$ downward motion. A curious feature of figure A.9 is that the sharp division of the ion gyromotion into upward and downward does not correspond to a sharp division in the γ-ray peak shape. In other words, the ion upward motion produces some events also in the region $E_\gamma < E_{\gamma 0}$; similarly, the ion downward motion is responsible for some counts in the region $E_\gamma > E_{\gamma 0}$. This is of interest in real applications when, due to an unfavorable line of sight of the spectrometer, only part of the ion gyromotion is seen. For example, when only the upward gyromotion is seen, few events are expected in the region $E_\gamma < E_{\gamma 0}$ and the peak shape presents a strong asymmetry, as experimentally observed in the measurements reported in Paper VI.

Acknowledgements

You're among friends now, Hank.
You can show off
– Charles Xavier

As I was writing down on a piece of paper the names of the people I wanted to include in the acknowledgements, I soon realized I had listed a quite numerous international crew of scientists. In these three years I had the opportunity to visit scientific institutions in several European countries and to attend conferences even on the other side of the Ocean (actually, the 2010 High Temperature Plasma Diagnostics Conference was my first trip ever to the United States). I have met a number of people I interacted with and I should say "thank you" to. I hope I won't forget anyone.

Giuseppe certainly deserves a special place in the list. He has been like a patron to me. He has supported my work as a PhD student and given me the opportunity (plus the money) to carry out experiments at several laboratories in Europe. Marco has been an irreplaceable help whenever there was some experimental activity to do and an inexhaustible source of good mood in so many circumstances. I certainly must acknowledge most of the people at Istituto di Fisica del Plasma "Piero Caldirola". In particular, Carlo, who has recently started his experience as a PhD student and has been my mate during the period I spent in Germany, and Gabriele, who has joined the "Fellowship of the neutrons and gammas" (quote) only recently but is already an important part of it.

The Department of Physics at Milano-Bicocca University has been my main habitat in this experience and my stay has certainly been made much more enjoyable by the inhabitants of the remote lands at the other end of the corridor: Marica, Roberta and Enrico. Zhongjing has been a very quiet office mate during my last months as a PhD student, which has been perfect to write this thesis. Besides, he has significantly broadened my knowledge on China that, so far, was essentially based on the Disney

movie “Mulan”. Jan deserves a special thank. He has been visiting Milan many times in these three years. His help and long experience on neutron spectroscopy were certainly precious for me and his volcanic attitude was a curious and appreciated variant of human behavior. Writing papers together was an essential part of my training.
At JET I have worked with many persons. I certainly must acknowledge all the members of the Neutron Spectroscopy group including Vasili, Brian, Sean and Luca. In particular Luca, who has been the Italian soldier at front and always so nice and helpful to anyone arriving at JET from Milan, and Sean, the MCNP guru with an irresistible British sense of humor. (Saints) Andre', Ana and Rita from Portugal were able to make miracles each time the γ-ray data acquisition systems decided not to work. Carl, Maria, Goran and all the other members of the Uppsala team had always some new exciting features to show me about TOFOR data and made good company in many lunches and dinners. Alexander, Dmitry and Igor welcomed me in the their laboratory in St. Petersburg and were a valuable help with photo-multipliers at JET. Silviu and Agata let us test our γ-ray spectroscopy system in Romania, besides fascinating me with their extraordinarily positive view of life.
Our campaign at ASDEX Upgrade would not have been possible without the help and patience of Arthur and the courtesy of Giovanni in finding a suitable location for our γ-ray spectrometer. Manolo has shed light on the mysterious world of fast ion driven instabilities. Each time I manage to learn some more on this topic, I soon realize there is a huge piece of the puzzle I am missing. Manolo, I hope you will lend me some more pieces of your Phial of Galadriel (second quote) in the future. Fernando has been an example for his incredible commitment in getting CTS work and a funny companion in many occasions with his cheerful mood. To all the young PhD students I met at ASDEX, I wish their work will be even better than mine.
E da ultimo, ma non per ultimi, vanno i ringraziamenti alle persone che mi sono state più vicine in questi anni. Alla mia famiglia devo tutto il sostegno e affetto ricevuti fino ad oggi, la possibilità di essere arrivato fino a questo traguardo e la sopportazione per avermi avuto a casa tutti questi anni (e spero ancora per qualche altro). Ai miei amici ringrazio di esserci sempre stati, da quando, bambini prima e ragazzini poi, andavamo ancora a scuola insieme, fino ad oggi e, spero, per molti anni ancora.

Bibliography

[1] Wesson J., "Tokamaks", 3rd edition, Clarendon Press (2004)

[2] `http://www.ipp.mpg.de/ippcms/eng/pr/exptypen/tokamak/index.html`

[3] T.H. Stix, "Waves in plasmas", Springer ed. (1992)

[4] D.G Swanson, "Plasma waves", Academic Press (2003)

[5] Gekelman W. et al., Plasma Phys. Controlled Fusion **39** (1997) 101

[6] Heidbrink W.W., Phys. Plasmas **15** (2008) 055501

[7] White R. B., "The theory of toroidally confined plasmas", Imperial College Press (2006)

[8] White R. B., Phys. Fluids **26** (1983) 2958

[9] Wong K.L., Plasma Phys. Controlled Fusion **41** (1999) R1

[10] I.H. Hutchinson, "Principles of plasma diagnostics", Cambridge University Press (2002)

[11] Tobias B.J. et al., Phys. Rev. Letters **106** (2011) 075003

[12] Garcia-Munoz M. et al., Rev. Sci. Instrum. **80** (2009) 053503

[13] Heidbrink W.W., Rev. Sci. Instrum. **81** (2010) 10D727

[14] Bindslev H. et al., Phys. Rev. Lett. **97** (2006) 205005

[15] Wolle B., Physics Reports **312** (1999) 1

[16] M. Tardocchi, "Neutron emission spectroscopy studies of fusion plasmas of deuterium-tritium in tokamaks", Ph.D. Thesis, Uppsala University (2000)

[17] L. Ballabio, "Calculation and Measurements of the Neutron Emission Spectrum due to Thermonuclear and Higher-Order Reactions in Tokamak Plasmas", Ph.D. Thesis, Uppsala University, (2003)

[18] Jarvis N.O., Fusion Eng. Design **34** (1997) 57

[19] Cecconello M. et al., Rev. Sci. Instrum. **81** (2010) 10D315

[20] Kiptily V.G. et al., Plasma Phys. Control. Fusion **48** (2006) R59

[21] Kiptily V.G. et al., Fusion Technology **22** (1992) 454

[22] Lehner G., Pohl F., Zeitschrift für Physik **207** (1967) 83

[23] C. Hellesen, "Diagnosing fuel ions in fusion plasmas using Neutron Emission Spectroscopy", Ph.D. Thesis, Uppsala University (2010)

[24] M. Gatu Johnson, "Fusion plasma observations at JET with the TOFOR neutron spectrometer", Ph.D. Thesis, Uppsala University (2010)

[25] Kuan H. et al., Nucl. Physics **51** (1964) 481

[26] Kiptily V G, Matukov A V, Mishin A S, Najdenov V O, Polunovskij I A, Rassadin L A and Chugunov I N, Izv. Rossiiskoi Akademii Nauk, Ser.Fiz. **56** (1992) 125

[27] Van Der Zwan L and Geiger K W Nucl. Phys. A **152** (1970) 481

[28] Lin C. et al., J. Phys. **19** (1981) 99

[29] Cecil F.E. et al., Nucl. Instrum. Meth. **221** (1984) 449

[30] Ognissanto F. et al., Nucl. Instrum. Meth. B **269** (2011) 786

[31] Källne J. et al., Phys. Rev. Letters **85** (2000) 1246

[32] Van Loef E.V.D. et al., Nucl. Instrum. Methods Phys. Res. A **486** (2002), 254

[33] M. Tardocchi et al., Rev. Sci. Instrum. **79** (2008) 10E524

[34] L.D. Landau, E.M. Lifshitz, *Mechanics*, vol. 1, 3rd edition

Paper I

Nucl. Fusion **51** (2011) 063011 (8pp) doi:10.1088/0029-5515/51/6/063011

Calculated neutron emission spectrum with knock-on effects for RF heated (^{3}He)D plasmas

M. Nocente[1,2], G. Gorini[1,2], J. Källne[1,3] and M. Tardocchi[2]

[1] Università degli Studi di Milano - Bicocca, Dipartimento di Fisica 'G. Occhialini', Piazza della Scienza 3, 20126, Milan, Italy
[2] Istituto di Fisica del Plasma 'Piero Caldirola', Associazione EURATOM-ENEA-CNR, via Cozzi 53, 20125, Milan, Italy
[3] Department of Engineering Sciences, Uppsala University, EURATOM-VR Association, 75121 Uppsala, Sweden

E-mail: massimo.nocente@mib.infn.it

Received 22 October 2010, accepted for publication 30 March 2011
Published 10 May 2011
Online at stacks.iop.org/NF/51/063011

Abstract
The neutron emission from (^{3}He)D plasmas with RF heating is calculated using a model that includes supra-thermal (knock-on) components of the deuteron population. The RF generation of fast ^{3}He ions is described and the knock-on components were determined with the help of newly derived ^{3}He + d scattering cross sections. Results are presented on the neutron emission spectrum and its contributions from different deuteron velocity components. It is shown that knock-on leaves an observable feature in the spectrum with a clear dependence on absorbed RF power. The importance of the nuclear interaction in the elastic cross section is demonstrated. The results represent a step forward in the use of neutron emission spectroscopy to diagnose fusion plasmas with minority supra-thermal components in their fuel ion composition.

(Some figures in this article are in colour only in the electronic version)

1. Introduction

Deuterium (D) plasmas emit neutrons through the reaction $d + d \rightarrow \tau + n$ where the neutron spectrum reflects the velocity distribution of the deuteron population; here τ is used to denote ^{3}He ions (helions) in analogy to d for deuterons. The deuteron population (d) is divided into bulk thermal (d′) and supra-thermal (d″) components with the fusion reaction combinations d′ + d′ and d″ + d′ in addition to d″ + d″. The d″ + d′ neutron emission can be significant for D plasmas with a small ^{3}He minority, denoted (^{3}He)D, and radio frequency (RF) heating; the ^{3}He concentration is at the level of $c_\tau = n_\tau/n_e \approx 1\%$. The RF frequency is tuned to the frequency of the ^{3}He ion cyclotron resonance whose plasma heating (ICRH) generates a supra-thermal minority component (τ'') which can affect the fusion reactions in two ways. One is that the τ'' population causes knock-on collisions with significant energy transfer which can give rise to a supra-thermal component in the majority population (d″). Second, the τ'' energy can be much above the thermal level (typically, 1–10 keV), so that the fusion $\tau + d \rightarrow \alpha + p$ cross section [1] becomes significant compared with $d + d \rightarrow \tau + n$ despite the concentration disadvantage. In this case, the α and p fusion products (with energies of 3.7 and 14.6 MeV) could also affect the supra-thermal d″ population through knock-on scattering. In this study, we consider only effects of the first type, i.e. knock-on by the τ'' population directly generated by RF. The purpose is to highlight the principles of the knock-on mechanism as controlled by the RF and its manifestation in the spectrum of the neutron emission $d + d \rightarrow \tau + n$ that can be measured; a later paper will include the higher orders involving the $\tau'' + d$ fusion reaction.

The interest in the investigation of knock-on effects is motivated by the ongoing effort to understand the physics of fast ions and their role in magnetic confinement fusion [2]. In the broad context, fast ions have been considered as drivers of MHD instabilities and as playing a role in the overall plasma equilibrium modelled through transport [3]. At the basis of understanding fast ion behaviour is the energy distribution such as affected by RF heating in (^{3}He)D plasmas or by α particles in DT plasmas. There are few diagnostic techniques for these studies. Alpha particle knock-on in DT plasmas has earlier been discussed in connection with experiments on neutral particles (NPA) [4, 5] and neutron emission spectra [6].

Experiments of the former type (NPA) have recently been reported [7] for RF heated (^{3}He)D plasmas. This study aims at making further progress on the diagnostic of neutron emission spectroscopy (NES).

The focus of this paper on RF heated (^{3}He)D plasmas derives from experiments conducted at JET [8], partly as a pre-study of a heating scheme of potential interest in next step fusion machines such as ITER. A second motivation for this study is the fact that (^{3}He)D plasmas can be observed with new neutron spectrometers, such as TOFOR [9, 10]. The experimental progress on NES diagnosis requires matching development in the modelling of the dd neutron emission including the effects of fast helion knock-on scattering controlled by the injected RF power. The study concerns the NES modelling calculation for (^{3}He)D plasmas with special reference to the conditions encountered at the JET tokamak.

In this work, the knock-on generated supra-thermal deuteron distribution in (^{3}He)D was calculated along the principles of the model of [11]. However, the d″ distribution generated by the τ'' distribution was determined numerically through Monte Carlo calculations rather than analytically. The τ'' + d knock-on source term was calculated using suitably parametrized cross sections for elastic τ + d scattering which have recently become available [12]. This term was, in turn, fed into the Fokker–Plank equation representing the steady state d″ slowing-down distribution. Special attention was paid to the matching of the thermal (d′) and supra-thermal (d″) distributions to each other so as to obtain the full description of the deuteron population (d). In this way it was possible to calculate the neutron emission spectrum due to d+d reactions based on a synthesized (full) deuteron velocity distribution and make comparison with a composite spectrum with separate contributions from d′+d′ and d″+d′. The neutron production was calculated with the model described in [13] which was upgraded and modified, for instance, so as to use the numerically calculated deuteron energy distributions.

This paper presents results on the neutron emission spectrum with knock-on effects for (^{3}He)D plasmas with RF. The diagnostic information embedded in neutron emission spectra is illustrated and the implications for plasma studies are discussed. In particular, it is shown that the temperature of the τ ions as well as the RF power density can be determined from the neutron spectrum. JET plasmas are used as a base for the studies and the results have also a bearing on RF heating in other tokamaks including the next generation ones.

2. Theoretical background and plasma conditions

The fast ^{3}He ions generated with the RF power can suffer knock-on collisions τ'' + d with large energy transfer resulting in the build-up of supra-thermal distribution of deuterons, $F_{d''}$. The knock-on source term $S_{d''}$, for the supra-thermal deuteron population (velocity distribution $F_{d''}$), is determined by the distribution $F_{\tau''}$ together with the τ'' + d $\rightarrow$ τ'' + d″ scattering cross section dσ/dΩ.

The speed distribution $F_{\tau''}(v)$ was calculated from the Stix formula for the effects of RF power deposition in the case of fundamental harmonic heating [14]

$$F_{\tau''}(v) = N \exp\left(-\frac{E}{T_\tau(E)}\right), \quad (1)$$

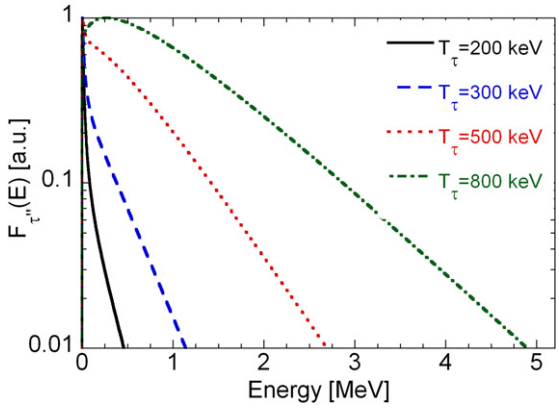

Figure 1. Calculated fast helion energy distribution $F_{\tau''}(E)$ in arbitrary units for several values of asymptotic tail temperature T_τ in a (^{3}He)D plasma of reference conditions (see text).

where $E = \frac{1}{2}mv^2$ and T_τ is referred to as the tail temperature. The latter is a function of energy through

$$T_\tau(E) = T_e\left(1 + \tfrac{3}{2}\xi\right)/g(\xi, E), \quad (2)$$

where ξ is a plasma dependent parameter and $g(\xi,E)$ an analytical function. The ξ parameter is inversely proportional to the density of the heated species (here $n_\tau = c_\tau \cdot n_e$) and the electron density n_e, and proportional to the absorbed RF power density (P_{RF}) and to the square root of the electron temperature ($\sqrt{T_e}$). In the supra-thermal region, $E \gg E_{th}$, one obtains $g(\xi, E) \rightarrow 1$ so that the tail temperature has the asymptotic value $T_\tau = T_e(1 + 3\xi/2)$. The results on the calculated energy distribution function for τ'' are shown in figure 1 for ξ values in the interval $\xi = 27$ to 106; correspondingly, the asymptotic tail temperatures range is $T_\tau = 200$ keV to 800 keV for 5 keV JET plasmas.

For a situation of known plasma conditions but for the RF related parameters P_{RF}, T_τ and n_τ, one can note the linear relationship between ξ and tail temperature, $\xi = \frac{2}{3}(T_\tau/T_e - 1) \approx \frac{2}{3}T_\tau/T_e$ while the power density would be proportional to the product $T_\tau \cdot n_\tau$. Experimentally, P_{RF} and T_τ can be related to observables of the amplitude of the d″ + d′ reaction component in the neutron emission spectrum and the shape of high-energy tail that we shall discuss later.

The pitch angle dependence in $F_{\tau''}(v)$ is not predicted but was assumed to be peaked in the direction perpendicular to the magnetic axis with a certain Gaussian spread Δ. The RF generated τ'' distribution in velocity and angle is thus determined through [14]

$$F_{\tau''}(v, \theta) = \exp\left(-\frac{E}{T_\tau(E)}\right)\exp\left(-\left(\frac{\theta - \pi/2}{\Delta}\right)^2\right). \quad (3)$$

A value of $\Delta = 4.25°$ was used in the calculations corresponding to FWHM $= 2.355\Delta = 10°$. This choice is based on previous work on the interpretation of neutron spectra from RF heated (D)T plasmas [15]. The adopted pitch angle spread is also close to that used in [7] for the analytical approximation of the τ energy distribution.

The angular distribution of cross section for τ+d scattering is available for the range $\theta_{c.m.} = 0$–180° for c.m. energies

of $E_{\mathrm{c.m.}} = 0.03$–$7\,\mathrm{MeV}$ [12]. These are mainly based on a parametrization of experimental data in addition to the angular dependence of pure Coulomb scattering ($\sin^{-4}(\theta_S/2)$) for the lowest energies which was also used for extrapolation into the region $\theta < 40^\circ$. The present knock-on calculations thus include the nuclear interaction in the scattering as compared with using the Coulomb approximation which is discussed in section 4.

Given the $\tau'' + \mathrm{d}$ scattering cross section $\mathrm{d}\sigma/\mathrm{d}\Omega(E,\theta)$ and the distribution $F_{\tau''}(v,\theta)$ of equation (3), the source term $S_{\mathrm{d}''}(v,\theta)$ was calculated using a Monte Carlo technique as described below. With $S_{\mathrm{d}''}(v,\theta)$, the stationary slowing-down velocity distribution of knock-on deuterons is obtained by direct integration of the Fokker–Planck equation [16, 17]

$$F_{\mathrm{d}''}(v,\theta) = \frac{\tau_s}{v^3 + v_c^3}\int_0^{+\infty} v^2 S_{\mathrm{d}''}(v,\theta)\,\mathrm{d}v. \qquad (4)$$

Here τ_s is the Spitzer slowing down time, v is the deuteron velocity and v_c its critical value [18]; only slowing down by energy drag is considered while pitch angle scattering is neglected.

Monte Carlo calculations were used to determine both the knock-on source term appearing in equation (4) and the neutron production reaction. The same non-relativistic two-body kinematics, i.e. $\mathrm{A} + \mathrm{B} \rightarrow \mathrm{C} + \mathrm{D}$, applies. From the input of the motional state of the incident ions, in terms of the relative velocity v_{rel} and the c.m. velocity $V_{\mathrm{c.m.}}$, the exit particle energy E_{D} in the laboratory frame can be determined for a given angle θ_{V} (between the c.m. velocity of D, w_{D} and $V_{\mathrm{c.m.}}$) [19]

$$E_{\mathrm{D}} = \frac{m_{\mathrm{C}}}{m_{\mathrm{D}} + m_{\mathrm{C}}}(Q + K) + V_{\mathrm{c.m}} \cdot \cos\theta_V \times \left[\frac{2m_{\mathrm{D}}m_{\mathrm{C}}}{m_{\mathrm{D}} + m_{\mathrm{C}}}(Q + K)\right]^{1/2} + \frac{1}{2}m_{\mathrm{D}}V_{\mathrm{c.m.}}^2; \qquad (5)$$

here, $K = \frac{1}{2}\mu v_{\mathrm{rel}}^2$ is the total incident kinetic energy and μ is the reduced mass. The Q-value specifies the process as elastic scattering ($Q = 0$) and neutron production by fusion ($Q = 3.27\,\mathrm{MeV}$). The energy distribution of particle D was obtained by sampling the energies of the incident particles. Particle D is a deuteron in the elastic scattering process and a neutron in the d+d fusion reaction.

In the case of scattering, the A and B particle distributions were $F_{\mathrm{d}'}(v,\theta)$ and $F_{\tau''}(v,\theta)$ which gave the supra-thermal deuteron velocity distribution, $F_{\mathrm{d}''}(v,\theta)$. The deuteron population is described by $F_{\mathrm{d}}(v,\theta)$ which is obtained by matching $F_{\mathrm{d}''}(v,\theta)$ to that of the thermal (Maxwellian) bulk of the population (d'). This is done by joining the calculated $F_{\mathrm{d}''}(v,\theta)$ at each pitch angle to a Maxwellian distribution that describes deuterons at low energies as defined by the ion temperature $T_{\mathrm{i}} = T$. In this way one arrives at $F_{\mathrm{d}}(v,\theta)$ which gives a complete description of the deuteron population under the influence of knock-on effects [11]. The neutron spectrum of the fusion reaction $\mathrm{d} + \mathrm{d} \rightarrow \tau + \mathrm{n}$ was calculated with the particle distribution $F_{\mathrm{d}}(v,\theta)$. This can be compared with the description of the spectrum as a superposition of the components $\mathrm{d}' + \mathrm{d}'$ and $\mathrm{d}' + \mathrm{d}''$, in addition to $\mathrm{d}'' + \mathrm{d}''$ which is negligible here [13]. A comparison of the two approaches is presented in section 4.

The code used for neutron production calculations was a modified version of that described in [20]. The $\mathrm{d} + \mathrm{d} \rightarrow \tau + \mathrm{n}$ neutron spectrum was thus calculated for a plasma assumed to be homogeneous with the following parameters: temperatures $T_{\mathrm{e}} = T_{\mathrm{i}} = 5\,\mathrm{keV}$, electron density $n_{\mathrm{e}} = 3 \times 10^{19}\,\mathrm{m}^{-3}$ with a standard helion concentration of $c_\tau = 1\%$, i.e. $n_\tau = 3 \times 10^{17}\,\mathrm{m}^{-3}$. The bulk plasma species were assumed to have a Maxwellian velocity distribution specified by T and n. The supra-thermal deuteron population (d'') was calculated as described above and controlled by the RF power injection as gauged by the asymptotic tail temperature (T_τ). Plasmas of the above parameter values combined with the RF effect parameter value $T_\tau = 500\,\mathrm{keV}$ constitute what is referred to as the reference case conditions. The RF power, as manifested by T_τ, was then varied to see the effect on the supra-thermal component of the τ population as observed in the neutron emission. The neutrons are assumed to be observed perpendicular to the magnetic axis of the tokamak. This maximizes the energy given to neutrons as a result of the Doppler effect for fast ions in orbits with a pitch angle of $\theta = 90^\circ$.

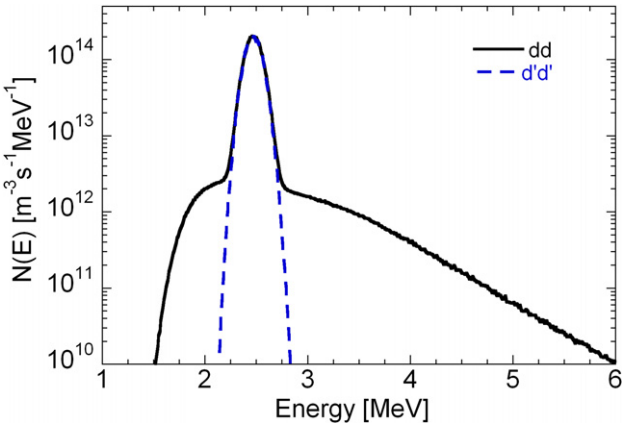

Figure 2. Calculated spectrum for $\mathrm{d} + \mathrm{d} \rightarrow \tau + \mathrm{n}$ neutron emission from a plasma with $c_\tau = 1\%$ and ICRH giving $T_\tau = 500\,\mathrm{keV}$ compared with that for a thermal D plasma (the $\mathrm{d}' + \mathrm{d}' \rightarrow \tau + \mathrm{n}$ reaction). The deuteron population in (^{3}He)D is described by the full velocity distribution with supra-thermal component d'' ($\mathrm{d} = \mathrm{d}' + \mathrm{d}''$ as described in the text).

3. Results

Neutron emission was calculated for the (^{3}He)D plasma subject to RF injection at different power levels. The result on the neutron spectrum from a plasma of reference conditions, as defined above, is presented in figure 2 and compared with neutron emission from thermal plasma without RF power. The supra-thermal $\mathrm{d}'' + \mathrm{d}'$ reactions (due to knock-on) manifest themselves as low- and high-energy tails starting at about $\pm 0.1\,\mathrm{MeV}$ from the peak at $E_{\mathrm{n}} = 2.45\,\mathrm{MeV}$ due to thermal $\mathrm{d}' + \mathrm{d}'$ reactions; the relative amplitude is about 1% of the peak. The knock-on results were obtained through Monte Carlo calculation with 10^8 events in the spectrum giving rise to the statistical scatter seen in the data.

There are shape differences between the low- and high-energy tails which have a kinematical origin. Using equation (5) one can calculate analytically the neutron energy (E_{n}) as a function of the energy E_{d} of fast deuterons interacting with deuterons at rest (figure 3). It is found that the minimum

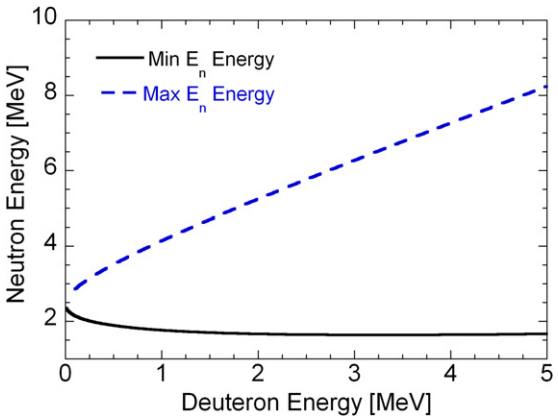

Figure 3. Maximum and minimum neutron energies of the reaction $d + d \rightarrow \tau + n$ as a function of the energy E_d of fast deuterons reacting with deuterons at rest.

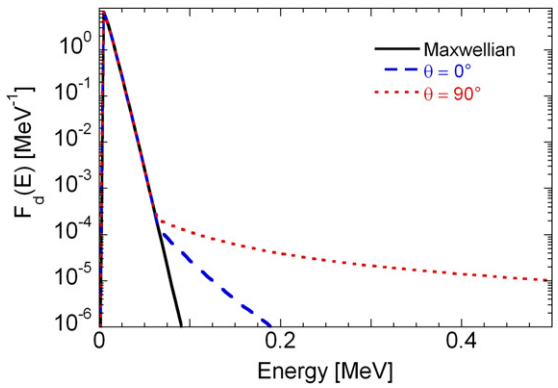

Figure 4. The calculated slowing-down deuteron distribution $F_{d''}(E, \theta)$ for pitch angles $\theta = 0°$ and $\theta = 90°$ resulting from the knock-on process $\tau'' + d \rightarrow \tau'' + d''$.

neutron energy is $E_n = 1.63$ MeV which equals $Q/2$ for an incoming energy of $E_d = Q = 3.27$ MeV; the graph also shows the expected result that the peak energy is $E_n = 2.45$ MeV for $E_d = 0$ MeV. The high-energy tail extends up to the value allowed kinematically by E_d, for instance, $E_n = 2Q = 6.54$ MeV for $E_d = Q$. This illustrates the origin of the spectral asymmetry around the peak energy which is most clearly displayed for the supra-thermal deuteron contributions.

The deuteron distribution used in the reference calculation is illustrated in figure 4 by the energy functions $F_d(E, \theta)$ for the fixed (pitch) angles $\theta = 0°$ and 90°. These distributions start to deviate from the Maxwellian shape at $E_d \approx 70$ keV with only a slight dependence on θ. The knock-on effect appears at an amplitude level of 10^{-4} compared with the peak maximum of the $F(E_d)$ distribution with a shape that mirrors the pitch angle anisotropy of the τ'' distribution as illustrated by the difference between the two curves. Clearly, the phase space for producing a high-energy deuteron in the $\theta = 90°$ direction through knock-on by τ'' moving in the $\theta = 0°$ direction is small. This explains why the supra-thermal d'' component retains the pitch angle anisotropy of the τ'' distribution.

The results on neutron spectra corresponding to different τ'' distributions, representing tail temperatures in the range $T_\tau = 100$ to 800 keV, are presented in figure 5. The relative

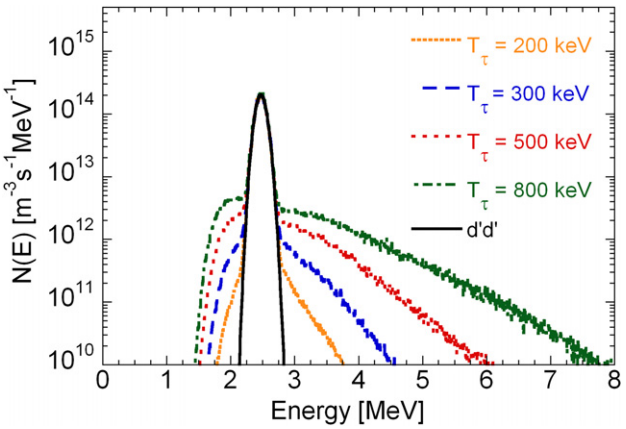

Figure 5. Calculated spectra for the neutron emission in a (^{3}He)D plasma with RF of varying power giving tail temperatures in the range $T_\tau = 200$–800 keV. Comparison is made with the emission from a thermal D plasma of $T_i = 5$ keV.

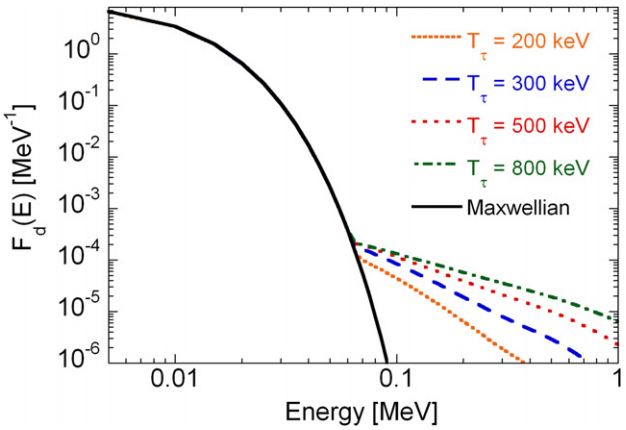

Figure 6. The calculated fast deuteron energy distribution $F_{d''}(E, \theta)$ at pitch angle $\theta = 90°$ for different levels of absorbed RF power densities as specified by the tail temperature T_τ. Comparison is made with a Maxwellian distribution for $T_i = 5$ keV.

importance of the knock-on signature can be seen to vary strongly with T_τ above 300 keV where it first appears as distinguishable low- and high-energy tails. In terms of energy integrated amplitude of the supra-thermal reaction ($d'' + d'$), the contribution relative to the dominant bulk thermal deuteron reactions ($d' + d'$) was estimated to vary approximately linearly with T_τ from 1.5% at 300 keV to 21% at 1000 keV.

The knock-on effects on the deuteron population can be seen from the results for the (full) velocity distributions, expressed by $F_d(E_d)$ at $\theta = 90°$, for different tail temperatures T_τ (figure 6). They show up for $E_d > 70$ keV (for a plasma assumed to have $T_i = 5$ keV) and form a tail whose fall off decreases systematically with T_τ. These results suggest that one can use $E_d \approx 70$ keV as a delimiter between the thermal ($F_{d'}$) and supra-thermal ($F_{d''}$) velocity components. The neutron production involving supra-thermal deuterons is thus $d'' + d'$ which would be responsible for the high-energy tail in the region $E_n \geqslant E_o = 3$ MeV in the spectra of figure 5. These tails for different T_τ can be described with the exponential function

$$N(E) = N_0 \exp(-k_1 \cdot (E - E_0) - k_2 \cdot (E - E_0)^2), \quad (6)$$

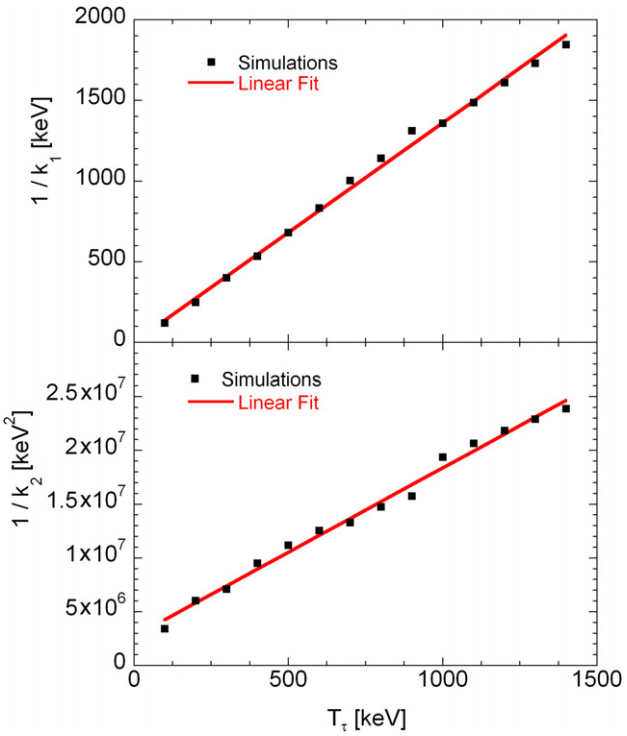

Figure 7. Relationship between the slope parameters k_1 and k_2 used in the description of the tail shape of the neutron spectrum and the temperature T_τ of fast helions (see the text).

where k_1 and k_2 are the first and second order slope parameters whose values are determined by fitting to the calculated data. It is found that there is approximately a linear relation between the inverse of the parameters and T_τ as borne out by the results in figure 7. Specifically, the calculated tail can be described with $1/k_1 = 1.4 \cdot T_\tau$ and $1/k_2 = 2.7\text{E}6 + 1.6\text{E}4 \cdot T_\tau$ in the RF heating range corresponding to $T_\tau = 100$–1400 keV.

4. Discussion

In this study we have used newly parametrized cross sections for the τ + d scattering. The latter includes the nuclear part of the interaction which is essential for recoil energies in the range $E_\text{d} > 70$ keV of relevance here. The effect of leaving out the nuclear scattering amplitude is illustrated by the examples in figure 8. This shows that the nuclear interaction affects the angular dependence of the cross section from about $\theta_\text{S} = 50^\circ$ and dominates in the backward direction. Generally, the relative importance of nuclear scattering is also revealed [12] in the τ + d elastic total cross section (for $\theta_\text{S} \neq 0^\circ$) which has a weaker fall off than that of pure Coulomb scattering (i.e. $1/E^2$). Details about the features of τ + d cross section including nuclear scattering of relevance for knock-on effects in the deuteron population can be found in [12]. Thus, the nuclear part is important for assessing τd knock-on effects on the deuteron population in the present (^{3}He)D plasmas with RF as was found for alpha particle knock-on for the fuel ion populations in DT plasmas in an earlier study [6, 20].

We now examine which ranges of the kinematics (θ_S and E) of the τ–d scattering are most important for the high-energy tail ($E_\text{n} > 3$) of the neutron spectrum. Calculations

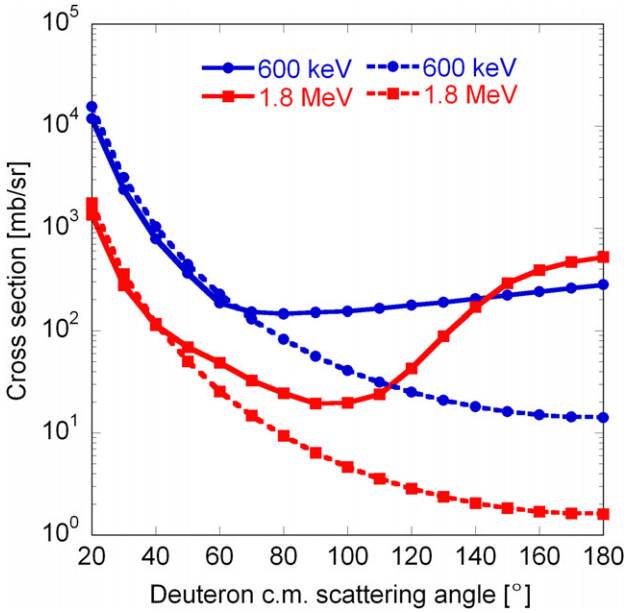

Figure 8. Comparison of the experimentally deduced angular distribution for τ + d elastic cross section (solid line) and that of Coulomb scattering (dashed line) for two energies in the c.m. frame.

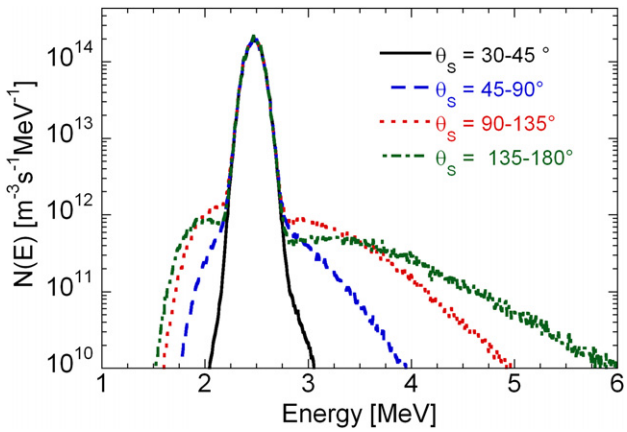

Figure 9. The calculated neutron spectrum for reference conditions where the knock-on scattering was limited to the angular ranges 30°–45°, 45°–90°, 90°–135° and 135°–180°.

were thus performed by restricting the scattering to the ranges $\theta_\text{S} = 30^\circ$–$45^\circ$, 45°–90°, 90°–135° and 135°–180° for plasma reference conditions specified in section 2 (figure 9). The tail is dominated by contributions for $\theta_\text{S} > 90^\circ$ and those for $\theta_\text{S} < 45^\circ$ are negligible. The extension to high E_n is determined by the contributions from highest θ_S. The tail dependence on helion energy was calculated for the cross section giving dominant contribution, i.e. angular range $\theta_\text{S} > 135^\circ$. It is found that, in terms of the divisions $E_\tau = 0$–1, 1–4 and >4 MeV, the middle range dominates with the small contribution near $E_\text{n} = 3$ MeV from the lowest helion energies. The high-energy range is responsible for the tail extension beyond $E_\text{n} = 6$ and negligible otherwise. These results have two implications. One is that the scattering kinematics range that dominates the tail is the one where nuclear interaction is important. The second is that the scattering cross sections used as input in the calculations are rather well determined

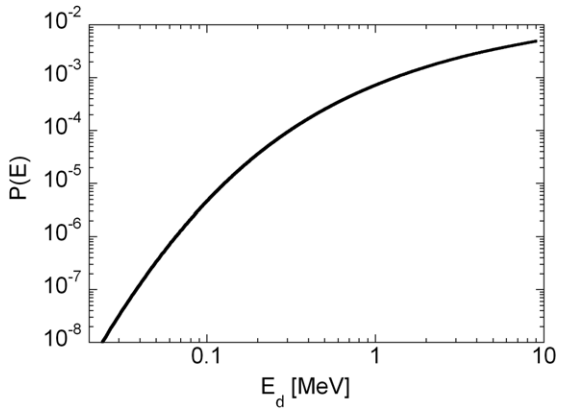

Figure 10. Neutron production probability as a function of the energy E_d of deuterons in their thermalization path in a D plasma.

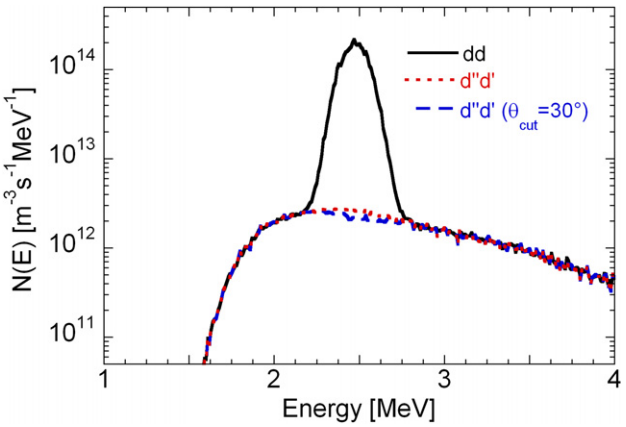

Figure 11. Comparison of the spectrum of the d + d → τ + n neutron emission from (^{3}He)D with RF ($T_\tau = 500$ keV) as calculated with the full deuteron velocity distribution developed here (dd) and the supra-thermal (d″d′) component without and with angular cut.

for the kinematics range that matters. The main uncertainty derives from the extrapolation to 180° from the measured range extending to between 130° and 150° [12]. It is judged that uncertainties in the τ + d scattering are limited at an indicative level of 10%.

A supra-thermal component in the d population of D plasmas has an effect on the neutron emission already at energies only slightly above the thermal range (say $E_d > 0.01$ MeV). This is illustrated in the probability distribution for the d″ + d′ reaction, $P(E_{d''})$, i.e. the probability for a fast deuteron to undergo a fusion reaction during its thermalization path in a D plasma,

$$P(E_{d''}) = \int_0^{E_d} d\varepsilon \frac{1}{|d\varepsilon/dt|} n_d \sigma(\varepsilon) \sqrt{\frac{2\varepsilon}{m_d}}. \quad (7)$$

Here, $\sigma(\varepsilon)$ is the cross section at the deuteron energy ε, n_d the deuteron bulk density, m_d the deuteron mass and $1/|d\varepsilon/dt|$ the energy loss per unit time. The graph $P(E_{d''})$ in figure 10 shows that the probability increases by 6 orders of magnitude from $E_{d''} = 10$ keV to 100 keV. The increasing trend continues even beyond but at a lower rate (roughly proportional to $\sqrt{E_{d''}}$). This energy dependence can be traced to the dd fusion cross section that increases sharply with E_d in the range up to above 100 keV to reach a maximum for $E_d > 1$ MeV. This means that the dd neutron production has a high sensitivity to supra-thermal components. Their presence is reflected in the d population with a clearly detectable tail in the neutron spectrum. This signature lends itself to diagnostics of plasma aspects related to the source of the knock-on which here is the absorbed RF power. From the progress made in describing NES with knock-on effects, the studies will be extended in a forthcoming paper. This will be concerned with a comparison of different knock-on sources affecting the neutron emission in (^{3}He)D with RF. It will also include (^{3}He)DT to illustrate the role of the energy dependence underlying fusion cross section as manifested by that of d + d → τ + n and d + t → α + n.

In this study the full velocity distribution F_d was used to describe the deuteron population to calculate the fusion reaction d + d → τ + n. However, it is also interesting to decompose the full dd spectrum into a superposition of the thermal and supra-thermal parts, i.e. d′d′ + d″d′ + d″d″ where the d″d″ contribution can be ignored. In the componential approach, $F_{d'}$ is represented by a Maxwellian and the $F_{d''}(\theta, E)$ distribution was defined in equation (4). The results in figure 11 show that the full calculation is made up of the supra-thermal contribution d″d′ in the regions ±0.3 MeV outside the peak. Inside this region, the calculated d″d′ component can include contributions from the relative low-energy end of $F_{d''}(\theta, E)$ where the deuterons cannot be uniquely attributed to the knock-on origin. The likelihood of a knock-on origin can be increased by applying a minimum angle cut (θ_{cut}) to $F_{d''}(\theta, E)$ implying that the deuteron energy has enhanced probability to come from knock-on. This is done by setting the τ + d scattering cross section to 0 for scattering angles $\theta < \theta_{cut}$. To demonstrate the effect of using the angular cut to detect thermal admixture, the d″d′ spectrum was calculated with a cut of 30° for comparison (figure 11). The results indicate that the admixture is small at the level of some 20% at the peak. It can be noted that the componential approach has been used earlier with an angular cut of 30° [20]. The present results where an energy cut was applied to the full distribution, obtained by matching the d′ and d″ distributions at $E_d \approx 70$ keV (figure 6), suggest that the componential approach is a reasonable approximation.

The results of this study show that the knock-on effect can be detected as a high-energy tail in the neutron emission spectrum. The tail appears where the dominant thermal component has fallen by a factor of 10^{-2} which is rather independent of absorbed RF power in the range $T_\tau > 300$ keV. Considering that the width (Gaussian equivalent) of the thermal and supra-thermal components differ by about a factor of 10, the counting statistics in the tail region would be about $>10^{-3}$ relative to that of the peak value. From this we can estimate that in order to observe the tail, with say 10% statistics, the spectrum would have to be recorded with a total number of events of $>100 \times 1000 > 10^5$. In addition, the energy resolution must be sufficient with corresponding immunity to background. This is presently attainable as demonstrated with the TOFOR spectrometer at JET [9, 10].

Given that the tail of the neutron spectrum can be observed and quantitatively determined, the present calculations indicate that the variation in the d″d′ reaction contribution can be related to the absorbed RF power density in the plasma (P_{RF}); for fixed plasma conditions, P_{RF} is proportional to the tail

temperature T_τ. Specifically, the slope of the high-energy tail (S) was shown to depend linearly on T_τ (figure 7) based on a parametric description (equation (7)) of the $E_n > 3$ MeV part of the neutron spectra. The amplitude of the neutron tail, A, is proportional to the power density, i.e. $A \propto P_{RF}$, which, in turn, depends on the tail temperature and density of the helions through $P_{RF} = T_\tau \cdot n_\tau$. This means that, for fixed helion density, changes in both observables S and A can be related to changes in the tail temperature. For a bulk plasma of reference conditions, ($n_e = 3 \times 10^{19}$ m^{-3}, $c_t = 1\%$, $T_e = T_i = 5$ keV), one obtains that $T_\tau = 500$ keV corresponds to $P_{RF} \approx 200$ kW m^{-3}. This power density level would be attainable at the resonance layer in JET experiments with an antenna power from about 4 MW.

By recasting equation (2) one obtains the plasma parameter dependence for the relationship between T_τ and P_{RF}, $T_\tau \propto (\sqrt{T_e} P_{RF}/c_\tau n_e^2)$. For the observables one obtains $S \propto k_S \cdot P_{RF}$ and $A \propto k_A \cdot P_{RF}$ where $k_S = \sqrt{T_e}/c_\tau \cdot n_e^2$ and $k_A = \sqrt{T_e}$. This shows that the slope shows the strongest plasma condition dependence through the $1/n_e^2$ factor. Hence, the cleanest knock-on signature in terms of S would fall rapidly with increasing n_e^2 for a given P_{RF}. In principle, the knock-on signal could be sustained with regard to the τ density c_τ. The latter would still have an upper limit of a few per cent because of the onset of RF power mode conversion into the Bernstein wave with an associated power transfer to the electrons instead of ions. The above implies that the knock-on effect can be detected and used for the diagnosis of plasmas from the highest RF power densities operated, for instance, at JET and downwards depending on plasma conditions as illustrated relative to the reference conditions defined here to be $n_e = 3 \times 10^{19}$ m^{-3}, $c_\tau = 1\%$ and $T_e = 5$ keV.

The question of neutron emission from RF accelerated ^{3}He ions with plasma impurities, such as ^{9}Be(^{3}He,n)^{11}C, that could appear along the knock-on spectral tails has been discussed recently in [21]. Such contributions were invoked to explain neutron spectra extending to $E_n = 10$ MeV for (^{3}He)D plasmas with raised ^{9}Be levels, but for an observed excess in the region 3 MeV $< E_n <$ 4 MeV, which was claimed as due to τ + d knock-on. A detailed study of the conditions under which ion-impurity reactions extraneous to fuel ion reactions may interfere with neutron emission is beyond the scope of this paper. However, the results reported in [21] suggest that components in the neutron spectrum due to τ + d knock-on can still be distinguishable in (^{3}He)D plasmas with ^{9}Be impurities. This result is of relevance for τ knock-on observations in next step fusion devices, such as ITER.

Finally we note that analysis and interpretation also hinges upon how well the τ velocity distribution can be determined for which we have used analytical prescription of Stix formula as a first-order approximation for the purpose of illustration.

5. Conclusions

The model describing the d + d $\rightarrow^3$ He + n neutron emission from (^{3}He)D plasmas with RF was extended to make full use of available d + ^{3}He scattering cross sections in the calculations of the knock-on source needed to determine the full velocity distribution of the deuteron population. It was demonstrated that nuclear interaction is essential for the knock-on term and that Coulomb scattering will not do as an approximation.

The calculations demonstrate the knock-on signature in the neutron emission spectrum and its variation with the absorbed power density P_{RF} giving helion temperatures in the range $T_\tau = 100$–1500 keV. Specifically, the relative amplitude of the knock-on spectral contribution was determined for different P_{RF} (linear relationship was found). Moreover, the high-energy tail signature was found to have a shape that was given a parametric description as a function of T_τ.

This study presents the tools for analysing neutron emission spectra affected by knock-on effects. Specifically, it is demonstrated how the knock-on source term, responsible for the supra-thermal velocity distribution of fusing ion populations, can be used to extract plasma information. This concerns RF effects in the present study but would differ depending on the knock-on source term at play.

Acknowledgments

This work has been performed under the auspices of European Fusion Development Agreement, and the Associations EURATOM ENEA-CNR (Milano, Italy) and EURATOM-VR (Uppsala, Sweden). One of the authors (M.N.) would like to thank Dr Thomas Johnson for his suggestions on the theoretical framework and the grant programme for young students in fusion research of the Italian Embassy in London for the economic support.

References

[1] Nocente M., Gorini G., Källne J. and Tardocchi M. 2010 *Nucl. Fusion* **50** 055001
[2] Heidbrink W.W. and Sadler G.J. 1994 *Nucl. Fusion* **34** 535
[3] Heidbrink W.W. 2008 *Phys. Plasmas* **15** 055501
[4] Kislyakov A.I., Khudoleev A.V., Kozlovskij S.S. and Petrov M.P. 1997 *Fusion Eng. Des.* **34–35** 107
[5] Korotkov A.A., Gondhalekar A. and Akers R.J. 2000 *Phys. Plasmas* **7** 957
[6] Källne J., Ballabio L., Frenje J., Conroy S., Ericsson G., Tardocchi M., Traneus E. and Gorini G. 2000 *Phys. Rev. Lett.* **85** 1246
[7] Zaitsev F.S., Gondhalekar A., Johnson T.J., Sharapov S.E., Testa D.S. and Kurbet I.I. 2007 *Plasma Phys. Control. Fusion* **49** 1747
[8] Van Eester D. *et al* 2009 *Plasma Phys. Control. Fusion* **51** 044007
[9] Gorini G and Källne J 1992 *Rev. Sci. Instrum.* **63** 4548
[10] Gatu Johnson M. *et al* 2006 *Rev. Sci. Instrum.* **77** 10E702
[11] Helander P., Lisak M. and Ryutov D.D. 1993 *Plasma Phys. Control. Fusion* **35** 363
[12] Ognissanto F., Gorini G., Källne J., Ballabio L., Nocente M. and Tardocchi M. 2011 The elastic 3He+d cross section of relevance for knock-on effects in radio frequency heated (3He)D plasmas *Nucl. Instrum. Methods* B **269** 786–92
[13] Ballabio L. 2003 Calculation and measurement of the neutron emission spectrum due to thermonuclear and higher-order reactions in tokamak plasmas *PhD Thesis* Acta Universitatis Upsaliensis No 797, Faculty of Science and Technology, Uppsala University
[14] Stix T H 1975 *Nucl. Fusion* **15** 737

[15] Tardocchi M., Conroy S., Ericsson G., Gorini G., Henriksson H. and Källne J. 2002 *Nucl. Fusion* **42** 1273
[16] Trubnikov B.A. 1965 *Rev. Plasma Phys.* **1** 105
[17] Sivukhin D.V. 1966 *Rev. Plasma Phys.* **4** 93
[18] Krall N. and Trivelpiece A. 1973 *Principles of Plasma Physics* (New York: McGraw Hill)
[19] Brysk H. 1973 *Plasma Phys.* **15** 611
[20] Ballabio L., Gorini G. and Källne J. 1997 *Phys. Rev.* E **55** 3358
[21] Gatu Johnson M. *et al* 2010 *Nucl. Fusion* **50** 045005

Paper II

IOP Publishing and International Atomic Energy Agency Nuclear Fusion

Nucl. Fusion **50** (2010) 055001 (6pp) doi:10.1088/0029-5515/50/5/055001

Cross section of the d + ^{3}He $\rightarrow \alpha$ + p reaction of relevance for fusion plasma applications

M. Nocente[1,2,a], G. Gorini[1,2], J. Källne[1,3] and M. Tardocchi[2]

[1] Dipartimento di Fisica 'G. Occhialini', Università degli Studi di Milano - Bicocca, Piazza della Scienza 3, 20126, Milan, Italy
[2] Istituto di Fisica del Plasma 'Piero Caldirola,' Associazione EURATOM-ENEA-CNR, via Cozzi 53, 20125, Milan, Italy
[3] Department of Engineering Sciences, Uppsala University, EURATOM-VR Association, 75121 Uppsala, Sweden

E-mail: massimo.nocente@mib.infn.it

Received 25 November 2009, accepted for publication 23 March 2010
Published 23 April 2010
Online at stacks.iop.org/NF/50/055001

Abstract
The cross section of the d + ^{3}He $\rightarrow \alpha$ + p fusion reaction has been determined with regard to its systematic variation with energy (E_{CM}) based on the available experimental data. Information is provided on the angular distribution $d\sigma/d\Omega(\theta_p, E)$ at energies up to $E_{CM} = 8.0$ MeV and the total cross section $\sigma(E_{CM})$ for the range $E_{CM} = 3.0$–8.0 MeV. The relevance of the presented results for fusion plasmas heated with RF heating of ^{3}He minority in D and DT plasmas is discussed.

PACS numbers: 25.55.-e, 29.30.Hs, 52.55.Pi

(Some figures in this article are in colour only in the electronic version)

1. Introduction

There are three main fusion reactions between nuclides of mass $A = 2$ and $A = 3$, namely, d + d $\rightarrow \tau$ + n (and d + d $\rightarrow$ t + p), d + t $\rightarrow \alpha$ + n and d + $\tau \rightarrow \alpha$ + p (where τ is used here to denote ^{3}He nuclei or ions). The total cross sections of these reactions are well analysed and parametrized for the ion energies encountered in fusion plasmas of typical Maxwellian velocity distributions of temperatures $T \leqslant 100$ keV [1]. This has been done in the framework of the R-matrix theory [2, 3]. The cross section for higher energies has not been similarly characterized which is especially true for the dτ reaction in the range of several megaelectronvolts. The suprathermal enhancement of the dτ has attracted increased interest recently because of the radio frequency (RF) power injection used to heat deuterium (D) or mixed deuterium–tritium (DT) plasmas with a small minority of τ [4]. In this case the RF power can be absorbed by the plasma through coupling to the ion cyclotron resonance frequency (ICRF) of τ. This leads to the creation of a suprathermal velocity component (τ'') in the τ population. The dτ reaction rate is typically insignificant relative to those of dd and dt, but for situations where it is enhanced by the presence of τ''d such as created and controlled by the injected RF power (P_{RF}). In order to assess the relationship between P_{RF} and the dτ fusion reaction, one needs to know the energy dependence of the cross section for energies over the range up to several megaelectronvolts.

Besides the issue of the magnitude of fusion power of the τd reaction, which can be driven by RF, there is also an interest because of the fast protons and α-particles (E_p = 15 MeV and $E_\alpha = 4.5$ MeV) produced. These fusion products together with τ'' can suffer knock-on collisions in the fuel ion populations (d and t), thus creating suprathermal components (d$''$and t$''$) whose presence will show up in the spectra of the neutron emission from the d + d $\rightarrow \tau$ + n or d + t $\rightarrow \alpha$ + n reactions. This work on the τ + d $\rightarrow \alpha$ + p cross sections in the megaelectronvolt range was initiated by the interest in determining the contribution of fast ion knock-on effects in the spectrum of dd neutron emission in RF heated (τ)D and (τ)DT plasmas, and the thus observable response of the plasma to RF power injection.

Information on the total cross section of d + $\tau \rightarrow \alpha$ + p can be found in the comprehensive review of light ion fusion reactions [1]. It contains detailed parametrizations of the total cross sections $\sigma(E)$ over the energy range of the first resonance

[a] Author to whom any correspondence should be addressed.

($E < 0.5$ MeV in the centre-of-mass system) whose use is extended up to 4.4 MeV. The experimental fusion data are rather scarce, especially, for the $\tau + d \rightarrow \alpha + p$ reaction, for which only a few measurements of angular distributions, $d\sigma/d\Omega(\theta_p)$, exist up to $E_{CM} = 8$ MeV. Information is needed on both $\sigma(E)$ and $d\sigma/d\Omega(\theta_p, E)$ in order to calculate the knock-effects in neutron emission spectra.

In this work we have done a survey of the literature for the experimental data. Parametric fitting analysis was performed to determine the systematic energy dependence of the total cross section and the angular distribution. This information has thus been completed up to $E = 8.0$ MeV as required for use in the description of the generation of suprathermal fuel ions that can show up in the spectra of neutron emission from RF heated (τ)D and (τ)DT plasmas. For the purpose of comparison with the $d + t \rightarrow \alpha + n$ and the dd fusion reactions, existing database information[4] was parametrized to obtain $\sigma(E)$ that extends up to 10 MeV. The results are discussed in view of their implications, especially on neutron emission spectra.

2. Cross section data and parametrization

The $\tau + d$ fusion cross section of interest for this study comes from $d + \tau$ experiments using deuteron beams in the energy range $E_d = 0.24$–14 MeV [5–7] with the fusion protons detected at different scattering angles in the laboratory system; the corresponding energy range in the centre of mass system is $E = 0.15$–8.2 MeV.[5] The energy steps of the data are roughly 300 keV below $E = 2.1$ MeV and 1 MeV above. The angular distributions are rather detailed, typically, every 10° but for the lack of back angle coverage, especially for low energies (table 1). In addition to data on differential cross section, $d\sigma/d\Omega$, there are measurements of the total cross section in the E_{CM} range 0.3–4.8 MeV.

The angular distribution of the differential cross sections $d\sigma/d\Omega(\theta_p)$ at a given energy was described using the Legendre polynomial expansion of order $N = 6$:

$$\frac{d\sigma}{d\Omega} = \sum_{l=0}^{N} a'_l P_l(\cos\,\theta_p), \tag{1}$$

where a'_l are energy dependent coefficients. This was used to make fits to the data which allowed determination of the value $d\sigma/d\Omega(\theta_p = 0)$ at each energy $E = E_{exp}$. The results were used to define normalized coefficients, $a_l(E) = a'_l(E)/d\sigma/d\Omega(0)$, resulting in the differential cross section expression

$$\frac{d\sigma}{d\Omega}(\theta_p, E) = \frac{d\sigma}{d\Omega}(\theta_p = 0, E) \sum_{l=0}^{N} a_l(E) P_l(\cos\,\theta_p). \tag{2}$$

The energy dependence of the coefficients $a_l(E)$ is described with 5th order polynomials

$$a_l(E) = \sum_{k=0}^{5} \alpha_{lk} E^k. \tag{3}$$

[4] www.nndc.bnl.gov/exfor/

[5] Additional experiments have been reported but not considered here because of the limited angular range covered [8] or at higher energies [9, 10].

Table 1. Summary of data on differential cross sections for $d + \tau$ fusion reaction from experiments listed in different CM energies, the angular range covered and number of data points.

CM energy (MeV)	Yarnell [5]	Stewart [6]	Gruebler [7]
0.16	15.5–131.5 (14)		
0.27	15.7–132.2 (14)		
0.59	16.1–133.2 (14)		
0.90	16.4–133.9 (14)		
1.21	16.5–134.5 (14)		
1.50	16.5–135 (14)		
1.68			23.3–152.7 (19)
1.81	16.8–135.4 (14)		
2.14	17–135.9 (14)		
2.40			24.8–160.4 (19)
3.00			24.9–159.8 (19)
3.54		11.7–146.2 (32)	
3.60			25.7–160.6 (19)
4.20			25.1–160.4 (19)
4.50		11.9–169.8 (25)	
4.80			26.2–161.8 (19)
5.40			26.3–161.9 (19)
6.00			26.5–162.0 (19)
6.24		12.1–174.0 (18)	
6.90			27.3–161.4 (18)
7.38		12.2–170.2 (22)	
8.22		12.3–170.4 (23)	

The values of the coefficients α_{lk} ($k = 0$–5) were obtained by fitting to the derived data $a_l(E = E_{exp})$. This result together with equation (2) gave a kinematically complete description of the angular distribution as a function of energy in the range $E = 0.6$–8.0 MeV, i.e. $d\sigma/d\Omega(\theta_p, E)$, but for the normalization factor $d\sigma/d\Omega(\theta_p = 0)$. The latter is related to the total cross section σ which is obtained by angular integration of equation (2) over 4π giving

$$\sigma = \frac{d\sigma}{d\Omega}(0) 4\pi a_0. \tag{4}$$

The energy dependence of the normalization factor is determined from $\sigma(E)$. For low energies ($E < 3$ MeV as described below) the parametrized results on $\sigma(E)$ of [1] were used. For energies $E > 3$ MeV, $\sigma(E)$ was determined by fitting an *ad hoc* function

$$\sigma_{d\tau}(E) = \frac{1}{E} \cdot \frac{A_0}{1 + B_1 E + B_2 E^2 + B_3 E^3} \tag{5}$$

to the results obtained for $\sigma(E)$; here A_0, B_1, B_2 and B_3 are fitting parameters.

In order to allow comparison of $\sigma(E)$ of the $d\tau$ fusion reaction with those of dt and dd, the data-based experimental cross sections were fitted with similar polynomials. However, to describe the data, more terms were required, which meant

$$\sigma_{dd}(E) = \frac{1}{E} \cdot \exp\left(-\frac{B_G}{\sqrt{E}}\right) \frac{A_0 + A_1 E + A_2 E^2 + A_3 E^3}{1 + B_1 E + B_2 E^2 + B_3 E^3} \tag{6}$$

and

$$\sigma_{dt}(E) = \frac{1}{E} \cdot \frac{A_0}{1 + B_1 E + B_2 E^2 + B_3 E^3 + B_4 E^4 + B_5 E^5} \tag{7}$$

for dd and dt, respectively, where A and B coefficients are fitting parameters. In equation (6) for dd the exponential factor has been included, which allowed describing the total cross section from $E = 10$ MeV down to 3 keV, where the B_G factor represents the Gamow constant.

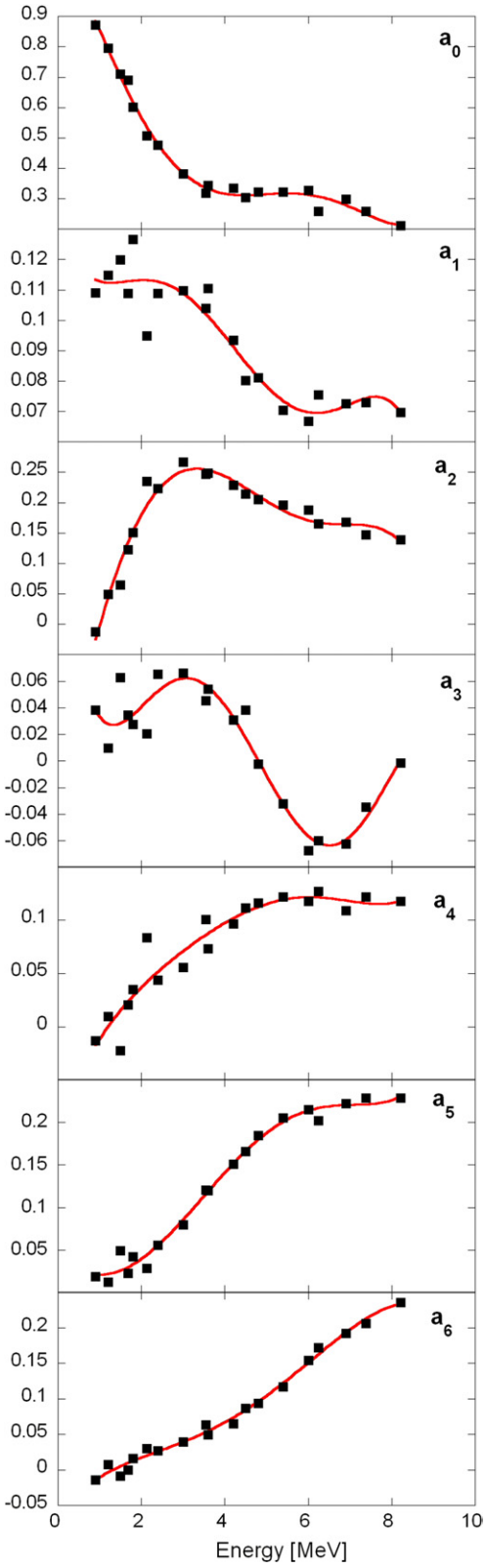

Figure 1. Results on the coefficients a_l ($l = 0$–6) from the Legendre polynomial analysis to measured angular distribution for different experiments at CM energies $E = E_{\rm exp}$ and the functions $a_l(E)$ representing the 5th order polynomial fit (solid lines).

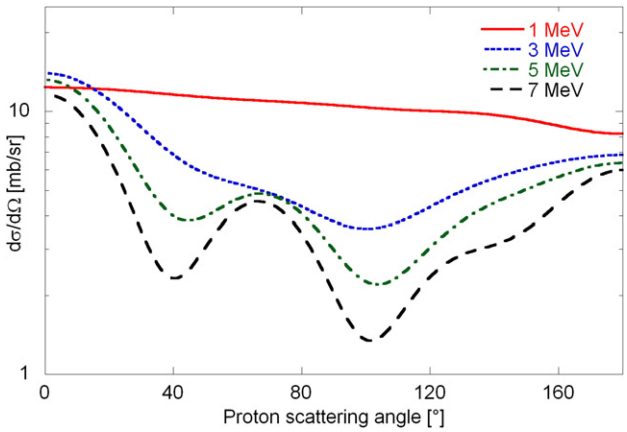

Figure 2. Examples of results for the differential cross sections as a function of the proton CM scattering angle at energies of $E = 1$, 3, 5 and 7 MeV obtained from the Legendre polynomial description and fitting (see text).

3. Results

The fits to $\mathrm{d}\sigma/\mathrm{d}\Omega(\theta_{\rm p})$ provide the values of the Legendre coefficients at the energies of the experiments, i.e. $a_l(E = E_{\rm exp})$. The results on $a_l(E = E_{\rm exp})$ for $l = 0$–6 are presented in figure 1 together with the polynomial functions $a_l(E)$ giving the best fits[6]. Here we can see that the $a_l(E = E_{\rm exp})$ values demonstrate marked energy dependent features which are well described with the fitted functions. There is a certain scatter in the deduced $a_l(E = E_{\rm exp})$ values, especially for $l = 1$ and 3 in the energy range $E_{\rm exp} < 3$ MeV where it exceeds the typical deviation level of about $\pm 10\%$. The enhanced scatter occurs for Legendre functions which have relatively small weight. This is the case for Y_1 and Y_3 compared with Y_0 and Y_2, which between them dominate $\mathrm{d}\sigma/\mathrm{d}\Omega(\theta_{\rm p})$ for low energies (cf figure 1). Generally, even functions $Y_1(\cos\theta_{\rm p})$ show more stable fitting (less scatter) than the odd ones which reflects the prevailing symmetry in $\theta_{\rm p}$ of the cross sections (figure 2). The results of the coefficients α_{lk} defining the $a_l(E)$ functions are presented in table 2.

With the results on α_{lk} in table 2, one can, with the help of (3), calculate $a_l(E)$ and, hence, obtain the desired results on $\mathrm{d}\sigma/\mathrm{d}\Omega(\theta_{\rm p}, E)$, as illustrated by the angular distributions at $E = 1$, 3, 5 and 7 MeV in figure 2. This shows that the angular dependence is weak for low energies $E < 1$ MeV so as to practically vanish for $E < 0.6$ MeV, i.e. $\mathrm{d}\sigma/\mathrm{d}\Omega(\theta_{\rm p})$ is constant to within 6%. For energies $E > 1$ MeV, there is a growing undulation pattern with increasing energy, showing forward and backward peaking with a typical amplitude swing of a factor 10 for the highest energy.

The results were derived on the $\sigma(E_{\rm exp})$ cross sections for the energy range 0.6–8 MeV. These were found to agree with the parametrized result $\sigma(E)$ of [1] for energies up to $E = 3$ MeV and no further information could be added in this region. The present results on $\sigma(E = E_{\rm exp})$ in the range $E > 1$ MeV are shown in figure 3 together with the $\sigma(E)$ determined by the fitting function (5) and the coefficients presented in table 3. The derived $\sigma(E)$ gives a good description

[6] The chosen normalization of the coefficients $a_l(E = E_{\rm exp})$ removes uncertainties in the cross section scale of the measurements.

Table 2. Results on best fit parameters of polynomial of order 5 used to represent the energy dependence of coefficients of Legendre polynomials describing the angular distribution in the energy range 0.6–8.0 MeV.

a_i	α_{l_0}	α_{l_1}	α_{l_2}	α_{l_3}	α_{l_4}	α_{l_5}
a_0	1.144	-2.219×10^{-1}	-1.131×10^{-1}	5.334×10^{-2}	-7.371×10^{-3}	3.347×10^{-4}
a_1	1.355×10^{-1}	-5.091×10^{-2}	3.964×10^{-2}	-1.305×10^{-2}	1.749×10^{-3}	-8.150×10^{-5}
a_2	-2.866×10^{-1}	3.186×10^{-1}	-2.004×10^{-2}	-1.745×10^{-2}	3.436×10^{-3}	-1.823×10^{-4}
a_3	1.929×10^{-1}	-3.258×10^{-1}	2.194×10^{-1}	-5.988×10^{-2}	6.879×10^{-3}	-2.793×10^{-4}
a_4	-9.471×10^{-2}	1.121×10^{-1}	-3.647×10^{-2}	8.610×10^{-3}	-1.074×10^{-3}	5.007×10^{-5}
a_5	4.324×10^{-2}	-4.425×10^{-2}	2.179×10^{-2}	9.399×10^{-4}	-7.215×10^{-4}	4.933×10^{-5}
a_6	-6.088×10^{-2}	6.944×10^{-2}	-2.301×10^{-2}	4.434×10^{-3}	-2.541×10^{-4}	-6.364×10^{-7}

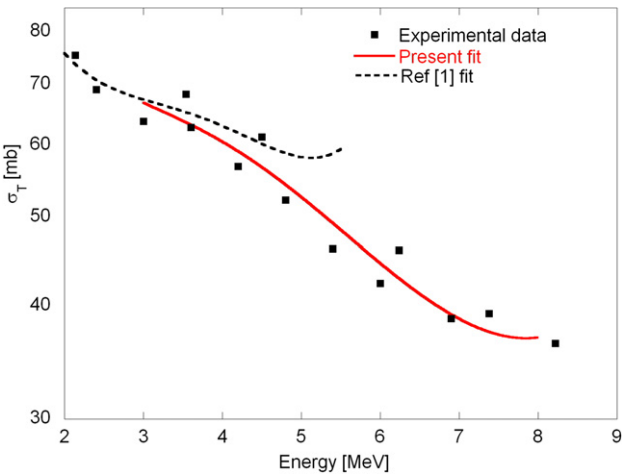

Figure 3. Results on total cross sections $\sigma(E = E_k)$ for the reaction $d + \tau \rightarrow \alpha + p$ at the discrete energies $E_k = E_{exp}$ for the energy range 2–8.0 MeV and the best fit function $\sigma(E)$ (solid curve). The result $\sigma(E)$ for the range $E < 4.5$ MeV from [1] is also shown.

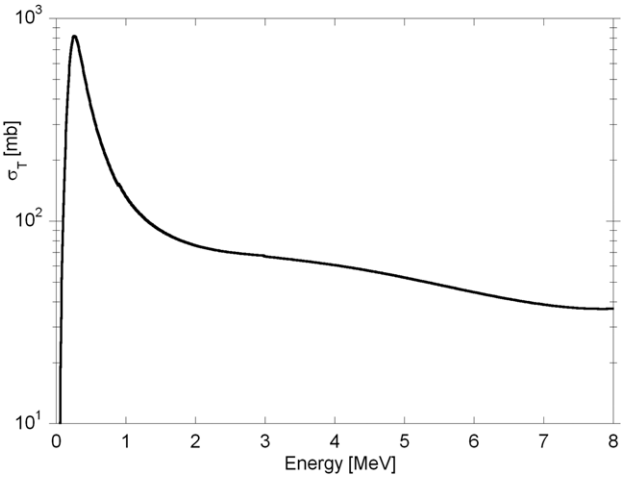

Figure 4. Total cross section for the reaction $d + \tau \rightarrow \alpha + p$ in the range 1 keV–8 MeV based on the present result on $\sigma(E)$ for $E \geqslant 3.0$ MeV and from [1] for $E < 3.0$ MeV.

Table 3. Results on best fit parameters used to represent the energy dependence of the total cross section $\sigma(E)$ of the fusion reactions $d + \tau \rightarrow \alpha + p$, $d + t \rightarrow \alpha + n$, $d + d \rightarrow \tau + n$ over the energy ranges $E = 3$–8 MeV for $d\tau$, $E = 3$–10 MeV for dt and 1 keV–8 MeV for dd.

Coefficient	$d\tau$	dt	dd
A_0	7.479×10^1	5.111×10^1	5.971×10^1
A_1	—	—	2.586×10^2
A_2	—	—	-3.377×10^2
A_3	—	—	3.325×10^2
B_1	-3.566×10^{-1}	-6.366×10^{-1}	-1.142
B_2	5.899×10^{-2}	1.922×10^{-1}	9.235×10^{-1}
B_3	-3.2605×10^{-3}	-2.825×10^{-2}	2.699×10^{-1}
B_4	—	2.003×10^{-3}	—
B_5	—	-5.482×10^{-5}	—
B_G			1.029

of $\sigma(E_{exp})$ for $E \geqslant 3$ MeV and thus complements the results on $\sigma(E)$ of [1], which starts to deviate at this energy. The results on $\sigma(E)$ of this study and of [1] were joined at $E = 3.0$ MeV to construct the energy dependent total cross section of $d + \tau \rightarrow \alpha + p$ shown in figure 4.

Parametrized results were also derived for the dt and dd fusion reactions for the purpose of providing comparisons with $\sigma(E)$ for $d\tau$ in the megaelectronvolt region. For energies above $E = 3$ MeV, a good description of the experimental data on $\sigma(E_{exp})$ for dt was obtained with the fitting function (7) using the coefficients presented in table 3. This is demonstrated by the results presented in figure 5 which also show that the present result complements those of [1], where information on $\sigma(E)$ is provided for $E < 3$ MeV. Similarly, the present results on $\sigma(E)$ for the dd reaction were successfully described with the fitting function (6) using the parameters presented in table 3. Here it is possible to describe the total cross section with a single function over the energy range 1 keV–8 MeV (figure 6). The present result is in close agreement with that of [1] while the covered energy range is extended beyond 4 MeV for energies up to 8 MeV.

4. Discussion and conclusion

RF accelerated τ's can undergo burn-up through fusion reactions $\tau + d \rightarrow \alpha + p$ during their thermalization, i.e. slowing down from $E_{\tau''}$ in the megaelectronvolt range to $E_{\tau'}$ in the kiloelectronvolt range. Considering that the slowing down rate varies as $1/\sqrt{E}$, the burn-up probability can be significant in the megaelectronvolt range, despite the fact that the cross section is only a fraction (about 1/10) of that of the maximum at about 0.25 MeV (figure 7). One can note that thermalization of 1 MeV τ-particles would have a burn-up fraction that is an order of magnitude lower than for those of $E_{\tau''} = 8$ MeV. This illustrates that the total cross section in the megaelectronvolt range is important to determine the τd fusion reactivity for RF heated (τ)D plasmas. For instance, the energy range of E_τ that we have provided information on, being at variance with that of an earlier study [1], is important due to the burn-up weight factor.

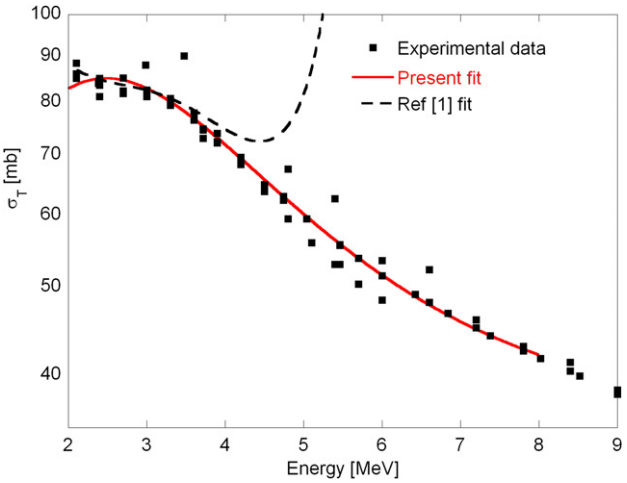

Figure 5. Results on the fitted total cross section $\sigma(E)$ for the $d + t \rightarrow \alpha + n$ reaction over the energy range $E = 2.0$–8.0 MeV (solid curve) with data taken from the EXFOR database[4]. Also shown is the result for $E < 4.7$ MeV from [1].

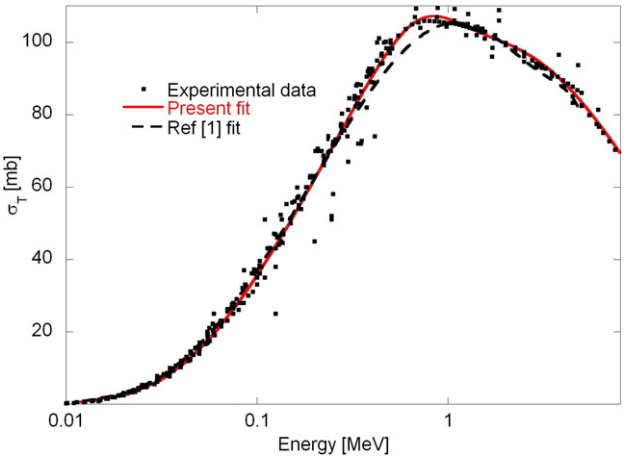

Figure 6. Results on fit of total cross section $\sigma(E)$ for $d + d \rightarrow n + {}^3He$ reaction over the energy range $E = 1$ keV–8.0 MeV with data taken from the EXFOR database[4] (solid curve). Also shown is the result for $E < 4.9$ MeV from [1].

The $\sigma(E)$ functions for the three fusion reactions $d\tau$, dt and dd are compared in figure 7. This displays the close similarity of the $d\tau$ and dt reactions if one accounts for the peak value shift (from 220 to 80 keV) due to the lower Coulomb repulsion effect for dt. In the region $E > 2.0$ MeV, these reactions have, essentially, the same slow fall-off with increasing energy, but for the slight enhancement for dt around 3 MeV that might not be present in $\sigma(E)$ of $d\tau$. The cross section magnitude is some 20% higher for dt relative to $d\tau$. It can be noted that the dd cross section is significantly larger for $E > 2$ MeV (at the level of about 50–30%) relative to both $d\tau$ and dt. In contrast to the $d\tau$ and dt reactions, one should also note that dd reaction lacks a resonance in the region $E < 1$ MeV so the cross section shows a monotonically accelerating fall off with decreasing energy. This means that RF heated (τ)D plasma of typical thermal energies, in the range of tens of kiloelectronvolts can have significant fusion reactivity due to $d\tau''$ compared with dd already for relatively small density ratios (say $n_{\tau''}/n_d \approx 10^{-6}$).

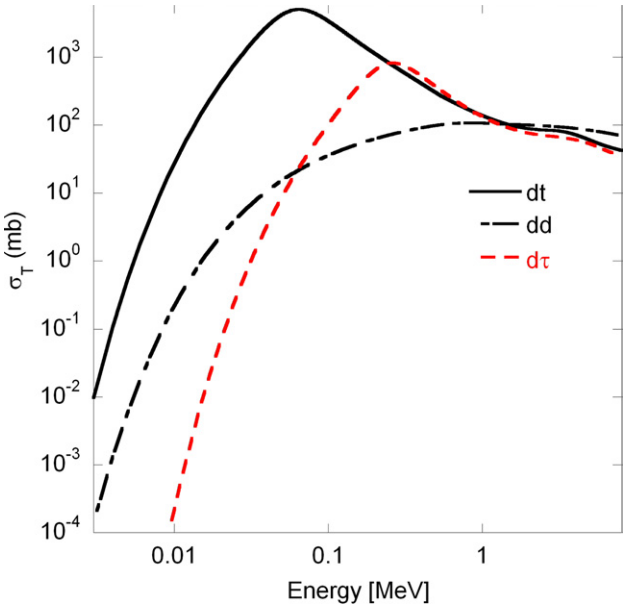

Figure 7. Comparison of total cross sections $\sigma(E)$ for the fusion reactions $d\tau$, dt, and dd in the energy range $E_{cm} = 1$ keV–8.0 MeV.

The $\tau + d \rightarrow \alpha + p$ cross section is of direct interest in calculating the total fusion power for (τ)D plasmas which includes that of dd with the reaction channels $d + d \rightarrow \tau + n$ and $d + d \rightarrow t + p$ (being of equal strength). The fusion power is normally determined through the measured neutron yield rate which thus directly gives the contribution from dd for (τ)D plasmas. However, the contribution from τd can be estimated from the effect it has on the spectrum of the neutron emission through the addition of a suprathermal component in the deuteron population through knock-on scattering involving both fast τ's directly and the fusion products p and α from $\tau + d \rightarrow \alpha + p$. This use of the present $\tau + d \rightarrow \alpha + p$ cross section result will be discussed in the forthcoming papers.

In conclusion, we have analysed and synthesized currently available cross sections for the $d + \tau \rightarrow \alpha + p$ reaction at energies up to 8 MeV with presented result in parametric form on $\sigma(E_{CM})$ and $d\sigma/d\Omega(\theta_p, E)$. With this information we have filled a gap in cross sections for fusion relevant reactions of nuclei in the mass region $A \leqslant 4$.

Acknowledgment

This work has been performed under the auspices of European Fusion Development Agreement, and the Associations EURATOM ENEA-CNR (Milano, Italy) and EURATOM-VR (Uppsala, Sweden). One of the authors (MN) would like to acknowledge the grant programme for young students in fusion research of the Italian Embassy in London for the economic support.

References

[1] Bosch H.S. and Hale G.M. 1992 *Nucl. Fusion* **32** 611–31
[2] Wigner E.P. and Eisenbud L. 1947 *Phys. Rev.* **72** 29

[3] Lane A.M. and Thomas R.G. 1958 *Rev. Mod. Phys.* **30** 257
[4] Van Eester D. *et al* 2009 *Plasma Phys. Control. Fusion* **51** 044007
[5] Yarnell J.L., Lovberg R.H. and Stratton W.R. 1953 *Phys. Rev.* **90** 292
[6] Stewart L., Brolley J.E. and Rosen L. 1960 *Phys. Rev.* **119** 1649
[7] Gruebler W., Konig V., Ruh A., Schmelzbach P.A., White R.E. and Marmier P. 1971 *Nucl. Phys.* A **176** 631–44
[8] Baker M.P., Cameron J.M., Chant N.S. and Mangelson N.F. 1972 *Nucl. Phys.* A **184** 97–104
[9] Bilaniuk O.M. and Slobodrian R.J. 1964 *Nucl. Phys.* **50** 585–92
[10] Roy R., Seiler F., Conzett H.E. and Rad F.N. 1981 *Phys. Rev.* C **24** 2421–34

Paper III

Nuclear scattering effects and neutron emission spectrum from fusion plasmas

M Nocente[1,2*], J Källne[1,3], G Grosso[2] , M Tardocchi[2] and G Gorini[1,2]

[1] Dipartimento di Fisica "G. Occhialini", Università degli Studi di Milano - Bicocca, Piazza della Scienza 3, 20126, Milano, Italy

[2] Istituto di Fisica del Plasma "Piero Caldirola," Associazione EURATOM-ENEA-CNR, via Cozzi 53, 20125, Milano, Italy

[3] Dept. of Eng. Sciences, Uppsala University, 75121 Uppsala, Sweden. EURATOM-VR Association

[*] Corresponding author. Electronic mail: massimo.nocente@mib.infn.it

Abstract

The effects of nuclear elastic scattering (knock-on) from energetic light ions on the neutron emission spectrum in fusion plasmas are studied. Each elastic scattering process leaves a distinct signature in the neutron spectrum that is manifested as a high energy component. The relative magnitude of knock on spectral features in D and DT plasmas without and with radio-frequency heating on a ^{3}He minority component is determined through Monte Carlo simulations. The results complete the map on nuclear elastic scattering effects induced by energetic ions in the neutron emission spectrum from D and DT plasmas, besides (^{3}He)D and (^{3}He)DT with radio-frequency heating, and are of relevance for diagnostics of fusion born α particles and fast ^{3}He ions through neutron emission spectroscopy in fusion plasmas.

PACS codes: 29.30.Hs, 52.20.Hv, 52.55.Pi, 52.65.Pp

1. Introduction

In a thermonuclear plasma, neutrons are produced by the main fusion reactions, d+d $\rightarrow$ n+^{3}He in a deuterium (D) plasma and d+t $\rightarrow$n + α in deuterium-tritium (DT). The neutron spectrum carries information on the reactant energy distribution, as demonstrated with dedicated work carried out mostly at the JET tokamak [1,2]. The fuel ion (f) population, deuterons and tritons, can be artificially divided into thermal (f') and suprathermal (f"), that in turn produce thermal (n') and suprathermal (n") components in the neutron emission spectrum, due to the reactions f'+f' and f'+f", respectively, f"+f" being generally negligible. f'+f' reactions produce a spectral feature of Gaussian shape, centred at E_0=2.5 MeV and E_0=14.5 MeV for d+d and d+t reactions, respectively, with a width that is proportional to the square root of the fuel ion bulk temperature [3].

The characteristics of spectral components from f'+f" reactions vary case by case and depend on properties of the f" energy distribution. In present day, low output power plasmas, suprathermal components in the fuel ion distribution are mostly generated by external heating, such as neutral beam injection (NBI) or radio-frequency (RF). Characteristic parameters of the energy distribution of externally heated fuel ions can be determined from comparison between neutron measurements and simulations, using as input a model for the energy distribution of energetic ions, as shown in dedicated works [4,5].

Besides external heating, suprathermal f" components can also be generated by nuclear elastic collisions between fast non fuel and thermal fuel ions and are in turn manifested in the high energy region ($E_n >> E_0$) of the spectrum from fusion neutrons. Energetic, non fuel ions are commonly found in thermonuclear plasmas and can be either products of the main fusion reactions (such as α particles from d+t$\rightarrow$n + α) or impurity ions that are heated on purpose. An example of the latter case is given by (^{3}He)D plasmas, where radio frequency heating is applied to ^{3}He ions (here denoted with the symbol τ) that are admixed to bulk D at a typical concentration level $c_\tau \approx 1\%$ [6]. The physics of energetic ions in fusion plasmas is the subject of a vast investigation in several tokamaks [7], given the role of α particles for the self sustainment of a burning plasma. The determination of the fast ion energy distribution lies at the heart of such studies, for example to assess the slowing down of α particles in a DT plasma or the efficiency of RF heating in certain schemes [8].

This work aims at completing the map on nuclear elastic scattering effects induced by energetic ions in the neutron emission spectrum from D and DT plasmas, besides (^{3}He)D and (^{3}He)DT plasmas with RF heating tuned to the fundamental harmonic of ^{3}He. The scope is to identify distinguishable components in the neutron emission spectrum that can be used to diagnose the energy distribution of fast non fuel ions, such as fusion products or τ ions heated by RF. Earlier studies on this topic were presented in references [9-11] for neutron spectroscopy and [12,13] to interpret data from the high energy Neutral Particle Analyzer diagnostic at JET [14]. This work extends the former neutron spectroscopy calculations by considering higher order

processes previously neglected, besides presenting novel results in plasma scenarios not studied before, such as (^{3}He)DT.

The paper is organized as follows. The theoretical framework behind the calculations is presented in section 2, with reference to previous works. In section 3 the obtained results on the neutron emission spectrum, besides knock-on induced distortions in the energy distribution of fuel ions, are summarized. The discussion in section 4 illustrates limitations of the present calculations and investigates diagnostic information on the distribution of fast ions that can be extracted from the measured neutron spectra. The findings of the paper are summarized in the Conclusion.

2. Theoretical framework and plasma conditions

Energetic ions produced by fusion reactions or accelerated by RF heating can suffer knock-on collisions on fuel deuterons and tritons. Knock on collisions result in a source term S(v,θ) of fast deuterons and tritons per unit time in phase space at each pitch angle θ. The source term depends on the energy distribution $F''(v,\theta)$ of fast ions, besides the differential cross section $d\sigma/d\Omega(E,\theta_{c.m.})$ for each scattering process, and can be calculated with a Monte Carlo method (see below) [11]. The presence of S(v,θ) in turn modifies the fuel ion energy distribution, that features a high energy component, $F_{f''}(v)$, resulting from slowing down of collision born suprathermal deuterons and tritons.

$F_{f''}(v,\theta)$ was calculated from integration of the Fokker-Planck equation [15,16] describing fast ion slowing down in a thermal plasma, namely

$$F_{f''}(v,\theta) = \frac{\tau_s}{v^3 + v_C^3} \int_0^{+\infty} v^2 S_{f''}(v,\theta) dv \qquad (1)$$

where τ_s is the Spitzer slowing down time, v the fuel ion velocity and v_C its critical value. Pitch angle scattering is neglected in equation (1) and only slowing down by energy drag is considered. The complete fuel ion energy distribution was obtained by joining the calculated $F_{f''}(v,\theta)$ at each pitch angle to a Maxwellian distribution that describes ions in thermal equilibrium at low energies, in a way similar to that described in references [11,17]. In this way, the complete fuel ion energy distribution $F_f(v,\theta)$ was obtained and was used as input for neutron spectrum calculations.

The neutron emission spectrum was calculated with a Monte Carlo method [18] from the known full energy distributions $F_f(v,\theta)$ of the reactants. Taking as input the motional state of the incident ions, expressed in terms of the relative velocity v_{rel} and the c.m. velocity V_{cm}, the neutron energy E_n in the laboratory frame can be determined from classical kinematics as [19]

$$E_n = \frac{m_C}{m_D + m_C}(Q + K) + V_{c.m}.\cos\theta \left[\frac{2m_D m_C}{m_D + m_C}(Q + K) \right]^{1/2} + \frac{1}{2} m_D V_{c.m.}^2 \qquad (2)$$

Here $K = \frac{1}{2}\mu v_{rel}^2$ is the total incident kinetic energy, μ is the reduced mass, *Q* the reaction Q-value and cosθ is the angle between the neutron velocity in the c.m. frame and $V_{c.m.}$. The neutron spectrum was calculated by sampling the energies of the incident particles. This method was also applied to calculate the fast deuteron and triton source terms S(v,θ) originated from nuclear elastic scattering on fast ions, as the same two-body classical kinematics applies, with the additional condition *Q*=0.

The fast ion content in each plasma scenario (D, DT, (^{3}He)D and (^{3}He)DT) is summarized in Table I and includes both fusion products and impurity ions that are externally heated by RF, such as helions (τ_{RF}). The mean energy of each ion is specified in Figure 1. In a thermal D plasma, fast ions come from the fusion reactions d+d $\rightarrow$ n+τ_1 and d+d $\rightarrow$ p_1+t_1, which have similar cross sections. The subscript 1 is here used to avoid confusion with same ions from different reactions, such as protons (p_3) from the d+$\tau_{RF}\rightarrow\alpha_3$+$p_3$ reaction in (^{3}He)D plasmas. In a DT plasma, α_2 particles are also generated, from d+t$\rightarrow\alpha_2$+n. When a small concentration of ^{3}He is added to a D or DT plasma, fast ^{3}He ions, τ_{RF}, can be accelerated by applying RF heating. These can in turn generate the fusion products α_3 and p_3, from the d+τ_{RF} $\rightarrow$ p_3+α_3 reaction, that add to the plasma fast ion content.

Through elastic scattering, each energetic ion ι produces a distinct fast fuel ion source term $S_\iota(v,\theta)$, that can be calculated with eq. (2). The total source $S_{f''}(v,\theta)$, that appears in eq. (1) and generates $F_{f''}(v,\theta)$ through slowing down, is given by

$$S_{f''}(v,\theta) = \sum_\iota S_\iota(v,\theta) \qquad (3)$$

where the sum is extended to the source terms $S_\iota(v,\theta)$ produced by each scattering process.

The differential cross sections $d\sigma/d\Omega(E,\theta_{c.m.})$ used as input to calculate $S_\iota(v,\theta)$ through equation (2), as well as those for fusion reactions, were taken either from dedicated works published in the literature [9,20,21], or retrieved from Evaluated Nuclear Data Files (ENDF)[1]. Data coverage was adequate in the energy range of interest for the calculations, but for the t+t and t+τ scattering reactions, for which $d\sigma/d\Omega(E,\theta_{c.m.})$ was tabulated up to $E_{c.m.}$=1.5 and 1.0 MeV only, respectively. In these cases, the differential cross section was extrapolated "by-eye " to higher energies, based on the energy dependence manifested at lower energies for each scattering angle in the c.m. frame. While this method is believed to be accurate enough for the t+t

[1] http://www-nds.iaea.org/exfor/endf.htm#1

reaction, the extrapolation for the t+τ reaction was undertaken with added uncertainty. The reason is illustrated in figure 2, where $d\sigma/d\Omega$ for t+τ is compared to that of d+α. For $E_{c.m.}$ < 0.4 MeV, i.e. where the Coulombian contribution to the scattering cross section is dominant, $d\sigma/d\Omega$ is identical for the two processes, due to the fact that t,τ have the same charge as d,α. As the energy is increased, nuclear scattering however dominates and differences are seen in the two cases. In particular, resonances appear for the d+α reaction at $E_{c.m.}\approx 2.3$ MeV and might also be present for t+τ, but were not included in the performed extrapolation. The implications are addressed in the Discussion.

Calculations of the neutron emission spectrum were performed in a point of the plasma, where an electron density of $n_e=5\cdot10^{19}$ m^{-3} and equal electron (T_e) and ion (T_i) temperatures of 5 keV were assumed. A ^{3}He concentration c_τ=1% was chosen when simulating (^{3}He)D and (^{3}He)DT plasmas, with the further prescription $n_d=n_t$ in the latter case. Maxwellian distributions were assumed for bulk fuel ions. The energy distribution $F_\tau(v,\theta)$ of RF accelerated τ_{RF} ions was expressed as

$$F_\tau(v,\theta) = \exp\left(-\frac{E}{T_\tau(E)}\right)\exp\left(-\left(\frac{\theta-\pi/2}{\Delta}\right)^2\right) \quad (4)$$

where $T_\tau(E)$ is the energy dependent tail temperature appearing in the Stix formulation [22] and a full width at half maximum FWHM=2.355·Δ=10° was used for the pitch angle spread. This choice is motivated in reference [11]. For E >> 5 keV, $T_\tau(E)$ reaches the (plasma parameter dependent) asymptotic value T_τ, that is here referred to as the "asymptotic tail temperature". A value T_τ=300 keV was set in the calculations and was later varied to study corresponding changes in the neutron emission spectrum. Neutrons were assumed to be viewed perpendicular to the magnetic field.

3. Results

The calculated slowing down energy distributions of the fusion products p_1, t_1, τ_1 and α_2 in D and DT plasmas are shown in figure 3, assuming plasma parameters specified in section 2. The majority of ions has energies E < 1 MeV, but the slowing down distribution extends up to the fast ion energy at birth $E_o=m_2/(m_1+m_2)\cdot Q$. E_0 depends on the fusion reaction (specified by its Q-value) and on the chosen fusion product of mass m_1, besides the mass m_2 of the remaining product. E_0 values for the fusion reactions considered here are summarized in figure 1 and Table I. As a result of the finite plasma ion temperature some particles have energies extending beyond E_0, which correspond to tails at E>E_0 in figure 3. This is a known feature of the slowing down energy distribution of fusion products as pointed out, for instance, in reference [9].

Figure 4 shows the fast deuteron and triton source terms $S(v,\theta)$ resulting from nuclear elastic scattering collisions between ions in figure 2 and the bulk plasma. The contribution of each collision process has a relative magnitude that varies case by case. In a D plasma, p_1+d scattering is the dominant process, with a contribution from t_1+d scattering in the region E < 1 MeV. Protons, born at energy $E_0 \approx 3.02$ MeV from the d+d→ p+t reaction, are on average more energetic than t_1 and τ_1 ($E_0 \approx 1.01$ MeV and 0.82 MeV, respectively) and can thus more efficiently transfer energy to bulk ions. When α_2 particles are generated by d+t fusion reaction, however, α_2 scattering dominates over all other nuclear processes by 1 to 2 orders of magnitude at high energies, say E > 1 MeV. This fact is not surprising, as the reactivity for the d+t→α+n reaction is about 2 orders of magnitude higher than both d+d→^{3}He+n and d+d→p+t, while the order of magnitude of the cross section for nuclear elastic scattering of fast fusion products on bulk ions is about the same for the different species. Besides, α particles are born at $E_0 \approx 3.52$ MeV, a value that is much higher than the energy of p_1 protons at birth. From figure 4, it is also seen that the source terms for fast deuterons and tritons are similar.

In RF heated (^{3}He)D and (^{3}He)DT plasmas a small amount of ^{3}He is added to the bulk plasma and is externally heated by RF waves. Figure 5 shows the energy distribution of τ_{RF} ions accelerated to an asymptotic temperature T_τ=300 keV and described by equation (4). The presence of a fast population of τ_{RF} ions enhances the reactivity for the d+τ_{RF}→α_3+p_3 reaction. The energy distribution of α_3 and p_3 is also shown in figure 5 and shares features similar to those described for figure 3.

The corresponding fast deuteron and triton source terms $S(v,\theta)$ are shown in figure 6. τ_{RF} knock on is the dominating process for E < 3 MeV and results in a decaying component with exponential slope. This feature was previously noted in the dedicated study of reference [11]. For E > 3 MeV, the contribution from nuclear elastic collision of p_3 protons emerges and extends to energies higher than 8 MeV, up to about 13 MeV and 11 MeV for scattering on deuterons and tritons, respectively. α_3 knock on is negligible in all energy ranges. As already observed for the DT plasma case, the source terms for fast deuterons and tritons are qualitatively similar, although quantitative differences appear and can be ascribed to differences in the scattering cross sections. The absolute scale of the source terms in figure 6 can be compared to that of figure 4. The comparison reveals that τ_{RF} knock on is about a 100 times more efficient source of fast fuel ions than α_2 nuclear elastic scattering, that is the dominant process in a DT plasma. p_3 knock-on is responsible for fast fuel ions at energies above E = 3.5 MeV in D or DT plasmas with a population of ^{3}He ions heated by RF.

The equilibrium fuel ion energy distribution $F(v,\theta)$, that takes into account contributions from the mentioned scattering processes, is shown in figure 7 for deuterons and tritons. Nuclear elastic scattering is manifested as deviations from the Maxwellian distribution at energies as low as ≈ 100 keV, where tails corresponding to suprathermal particles are seen and extend to energies in the MeV range. The level of the tails is between 10^{-8} and 10^{-4} with respect to the peak value of the distribution, with variations depending on the plasma

admixture. Distortions from a Maxwellian distribution are more pronounced in plasmas containing RF heated τ_{RF} ions, as was found for the source terms.

The neutron emission spectra calculated from the results of figure 7 are shown in figure 8 and 9. Although the calculations behind the spectra were performed considering all relevant scattering processes described in Table I, only those components that give a non negligible contribution to the total spectrum are separately marked in the figures. The neutron spectra present low and high energy tails as a result of d+d and d+t reactions between suprathermal and bulk ions, with an asymmetry for neutron producing d+d reactions that was already described in [11] as being of kinematic origin. The amplitude of the neutron component from each nuclear elastic scattering process reflects the magnitude of the corresponding contribution to the fast d,t source terms. This is, for instance, shown by the d+d neutron spectrum in the D plasma of figure 8 (top), where the total spectrum almost coincides with that calculated considering the contribution from p_1+d scattering reactions only, as it was found for the source term of figure 4; τ_1+d and t_1+d scattering contribute only to a 30% enhancement of the number of neutrons in the narrow energy range from E_n=3 MeV to 3.2 MeV.

A similar argument applies for 14 MeV neutrons produced by d+t reactions in a DT plasmas. Here α_2 knock on is the dominating process, besides a component from triton burn up (TBN) that compares to α_2 knock on in the energy region E_n=11 to 18 MeV. Triton burn up neutrons are generated by reactions between burn up t_1 tritons from the d+d$\rightarrow$ p + t_1 reaction, that in turn produce 14 MeV neutrons through d+$t_1\rightarrow\alpha$+n [23].

The addition of RF heated τ_{RF} ions in the plasma admixture significantly changes the neutron spectrum. τ_{RF} knock on by far dominates over any other nuclear elastic scattering process from fusion products, with the exception of p_3 knock on. The latter manifests itself as a component extending to high energies from E_n=4.5 and 18 MeV in the neutron emission spectrum of (^{3}He)D and (^{3}He)DT plasmas respectively. The relative magnitude of these components in the neutron spectrum again reflects that in the source terms of figure 6.

4. Discussion

Uncertainties on nuclear elastic scattering cross sections are a source of systematic error in the calculated neutron emission spectra of figure 7 and 8. As stated in section 2, the completeness of nuclear elastic scattering cross section data was acceptable for all reactions but for t+t and t+τ scattering. In these cases, extrapolations were made, which might have led to underestimations of the true cross section values, as possible resonances in the MeV range were neglected (figure 2). An error on the t+t cross section is judged to be of minor relevance, as t+t is generally an ignorable process, but in the neutron spectrum of D plasmas, where it is manifested as an excess of events at a level of 30% in the region 3.0< E_n <3.2 MeV only. The uncertainty on t+τ has in principle a stronger impact on the calculated neutron spectrum, as t+τ_{RF} scattering is responsible for the dominating high energy component in the neutron spectrum of RF heated (^{3}He)DT

plasmas shown in figure 9. However, the resulting systematic error on the neutron spectrum can be estimated to be of the order of unity at most, which does not change the overall picture at a qualitative level. A further source of uncertainty comes from the confinement of d+τ fusion born 14.7 MeV protons, that were assumed to be fully confined in the simulations, but are likely to be affected by prompt losses in real experiments. This would affect components produced by p_3 scattering, that might have a more pronounced fall off at high neutron energies than that shown in figures 8 and 9.

The calculated neutron spectra presented in section 3 are of relevance for diagnostics of fast ions and fusion products, as changes in their energy distribution could be tracked by observing modifications to the corresponding spectral signature in the neutron emission from a burning plasma. The relevance of the α knock on component in the spectrum from DT plasma has been already discussed in references [9,10] and hinges upon the possibility to study anomalies affecting the slowing down of α particles in a burning plasma by measuring neutron emission in the energy region E_n > 15 MeV. A difficulty in the interpretation of neutron emission for E_n > 15 MeV can however arise from TBN neutrons, that interfere with the α knock on spectral component in a DT plasma as shown in figure 9 for T_i=5 keV. Interference from other scattering processes, such as p_1 knock on, was here ruled out. The relative importance of TBN and α knock-on in producing E_n > 15 MeV neutrons is studied in figure 10, where calculations of the neutron emission spectrum from a DT plasma are performed assuming higher T_e=T_i bulk temperatures set at the values 10 and 20 keV respectively. TBN neutrons are of relevance at low T_i only and are negligible at the higher temperatures expected in a burning plasma. A similar result also holds if T_i only is increased, maintaining T_e constant. This in particular reveals that slowing down, which is affected by changes in T_e, has a weaker role in determining the relative magnitude of the α knock on and TBN components. The negligible effects of scattering processes besides α_2 knock on in DT plasmas, together with the limited importance of TBN for T_i>5 keV, further confirms the interpretation of counts at E_n>15 MeV in the neutron spectrum from reference [10] as originating from α_2 knock on only.

The neutron spectrum from RF heated (^{3}He)D plasmas was previously studied in reference [11], where it was found that the slope of the high energy component produced by τ_{RF} knock on is proportional to the asymptotic tail temperature T_τ of τ_{RF} ions. Those calculations were here extended by including the effect of second order processes, such as collisions from fusion born p_3 and α_3 ions. Besides, a similar study for a (^{3}He)DT plasma was also undertaken. Proton knock on was found to result in an additional high energy tail, from E_n=4.5 MeV and E_n=18 MeV in the neutron spectrum from (^{3}He)D and (^{3}He)DT plasmas, respectively. The magnitude of this component is however of decreasing importance as T_τ is raised from 300 keV to 700 keV, as shown with the results of figure 11 and 12, where τ_{RF} knock on is by far the dominating process. This makes it almost impossible to study fusion born p_3 protons from the neutron emission spectrum at high T_τ. Besides, information on α_2 particles produced by the d+t reaction is lost already at relatively low T_τ

temperatures (say, $T_\tau \geq 300$ keV) in a (^{3}He)DT plasma. On the other hand, the τ_{RF} component shows significant variations in slope and magnitude also for a (^{3}He)DT plasma, in a way similar to the findings for the (^{3}He)D plasma case of reference [11], and can be used to study the energy distribution of τ_{RF} ions accelerated by radio frequency.

The results of this study show that p_1 knock on in D plasmas, α_2 knock on in DT plasmas and τ_{RF} knock on in (^{3}He)D and (^{3}He)DT plasmas are manifested as distinguishable high energy components in the neutron emission spectrum. The relative intensity of these spectral features with respect to the peak from thermal emission can be compared with the present sensitivity of advanced neutron spectrometers. The instruments that have demonstrated the best performance so far in magnetic confinement devices were MPR [2] for 14 MeV and TOFOR [1,24] for 2.5 MeV neutrons. These detectors, based on different principles, can distinguish spectral features at a level of about 10^{-5} and 10^{-3} with respect to the thermal emission peak and are therefore suitable for observation of α_2 and τ_{RF} knock on signature in the neutron emission spectrum from DT, (^{3}He)D and (^{3}He)DT plasmas. p_1 knock on in D plasmas appears at a level about 100 times lower than the quoted TOFOR instrumental sensitivity and might be observed only if significant advances are made in spectrometers for 2.5 MeV neutrons, particularly in the field of background rejection, that is presently the main limiting factor of such instruments [24]. All other knock on signatures are within the present instrumental sensitivity, or even significantly above, such are τ_{RF} knock on in (^{3}He)DT plasmas.

The results presented in this paper were obtained with simplified assumptions on plasma parameters and energy distributions. The purpose was to have a complete map of the role of fast ion and fusion product scattering processes in the neutron emission spectrum from D, DT, (^{3}He)DT and (^{3}He)DT plasmas. The calculations aimed at elucidating the relative magnitude of different processes, rather than to provide results at a quantitative accuracy suitable for comparison with measurements. Besides, this work does not deal with aspects that are expected to complicate the interpretation of neutron emission spectra in real measurements, such as distortions of the fuel ion energy distribution due to parasitic absorption of the RF power. This, for example, is of particular relevance in (^{3}He)DT plasmas, where parasitic absorption from bulk tritons is expected, as triton 2nd harmonic ion cyclotron frequency coincides with first harmonic τ_{RF}. A dedicated work was performed in reference [25], where the effect of α_2 knock on in the neutron spectrum from (^{3}He)DT plasmas was calculated for a standard ITER scenario with the input of realistic fuel ion distributions, that included distortion from parasitic RF power absorption by tritons. The results showed that the distortion is manifested as a high energy component at the level of that from α_2 knock on, with quantitative changes depending on details of the heating parameters. It is to be noted, however, that τ_{RF} knock on was not considered in reference [25], although, from the results of figure 9, this is expected to be the dominant spectral component at E_n>15 MeV, already for T_τ=300 keV. The distribution used as input in reference [25] had $T_\tau \approx 1$ MeV.

Recent experiments performed in RF heated (^{3}He)D plasmas with injected ^{9}Be impurities have shown that neutrons from the ^{9}Be(^{3}He,n)^{11}C reaction can appear along the spectral tails from τ_{RF} knock on [26]. ^{9}Be is expected to be found as impurity in plasmas of next generation devices, such as ITER, given the composition of the tokamak walls. Besides the ^{9}Be(^{3}He,n)^{11}C reaction, an additional source of neutrons in DT plasmas is expected to come from the ^{9}Be(α,n)^{12}C reaction [27], due to fusion born α particles. These processes must be included for the interpretation of neutron emission measurements from a real experiments, but its inclusion goes beyond the scope of this work, that is focused on effects from scattering processes only.

5. Conclusion

In this work the neutron emission spectrum from D and DT plasmas, besides (^{3}He)D and (^{3}He)DT with RF heating tuned to the fundamental ^{3}He ion cyclotron harmonic, was determined. The calculations included distortions of the fuel ion energy distribution produced by knock on effects of energetic ions, that were shown to result in distinctive components in the high energy part of the neutron spectrum. Proton knock on collisions produce high energy components in the neutron spectrum of D plasmas, at a level of 10^{-5} with respect to the peak from thermal emission, that might be too low to be observed given the sensitivity of current neutron spectrometers. In DT plasmas, α knock on is manifested for E_n > 15 MeV and dominates over other scattering processes, but for triton burn up neutrons, that give a comparable contribution at low Ti only. When ^{3}He is admixed to the plasma and heated by RF, τ knock on dominates the high energy region of the neutron spectrum both in (^{3}He)D and (^{3}He)DT plasmas. Protons produced by the d+$\tau\rightarrow\alpha$+p reaction contribute to a further distinguishable component at low τ temperatures only.

The results presented in this paper complete the map on nuclear elastic scattering effects induced by energetic ions in the neutron emission spectrum from D and DT plasmas, besides (^{3}He)D and (^{3}He)DT with RF heating tuned to the fundamental harmonic of ^{3}He, and are of relevance for diagnostics of fusion born α particles and radio frequency heated τ ions through neutron emission spectroscopy in fusion plasmas.

References

[1] Gatu Johnson M *et al.* 2006 *Rev. Sci. Instrum*. **77**, 10E702

[2] Ericsson G, Ballabio L, Conroy S, Frenje J, Henriksson H, Hjalmarsson A, Källne J and Tardocchi M 2001 *Rev. Sci. Instrum*. **72**, 759

[3] Faust W R and Harris E G 1960 *Nucl. Fusion* **1**, 62

[4] Hellesen C *et al.* 2010 *Plasma Phys. Control. Fusion* **52**, 085013

[5] Hellesen C *et al.* 2010 *Nucl. Fusion* **50** 084006

[6] Van Eester D *et al.* 2009 *Plasma Phys. Control. Fusion* **51** 044007

[7] Breizman B N and Sharapov S E 2011 *Plasma Phys. Control. Fusion* **53** 054001

[8] Lerche E *et al*. 2011 *Plasma Phys. Control. Fusion* **53**, 124019

[9] Ballabio L, Gorini G and Källne J 1997 *Phys. Review E* **55**, 3358

[10] Källne J, Ballabio L, Frenje J, Conroy S, Ericsson G, Tardocchi M, Traneus E and Gorini G 2000 *Phys. Rev. Lett.* **85** 1246

[11] Nocente M, Gorini G, Källne J and Tardocchi M 2011 *Nucl. Fusion* **51**, 063011

[12] Korotkov AA, Gondhalekar A and Akers R J 2000 *Phys. of Plasmas* **7** 957

[13] Zaitsev F S, Gondhalekar A, Johnson T J, Sharapov S E, Testa D S, Kurbet I I 2007 *Plasma Phys. Control. Fusion* **49** 1747

[14] Kislyakov A I, Khudoleev A V, Kozlovskij S S and Petrov M P 1997 *Fusion Eng. Des.* **34** 107

[15] Trubnikov B A 1965 *Reviews of Plasma Physics* **1**105

[16] Sivukhin D V 1966 *Reviews of Plasma Physics* **4** 93

[17] Helander P, Lisak M and Ryutov D D 1992 *Plasma Phys. Control. Fusion* **35** 363

[18] Ballabio L, Calculation and measurement of the neutron emission spectrum due to thermonuclear and higher-order reactions in tokamak plasmas, *PhD Thesis, Acta Universitatis Upsaliensis No 797,* Faculty of Science and Technology, Uppsala University

[19] Brysk H 1973 *Plasma Phys.* **15** 611

[20] Nocente M, Gorini G, Källne J and Tardocchi M 2010 *Nucl. Fusion* **50**, 055001

[21] Ognissanto F, Gorini G, Källne J, Ballabio L, Nocente M and Tardocchi M 2011 *Nucl. Instrum. Meth. B* **269**, 786

[22] Stix T H 1975 *Nucl. Fusion* **15** 1063

[23] Ballabio L, Frenje J, Källne J, Conroy S W, Ericsson G, Tardocchi M, Traneus E, Gorini G 2000 *Nucl. Fusion* **40**, 21

[24] Gatu Johnson M *et al.* 2008 *Nucl. Instrum. Meth. A* **591**, 417

[25] Eriksson L-G *et al*. 2007 Final report on the EFDA task TW6-TPDS-DIADEV: ICRF, NBI and ITER diagnostics

[26] Gatu Johnson M *et al.* 2010 *Nucl. Fusion* **50** 045005

[27] Gatu Johnson M *et al.* 2010 *Rev. Sci. Instrum*. **81** 10D336

Figures

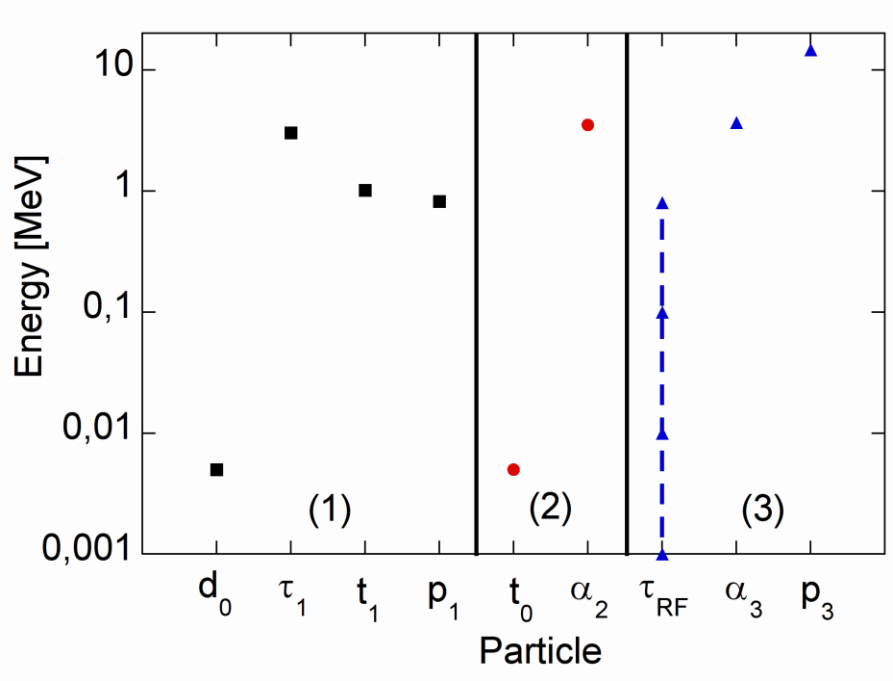

Figure 1. Scheme of suprathermal and thermal ions found in D, DT, (^{3}He)D and (^{3}He)DT plasmas. The mean energy of each ion is indicated on the y axis. The adopted notation is that of Table I.

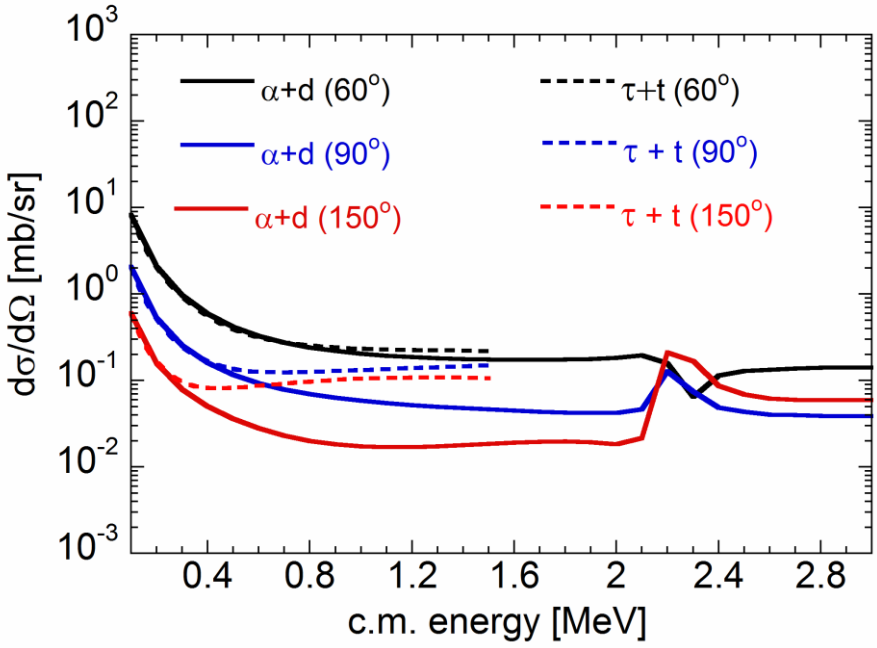

Figure 2. Comparison of the differential cross sections for the nuclear elastic scattering reactions α+d and τ+t at different c.m. energies and scattering angles θ in the c.m. frame.

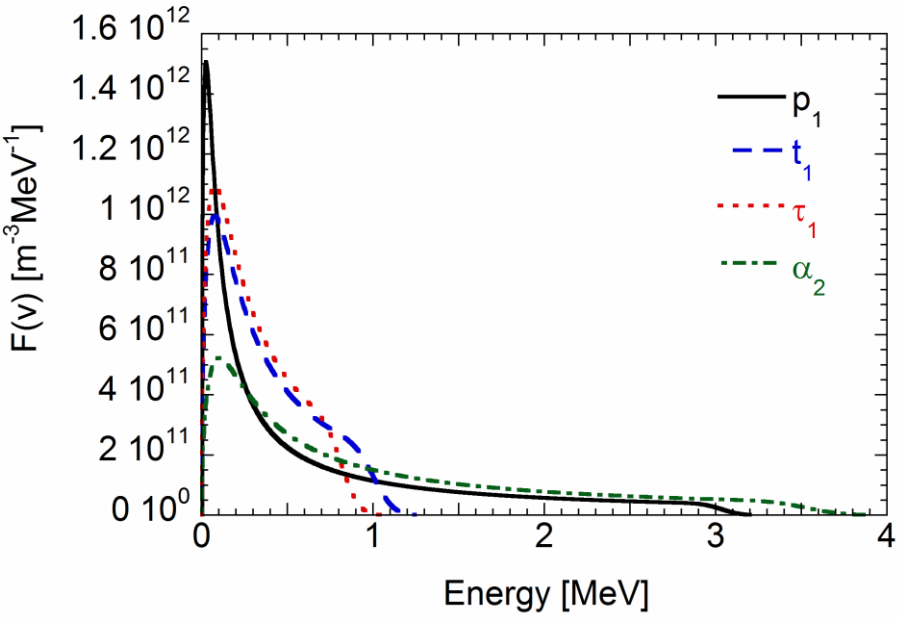

Figure 3. Slowing down energy distributions of p_1, t_1 and τ_1 ions in a D plasma, besides α_2 in a DT plasma.

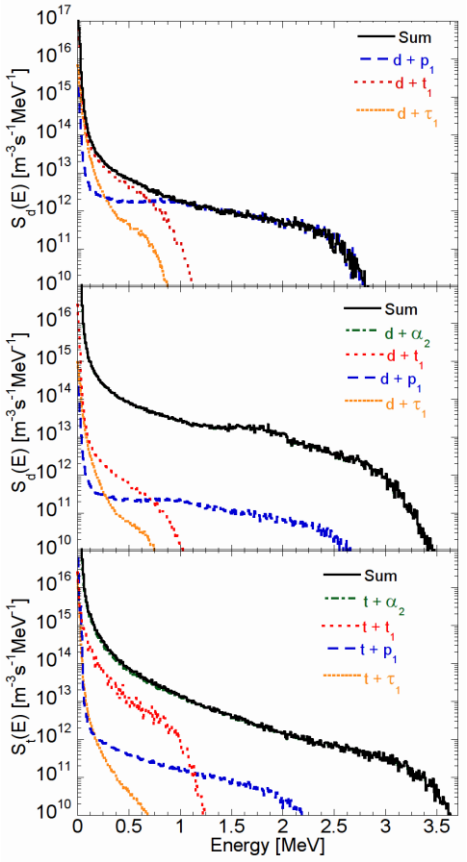

Figure 4. Fast deuteron source terms S(v,θ=90°) produced by nuclear elastic scattering of fast ions in D (top panel) and DT (middle panel) plasmas. The bottom panel shows the fast triton source term in a DT plasma. In DT plasmas α_2 knock on dominates the source term of fast fuel ions.

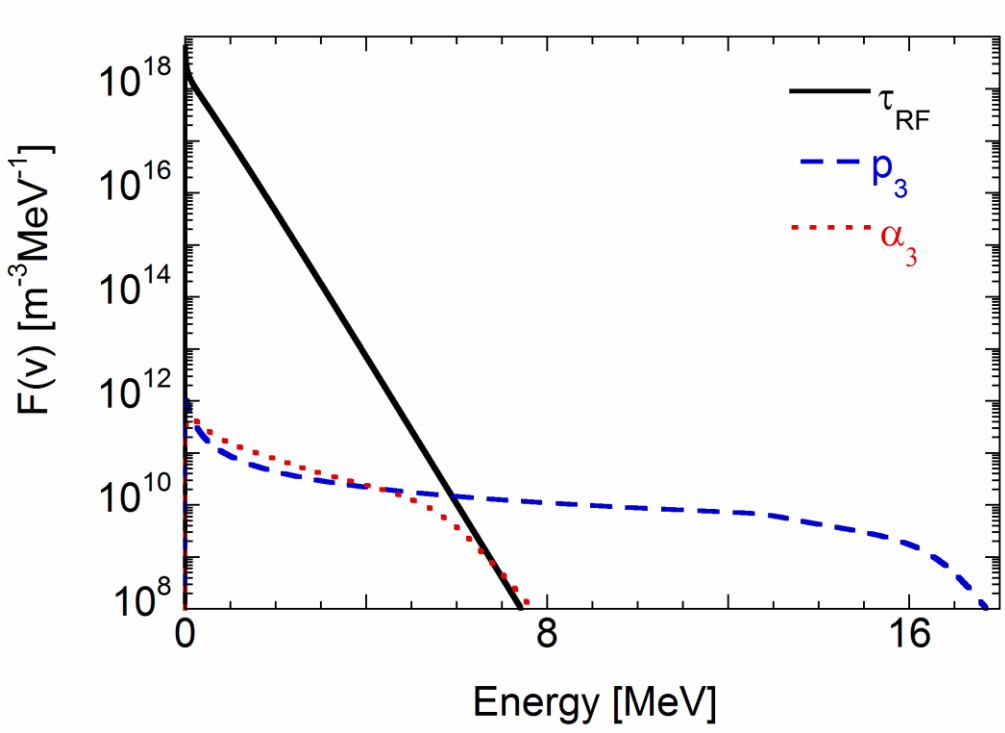

Figure 5. Slowing down energy distribution of τ_{RF}, α_3 and p_3 ions in a (^{3}He)D plasma

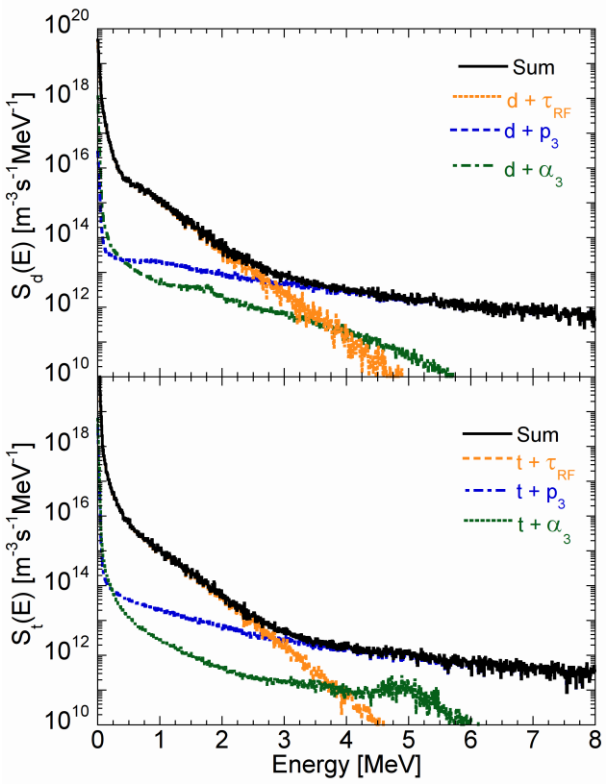

Figure 6. Fast deuteron (top) and triton (bottom) source terms S(v,θ=90°) in a (^{3}He)DT plasma considering nuclear elastic collisions induced by τ_{RF}, besides α_3 and p_3 fusion products from the $d+\tau_{RF}\rightarrow\alpha_3+p_3$ reaction.

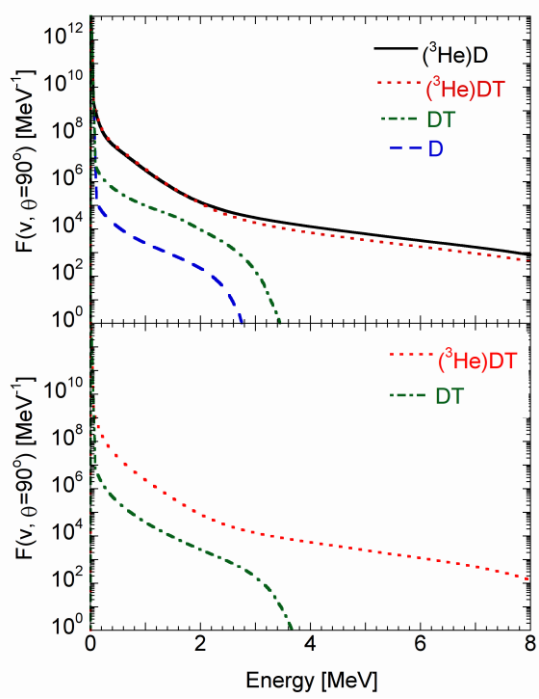

Figure 7. Slowing down energy distribution of fuel deuterons (top) and tritons (bottom) including distortions due to knock on reactions from fast ions in D, DT, (^{3}He)D and (^{3}He)DT plasmas.

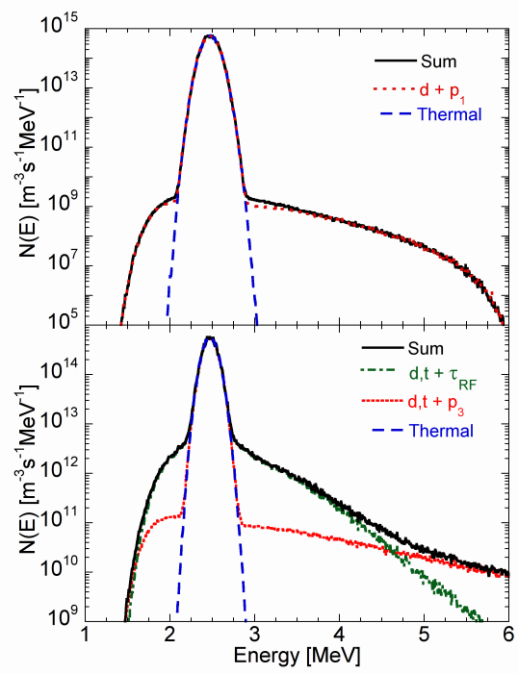

Figure 8. Neutron spectrum from D and (^{3}He)D plasmas including components due to different knock-on processes from fast ions. Only distinguishable components are shown in the figure and are labelled by the corresponding scattering process. The expected neutron spectrum from a thermal D plasma is also shown for comparison.

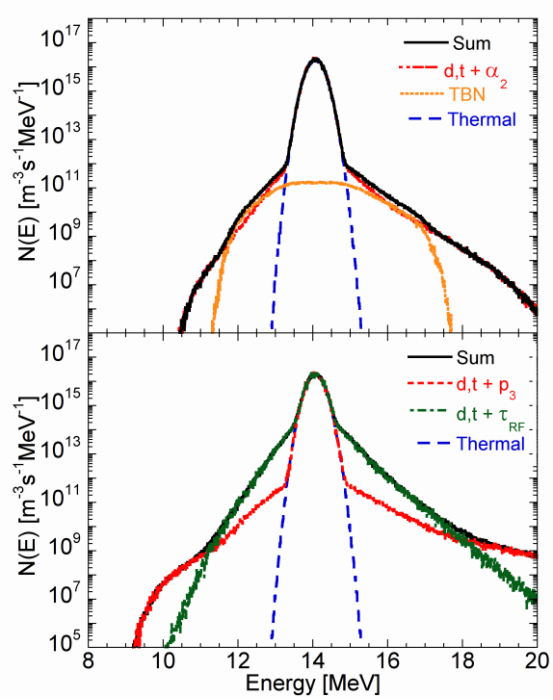

Figure 9. Neutron spectrum from DT and (^{3}He)DT plasmas including components due to different knock-on processes from fast ions. Only distinguishable components are shown in the figure and are labelled by the corresponding scattering process. The expected neutron spectrum from a thermal DT plasma is also shown for comparison.

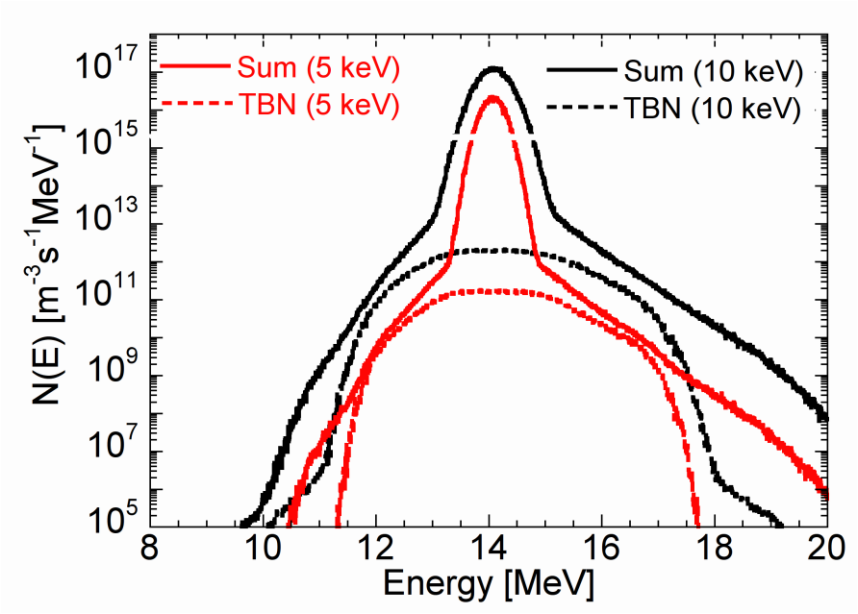

Figure 10. Comparison between the neutron spectrum from DT plasmas at T_i=5 keV and T_i=10 keV. The spectrum includes effects of knock on collisions from fast ions, besides triton burn up neutrons.

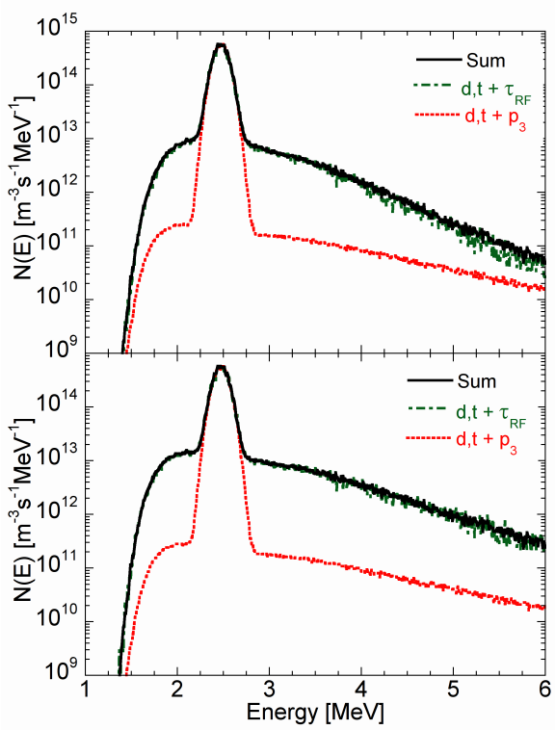

Figure 11. Neutron spectrum from a (^{3}He)D plasma with RF heating applied to ^{3}He at tail temperatures T_τ=500 keV (top) and T_τ=700 keV (bottom).

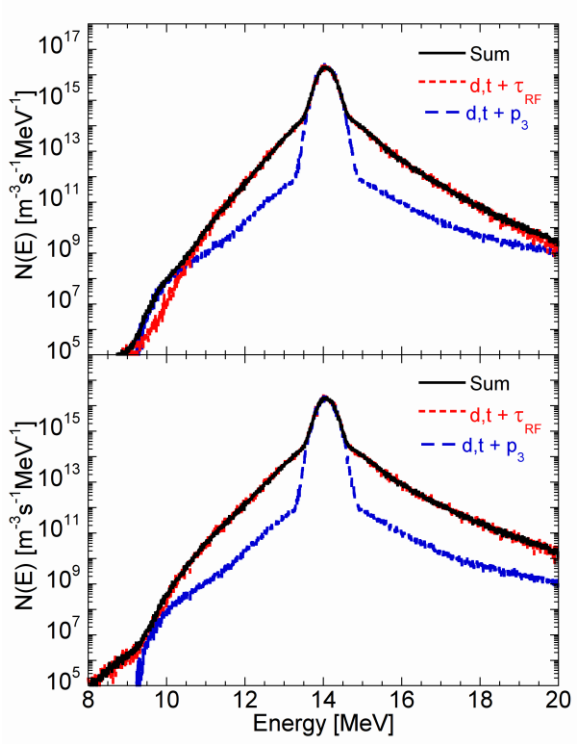

Figure 12. Neutron spectrum from a (^{3}He)DT plasma with RF heating applied to ^{3}He at tail temperatures T_τ=500 keV (top) and T_τ=700 keV (bottom).

List of tables

Table I Summary of ion populations organized by groups in D and DT plasmas without and with RF heating on a ^{3}He minority component. The τ_{RF} energy is given as the asymptotic tail temperature T_τ (equation 4). Ions of groups (1) and (2) are those found in D and DT plasmas, respectively; a (^{3}He)D plasma includes ions of group (1)+(3). Ions belonging to groups (1)+(2)+(3) are found in (^{3}He)DT plasmas.

Group number	Ion (mean energy in MeV)
(1)	d_0 (0.005), p_1 (3.0), t_1 (1.0),τ_1 (0.82)
(2)	t_0(0.005), α_2 (3.5)
(3)	τ_{RF} (0-0.7), p_3 (14.7), α_3 (3.7)

Paper IV

The $^{12}C(^3He,p\gamma)^{14}N$ reaction cross section for γ-ray spectroscopy simulation of fusion plasmas[a)]

I. Proverbio,[1] M. Nocente,[1,b)] V. G. Kiptily,[2] M. Tardocchi,[1] G. Gorini,[1] and JET-EFDA Contributors[3,c)]

[1]*Dipartimento di Fisica, Università degli Studi di Milano-Bicocca and Istituto di Fisica del Plasma, EURATOM-ENEA-CNR, 20125 Milano, Italy*

[2]*Culham Centre for Fusion Energy, Culham Science Centre, Abingdon, Oxfordshire OX14 3DB, United Kingdom*

[3]*JET-EFDA, Culham Science Centre, Abingdon OX14 3DB, United Kingdom*

(Presented 17 May 2010; received 16 May 2010; accepted 2 June 2010; published online 26 October 2010)

High resolution γ-ray spectroscopy measurements were performed in JET (^{3}He)D plasmas with high energy ion populations driven by radio-frequency (RF) heating. One of the first reactions investigated was $^{12}C(^3He,p\gamma)^{14}N$, which was observed at low ^{3}He concentrations. In order to interpret the measurements in this work, cross section data for the $^{12}C(^3He,p\gamma)^{14}N$ reaction are evaluated. Available data for the population of excited states in ^{14}N up to the eighth level are assessed in the range $E_{3He}=0-5$ MeV. Discrepancies and gaps in the database have been solved by means of interpolations and consistency analysis. The evaluated cross section data are used to predict the intensity ratio of characteristic 2.31 and 1.63 MeV γ-rays. [doi:10.1063/1.3502037]

I. INTRODUCTION

γ-ray spectrometry is in use at the JET fusion experiment as a diagnostics of energetic ions with energies in the range of 0.5–5.0 MeV.[1] These are created in JET (^{3}He)D plasmas by ion cyclotron resonance heating (ICRH) tuned to the first harmonic frequency of minority ^{3}He ions. When the injected RF power is above 4 MW and at low ^{3}He concentrations ($X[^3He]<10\%$) energetic tails in the ^{3}He energy distribution function are driven. Depending on $X[^3He]$, minority heating regimes were achieved, while strong MHD activity was observed for very low ^{3}He concentrations (for example, $X[^3He]<1\%$).[2] Typical measurements involve the observation of γ-ray emission peaks due to reactions between light plasma impurities and fast ions produced by ICRH. A good example is the $^{12}C(^3He,p\gamma)^{14}N$ reaction. Emitted γ-rays have typical energies of $E_{\gamma 1}=2.31$ and $E_{\gamma 2}=1.63$ MeV that are well within the range of available spectrometers. Somewhat more challenging is the interpretation of the measurements. The $^{12}C(^3He,p\gamma)^{14}N$ reaction is exothermic, with a Q value of 4.78 MeV, which exceeds the energy of the first two ^{14}N excited states at 2.31 and 3.95 MeV. Gamma ray emission is negligible for $E_{3He}<1$ MeV. At ^{3}He energies in the MeV range, ^{14}N excited states higher than the second contribute to the peaks at $E_{\gamma 1}$ and $E_{\gamma 2}$ through cascade transitions (Fig. 1 and Table I). A good knowledge of the reaction cross sections for the population up to the eighth excited state of ^{14}N is required for accurate simulations of the I_1/I_2 intensity ratio in the range $E_{3He}=0-5$ MeV. However, available data[3–7] show discrepancies and gaps in the database that are solved here by means of interpolations and consistency analysis. The evaluated differential cross section data $d\sigma_i/d\Omega$ and $(i=1-8)$ are used to predict the intensity ratio of characteristic γ-rays at $E_{\gamma 1}=2.31$ and $E_{\gamma 2}=1.63$ MeV.

II. CROSS SECTION DATA AND INTERPOLATIONS

Available cross section data for the $^{12}C(^3He,p\gamma)^{14}N$ reaction were obtained at accelerators with ^{3}He beams in the energy range $E_{3He}=1.1-5.5$ MeV (laboratory system). The available data can be divided into two groups. The first group[3–5] contains data from experiments aimed at a systematic investigation of ^{15}O nuclear structure and decays. Data on the proton angular distributions (differential cross sections $d\sigma_i/d\Omega$) at selected angles are provided as a function of E_{3He} for several excited states of ^{14}N, as well as $d\sigma_i/d\Omega(\theta)$ data provided for the full angular range of 0°–180° at selected energies. A second more recent set of measurements[6,7] was motivated by the interest in an alternative technique for profiling ^{12}C below a surface. The differential cross section $d\sigma/d\Omega(\theta=90°)$ was measured in the energy range $E_{3\,He}=1.5-3$ MeV for the ground, first, and second ^{14}N excited states, and in the range $E_{3He}=2-3$ MeV for the third and fourth excited states. No information is provided by the more recent measurements on higher excited states, nor on the angular dependence of the cross section.

The available data set above $E_{3He}=3$ MeV is complete and consistent and does not require corrections or interpola-

[a)]Contributed paper, published as part of the Proceedings of the 18th Topical Conference on High-Temperature Plasma Diagnostics, Wildwood, New Jersey, May 2010.

[b)]Author to whom correspondence should be addressed. Electronic mail: massimo.nocente@mib.infn.it.

[c)]See the Appendix of F. Romanelli *et al.*, Proceedings of the 22nd IAEA Fusion Energy Conference, Geneva, Switzerland, 2008 and the Appendix of Nucl. Fusion 49, 104006 (2009).

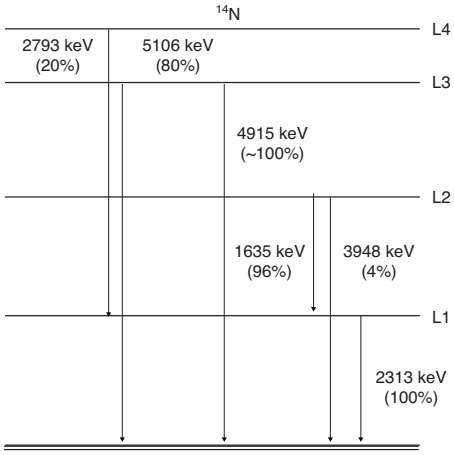

FIG. 1. Level scheme for the first four excited levels of ^{14}N nucleus. The branching ratios for allowed transitions are indicated.

tions. The situation is less satisfactory in the range 1 MeV $<E_{3He}<3$ MeV. This is illustrated in Fig. 2, where some cross section data from Refs. 3 and 7 are shown. The main observations are the following.

(i) Above $E_{3He}=1.8$ MeV, data for $d\sigma_1/d\Omega(\theta=90°)$ from Ref. 3 are systematically underestimated if compared to those of Ref. 7, whose values are, however, in agreement with Ref. 6. The same is also true when comparing data for $d\sigma_2/d\Omega(\theta=90°)$.

(ii) Data at $E_{3He}=2$ MeV indicate that $d\sigma_4/d\Omega(\theta=90°)$ is higher than $d\sigma_4/d\Omega(\theta=90°)$, and $d\sigma_2/d\Omega(\theta=90°)$ for $E_{3He}<2$ MeV; however, no $d\sigma_4/d\Omega(\theta=90°)$ values are available below $E_{3He}<2$ MeV.

In order to obtain the complete differential cross section in the range $E_{3He}=0-5$ MeV, data on $d\sigma_i/d\Omega$, (θ), and $(i=1-8)$ were completed with suitable interpolations and extrapolations. To fill in the gap in the data for $d\sigma_4/d\Omega(\theta=90°)$ below 2 MeV, an exponential extrapolation with slope taken from the data in the range $E_{3He}=2.0-2.5$ MeV was performed down to $E_{3He}=1.4$ MeV. A second exponential extrapolation was used to produce data in the range $E_{3He}=0-1.4$ MeV with a slope chosen so as to have $d\sigma_4/d\Omega$, $(\theta=90°)=d\sigma_1/d\Omega$, and $(\theta=90°)$ at $E_{3He}=1.1$ MeV. Below this value, $d\sigma_i/d\Omega(\theta=90°)$ was assumed to be the same for $i=1,2,4$. The latter choice is based on the observation that $d\sigma_1/d\Omega(\theta=90°)$ and $d\sigma_2/d\Omega(\theta=90°)$ are almost equal in the range $E_{3He}<1.8$ MeV (Fig. 2). For higher excited states,

TABLE I. Energies of the first eight ^{14}N excited states.

Level	Energy (keV)
L1	2313
L2	3948
L3	4915
L4	5106
L5	5691
L6	5834
L7	6204
L8	6446

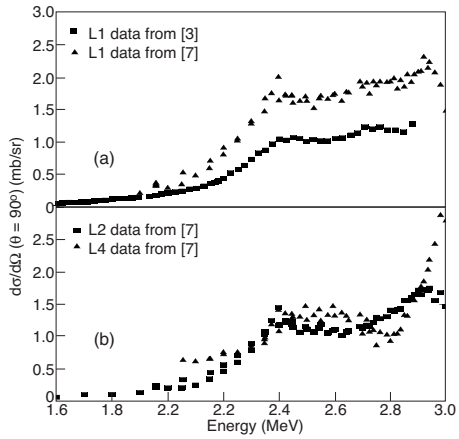

FIG. 2. (a) Differential cross section $d\sigma/d\Omega(\theta=90°)$ for the reaction $^{12}C(^3He,p\gamma)^{14}N$ populating the first excited state of ^{14}N. Data taken from Ref. 7. Cross section data from Ref. 3 are also shown for comparison. (b) Same as (a) but for the second and fourth excited states of ^{14}N. Data for the fourth excited state are not available for $E_{3He}<2$ MeV.

$(i=5-8)$ and $d\sigma_i/d\Omega=0$ was assumed in the energy range of up to $E_{3He}=2$ MeV, where no experimental data are available. Data from Ref. 3 were used for $d\sigma_1/d\Omega(\theta=90°)$ and $d\sigma_2/d\Omega(\theta=90°)$ only in the range $E_{3He}=1.1-1.6$ MeV, while data from Ref. 7 were used wherever available below $E_{3He}=3$ MeV. Above this energy, data availability was sufficiently adequate for all levels to avoid interpolations for $d\sigma_i/d\Omega$ and $(i=1-8)$. In this way, $d\sigma_i/d\Omega(\theta=90°)$ was determined at all energies up to 5 MeV.

The total cross section σ_i for populating the *i*th excited level was calculated by assigning the angular dependence of the differential cross sections as a function of E_{3He}. This was available (e.g., from Ref. 3) for a number of E_{3He} energies. Available information was completed by linear interpolation from values at the nearest neighbor points, including a point at $E_{3He}=0$ MeV, where cross section isotropy was assumed.

The resulting cross section values are shown in Fig. 3. For $E_{3He}<2$ MeV, only the cross sections for the population of the first, second, and fourth excited states contribute to γ-ray emission (the third excited state is disregarded here

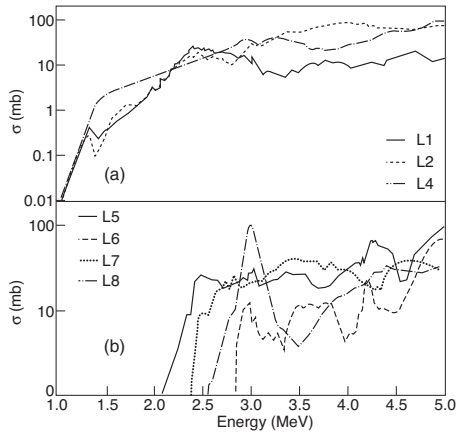

FIG. 3. (a) Excitation functions (integral cross sections) for the first to the fourth ^{14}N states populated in the $^{12}C(^3He,p\gamma)^{14}N$ reaction obtained from the interpolations of experimental data. (b) Same as (a) but for the fifth to the eight excited states of ^{14}N.

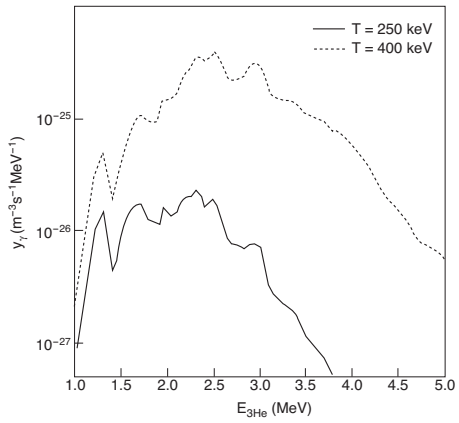

FIG. 4. Differential reactivity for the production of 2.31 MeV γ-rays assuming Maxwellian ^{3}He ions with tail temperatures equal to 250 (solid line) and 400 keV (dashed line).

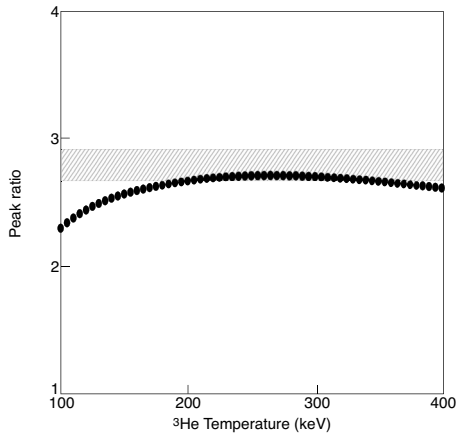

FIG. 5. Intensity ratio of 1.63 and 2.31 MeV γ-rays from the $^{12}C(^3He,p\gamma)^{14}N$ reaction for Maxwellian ^{3}He ions of different temperatures. The shadowed band is the intensity ratio determined from experimental data.

because it does not yield γ-rays of $E_{\gamma 1}=2.31$ MeV or $E_{\gamma 2}=1.63$ MeV). The general trend is that of an exponential, but for a resonance in the cross section for the first and second excited states at $E_{3He}=1.3$ MeV, followed by a second broader resonance for the second excited state at $E_{3He}=1.6$ MeV. Above $E_{3He}=2$ MeV, higher excited states start to be populated and contribute to γ-ray emission. This is particularly true for the fifth and seventh excited states with a cross section about half of that for the second state, which is the largest in this energy range.

III. REACTIVITY AND PEAK INTENSITIES

The evaluated σ_i database can be used to predict the intensity of characteristic γ-rays in fusion plasmas. The effective cross sections $\sigma_{\gamma 1}$ and $\sigma_{\gamma 2}$ for production of γ-rays with $E_{\gamma 1}=2.31$ and $E_{\gamma 2}=1.63$ MeV are determined as a weighted sum of σ_i values with the branching ratios for the relevant transitions as weights.

The reactivities for γ-ray emission in the plasma are

$$Y_{\gamma 1}=\int y_{\gamma 1} dE_{3He} \quad Y_{\gamma 2}=\int y_{\gamma 2} dE_{3He}, \tag{1}$$

where $y_{\gamma 1}$ and $y_{\gamma 2}$ are the differential reactivities given by

$$y_{\gamma 1}=f(E_{3He})\sigma_{\gamma 1}(E_{3He})v,$$
$$y_{\gamma 2}=f(E_{3He})\sigma_{\gamma 2}(E_{3He})v. \tag{2}$$

The differential reactivities reflect the combined energy dependence of the cross sections and of the ^{3}He distribution. For Maxwellian ^{3}He ions, $y_{\gamma 1}$ varies as illustrated in Fig. 4 for temperatures $T_{3He}=250$ and 400 keV. At $T_{3He}=250$ keV, $y_{\gamma 1}$ is practically negligible above $E_{3He}=3$ MeV, i.e., most of the γ-ray emission comes from the lower excited states L1, L2, and L4. As T_{3He} is raised to 400 keV, ^{3}He energies up to 5 MeV contribute to γ-ray emission and levels up to L8 need to be included in the calculation. The qualitative behavior of $y_{\gamma 1}$ is similar. Our evaluation of cross section data was limited to $E_{3He}<5$ MeV; therefore, one should expect to accurately predict γ-ray emission for ^{3}He temperatures up to about 500 keV. There is some systematic uncertainty in the calculations, especially at lower T_{3He} values, due to the use of evaluated σ_i values. This can be reduced if new cross section measurements become available for $E_{3He}<3$ MeV.

The ratio of the reactivities $Y_{\gamma 1}$ and $Y_{\gamma 2}$ is $r=Y_{\gamma 1}/Y_{\gamma 2}$. Its value is always above 2 because the second excited state contributes equally to the $E_{\gamma 1}=2.31$ and $E_{\gamma 2}=1.63$ MeV peaks, whereas the first and several other levels only contribute to the $E_{\gamma 1}$ peak. An exception is the eighth level that has a resonant contribution to γ_2 at $E_{3He}\approx 3$ MeV. Shown in Fig. 5 is the variation of r versus T_{3He}. As T_{3He} is raised from 100 to 200 keV, r increases from 2.4 to 2.7. It is then practically independent of T_{3He} up to $T_{3He}=350$ keV. The slow decrease of r above 350 keV is due to the relatively larger contribution of the second excited state σ_2 at higher energies, see Fig. 3.

Also shown in Fig. 5 is a value for r derived from the γ-ray spectrometry measurements at JET. One can see that the measured ratio is of limited use as a T_{3He} diagnostics. On the other hand, the measured ratio agrees with the predicted value over a broad range of temperatures. This confirms that the systematic errors on the cross sections should not be too large.

IV. CONCLUSIONS

Cross section values for the $^{12}C(^3He,p\gamma)^{14}N$ reaction of relevance for γ-ray spectrometry of fusion plasmas were evaluated in the range $E_{3He}=0-5$ MeV. Available data for the production of up to the eighth excited state of ^{14}N were assessed, and discrepancies as well as missing data were found for $E_{3He}<3$ MeV. Discrepancies and gaps in the database were solved by means of interpolations and consistency analysis. The evaluated cross section data were used to predict the intensity ratio of characteristic γ-ray peaks at 2.31 and 1.63 MeV, which was found to be in reasonable agreement with the measured value.

ACKNOWLEDGMENTS

This work was supported by EURATOM and carried out within the framework of the European Fusion Development Agreement. The views and opinions expressed herein do not necessarily reflect those of the European Commission.

[1] V. G. Kiptily, F. E. Cecil, O. N. Jarvis, M. J. Mantsinen, S. E. Sharapov, L. Bertalot, S. Conroy, L. C. Ingesson, T. Johnson, K. D. Lawson, S. Popovichev, and Contributors to the EFDA-JET Workprogramme, Nucl. Fusion **42**, 999 (2002).
[2] D. Van Eester, E. Lerche, Y. Andrew, T. M. Biewer, A. Casati, K. Crombé, E. de la Luna, G. Ericsson, R. Felton, L. Giacomelli, C. Giroud, N. Hawkes, C. Hellesen, A. Hjalmarsson, E. Joffrin, J. Källne, V. Kiptily, P. Lomas, P. Mantica, A. Marinoni, M.-L. Mayoral, J. Ongena, M.-E. Puiatti, M. Santala, S. Sharapov, M. Valisa, and JET-EFDA Contributors, Plasma Phys. Controlled Fusion **51**, 044007 (2009).
[3] D. A. Bromley, E. Almqvist, H. E. Gove, A. E. Litherland, E. B. Paul, and A. J. Ferguson, Phys. Rev. **105**, 957 (1957).
[4] R. L. Johnston, H. D. Holmgren, E. A. Wolicki, and E. Geer Illsley, Phys. Rev. **109**, 884 (1958).
[5] H.-M. Kuan, T. W. Bonner, and J. R. Risser, Nucl. Phys. **51**, 481 (1964).
[6] S. Y. Tong, W. N. Lennard, P. F. A. Alkemade, and I. V. Mitchell, Nucl. Instrum. Methods Phys. Res. B **45**, 91 (1990).
[7] G. Terwagne, Nucl. Instrum. Methods Phys. Res. B **122**, 1 (1997).

Paper V

Spectral Broadening of Characteristic γ-Ray Emission Peaks from $^{12}C(^3He, p\gamma)^{14}N$ Reactions in Fusion Plasmas

M. Tardocchi,[1,2] M. Nocente,[2,1] I. Proverbio,[2] V. G. Kiptily,[3] P. Blanchard,[4] S. Conroy,[5] M. Fontanesi,[2] G. Grosso,[1] K. Kneupner,[3] E. Lerche,[6] A. Murari,[7] E. Perelli Cippo,[2] A. Pietropaolo,[2] B. Syme,[3] D. Van Eester,[6] and G. Gorini[2,1]

[1]*Istituto di Fisica del Plasma, EURATOM-ENEA-CNR Association, Milan, Italy*
[2]*Università degli Studi di Milano-Bicocca, Dipartimento di Fisica "G. Occhialini," Milan, Italy*
[3]*EURATOM-CCFE Association, Culham Science Centre, Abingdon, United Kingdom*
[4]*Centre de Recherches en Physique des Plasmas–CRPP, EPFL-SB, Lausanne, Switzerland*
[5]*EURATOM-VR, Department of Physics and Astronomy, Uppsala University, Uppsala, Sweden*
[6]*LPP-ERM/KMS, Association Euratom-"Belgian State," TEC Partner, B-1000, Brussels, Belgium*
[7]*Consorzio RFX, Padova, Italy*

(Received 2 May 2011; published 8 November 2011)

The spectral broadening of characteristic γ-ray emission peaks from the reaction $^{12}C(^3He, p\gamma)^{14}N$ was measured in $D(^3He)$ plasmas of the JET tokamak with ion cyclotron resonance heating tuned to the fundamental harmonic of ^3He. Intensities and detailed spectral shapes of γ-ray emission peaks were successfully reproduced using a physics model combining the kinetics of the reacting ions with a detailed description of the nuclear reaction differential cross sections for populating the $L1$-$L8$ ^{14}N excitation levels yielding the observed γ-ray emission. The results provide a paradigm, which leverages knowledge from areas of physics outside traditional plasma physics, for the development of nuclear radiation based methods for understanding and controlling fusion burning plasmas.

DOI: 10.1103/PhysRevLett.107.205002 PACS numbers: 52.70.La, 29.30.Kv, 52.55.Fa

Investigations of neutron and γ-ray emission from plasmas are motivated by the need to understand the nuclear processes occurring at the heart of a fusion burning experiment. Understanding and controlling the neutron emission at high power levels is the ultimate measure of the development of fusion research towards the goal of energy production. Fusion γ-ray emission rates are comparatively weaker but the role of γ rays as providers of information on the underlying fusion burning plasma state is emerging as a key asset. This is true for both inertial confinement fusion implosion experiments—where neutron and γ-ray emission can be used to understand the fusion reaction history, or measure fundamental parameters including the reacting fuel composition, ion temperature, ablator areal density, etc. [1–5]—and for magnetic confinement fusion—where neutron and γ-ray emission is expected to provide key information on the fusion burn conditions as well as on the physical processes involving α particles [6–14].

In order to develop neutron and γ-ray measurements in fusion burning plasmas the underlying physics must be discovered first. Even though the main reaction mechanisms may seem well identified, a lot remains to be done in order to unfold the underlying blend of plasma and nuclear physics. This task can be undertaken in present-day fusion experiments.

This Letter reports the first high-resolution investigation of γ-ray emission from a fusion plasma. The experiments were carried out on JET [15] under favorable experimental conditions such as large distance from the tokamak in a shielded low-background area, and interpreted using a model combining the kinetics of the reacting ions with a detailed description of the nuclear reaction differential cross sections and branching ratios for γ-ray emission.

The measurements were performed with a high purity germanium detector featuring 100% relative photopeak efficiency and 2.4 keV energy resolution at the calibration energy $E_\gamma = 1.33$ MeV [16]. Although commonly available at nuclear radiation laboratories, spectrometers of this kind were never used in fusion experiment. Operation in a present-day fusion environment was made possible by choosing N-type germanium, which is more resilient to neutron damage, and by equipping the detector with an electromechanical cooling system instead of liquid nitrogen cooling to facilitate operation in restricted areas. List mode digital acquisition recorded pulse height and time of each detection event; these data were converted to energy spectra after calibration with radiation sources providing <1 keV accuracy. The detector was placed in a shielded location 23 m above the tokamak viewing the plasma along a vertically collimated line of sight orthogonal to the toroidal magnetic field [17]. In these experiments the toroidal field value was 3.45 T and the plasma current ranged from 1.8 to 3.0 MA, which ensured good confinement of the fast ions. Ion cyclotron resonance heating (ICRH) was operated at a frequency of 33 MHz which is the fundamental resonance frequency of ^3He at the plasma axis major radius location of 2.84 m. Steady state ICRH power levels up to 6 MW were coupled to deuterium plasmas with electron densities of $2–3 \times 10^{19}$ m^{-3} and

electron and ion temperatures of $T_e \approx 3$-8 keV and $T_i \approx 3$-5 keV, respectively. The plasmas contained a moderate level of carbon and other impurities; ^{3}He minority concentration levels of 1%–5% were achieved after injecting small amounts of ^{3}He gas. These conditions are suitable for the generation of a population of energetic ^{3}He ions in the plasma in predominantly trapped orbits with velocities nearly perpendicular to the magnetic field. The presence of energetic ^{3}He ions was demonstrated by the γ-ray observations reported here.

A total of seven plasma discharges with several seconds of γ-ray emission were produced. Data collected from all discharges were added up to achieve good statistics in the γ-ray energy spectra. Evidence on energetic ^{3}He ions comes mainly from the two γ-ray spectral peaks at $E_{\gamma 1} = 2313$ keV and $E_{\gamma 2} = 1635$ keV shown in Fig. 1. Both peaks ride on top of a nearly flat background.

Statistical analysis of the $E_{\gamma 1}$ and $E_{\gamma 2}$ peaks after background subtraction yields intensities of $I_1 = 6516 \pm 80$ and $I_2 = 2755 \pm 53$ and peak widths—defined here as $W = 2.355\sigma$ where σ is the standard deviation—of $W_1 = 39.4 \pm 0.3$ keV and $W_2 = 26.5 \pm 0.4$ keV, respectively. For comparison the instrumental energy resolution is about 3.5 keV at these energies, which means that instrumental broadening of the peak shape is negligible. From the calculated HPGe photopeak efficiency and γ-ray attenuation along the viewing line the relative γ-ray yield is determined to be $r = Y_{\gamma 1}/Y_{\gamma 2} = 2.8 \pm 0.2$; the uncertainty is dominated by systematic error of photon transport simulations relating the plasma emissivity to the observed event rates. The analysis of the peaks and their shapes requires detailed knowledge of the underlying nuclear reaction differential cross sections and branching ratios for γ-ray emission. The ^{12}C(^{3}He, p)^{14}N* reaction is exothermic, with a Q value of 4.78 MeV, which exceeds the energy of the first two ^{14}N excitation levels. Level $L1$ at

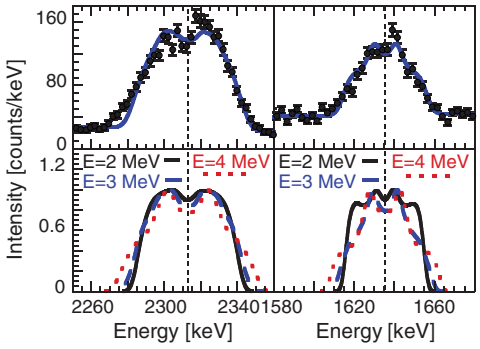

FIG. 1 (color). Top: experimental and fitted (solid line) peak shapes for the $E_{\gamma 1}$ (left) and $E_{\gamma 2}$ (right) γ-ray emission peaks. The unshifted $E_{\gamma 1} = 2313$ keV and $E_{\gamma 2} = 1635$ keV values are marked with vertical dashed lines. Bottom: Normalized simulated $E_{\gamma 1}$ (left) and $E_{\gamma 2}$ (right) peak shape for monoenergetic ^{3}He ions with Gaussian pitch angle distribution centered at $\theta_p = 90°$ and with FWHM = 10°.

2313 keV decays to the ground state with emission of $E_{\gamma 1}$ γ rays with $b_1 = 100\%$ probability (branching ratio). Level $L2$ at 3948 keV has a $b_2 = 96\%$ probability of decaying to level $L1$ thus emitting a cascade of $E_{\gamma 2}$ and $E_{\gamma 1}$ γ rays of equal intensities. At ^{3}He energies in the MeV range, ^{14}N excitation levels above $L2$ contribute to the peaks at $E_{\gamma 1}$ and $E_{\gamma 2}$ through cascade transitions as summarized in Table I. The effective cross section for emission of $E_{\gamma 1}$ and $E_{\gamma 2}$ γ rays is given by $\sigma_{\gamma 1} = \Sigma b_{i1} \cdot \sigma_{Li}$ and $\sigma_{\gamma 2} = \Sigma b_{i2} \cdot \sigma_{Li}$ where σ_{Li} ($i = 1$–8) is the cross section for populating the ith ^{14}N excitation level. These cross sections were determined from the differential cross section values available in the literature after some interpolation and consistency analysis [18]. All cross sections rise rapidly above 1 MeV and reach their largest values above 2 MeV. Main contributions to the $E_{\gamma 1}$ peak come from $L1$ and $L2$; however, contributions from the upper levels cannot be neglected. The situation is simpler for the $E_{\gamma 2}$ peak which is entirely due to $L2$ except for a resonance in the $L8$ cross section around $E_{3\mathrm{He}} = 3$ MeV. The relative γ-ray yield $r = \sigma_{\gamma 1}/\sigma_{\gamma 2}$ for monoenergetic ^{3}He is readily determined from the cross section values and is shown in Fig. 2. A detailed discussion of its wide oscillations in terms of the underlying nuclear structure properties is beyond the scope of the present work. The measured value $r = 2.8 \pm 0.2$ suggests that most of the γ-emitting ^{3}He ions in the plasma must have an energy below 3 MeV. One can go one step further and determine the yield ratio for the case of ^{3}He ions described by a Stix distribution with an asymptotic tail temperature $T_{3\mathrm{He}}$ (Fig. 2). The simulations show that the r value is only slightly sensitive to $T_{3\mathrm{He}}$ in the range 100 keV $< T_{3\mathrm{He}} <$ 500 keV. Any $T_{3\mathrm{He}}$ value within this range is compatible within the uncertainties of the measured r value.

The absolute level of the γ-ray count rate in the detector can be used to estimate the ^{3}He density $n_{3\mathrm{He}}$ in the plasma. The average rate at the $E_{\gamma 2} = 1635$ keV full energy peak was 98 ± 2 count/s, with a minimum and maximum value of 54 and 157 counts/s, respectively, during the seven discharges under analysis. This corresponds to an

TABLE I. Energies of the first eight ^{14}N excited states with branching ratios for emission of γ rays of energy $E_{\gamma 1} = 2313$ keV and $E_{\gamma 2} = 1635$ keV.

Level	Energy	b_1 (%)	b_2 (%)
$L1$	2313	100	0
$L2$	3948	96	96
$L3$	4915	0	0
$L4$	5106	20	1
$L5$	5691	64	0
$L6$	5834	16	1
$L7$	6204	77	0
$L8$	6446	21	19

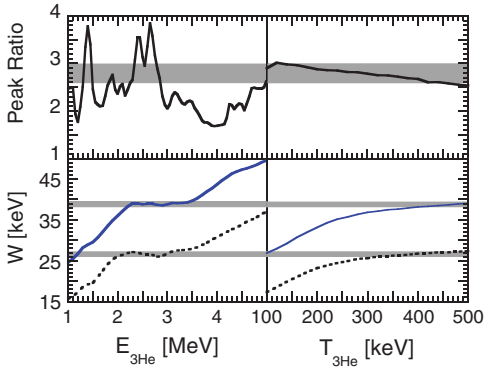

FIG. 2 (color). Peak ratio (top) and width (bottom) of the simulated $E_{\gamma 1}$ and $E_{\gamma 2}$ γ-ray emission peaks for monoenergetic ^{3}He ions of different energies (left) and Maxwellian ^{3}He ions of different temperatures (right). The horizontal bands are the experimental values.

estimated γ-ray emissivity of 1.7×10^{12} s^{-1} in the plasma core with systematic uncertainties of a factor 2 mainly due to the viewing line geometry. The emissivity changes significantly with the ^{3}He temperature with an increase of about 3 orders of magnitude as $T_{3\mathrm{He}}$ is raised from 200 to 500 keV. Assuming $T_{3\mathrm{He}} \approx 400$ keV and a ^{12}C density of 8.5×10^{-17} m^{-3} determined by CXRS data, the value $n_{3\mathrm{He}} = 6.8 \times 10^{17}$ m^{-3} is found. This is consistent with ^{3}He concentration values between 1% and 5% measured in real time during the discharges. Similar results are obtained by analyzing the $E_{\gamma 1} = 2313$ keV full energy peak.

We can now analyze the spectral broadening of the γ-ray peaks. The γ-ray energy in the lab system is Doppler shifted with respect to the reference value $E_{\gamma 0}$ by the amount $\Delta E_\gamma / E_{\gamma 0} = (V_N/c)\cos\theta_{\gamma N}$, where V_N is the ^{14}N* velocity and $\theta_{\gamma N}$ is the angle between the emitted γ ray and the excited ^{14}N* nucleus. In turn, the velocity of a γ ray is determined by simple kinematics from the initial ^{3}He velocity and the angle θ between the directions of the ^{3}He and the outgoing proton. Thus the final γ-ray energy spectrum reflects the energy and direction distribution of the initial ^{3}He population in the plasma, with weights provided by the differential cross section $d\sigma_i/d\Omega(\theta)$ ($i = 1$–8) for populating the $L1$-$L8$ ^{14}N levels.

The γ-ray spectrum is determined here using the Monte Carlo code GENESIS, a modified version of a code developed for neutron emission spectrometry applications [6]. An assumption made in the simulations is the absence of correlation in the γ-ray direction relative to the proton direction; i.e., each γ-ray emission direction with respect to the ^{14}N velocity is equally probable. This allows us to simulate the two reaction steps independently. Although the code can simulate the γ-ray spectrum from an extended ^{3}He distribution in the plasma volume, in this Letter we consider the simpler case of emission from a point in the plasma. Furthermore, we assume a Gaussian pitch angle distribution of the ^{3}He ions centered at $\theta_p = 90°$ and with FWHM $= 10°$; i.e., the ^{3}He ions gyrate with nearly perpendicular velocities around the horizontal magnetic field. Since the γ-ray spectrometry viewing line is also perpendicular to the magnetic field we expect the resulting γ-ray spectrum to be double humped. This is a well-known feature of fusion neutron, as well as proton, spectra for similar viewing geometries [19,20]. Examples of simulated γ-ray spectra for monoenergetic ^{3}He ions are shown in Fig. 1 for the $E_{\gamma 1}$ and $E_{\gamma 2}$ peaks and $E_{3\mathrm{He}} = 2$, 3, and 4 MeV. All spectra are symmetric around the unshifted energies $E_{\gamma 1}$ and $E_{\gamma 2}$ and do have a double hump shape though modulated by the angular dependence of the differential cross sections $d\sigma_i/d\Omega(\theta)$. To be noted is the spectral width. This is shown in Fig. 2 where the broadening $W = 2.355\sigma$ of the simulated γ-ray emission peaks is plotted for monoenergetic ions of energy up to 5 MeV. The peculiar behavior of the ^{12}C(^{3}He, $p\gamma$)^{14}N reaction cross sections results in a peak width that is practically independent of ^{3}He energy over the 2.0–3.5 MeV energy range. In the case of Maxwellian ^{3}He ion population of different temperature $T_{3\mathrm{He}}$ (Fig. 2), it is found that the broadening increases with the temperature. However, for $T_{3\mathrm{He}}$ values from 300 to 500 keV the variation is small (7%). Thus the experimental spectral width value is compatible with a broad range of $T_{3\mathrm{He}}$ values.

A similar conclusion is reached by detailed shape analysis of the γ-ray peaks. The simulated spectra fitted to the data in Fig. 1 assume ^{3}He ions described by a Stix distribution [21] with an asymptotic tail temperature $T_{3\mathrm{He}} = 400$ keV. The resulting reduced χ^2 values are $\chi^2 = 1.8$ for the $E_{\gamma 1}$ peak and $\chi^2 = 1.7$ for the $E_{\gamma 2}$ peak. The lower limit $T_{3\mathrm{He}}$ value resulting in a χ^2 increase by one is $T_{3\mathrm{He}} = 200$ keV. No useful upper limit to $T_{3\mathrm{He}}$ can be inferred: the simulated spectra shown in Fig. 3 feature a remarkable shape invariance above 300 keV. We conclude that a temperature value $T_{3\mathrm{He}} > 300$ keV was reached in the experiments reported here, $T_{3\mathrm{He}} \approx 400$ keV being a likely value based on the agreement between the expected γ-ray yield and the measured one for ^{3}He densities of a few percent and due to the minimum reduced χ^2 value obtained at this temperature.

Simulations of the rf heated ^{3}He energy distribution were performed with the CYRANO/TOMCAT wave codes [22,23]. The results indicate that temperatures above $T = 300$ keV were reached in all discharges, in agreement with the experimental evidence reported in this Letter.

When observed more carefully, the measured spectra in Fig. 1 seem to have an asymmetry in the top part of the spectrum: a few data points on the high energy side are systematically above the fitted curve whereas a few data points on the low energy side are systematically below the fitted curve. Our present model cannot account for the asymmetry, which is at the limit of statistical significance. Should better data confirm the evidence of asymmetry, a possible explanation can be sought by taking into account

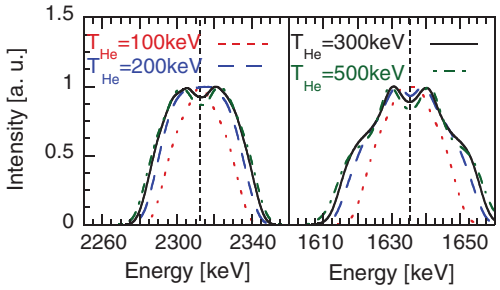

FIG. 3 (color). Simulated $E_{\gamma 1}$ (left) and $E_{\gamma 2}$ (right) γ-ray emission peak shapes normalized to unit height for ^{3}He ions described by a Stix distribution with several asymptotic tail temperatures $T_{3\mathrm{He}}$. The unshifted $E_{\gamma 1} = 2313$ keV and $E_{\gamma 1} = 1635$ keV values are marked with vertical dashed lines.

the viewing geometry and how it affects the full observation of gyration orbits around the magnetic field. Indeed we can reproduce the observed asymmetry if we assume that a $\sim$10% fraction of the gyrating ions falls out of the volume viewed by the spectrometer when moving downwards (i.e., away from the spectrometer). Evidence for effects of this kind can be sought, e.g., by looking for correlation with the ion orbit size: i.e., larger ion orbits should result in a stronger asymmetry in the gamma ray emission spectrum.

Another feature which seems to be marginally outside the statistical uncertainty and not accounted for by our model is an excess of events in the low energy side of the $E_{\gamma 1}$ peak. Peaks from the ^{3}He(^{9}Be, $p\gamma$)^{11}B reaction were also observed in the collected γ ray spectrum, but with lower intensities with respect to those from ^{3}He(^{12}C, $p\gamma$)^{14}N. Transitions from ^{11}B* excited states are expected to yield gamma rays of energies 2298 and 2265 keV, i.e., in the region where the excess of events for the $E_{\gamma 1}$ peak is observed. A detailed Monte Carlo simulation has not been done for this particular reaction, but we speculate that emission from ^{11}B* may be the reason of the observed excess of counts in the low energy side for the $E_{\gamma 1}$ peak. Because of this unaccounted component only the right-hand side ($E > E_{\gamma 1} = 2313$ keV) of the $E_{\gamma 1}$ peak was used to determine W_1 and χ^2 values.

In conclusion, high-resolution investigations of γ-ray emission from $D(^3\mathrm{He})$ fusion plasmas of the JET tokamak were reported. Intensities and detailed spectral shapes of γ-ray emission peaks from the reaction ^{12}C(^{3}He, $p\gamma$)^{14}N were successfully reproduced using a physics model combining the kinetics of the reacting ions accelerated by radio frequency waves in the plasma with a detailed description of the nuclear reaction differential cross sections $d\sigma_i/d\Omega(\theta)$ ($i = 1$–8) for populating the $L1$-$L8$ ^{14}N excitation levels yielding the observed γ-ray emission. The results represent a step forward in, and provide a paradigm for, the development of nuclear radiation based methods for understanding and controlling fusion burning plasmas.

This work was supported by EURATOM and carried out within the framework of the European Fusion Development Agreement. The views and opinions expressed herein do not necessarily reflect those of the European Commission. This work was done under the JET-EFDA workprogramme [24].

[1] J. A. Frenje *et al.*, Phys. Plasmas **17**, 056311 (2010).
[2] M. D. Cable *et al.*, Phys. Rev. Lett. **73**, 2316 (1994).
[3] H. W. Herrmann *et al.*, Rev. Sci. Instrum. **81**, 10D333 (2010).
[4] A. M. McEvoy *et al.*, Rev. Sci. Instrum. **81**, 10D322 (2010).
[5] N. M. Hoffmann *et al.*, Rev. Sci. Instrum. **81**, 10D332 (2010).
[6] L. Ballabio, G. Gorini, and J. Källne, Phys. Rev. E **55**, 3358 (1997).
[7] M. Nocente, G. Gorini, J. Källne, and M. Tardocchi, Nucl. Fusion **51**, 063011 (2011).
[8] J. Källne, L. Ballabio, J. Frenje, S. Conroy, G. Ericsson, M. Tardocchi, E. Traneus, and G. Gorini, Phys. Rev. Lett. **85**, 1246 (2000).
[9] L. Giacomelli *et al.*, Nucl. Fusion **45**, 1191 (2005).
[10] F. E. Cecil and D. E. Newman, Nucl. Instrum. Methods Phys. Res. **221**, 449 (1984).
[11] V. G. Kiptily, F. E. Cecil, and S. S. Medley, Plasma Phys. Controlled Fusion **48**, R59 (2006).
[12] W. W. Heidbrink and G. J. Sadler, Nucl. Fusion **34**, 535 (1994).
[13] W. W. Heidbrink, Phys. Plasmas **15**, 055501 (2008).
[14] B. N. Breizman and S. E. Sharapov, Plasma Phys. Controlled Fusion **53**, 054001 (2011).
[15] M. Keilhacker, A. Gibson, C. Gormezano, and P. H. Rebut, Nucl. Fusion **41**, 1925 (2001).
[16] I. L. Proverbio, Ph.D. thesis, Milano-Bicocca University, Italy, 2009.
[17] M. Gatu Johnson *et al.*, Plasma Phys. Controlled Fusion **52**, 085002 (2010).
[18] I. Proverbio, M. Nocente, V. G. Kiptily, M. Tardocchi, and G. Gorini, Rev. Sci. Instrum. **81**, 10D320 (2010).
[19] M. Tardocchi, S. Conroy, G. Ericsson, G. Gorini, H. Henriksson, and J. Källne, Nucl. Fusion **42**, 1273 (2002).
[20] W. W. Heidbrink, Nucl. Fusion **24**, 636 (1984).
[21] T. H. Stix, Nucl. Fusion **15**, 737 (1975).
[22] D. Van Eester and R. Koch, Plasma Phys. Controlled Fusion **40**, 1949 (1998).
[23] P. U. Lamalle, Plasma Phys. Controlled Fusion **40**, 465 (1998).
[24] F. Romanelli *et al.*, in *Proceedings of the 22nd Fusion Energy Conference, Geneva, Switzerland, 2008* [International Atomic Energy Agency (IAEA), Vienna, 2008]. (All the members of the JET-EFDA Collaboration appear in the appendix of this paper.)

Paper VI

High resolution gamma ray spectroscopy measurements of the fast ion energy distribution in JET ^{4}He plasmas

M. Nocente[1,2*], M. Tardocchi[2], V.G. Kiptily[3], P. Blanchard[3], I. Chugunov[4], S. Conroy[5], T. Edlington[3], A.M. Fernandes[6], G. Ericsson[5], M. Gatu Johnson[5], D. Gin[4], G. Grosso[2], C. Hellesen[5], K. Kneupner[3], E. Lerche[7], A. Murari[8], A. Neto[5], R.C. Pereira[6], E. Perelli Cippo[1], S. Sharapov[3], A. Shevelev[4], J. Sousa[5], D.B. Syme[3], D. Van Eester[7], G. Gorini[1,2] and JET-EFDA contributors[†]

JET-EFDA, Culham Science Centre, Abingdon, OX14 3DB, UK

[1]Dipartimento di Fisica "G. Occhialini", Università degli Studi di Milano-Bicocca, Piazza della Scienza 3, 20126, Milano, Italy

[2] Istituto di Fisica del Plasma "Piero Caldirola," Associazione EURATOM-ENEA-CNR, via Cozzi 53, 20125, Milan, Italy

[3]JET-EFDA, Culham Science Centre, Abingdon OX14 3DB, United Kingdom

[4]A.F. Ioffe Physico-Technical Institute, 194021, St. Petersburg, Russian Federation

[5]Department of Physics and Astronomy, EURATOM-VR Association, Uppsala University, Uppsala, Sweden

[6] Instituto Superior Técnico, Centro de Fusão Nuclear, Associação EURATOM/IST, 1049-001, Lisboa, Portugal

[7]LPP-ERM/KMS, Association Euratom-"Belgian State", TEC Partner, B-1000, Brussels, Belgium

[8]Consorzio RFX, Padova, Italy

[†]*See the Appendix of F. Romanelli et al., Proceedings of the 23rd IAEA Fusion Energy Conference 2010, Daejeon, Korea*

[*] Corresponding author. Electronic mail: massimo.nocente@mib.infn.it

Abstract

High resolution γ ray measurements were carried out on the Joint European Torus (JET) in an experiment aimed at accelerating ^{4}He ions in the MeV range by coupling third harmonic radio frequency heating to an injected ^{4}He beam. For the first time, Doppler broadening of γ ray peaks from the ^{12}C(d, pγ)^{13}C and ^{9}Be(α, nγ)^{12}C reactions was observed and interpreted with dedicated Monte Carlo codes based on the detailed nuclear physics of the processes. Information on the confined ^{4}He and deuteron energy distribution was inferred and confined ^{4}He ions with energies as high as 6 MeV were assessed. A signature of MHD activity in γ ray traces was also detected. The reported results have a bearing on diagnostics for fast ions in the MeV range in next step fusion devices.

PACS codes: 29.30.Kv, 52.70.La, 52.65.Pp, 52.55.Pi

1. Introduction

Understanding the behaviour of fast ions is widely considered a still open problem for reliable operation of a fusion device. There has been remarkable progress in the past decade in this field of research, both on the theoretical as well as on the experimental side, as recently reviewed in [1]. Many of the predicted magneto hydrodynamic (MHD) modes driven by fast particles have been identified and their non linear frequency evolution has been measured and theoretically explained. A certain degree of uncertainty however still remains on the effects of the interaction between these modes and fast ions which has a bearing on α particles in a fusion reactor. Fast ion redistribution and losses due to the excitation of many MHD instabilities, besides the consequent role of energetic particles on the overall transport, are largely unknown and dedicated experiments are presently carried out in several machines [1]. On the diagnostics side, most of the present knowledge derives from measurements of fast ions on middle-size machines, where instabilities are driven by particles with energies in the 100 keV range, either due to neutral beam injection (NBI) or generated by radio frequency (RF) heating. Recent progress in the detection of lost ions allowed phase space characterization of the losses [2,3], while a charge exchange recombination spectroscopy technique based on fast ion D_α emission (FIDA) [4] showed flattening of the fast ion profile correlated to the onset of energetic particle instabilities [5,6]. As the energy of the ions is increased towards the MeV range, such as that of α particles in a burning plasma, many diagnostics presently used for these studies on middle size machines show limitations and new methods need to be sought. For example, the considerably small cross sections for D_α emission in the MeV range limit the applicability of the FIDA technique [4]. On the other hand, the increased size of next step devices demands methods to diagnose confined energetic ions and complement information on losses.

Gamma ray spectroscopy is one of the proposed techniques for the observation of ions in the MeV range in next step fusion devices and a number of studies have been made on the JET tokamak, the only present machine that can confine ions in that energy range [7]. In recent years, the upgrade of the JET γ-ray spectrometers with the installation of a High Purity Germanium (HpGe) and a Lanthanum Bromide- Cerium ($LaBr_3(Ce)$) detectors [8] has greatly enhanced the quality of the observations and the information that can be derived from the data. For the first time, the Doppler broadened peak shape produced by interaction of ^{3}He ions on ^{12}C impurities has been measured and interpreted in terms of the nuclear physics of the reaction and tail temperature of the energetic ions [9]. In this paper we report, for the first time, observations of Doppler broadened peak shapes from energetic ^{4}He ions and deuterons on JET. The measurements were carried out in an experiment aimed at accelerating ^{4}He ions by coupling RF heating at the third harmonic to a helium beam injected approximately at 40° to the magnetic axis in a (D)^{4}He plasma [10]. The plasma current was I_p=2 MA and the toroidal magnetic field at plasma centre was B_T=2.25 T, which placed the 51.4 MHz resonance layer on the magnetic axis for both ^{4}He and d ions. Core Electron densities in the range 2.5 - $4\cdot10^{19}$ m^{-3} with average on axis electron temperatures of 3.4 keV were available for applied antenna powers in the

range 3-6 MW. The collected experimental data are interpreted in this paper by means of simulations with the GENESIS (Gamma Emission and Neutron Emission Simulation and Interpretation Software) Monte Carlo code that is an extended version of a previous programme [11,12] adopted for neutron emission calculations. A simplified semi-analytical model, described in section 3, is adopted for the distribution of RF heated ^{4}He and d ions as input for calculations. This simplification was found convenient to numerically investigate changes in the peak shapes and ratios as effect of modifications in parameters describing the energetic ion distribution, while still retaining the main features of the employed heating scheme. After a short overview of the γ emitting reactions of interest for this study in section 2, the experimental results and simulations are presented and the findings compared with information from other diagnostics. Implications of these results on observations of confined fast ions in the MeV range on next generation devices are finally discussed.

2. Gamma emitting reactions and cross sections

Gamma ray emission can occur when fast ions interact with impurities, either coming from the machine vacuum vessel or injected on purpose. On JET there are two reactions of interest for the observation of fast ^{4}He ions and deuterons, the ^{9}Be(α, nγ)^{12}C and ^{12}C(d, pγ)^{13}C reactions, respectively [13]. The level scheme of the emitting nuclei is presented in figure 1. The ^{9}Be(α, nγ)^{12}C reaction is the main candidate for α particle observations through gamma ray spectrometry on ITER [14,15] and has a positive Q value of 1.27 MeV for populating ^{12}C in his first excited state, which in turn de-excites by emission of a 4.44 MeV gamma ray. If the α particle energy exceeds E_α=1.35 MeV the second ^{12}C excited state starts to be populated and de-excites with the emission of a 3.22 MeV and 4.44 MeV gamma rays in cascade. The ^{12}C(d, pγ)^{13}C reaction is instead endothermic, with negative Q values of -0.37 MeV, -0.96 MeV and -1.13 MeV for the population of the 1st, 2nd and 3rd ^{13}C excited states, respectively, yielding gamma rays of energies 3.09 MeV, 3.68 MeV and 3.85 MeV. In the discharges analyzed in the present paper ^{9}Be was evaporated overnight while ^{12}C was present at a typical concentration level of about 1% due to the composition of the JET vacuum vessel.

The cross sections for the production of gamma rays observed during the measurements reported here are shown in figure 2 and were obtained by merging experimental data from several authors in a way similar to the methods described in reference [16]. In particular, data from references [17,18] were used to obtain the total, as well as differential, cross section for production of the 4.44 MeV peak from the ^{9}Be(α, nγ)^{12}C reaction up to E_α= 6 MeV (figure 2, top). The cross section is negligible below E_α < 1 MeV and displays a non trivial behaviour as a function of energy with major resonances at E_α≈2.0, 2.9, 4.3, 5.5 MeV. The angular distribution of the emitted neutrons in the c.m. frame is not isotropic and shows an increased forward peaking as the energy of ^{4}He ions is raised, which affects the Monte Carlo simulated peak shape [17,18].

Cross section data for the $^{12}C(d, p\gamma)^{13}C$ reaction were obtained from reference [19] and are shown in figure 2, bottom part, for laboratory energies in the range 1-4 MeV. The values are those for the production of 3.09 MeV and 3.69 MeV gamma rays, which are weighted by the branching ratios of figure 1. Similarly to the $\alpha+^{9}Be$ reaction, the cross section for the $d+^{12}C$ reaction has a complex trend as function of energy, with several resonances appearing in the MeV region.

3. Fast ion energy distribution

For energies far from the thermal ion region, an approximate form for the anisotropic fast ^{4}He energy distribution f is obtained from the Fokker-Planck equation

$$\frac{\partial f}{\partial t} + S(v_p) + L(v_p) = C(f) + Q(f) \quad (1)$$

where all the quantities are expressed in terms of the velocity component perpendicular to the magnetic field v_p only. $S(v_P)$ represents the source term due to perpendicular NBI injection and is expressed as $S(v_P) = S_0/(2\pi v_p)\cdot\delta(v_p - v_0)$ with v_0 indicating the NBI injection velocity and S_0 a constant. $L(v_P)$ is a loss term that absorbs ions at the same rate as $S(v_p)$, but at thermal speed. $C(f)$ and $Q(f)$ are operators representing the effect of collisions and radio frequency heating on the alpha particles respectively. Following the treatment of reference [20] they can be expressed as

$$C(f) + Q(f) = \frac{1}{v_p}\frac{\partial}{\partial v_p}\left[-\alpha v_p f + \frac{1}{2}\frac{\partial}{\partial v_p}(\beta v_p f) + \frac{1}{4}\gamma f + D_{RF} v_p \frac{\partial f}{\partial v_p}\right] \quad (2)$$

where α, β and γ are the Spitzer collision coefficients [21] and D_{RF} the radio frequency diffusion coefficient. In the steady state condition equation (1), combined with equation (2), is reduced to a 1^{st} order ordinary differential equation for f and the solution is readily expressed in terms of one dimension velocity integrals to be evaluated numerically.

The specific form of the solution depends on the diffusion coefficient D_{RF}, which is expressed as [20,21]

$$D_{RF} = K\left|J_{n-1}\left(\frac{k_p v_p}{\omega_c}\right) + \frac{E_-}{E_+}J_{n+1}\left(\frac{k_p v_p}{\omega_c}\right)\right|^2 \quad (3)$$

For harmonics higher than the fundamental, D_{RF} has an oscillating behaviour due to the presence of Bessel functions of the first kind $J_n(x)$ (figure 3) and contains parameters pertaining to wave propagation and absorption at the resonance that need to be known. Specifically, E_- (E_+) are the right (left) handed component of the electric field at the resonance, k_P is the perpendicular wave number and ω_C the cyclotron frequency of the resonating ion. K is a constant representing the amount of RF absorption. In this work K was varied in

equation (3) until a chosen value was matched by the total absorbed power density P_{RF}. The latter was expressed as

$$P_{RF} = 2\pi n_s \int dv_p v_p \left(\frac{m_s v_p^2}{2} \right) Q(f) \qquad (4)$$

where the known mass m_s and density n_s of the resonating ion appear. P_{RF} depends on K in equation (4) through the $Q(f)$ term [20]. The power density absorbed by ^{4}He ions can be estimated to be of the order $\approx 10^5$ W/m^3 for the scenario under study.

Figure 3 shows the calculated ^{4}He ion distribution assuming P_{RF}= 500 kW/m^3 and using cold plasma theory (equations (1.18) and (1.58) of [21]) to calculate the resonance parameters k_P and E/E_+ from measured values. ^{4}He ions accelerated at the third harmonic resonance develop a rather flat tail in phase space extending to high energies from the NBI injection energy up to a certain cut value E_α*. The latter is determined by the appearance of the first zero in the diffusion coefficient D_{RF} (figure 3b). Correspondingly, a sharp drop is seen in the ^{4}He ion energy distribution and almost no particles have energies extending above E_α* [21]. Figure 3 also shows the deuteron energy distribution calculated with equation (1), letting $S(v_p)=L(v_p)=0$. As ^{4}He ions and deuterons have the same ion cyclotron frequency, part of the incoming wave power is damped on thermal deuterons that also develop energetic tails up to a certain energy E_d*. The deuteron tail level is however some orders of magnitude lower compared to that of ^{4}He ions due to the absence of a fast ion seed provided by NBI. As E_d* is also determined by the appearance of the first zero in the diffusion coefficient D_{RF}, the relation $E_\alpha^*=2 \cdot E_d^*$ holds between the two cut energies. In fact, being k_p and ω_c the same for the two species, the cut velocity v_p* is the same and the relation between the cut energies $E^*=1/2mv^{*2}$ is given by the mass ratios of the resonating species.

In order to investigate the fractions of RF power absorbed by the different species, simulations were performed with the TOMCAT wave code for single pass absorption [22]. The ^{4}He ion and deuteron distribution were represented as Maxwellians at temperatures $T_\alpha >> T_i$ and T_i respectively and a scan was made in ^{4}He temperature and beam density. Figure 4 shows the power fraction absorbed by different species for a case with T_α=50 keV and a beam density equal to 6% of the electron density. The incoming wave is mainly damped on the ^{4}He beam ions and electrons, with only about 1% of the power coupled to deuterons. The simulations show quantitative changes depending on the exact value of T_α and the beam fraction. However in all cases only a fraction around 1% of the power is coupled to deuterons and can be considered independent of the simplistic representation of the ^{4}He ion energy distribution as a Maxwellian at $T_\alpha >>$ Ti. Thus one can expect P_{RF} to be of the order $\approx 10^3$ W/m^3 for deuterons at resonance. In figure 3 the value $P_{RF}=5 \cdot 10^3$ W/m^3 was used to calculate the deuteron distribution.

Figure 5 shows variations of the ^{4}He ion distribution by changes of ±10% in P_{RF} and k_p around the values predicted by cold wave theory. A small variation in k_P strongly affects the energy distribution, as it directly acts on the cut energy E*, while P_{RF} mainly acts on the level of the plateau, without significant influence on E*. Similar trends are seen in the deuteron energy distribution.

4. Experimental results and modelling

The measured gamma-ray emission spectrum in the region $E_\gamma > 3$ MeV for JET discharges #79168 to #79171 is shown in figure 6 in the time window 12 to 17 s. The spectrum was collected with a HpGe detector, time integrated during RF heating and summed over these similar 4 discharges to improve statistics. The resolution of the measurement in this energy region is about 1 keV, which allows one to appreciate broadening of the peak shapes besides identifying signatures of de-excitation from different states of the same emitting nucleus. The most intense peak appears at E_γ=3.09 MeV that corresponds to de-excitation of the first ^{13}C* excited level produced by the d+^{12}C reaction. The 3.68 MeV and 3.85 MeV peaks from de-excitation of the second and third ^{13}C* states (the latter barely emerging from the background) are also seen and qualitatively indicate deuteron energies greater than 1.13 MeV. ^{4}He ions with energies in excess of 1 MeV are manifested by the appearance of the E_γ=4.44 MeV peak. This is in turn mirrored in the single escape peak at E_γ=3.93 MeV which depends on the detector response function and does not correspond to a new reaction occurring in the plasma. No clear evidence of the 3.22 MeV peak from de-excitation of the second ^{12}C* excited state is seen in the data.

Besides qualitatively indicating that ions exceeding a certain energy were produced in the analyzed discharges, quantitative information can be derived from the measured spectrum by comparison with modelling. From the experimental data shown in figure 6 one can derive the peak ratio *r* between counts due to de-excitation of the first and second ^{13}C* levels, yielding $r = 6.5\pm0.6$ after correcting for the difference in detector intrinsic efficiency at the two peaks and background subtraction. The peak ratio is related to the ratio of the reactivities Y_γ through the relation [16]

$$r = \frac{Y_{\gamma 1}}{Y_{\gamma 2}} = \frac{\int d^3\vec{v}\,\sigma_{\gamma 1} v f(\vec{v})}{\int d^3\vec{v}\,\sigma_{\gamma 2} v f(\vec{v})} \quad (5)$$

where $\sigma_{\gamma i}$ represents the cross section for populating the i-th ^{13}C* level. The advantage of distinguishing several excited states of the same emitting nucleus is that the calculated peak ratio is independent of the densities of the reactant (d and ^{12}C for the present reaction) and of the effective emission volume, that both simplify in the ratio expressed by equation (5).

The expected peak ratio was evaluated with equation (5) and is compared to the measured value in figure 7. The fast deuteron distribution was varied by independently changing the P_{RF} and k_p parameters and resulted

in the calculated curves shown in the figure. The wave polarization was set to the constant value obtained by applying cold plasma theory as it did not significantly affect the distribution. The horizontal shadowed bar represents the experimental value *r* with its uncertainty. The calculated curves are rather independent of P_{RF} but for very low power densities, say $P_{RF} < 1$ kW/m^3. Here a sharp rise is seen that is due to the rapidly decreasing cross section for populating the second ^{13}C* state.

From the results of figure 7, k_p must lie in the range 44 m^{-1} to 47 m^{-1} that corresponds to $E_d^* = 3.0 \pm 0.2$ MeV. This interval is consistent with the estimated P_{RF} in the range 10^3-10^4 W/m^3 and reproduces the absolute number of counts measured under the E_γ=3.09 MeV and E_γ=3.68 MeV peaks assuming ^{12}C concentrations of a few percent. Lower k_P values are, for instance, ruled out, as the number of counts under E_γ=3.68 MeV peak would be underestimated by 1 to 2 orders of magnitude. As the electron density varied between $2.3 \cdot 10^{19}$ m^{-3} and $3.6 \cdot 10^{19}$ m^{-3} in the time window 12 to 17 s, which changed k_p in time, the value k_p=44-47 m^{-1} must be regarded as effective, i.e inferred by time integrating γ-ray spectra for statistical reasons. Temporal changes in k_p could be resolved in future measurements with better statistics (see discussion). From the relation $E_\alpha^* = 2 \cdot E_d^*$ one can also derive the cut energy of ^{4}He ions to be $E_\alpha^* = 6.0 \pm 0.4$ MeV.

We now move to the analysis of the detailed E_γ=4.44 MeV peak shape from the ^{9}Be(α, nγ)^{12}C reaction. Data collected with the HpGe detector for the sum of four discharges during RF heating are presented in figure 8. The error bars are those associated to the Poisson statistics of the measurement. The energy calibration is linearly extrapolated from known calibration source peaks at lower energy, with an estimated error of ≈ 3 keV in the region of the α+^{9}Be peak. Two features are clearly displayed by the data. The first one is that the α+^{9}Be peak is Doppler broadened, as it was found for gamma ray peaks from reactions between radio frequency heated ^{3}He ions and ^{12}C in reference [9]. The second is that the centroid of the peak is around 4470 keV, i.e. ≈ 30 keV upward shifted with respect to the expected value of 4439 keV.

The reason of this shift is clarified when simulating the expected peak shape produced by ^{4}He ions described by the distribution in figure 5. The simulations were performed with the GENESIS Monte Carlo code [9]. The ^{12}C* energy spectrum is determined through classical kinematics by sampling the reactant energy distributions. In a second stage, the resulting gamma ray emission spectrum is evaluated along a specified line of sight. Isotropic γ-ray emission with respect to the excited nucleus direction in the laboratory frame is assumed and branching ratios are taken into account so to simulate cascade transitions when necessary [16]. The result of the simulation is presented in figure 8 (dashed line). The only parameter fitted is the normalization of the spectrum with the addition of a linear background. Quite surprisingly, the curve completely fails to describe the lower half of the peak, which is not present in the measured data. The reason for this effect may be explained by considering the orbit of RF heated ^{4}He ions at the resonance. The calculated trajectory of 4 MeV ^{4}He ions projected on to the poloidal plane is shown in figure 9. The particles

are generated on the magnetic axis with 90° pitch angle. The line of sight of the HpGe detector is determined by collimators designed for the JET Roof Laboratory and is the same of that of TOFOR neutron spectrometer [23,24]. The latter was evaluated in reference [25] and covers the region in major radius 2.74 – 3.02 m, with an uncertainty of about 1 cm at the edges. When the line of sight is taken into account in figure 9, it is revealed that only the upward gyro-motion of the particle is seen by the detector. This explains why the lower half of the peak, which corresponds to downward motion, is missing from the data. In order to quantitatively describe the measurements, an "ad hoc" orbit effect was introduced in the code. This was done by sampling the radial position of the ^{4}He ions with Gaussian probability. The centre of the radial distribution was placed at the resonance location while the FWHM was varied between 5 cm and 30 cm. At each particle location only the fraction of gyroradius falling inside the line of sight was considered for the calculation of the resulting γ-ray spectrum. In this way, the measured peak shape is described when the FWHM of the ^{4}He ion radial distribution lies in the range 10 cm to 20 cm (figure 8, solid line); here a reduced $\chi^2 \approx 1.5$ is found, with little variations depending on the exact value of the chosen FWHM in the interval 10 to 20 cm.

Simulations of the 4.44 MeV peak show changes in shape depending on the k_p parameter of the ^{4}He ion energy distribution. Figure 10 compares the upper half of the 4.44 MeV peak with calculations. The comparison is limited to this part of the peak so to discard the orbit effect discussed above. The best fit is obtained for $k_p \approx 45$ m^{-1} (reduced χ^2=1.0). The range of variation for k_p, determined by an increase of ± 1 in reduced χ^2 is 35-55 m^{-1}, which is rather large because of the limited statistics of the measurement. k_p=45±10 m^{-1} is in good agreement with the interval 44 to 47 m^{-1} obtained from analysis of the ^{13}C* peak ratio *r* and confirms the value 6.0±0.4 MeV for E_α*. This result shows that information on the confined ^{4}He energy distribution can indeed be derived from the detailed peak shape for the scenario of this experiment and independently benchmarks the information obtained from the ^{13}C* peak ratio. In figure 10 k_p was varied in steps of 5 m^{-1}, but smaller variations may be appreciable in future measurements with improved statistics.

A $LaBr_3$(Ce) spectrometer was also used in the measurements. The detector, designed for high rates, has been already described in [8]. Although its resolution is not as good as that of HpGe, its enhanced detection efficiency allows for better statistics. Figure 11 shows the measured gamma emission spectrum for JET discharge #79174. Besides peaks from the d+^{12}C and α+^{9}Be reaction, a further peak at E_γ=3.37 MeV appears. This is produced by the ^{9}Be(d, pγ)^{10}Be reaction and was not observed in shots #79168-79171. As the antenna had ±90° phasing in discharge #79174 (to be compared with dipole phasing for #79168-79171), cold plasma theory predicts an increased k_P, which would correspond to a decreased E_d*. Indeed, according to figure 7, an augmented k_p is compatible with an increased peak ratio *r*, which for this discharge equals 17 ± 8. The large error on this value comes from background subtraction below the E_γ=3.68 MeV peak and is partially due to the still not optimized detector parameters adopted in this discharge. As E_d* is lowered, the appearance of the peak from the ^{9}Be(d, pγ)^{10}Be reaction can be explained only by higher P_{RF}. The temporal

evolution of the E_γ=3.09 MeV and E_γ=4.44 MeV count rates are shown in figure 12 every 20 ms between 3 and 8 s. The count rate starts to rise at 4 s and drops between 7.2 and 7.6 s, i.e. 0.4 s before the end of the RF heating phase, between 4 and 8 s in this discharge. The reason is that core electron density experiences a jump from $3\cdot10^{19}$ m^{-3} at 7 s to $3.8\cdot10^{19}$ m^{-3} at 7.2 s that impedes fast ion acceleration, with a delayed drop in the γ count rate due to slowing down. Between 5.6 and 5.8 s a further sharp drop of a factor ≈ 1.6 that exceeds the statistical fluctuation of the data is observed in the E_γ=3.09 MeV count rate. This drop corresponds to the appearance of toroidal Alfvén eigenmodes (TAE) in the magnetic traces at 5.75 s and suggests redistribution of fast deuterons. A similar drop is not observed in the count rate for the E_γ=4.44 MeV peak ($\alpha+^9$Be reaction) but might be masked by the larger statistical data fluctuation. No signs of MHD activity was observed in the magnetic traces, as well as in the γ-ray count rates, for shots #79168-79171 where the HpGe detector was used.

5. Discussion

γ-ray observations can be compared to neutron measurements with the TOFOR spectrometer on JET [23,24]. The instrument measures the neutron time of flight t_n between two arrays of scintillators so that the neutron energy E_n is univocally related to t_n through $E_n=1.04\cdot10^4/t_n^2$ where E_n is expressed in MeV and t_n in nanoseconds. This relation implies that higher neutron energies correspond to smaller time of flights. Figure 13 shows the measured neutron spectrum for the sum of JET discharges #79168-79171 in the time window 12 to 17 s that directly compares to the γ-ray spectrum of figure 6. Neutron emission is expected mainly from the d+d→n+^{3}He reaction, but there is a component from the $\alpha+^9$Be→n+^{12}C reaction as well. Noticeably, the highly non Maxwellian character of the energy distribution is manifested in the neutron spectrum that does not show a Gaussian peak centred at t_n=65 ns (E_n = 2.45 MeV) due to thermal emission. The GENESIS code was used to calculate the expected neutron spectrum from the d+d→n+^{3}He and $\alpha+^9$Be→n+^{12}C reactions using as input the distributions calculated as described in section 3 and setting k_p to the value 45 m^{-1} inferred from γ-ray measurements. As the result of equation (2) is not adequate in the thermal region, the deuteron distribution was here joined to an isotropic Maxwellian representing the bulk component with a procedure similar to that adopted in [26]. This choice, although simplistic, was found adequate to describe the data within the statistics. The same procedure was not necessary for the neutron component from the $\alpha+^9$Be reaction, as neutron emission for thermal ^{4}He ions is negligible. The result of the simulation is shown in figure 13 and confirms the presence of ^{4}He ions with energies as high as 6 MeV determined through γ-ray spectroscopy. It is also revealed that the d+d contribution has a sharp cut off at t_n=42 ns which sets $E_d^*\approx3$ MeV, consistent with γ observations. More details on neutron measurements for this experiment can be found in reference [27]. Here we just add that orbit effects do need to be taken into account also to describe neutron data, for which the empirical model illustrated in section 3 was adopted in the simulations of figure

13. A more accurate procedure was used in [27] and its developments are the subject of [28]. A similar study of the energy distribution of fast deuterons accelerated by RF at the third harmonic using neutron emission spectroscopy at JET is reported in [29] for a different experiment and confirms the results presented here. In reference [30] measurements with a Faraday cup array are reported for the experiment considered here. A signal in terms of current from ^{4}He ions in the energy range 2.3 MeV – 5.9 MeV was detected for the first time throughout all the discharges, while no evidence of ^{4}He ions exceeding 6 MeV was seen. This is also consistent with the values stated in this paper.

In this work we have derived information on energy distribution of ^{4}He ions by considering both variations in the ratio of peaks produced by different excited states of the same emitting nucleus (^{13}C* in this case) and by studying the detailed shape of the α+^{9}Be peak at E_γ=4.44 MeV. Although qualitative results could be derived by simple arguments based on the observed emission spectra, quantitative information were obtained only by considering the detailed nuclear physics behind the reaction in terms of differential cross section, energy levels and branching ratios of the emitting nuclei, which can be quite different depending on the emission process. Indeed, the extremely variegated properties of reactions between light nuclei and impurities (see for example [31,32] and references therein) can sometimes produce undesirable effects, such as limiting changes of an observable even over significant modifications in the plasma parameters. An example is given by the peak ratio of the ^{12}C(^{3}He, pγ)^{14}N reaction, which is rather independent of the fast ^{3}He distribution as shown in reference [16], in clear contrast with the peak ratio from the ^{12}C(d, pγ)^{13}C reaction considered in this paper. Similar arguments hold for the peak shape that is found to depend on the detailed angular distribution of the emitting nuclei and can also show limited variations for certain reactions. These issues will be more extensively addressed in forthcoming papers. Clearly, due to the Poissonian nature of the process, the possibility to observe changes in the γ-ray emission spectrum benefits from increased statistics which sets a trade-off between time resolution and the required precision in determining the parameter of interest (for example E_α* in this paper).

Similarly to neutron spectroscopy [33,34], as shown with the result of figure 12, γ-ray spectroscopy can also be used to derive information on the effect of MHD modes on fast ions by studying the time dependence of the measured counting rate [34]. The energies of the interacting ions are related to the counting rate through the differential reactivity $y_\gamma(E) = v\sigma(E)\, f(E)$. The latter represents the γ-ray emission intensity as a function of the fast ion energy and is the integrand appearing in equation (5). The differential reactivity for the E_γ=3.09 MeV peak of the ^{12}C(d, p)^{13}C reaction is shown in figure 14 for discharge #79174. The curve is significantly non null only in the energy range E_d=0.8 to 2.5 MeV, with a peak at $E_d \approx$1.7 MeV. By inspecting figure 14, we speculate that a redistribution of fast deuterons with $E_d \approx$1.7 MeV (i.e. around the peak in the differential reactivity curve) must have occurred in discharge #79174 to justify a factor 1.6 drop as observed in the counting rate. Further insights on mode-particle interaction could be obtained by calculating resonance curves between the observed TAEs and fast ions, as done for instance in reference [35], but this goes outside

the scope of the present paper. Here we note the following fact. The fast ion energies, to which γ-ray spectroscopy is sensitive, are determined by the differential reactivity of each specific reaction, which comprises the combined product of the cross section and the ion energy distribution. When resonances in the cross sections appear [31,32], the evolution of the γ-ray counting rate can be dominated by ions with energies near resonance, despite those with energies off-resonance. For example, in the case of figure 14, a change in the fast deuteron population having $E_d \approx 0.8$ MeV would hardly be manifested in the observed γ-ray counting rate. This strengthens the need to consider the detailed nuclear physics behind each reaction to derive conclusions also on the fast ion dynamics based on the observed γ-ray emission rate. From the instrumental point of view, observations on the interaction between fast ions and instabilities through γ spectroscopy would be boosted by the capability to perform spatially resolved measurements, for example to study the effects of α particles in a DT plasma. This could be done through a tomographic system, such as the JET γ-ray camera [7], but with spectroscopy capabilities at each channel and an increased number of line of sights. Concept studies are currently undergoing in view of ITER and some solutions are reported in reference [36].

6. Conclusions

In this paper first high resolution measurements of Doppler broadened peak shapes from γ emitting reactions induced by energetic α particles and deuterons were reported. The data were interpreted through Monte Carlo simulations of the γ-ray emitting reactions and good agreement was found with measured data. Information on the ^{4}He and deuteron energy distribution was inferred and found consistent with observations from other diagnostics. In particular, the confinement of deuteron and ^{4}He ions with energies as high as 3 and 6 MeV, respectively, was assessed. A drop in the γ–ray count rate was found in one discharge and corresponded to the appearance of TAE in the magnetic traces. The need to consider the detailed nuclear reaction data and physics of each reaction to derive quantitative information on the energetic ions from the γ-ray emission spectrum was pointed out. The methods and results reported here are of relevance for confined fast ion studies in the MeV range on next generation devices, such as α particles in ITER DT plasmas, where observations would significantly be boosted by spatially resolved measurements through a tomographic γ-ray system with spectroscopic capabilities.

7. Acknowledgments

This work was supported by EURATOM and carried out within the framework of the European Fusion Development Agreement. The views and opinions expressed herein do not necessarily reflect those of the European Commission.

References

[1] Breizman B N and Sharapov S E 2011 *Plasma Phys. Control. Fusion* **53** 054001

[2] García-Muñoz M, Fahrbach H U, Günter S, Igochine V, Mantsinen M J, Maraschek M, Martin P, Piovesan P, Sassenberg K, Zohm H 2008 *Phys. Rev. Lett.* **100** 055005

[3] García-Muñoz M *et al.* 2010 *Phys. Rev. Lett.* **104** 185002

[4] Heidbrink W W 2010 *Rev. Sci. Instrum.* **81** 10D727

[5] Heidbrink W W *et al.* 2007 *Phys. Rev. Lett.* **99** 245002

[6] White R B, Gorelenkov N, Heidbrink WW, Van Zeeland M A 2010 *Phys. of Plasmas* **17** 056107

[7] Kiptily V G, Cecil F E, Medley S S 2006 *Plasma Phys. Control. Fusion* **48** R59

[8] Nocente M *et al.* 2010 *Rev. Sci. Instrum.* **81** 10D321

[9] Tardocchi M *et al.* 2011 *Phys. Rev. Lett.* **107** 205002

[10] Mantsinen M J *et al.* 2002 *Phys. Rev. Lett.* **88** 105002

[11] Ballabio L. 2003 Calculation and measurement of the neutron emission spectrum due to thermonuclear and higher-order reactions in tokamak plasmas *PhD Thesis* Acta Universitatis Upsaliensis No 797, Faculty of Science and Technology, Uppsala University

[12] Ballabio L, Gorini G and Källne J 1997 *Phys. Rev. E* **55** 3358

[13] Kiptily V G *et al.* 2002 Nucl. Fusion **42** 999

[14] Kiptily V G *et al.* 1990 *Fusion Technology* **18** 583

[15] Kiptily V G *et al.* 1992 *Fusion Technology* **22** 454

[16] Proverbio I, Nocente M, Kiptily V G, Tardocchi M and Gorini G 2010 *Rev. Sci. Instrum.* **81** 10D320

[17] Kiptily V G, Matukov A V, Mishin A S, Najdenov V O, Polunovskij I A, Rassadin L A and Chugunov I N1992 *Bull Russ. Acad. Sci. Phys.* **56** 125

[18] Van Der Zwan L and Geiger K W 1970 *Nucl. Phys. A* **152** 481

[19] Papillon F and Walter P 1997 *Nucl. Instrum. Meth. B* **132** 468

[20] Salmi A, Mantsinen M J, Beaumont P, De Vries P, Eriksson L-G, Gowers C, Helander P, Laxåback M, Noterdaeme J-M, Testa D 2006 *Plasma Phys. Control. Fusion* **48** 717

[21] Stix T H 1992 *Waves in plasmas* ed. Springer

[22] Van Eester D and Koch R 1998 *Plasma Phys. Contr. Fusion* **40** 1949

[23] Gorini G and Källne J 1992 *Rev. Sci. Instrum.* **63** 4548

[24] Gatu Johnson M *et al.* 2008 *Nucl. Instrum. Meth. A* **591** 417

[25] Gatu Johnson M *et al.* 2010 *Plasma Phys. Control. Fusion* **52** 085002

[26] Nocente M, Gorini G, Källne J and Tardocchi M 2011 *Nucl. Fusion* **51** 063011

[27] Gatu Johnson M *et al.* 2010 *Rev. Sci. Instrum.* **81** 10D336

[28] Eriksson J *et al.* 2011 “Finite Larmor radii effects in fast ion measurements as demonstrated using neutron emission spectrometry of JET plasmas heated with 3rd harmonic ICRF” Proceedings of the 38th EPS Conference on Plasma Physics and Controlled Fusion, Strasbourg, France, 27th June – 1st July 2011; and Eriksson J *et al.* 2011 submitted to *Plasma Phys. Control. Fusion*

[29] Hellesen C et al. 2011 "Fast ion distributions from 3rd harmonic ICRF heating studied with neutron emission spectroscopy" submitted to *Nucl. Fusion*

[30] Darrow D S, Cecil F E, Kiptily V, Fullard K, Horton A, Murari A 2010 *Rev. Sci. Instrum.* **81** 10D330

[31] Ajzenberg-Selove F 1990 Nucl. Phys. **A506** 1

[32] Ajzenberg-Selove F 1991 Nucl. Phys. **A523** 1

[33] Hellesen C *et al.* 2010 *Nucl. Fusion* **50** 022001

[34] Hellesen C *et al.* 2010 *Nucl. Fusion* **50** 084006

[35] Nocente M et al. "Gamma-ray spectroscopy measurements of fast ions on ASDEX Upgrade", submitted to *Nucl. Fusion*

[36] Chugunov I N, Shevelev A E, Gin D B, Kiptily V G, Gorini G, Nocente M, Tardocchi M, Doinikov D N, Naidenov V O and Khilkevitch E M 2011 *Nucl. Fusion* **51** 083010

Figures

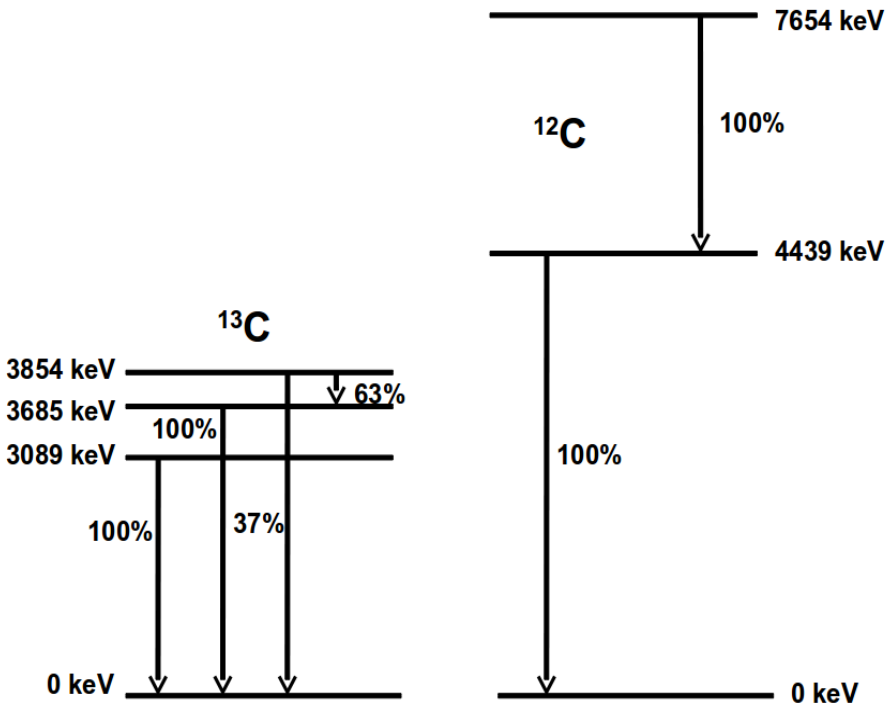

Figure 1. Level scheme of the ^{13}C and ^{12}C γ emitting nuclei produced in the $^{12}C(d, p\gamma)^{13}C$ and $^{9}Be(\alpha, n\gamma)^{12}C$ reactions.

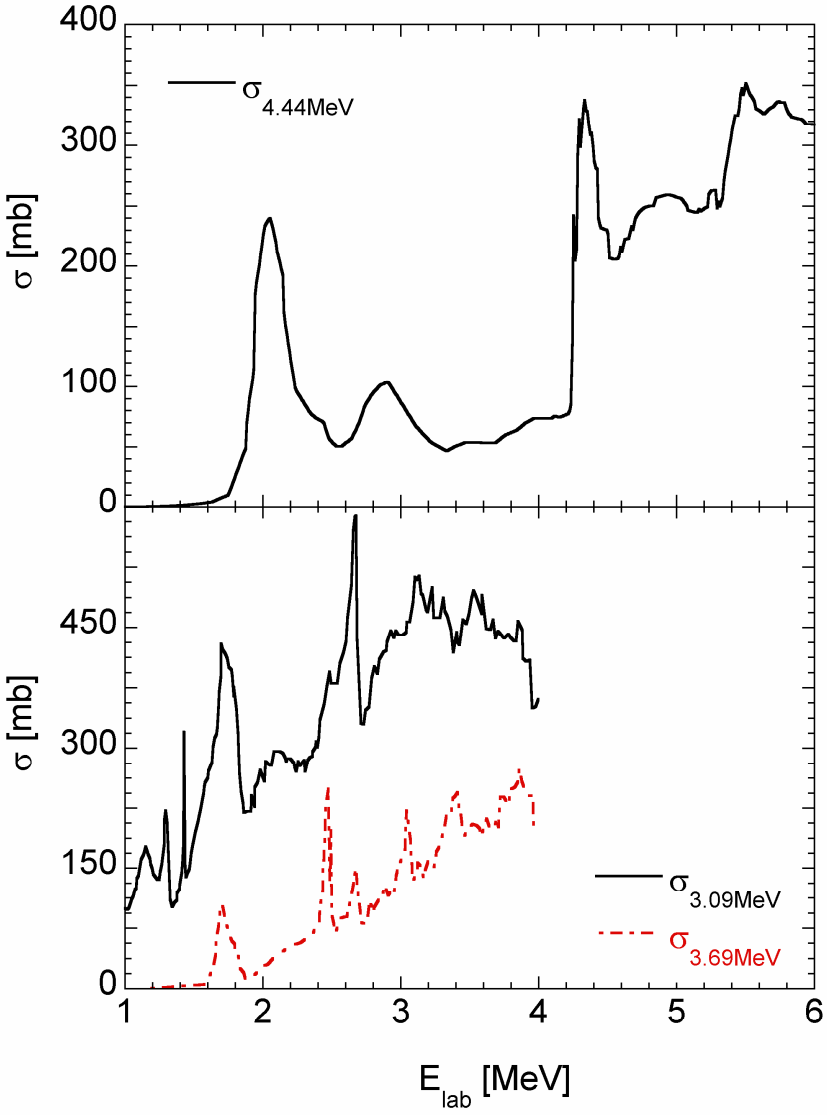

Figure 2. Cross section for the production of γ-rays at energies E_γ=4.44 MeV (top, ^{9}Be(α, nγ)^{12}C reaction), E_γ=3.09 MeV and 3.69 MeV (bottom, ^{12}C(d, pγ)^{13}C reaction)as a function of the light ion energy in the laboratory frame. The values shown are weighted by the branching ratios of figure 1.

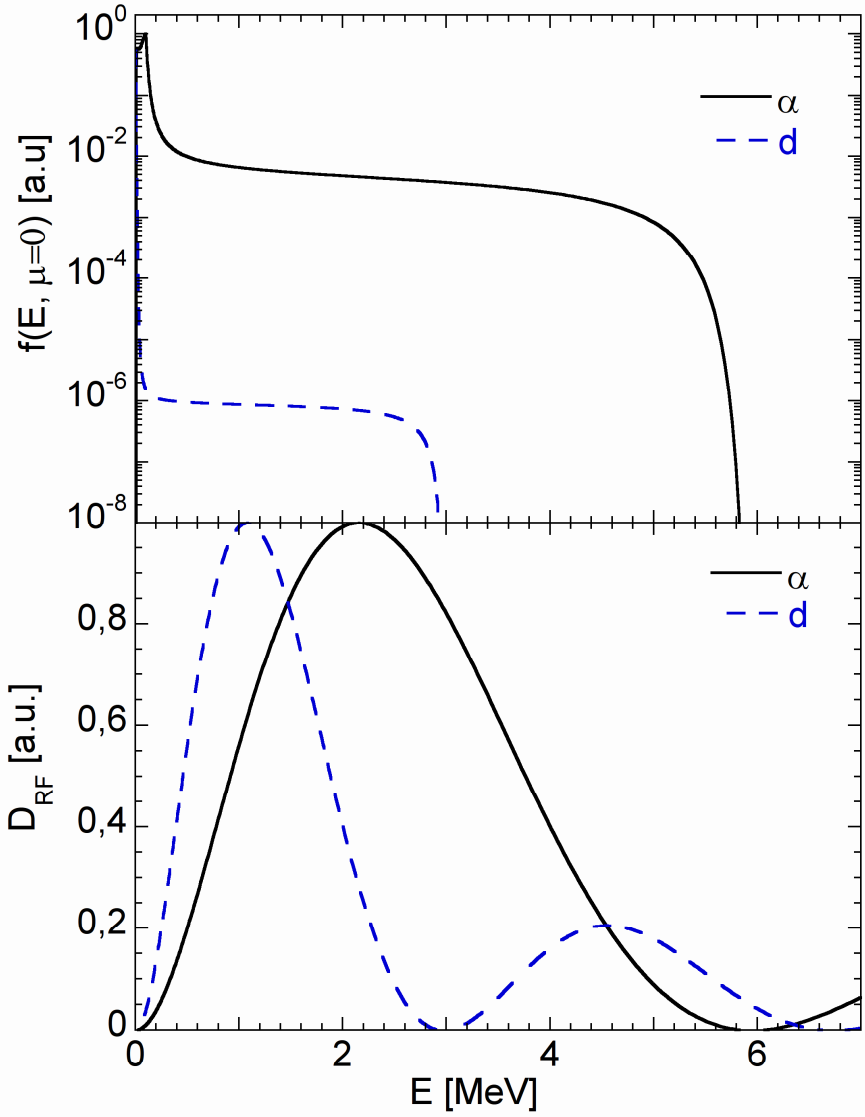

Figure 3. Calculated perpendicular (μ=0) energy distribution for deuterons and ^{4}He ions accelerated at the third harmonic as described in the text (top) and corresponding RF diffusion coefficient D_{RF} (bottom). Coupled power densities $P_{RF}=5\cdot10^5$ W/m^3 and $5\cdot10^3$ W/m^3 are assumed for ^{4}He ions and deuterons respectively.

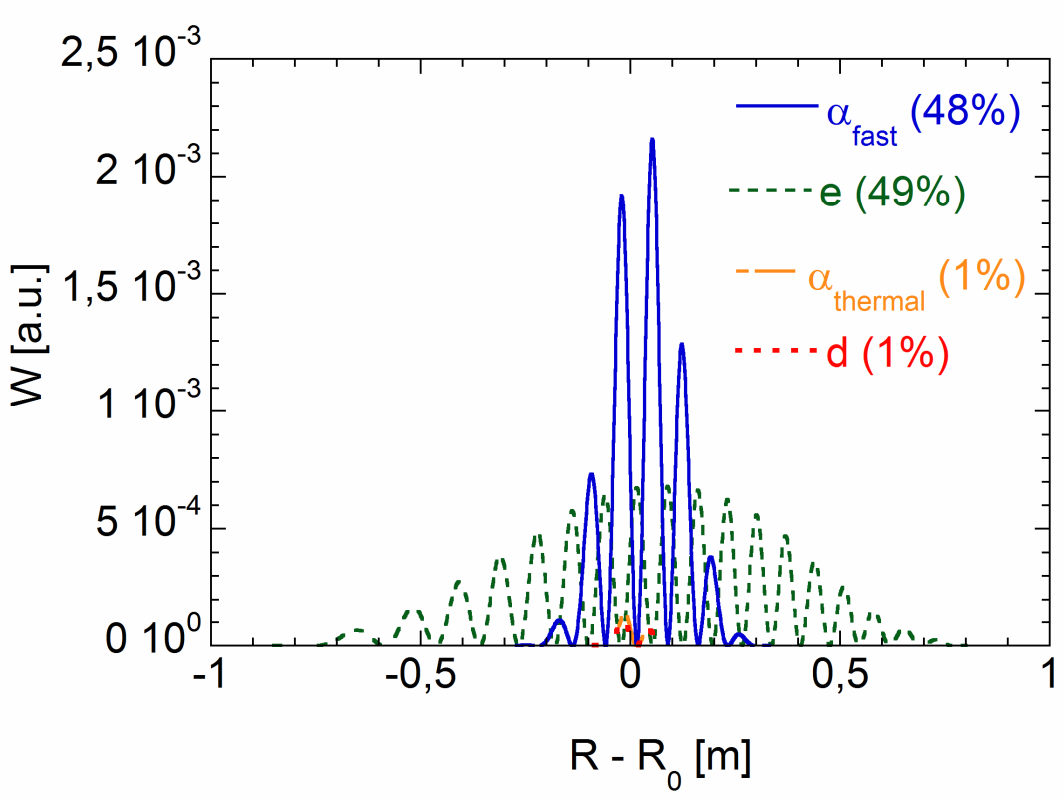

Figure 4. Single pass wave absorption simulated with the TOMCAT code for a (D)^{4}He plasma with ^{4}He neutral beam injection. The beam was represented in the code as a T_α=50 keV Maxwellian with 6% concentration. The power fractions absorbed by the different species are written in parentheses.

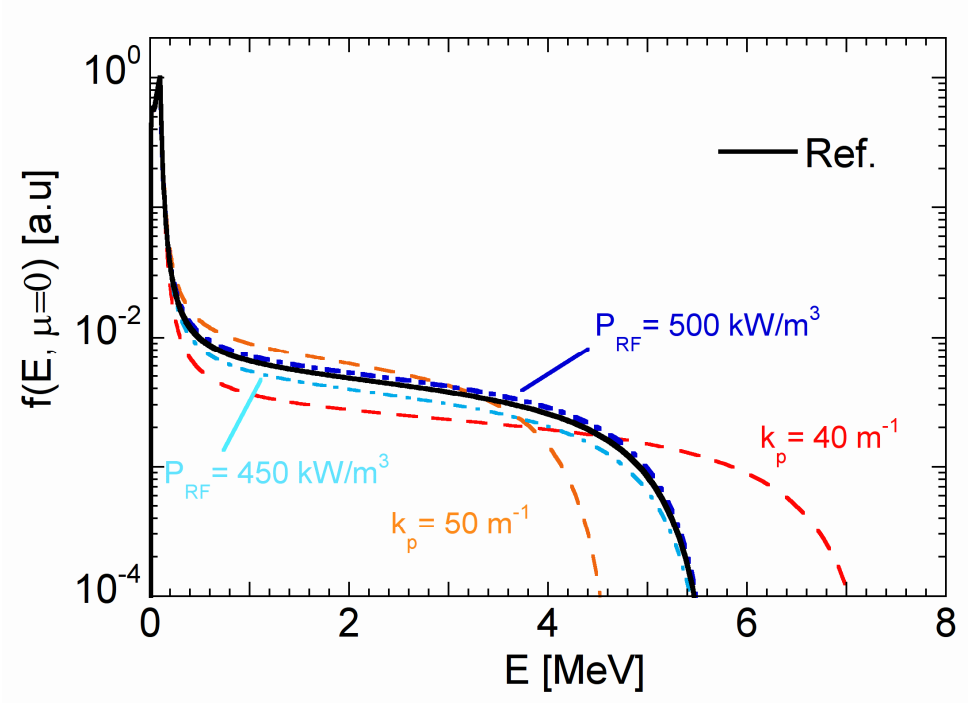

Figure 5. Changes in the ^{4}He ion perpendicular energy distribution by variations of the coupled power density P_{RF} and perpendicular wave number k_P of ±10% around reference values.

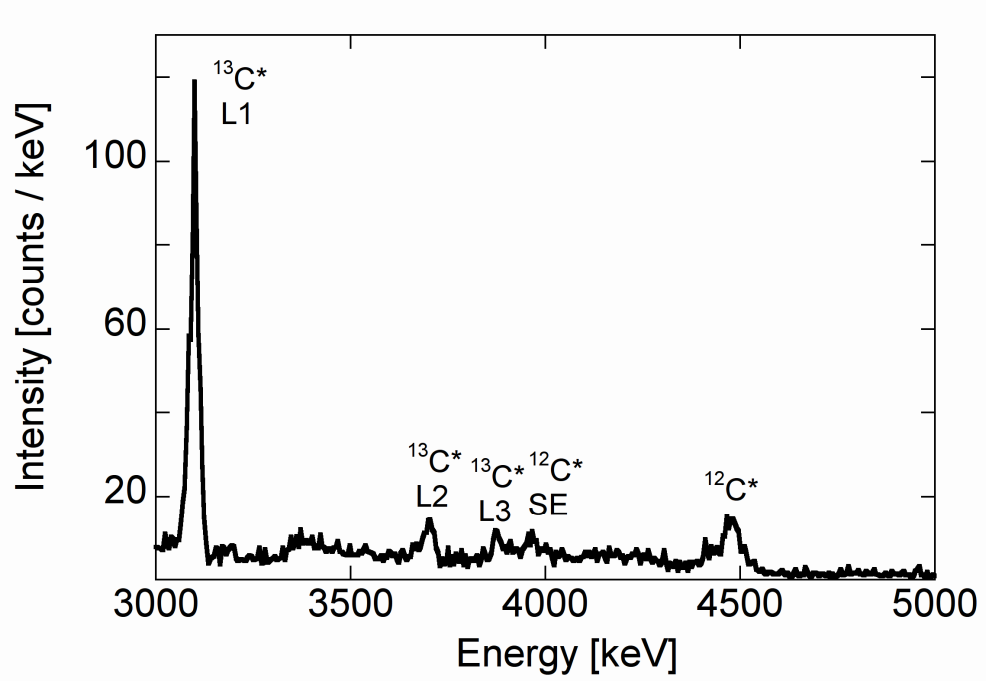

Figure 6. γ–ray emission spectrum recorded with a HpGe detector for the sum of JET discharges #79168-79171 in the time window 12-17 s. Labels indicate peaks from different excited states of ^{13}C* (L1-L3) and ^{12}C*, the latter also with its single escape (SE) peak.

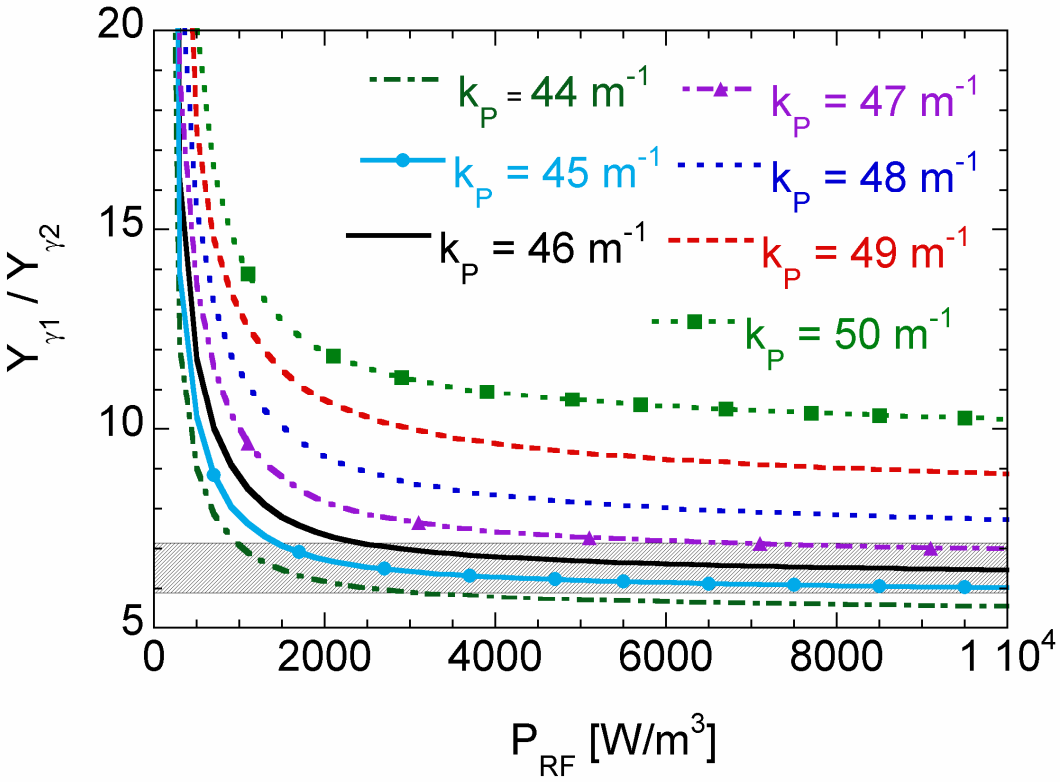

Figure 7. Calculated peak ratio $r=Y_{\gamma 1}/Y_{\gamma 2}$ between the first and second level of ^{13}C* as a function of the perpendicular wave number k_p and coupled power density P_{RF} of the deuteron energy distribution. The shadowed bar represents the measured value with its uncertainty.

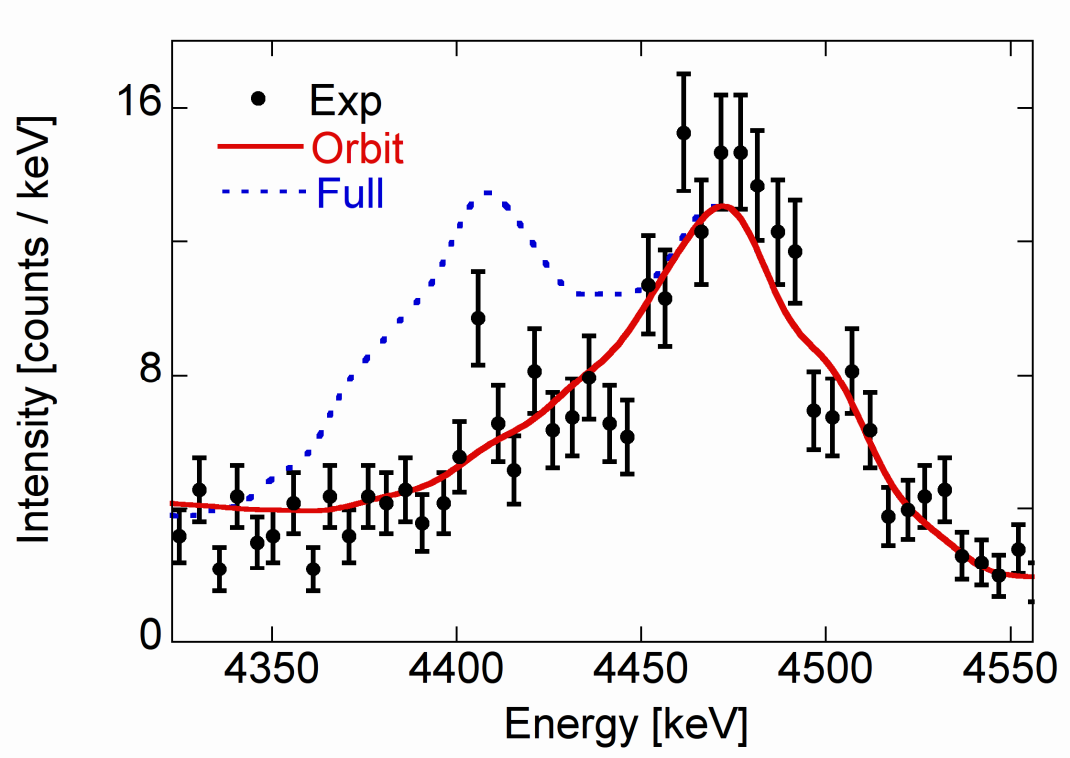

Figure 8. Doppler broadened E_γ=4.44 MeV peak from the $^{9}Be(\alpha, n\gamma)^{12}C$ reaction as measured with the HpGe detector for the sum of JET discharges #79168-79171 in the time window 12-17 s. The curves are the result of Monte Carlo simulations with the GENESIS code with (solid line) and without (dashed line) correlation between the gyro-radius of ^{4}He ions and the width of the line of sight.

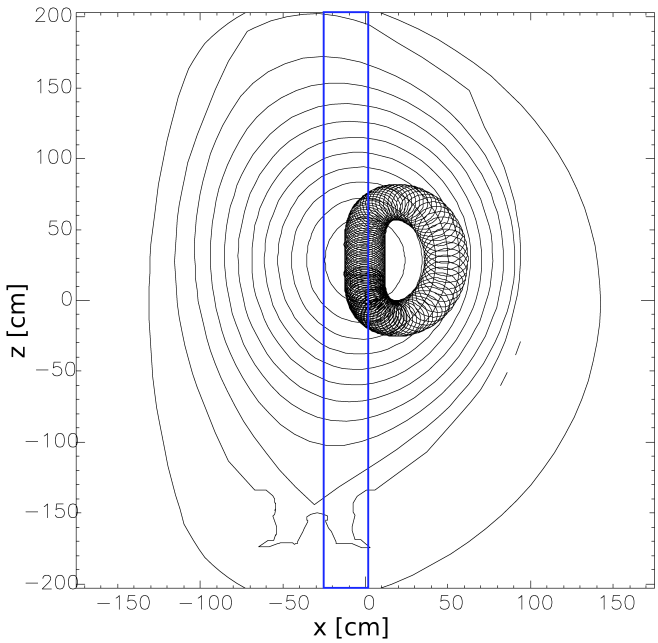

Figure 9. Orbit of a 4 MeV ^{4}He ion projected onto the poloidal plane. The particle is originated on the magnetic axis (z = 0 cm, x = 0 cm) with pitch angle of 90°. The rectangle represents the detector line of sight.

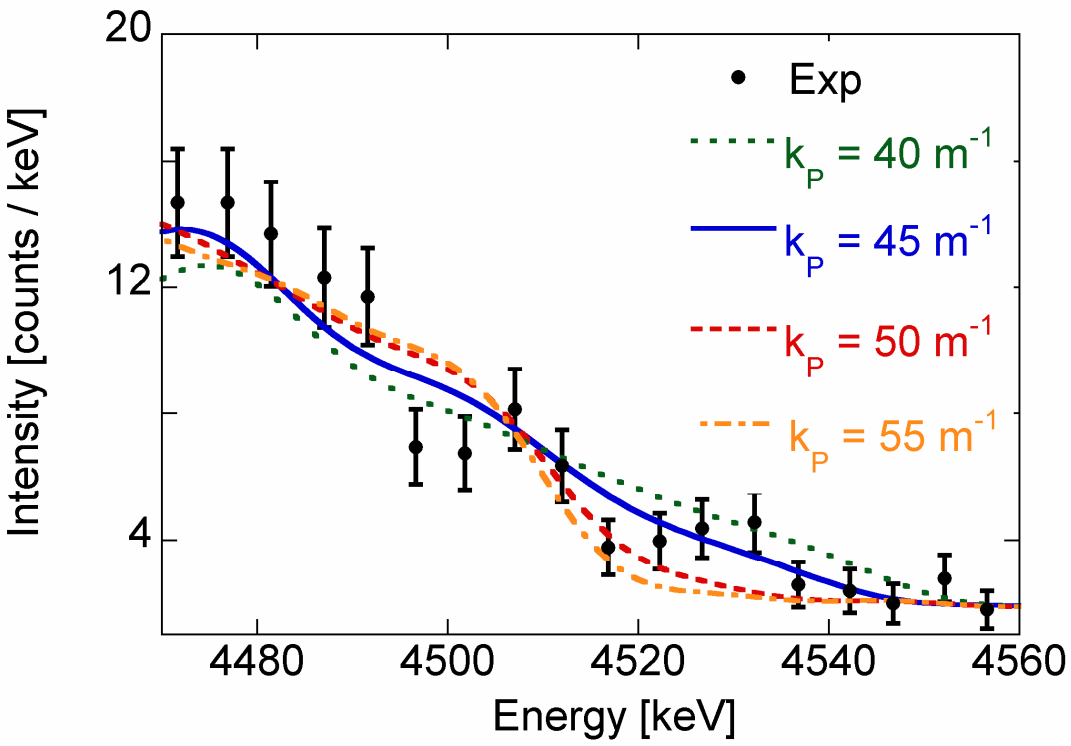

Figure 10. Upper half of the E_γ=4.44 MeV peak from the $^{9}Be(\alpha, n)^{12}C$ reaction and simulations with the GENESIS Monte Carlo code for several values of the perpendicular wave number k_p.

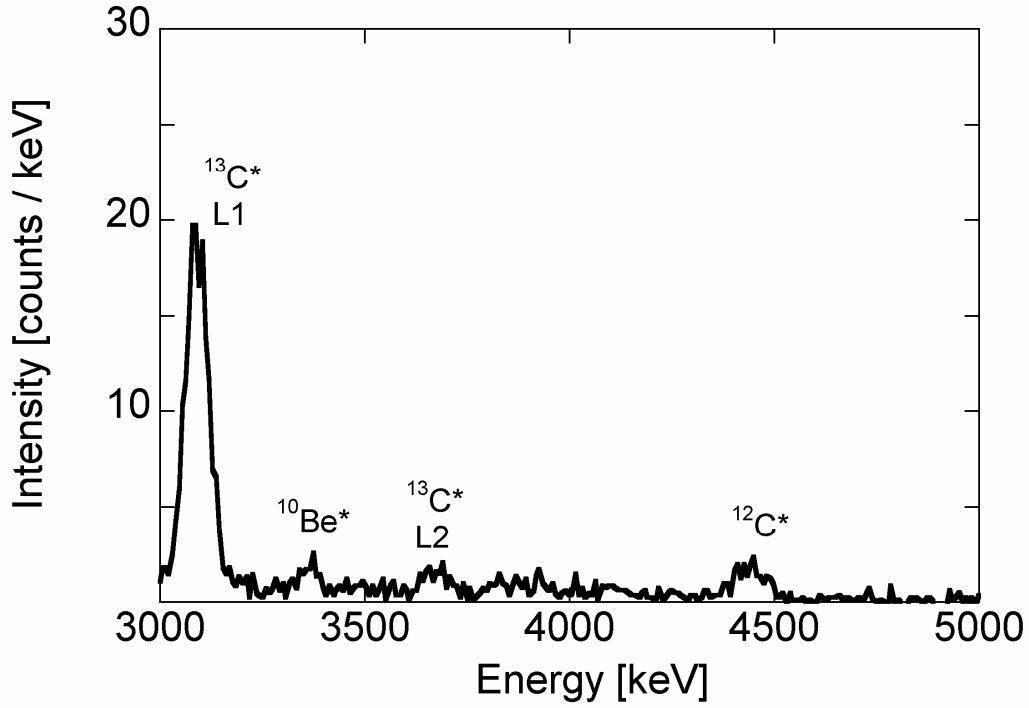

Figure 11. γ–ray emission spectrum recorded with a $LaBr_3(Ce)$ detector for JET discharge #79174 in the time window 4-8 s. Shown are peaks from different excited states of $^{13}C^*$ (L1 and L2) as well as peaks from $^{12}C^*$ and $^{10}Be^*$.

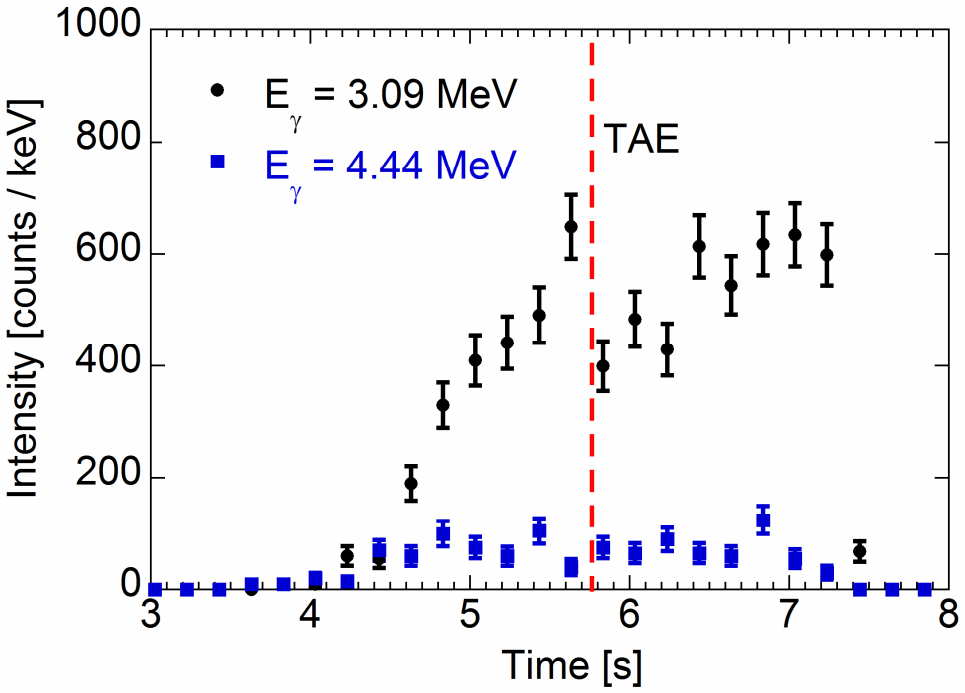

Figure 12. Count rates of the E_γ=3.09 MeV and E_γ=4.44 MeV peaks from the $^{12}C(d, p\gamma)^{13}C$ and $^{9}Be(\alpha, n\gamma)^{12}C$ reactions measured for discharge #79174. The vertical dashed line represents the instant when a Toroidal Alfvén Eigenmode (TAE) was detected in the magnetic traces.

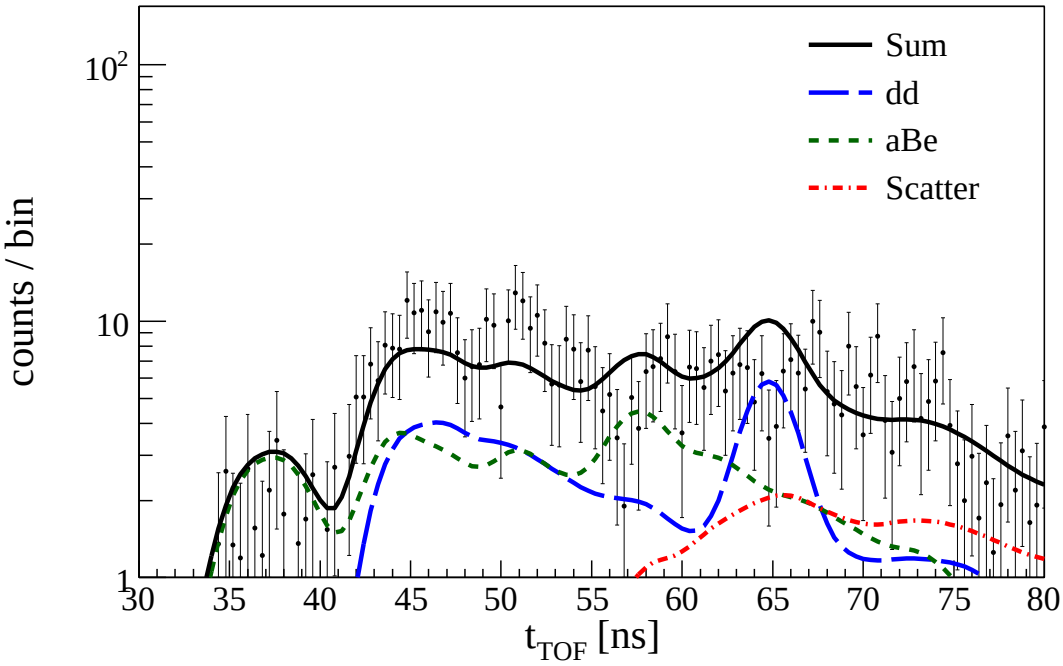

Figure 13. Neutron spectrum measured with the TOFOR spectrometer for the sum of JET discharges #79168-79171 in the time interval 12 to 17 s. The curves are simulations of the expected d + d→n + ^{3}He (long dash) and α + ^{9}Be→n + ^{12}C (short dash) neutron spectra, plus a scatter component (dash-dotted) taking into account neutron diffusion from the tokamak walls.

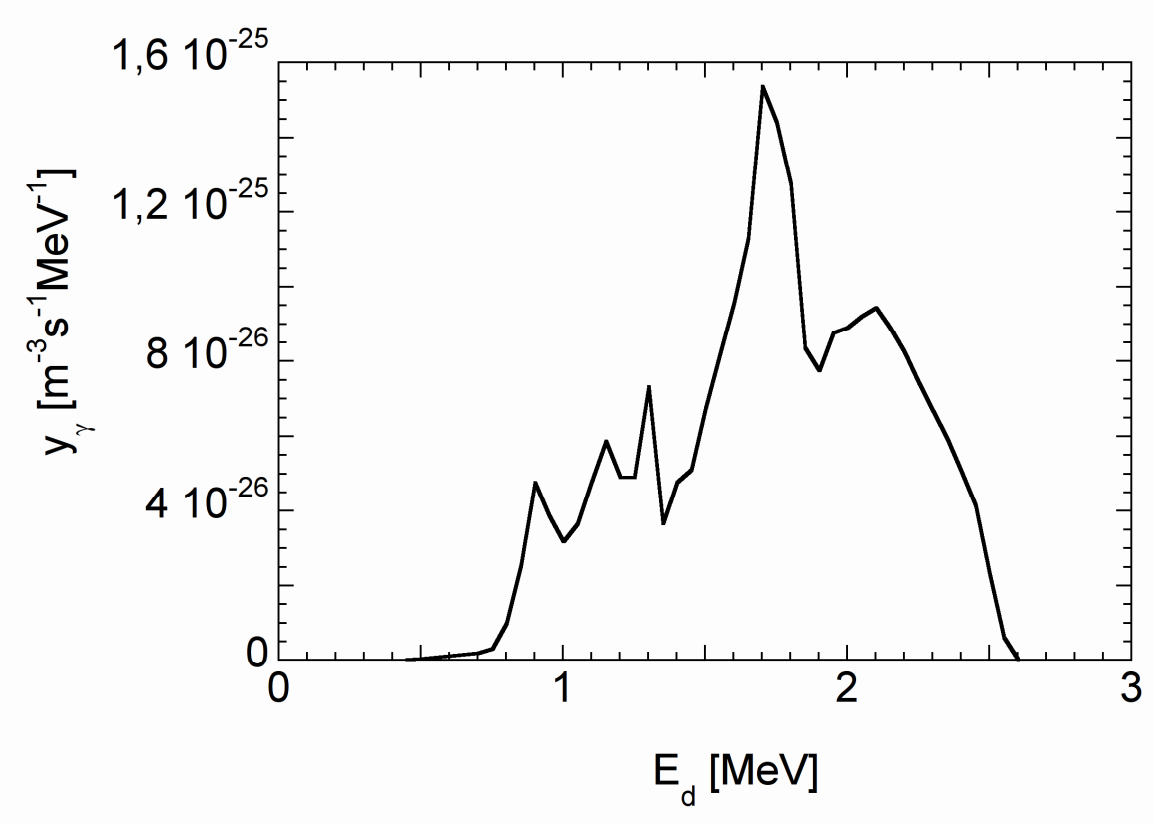

Figure 14. Differential reactivity for the production of E_γ=3.09 MeV γ-rays from the $^{12}C(d, p\gamma)^{13}C$ reaction for third harmonic RF heating and parameters described in the text.

Paper VII

Energy resolution of gamma-ray spectroscopy of JET plasmas with a $LaBr_3$ scintillator detector and digital data acquisition[a)]

M. Nocente,[1,b)] M. Tardocchi,[1] I. Chugunov,[2] R. C. Pereira,[3] T. Edlington,[4] A. M. Fernandes,[3] D. Gin,[2] G. Grosso,[1] V. Kiptily,[4] A. Murari,[5] A. Neto,[3] E. Perelli Cippo,[1] A. Pietropaolo,[1] I. Proverbio,[1] A. Shevelev,[2] J. Sousa,[3] B. Syme,[4] G. Gorini,[1] and JET-EFDA Contributors[6,c)]

[1]*Dipartimento di Fisica, Università degli Studi di Milano-Bicocca and Istituto di Fisica del Plasma, Associazione EURATOM-ENEA-CNR, 20125 Milano, Italy*
[2]*A. F. Ioffe Physico-Technical Institute, St. Petersburg 194021, Russia*
[3]*Associação EURATOM/IST Centro de Fusão Nuclear, Instituto Superior Técnico, 1049-001 Lisboa, Portugal*
[4]*Culham Centre for Fusion Energy, Culham OX143DB, United Kingdom*
[5]*Consorzio RFX, 35127 Padova, Italy*
[6]*JET-EFDA, Culham Science Centre, Abingdon OX14 3DB, United Kingdom*

(Presented 17 May 2010; received 16 May 2010; accepted 24 May 2010; published online 26 October 2010)

A new high efficiency, high resolution, fast γ-ray spectrometer was recently installed at the JET tokamak. The spectrometer is based on a $LaBr_3$(Ce) scintillator coupled to a photomultiplier tube. A digital data acquisition system is used to allow spectrometry with event rates in excess of 1 MHz expected in future JET DT plasmas. However, at the lower rates typical of present day experiments, digitization can degrade the energy resolution of the system, depending on the algorithms used for extracting pulse height information from the digitized pulses. In this paper, the digital and analog spectrometry methods were compared for different experimental conditions. An algorithm based on pulse shape fitting was developed, providing energy resolution equivalent to the traditional analog spectrometry method. [doi:10.1063/1.3501386]

I. INTRODUCTION

Gamma-ray spectrometry (GRS) is used on the JET fusion device for observation of reactions between energetic ions and plasma impurities.[1–3] Different γ-ray spectrometers are available since 2009:

(i) A high purity germanium was installed because of its very high energy resolution.[4] The crystal is sensitive to neutron damage, which limits the use of this detector in a fusion environment. When used, it provides data of excellent quality in the γ-ray energy range up to 5 MeV.
(ii) Bismuth germanate (BGO) and sodium iodide (NaI) detectors. These detectors were used at JET for a number of years[3] because of their high efficiency and reasonably good energy resolution over a broad range of γ-ray energies.
(iii) The latest addition to the GRS instrument suite is a lanthanum bromide (Brillance) detector. $LaBr_3$(Ce) is a new scintillating material[5] delivering a very high light yield and hence energy resolution. It is also fast (see pulse shape in Fig. 1) and insensitive to neutrons. Our 3 in.$\times$6 in. $LaBr_3$(Ce) crystal is coupled to a Hamamatsu photomultiplier tube (PMT) designed to allow operations at rates up to 2 MHz.[6] The PMT signal is fed into a fast preamplifier with five times gain before being digitized. High rate capability is enabled by a dedicated pulse digitization data acquisition system[7] based on the ATCA platform with a sampling frequency up to 400 MSPS and a nominal 14-bit resolution. The acquisition board has channels with ac or dc coupling. A threshold on the signal coming from the PMT is set to avoid noise peak-up. When the signal exceeds the threshold, a trigger is set and a data segment is stored consisting of 128 samples. The first 30 sample points are taken immediately before the trigger. This provides the baseline level for each event. The remaining points contain the actual digitized pulse. Each digitized event has an associated time-stamp to allow for time resolved data analysis.

The digital data acquisition system is used to allow for spectrometry measurements with event rates in excess of 1 MHz, expected in future JET DT plasmas. However, at the lower rates typical of present day experiments, digitization can degrade the energy resolution of the system, depending on the algorithms used for extracting pulse height information from the digitized pulses. The effect of digitization and different processing algorithms is studied here by comparing the results of digital and analog spectrometry for different experimental conditions.

[a)]Contributed paper, published as part of the Proceedings of the 18th Topical Conference on High-Temperature Plasma Diagnostics, Wildwood, New Jersey, May 2010.
[b)]Author to whom correspondence should be addressed. Electronic mail: massimo.nocente@mib.infn.it.

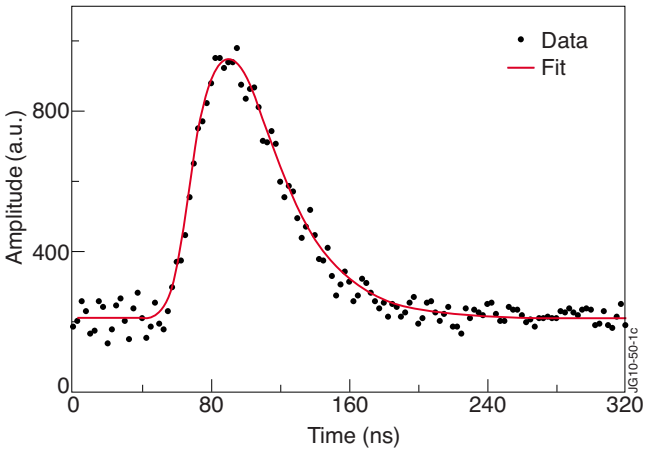

FIG. 1. (Color online) Example of $LaBr_3(Ce)$ digitized pulse from a 1.5 MeV γ-ray. The solid line is the best fit to the data using Eq. (1).

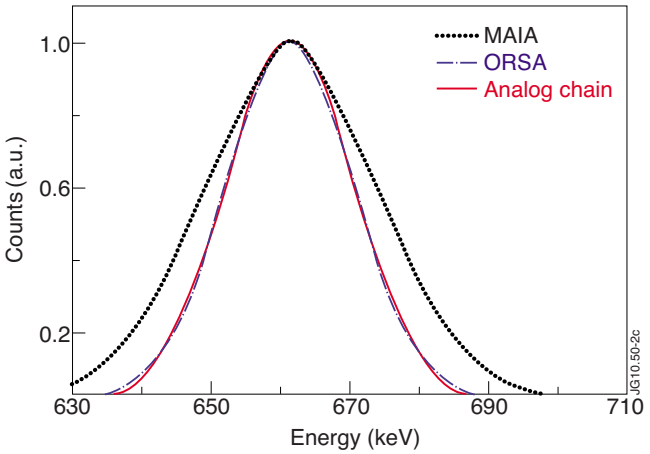

FIG. 2. (Color online) Comparison of a reconstructed ^{137}Cs peak at 661.66 keV using the digitized data processed with the MAIA (dashed line) and ORSA (dashed-dotted line) algorithms. Results from an analog spectrometry chain are also shown for comparison (full line). Measurements were performed in low noise laboratory conditions.

II. SPECTRUM RECONSTRUCTION ALGORITHMS

Dedicated algorithms were developed to build the event pulse height spectrum. A first algorithm named MAIA (maximum algorithm for intershot analysis) was written with the aim of providing a spectrum immediately after a JET discharge. The code is written in C and takes about 15 s to reconstruct a spectrum made of 10^5 events when running on a computer of the JET analysis cluster. The event pulse height is extracted from the corresponding data segment by taking the difference between the sample with maximum height inside the segment and the baseline. The latter is evaluated as an average of the first 20 points of the segment.

A second algorithm named ORSA (offline reconstruction simple algorithm) was developed to better cope with noisy data. The absence of an hardware noise filtering stage between the PMT and the ATCA implies that baseline noise is reflected into the sampled pulse. Moreover, amplitude walks can introduce an uncertainty on the baseline value determined as average of the first 20 points of each segment. Noise filtering is achieved in ORSA by pulse fitting. The shape $S(t)$ of each digitized event is described as

$$S(t) = \begin{cases} y_0 \quad if \ \ t < t_0 \\ y_0 + N\{1 - \exp[-(t-t_0)/\tau_1]\}^P \\ \exp[-(t-t_0)/\tau_2] \quad if \ \ t > t_0, \end{cases} \tag{1}$$

where y_0, N, and t_0 are fit parameters. τ_1, τ_2, and P are instead determined by a prefit and kept constant for all the pulses; i.e., the pulse shape is assumed not to depend on γ-ray energy. The best values for these parameters were found to be $\tau_1 = 31.6$ ns, $\tau_2 = 23.8$ ns, and $P = 3.5$ when the accelerating voltage V_{HV} between the anode and the photocathode of the PMT was 800 V. τ_1 was found to have a slight dependence on V_{HV}, while τ_2 and P were independent of V_{HV}. An example of the fit accuracy is shown in Fig. 1. Like MAIA, the pulse height of each event is determined from the difference between the maximum and the baseline, but now the fitted pulse shape is used instead of the raw data. ORSA is slow compared to MAIA but provides better results.

III. RESULTS

The pulse height resolution of the system was investigated in laboratory tests and compared to that of an analog spectrometry chain consisting of a preamplifier+shaping amplifier and an ADC unit. The PMT was operated with $V_{HV} = 800$ V. Gamma rays from ^{137}Cs and ^{60}Co radioactive sources were detected and the pulse height spectrum reconstructed using both ORSA and MAIA algorithms. The reconstructed ^{137}Cs peak at 661.66 keV is shown in Fig. 2 as resulting from the three approaches in the case of measurements performed in low noise laboratory conditions. Pulse height resolution (FWHM) values at the three calibration peaks can be compared in Table I. One can see that the values obtained with the ORSA algorithm are close to the analog spectrometry values. This is an important result since it shows that digitization in itself does not degrade the resolution of the measurement. On the other hand, it is essential for enabling spectrometry at high rates. The results obtained with MAIA, although not optimal, are still better than the NaI and BGO detectors previously used at JET: they feature a resolution of about 7% at the same energy.

Figure 3 shows the achieved resolution (FWHM in keV and in percent) of the ^{137}Cs line at 661.66 keV during experiments at a Tandem accelerator for different photomultiplier voltages. For comparison, the best resolution obtained with an analog chain in low noise laboratory conditions is also shown. Again, the analog spectrometry chain and the

TABLE I. Comparison of pulse height resolution values obtained with the digital spectrometry system and the ORSA and MAIA algorithms described in the text for characteristic calibration of γ-ray peaks. Results from an analog spectrometry chain are also shown for comparison.

Gamma-ray peak	MAIA (%)	ORSA (%)	Analog chain (%)
662 keV (^{137}Cs)	4.4	3.3	3.2
1173 keV (^{60}Co)	3.2	2.5	2.4
1333 keV (^{60}Co)	3.0	2.4	2.3

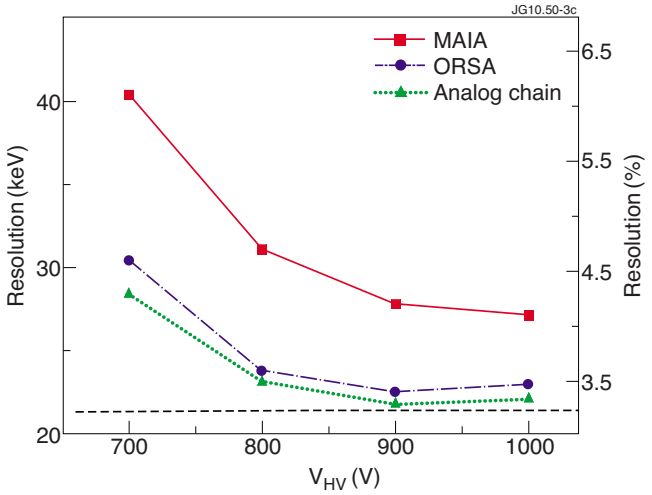

FIG. 3. (Color online) Resolution (FWHM in keV and in %) of the ^{137}Cs line at 661.66 keV during experiments at a Tandem accelerator for different photomultiplier voltage. The analog spectrometry chain (triangles) and the ORSA algorithm (circles) provide similar results. The MAIA algorithm (squares) is somewhat worse. The dashed line represents the best resolution obtained with an analog chain in low noise laboratory conditions.

ORSA algorithm are found to provide similar results. Optimal resolution is achieved when $V_{HV} \geq 800$ V, with no significant improvement in resolution at higher PMT operating voltages. Resolution with the MAIA algorithm is instead improved by choosing a higher voltage value. This suggests that cable noise is the main cause for resolution deterioration and is partly compensated for by increasing the signal amplitude.

The $LaBr_3$ spectrometer was successfully used at JET to measure γ-ray spectra in recent experiments where fast ions were produced by ion cyclotron resonance heating (ICRH). The digital data acquisition proved to be high reliable with practically no loss of data due to malfunction. Figure 4 shows a pulse height spectrum measured during an experiment in a (^{3}He)H plasma meant to study minority and mode conversion heating in inverted (^{3}He)H scenarios[8,9] of relevance for the nonactive phase of ITER. The first harmonic

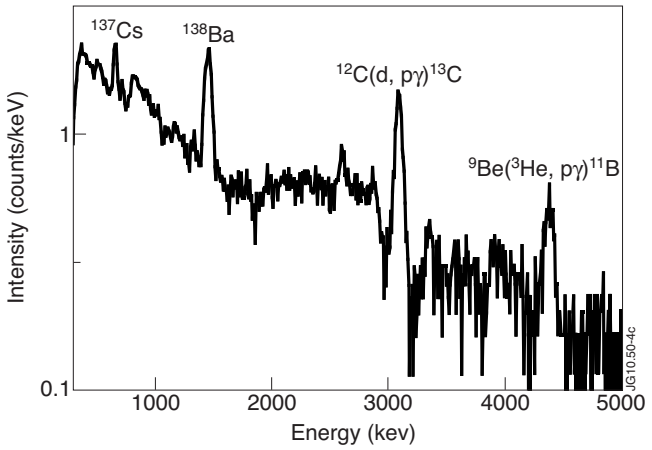

FIG. 4. Gamma-ray spectrum from JET pulse No. 79352 obtained with the digital spectrometry system and the ORSA algorithm described in the text. Gamma-ray peaks due to the ^{12}C(d,pγ)^{13}C and ^{9}Be(^{3}He,pγ)^{11}B reactions are marked. Other peaks due to calibration sources or intrinsic detector radioactivity can also be identified.

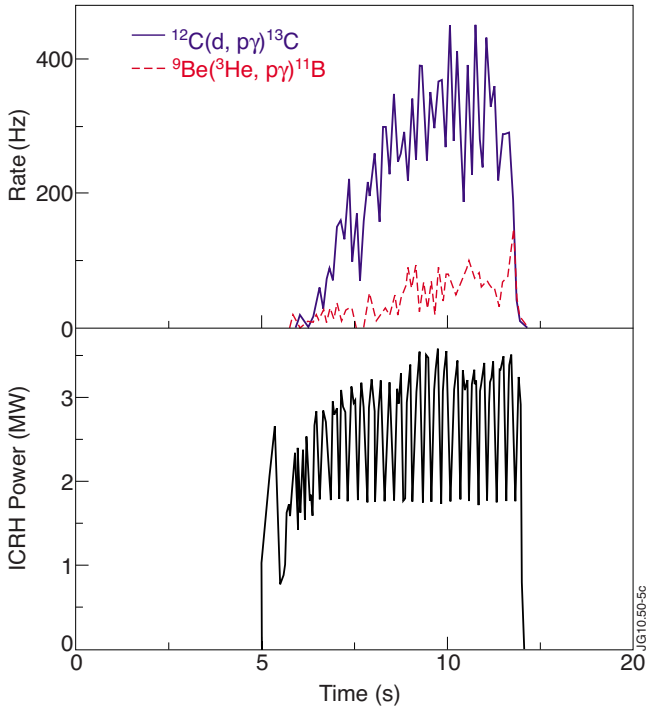

FIG. 5. (Color online) Time traces of measured rates in the pulse height energy regions E=3.0–3.2 MeV and E=4.3–4.6 MeV corresponding to γ-ray peaks from the reactions ^{12}C(d,pγ)^{13}C and ^{9}Be(^{3}He,pγ)^{11}B observed in JET pulse No. 79352. The corresponding ICRH power time trace is also shown for comparison.

ICRH was tuned to fundamental ^{3}He frequency. When the ^{3}He concentration was sufficiently low, high energy tails in the ^{3}He distribution function were created as a result of ICRH heating. These fast ions in turn induced γ-ray emission when interacting with impurities inside the machine (typically ^{12}C and ^{9}Be at JET).[3] In (^{3}He)H plasmas, γ-rays from the reaction ^{9}Be(^{3}He,pγ)^{11}B were expected to be observed. These are represented by the peak at 4.44 MeV in Fig. 4 due to a transition from the second to ground state of ^{11}B. However, γ-ray emission from the reaction ^{12}C(d,p)^{13}C was also observed, which implied production of deuterons with energy greater than 0.5 MeV.[3] This unexpected event is represented by the peak at 3.09 MeV in Fig. 4 due to transition from the first to the ground state of ^{13}C. The two peaks at lower energies are instead due to calibration sources (the peak at 661.66 keV is due to ^{137}Cs) or to the detector intrinsic radioactivity (peak at 1473 keV due to excited ^{138}Ba, produced after electron capture on ^{138}La). Figure 5 shows the temporal evolution of signal proportional to the γ-ray emission due to the reactions ^{9}Be(^{3}He,pγ)^{11}B and ^{12}C(d,p)^{13}C. The coherent trend shows that ^{3}He and d ions were both accelerated by the applied ICRH and illustrates the time resolution achieved with the new $LaBr_3$ spectrometry system. Much higher rates and better time resolutions are expected from this system when plasmas with alpha particles and ^{9}Be impurities are available, e.g., in DT fusion experiments in JET and ITER.

IV. CONCLUSIONS

A $LaBr_3$(Ce) scintillator with fully digital data acquisition designed for high rate operation was installed at JET.

Dedicated spectrum reconstruction algorithms were written to allow for immediate visualization of the measured γ-ray spectrum or to provide pulse height resolution matching the best resolution available from conventional analog spectrometry chains. The system was successfully used during recent JET experiments where it provided data at relatively low rates. Much higher rates are envisaged in future DT plasmas due to the presence of energetic alpha particles.

ACKNOWLEDGMENTS

This work was supported by EURATOM and carried out within the framework of the European Fusion Development Agreement. The views and opinions expressed herein do not necessarily reflect those of the European Commission.

[1] F. E. Cecil and D. E. Newman, Nucl. Instrum. Methods Phys. Res. **221**, 449 (1984).
[2] V. G. Kiptily, S. Popovichev, S. E. Sharapov, L. Bertalot, F. E. Cecil, S. Conroy, and M. J. Mantsinen, Rev. Sci. Instrum. **74**, 1753 (2003).
[3] V. G. Kiptily, F. E. Cecil, O. N. Jarvis, M. J. Mantsinen, S. E. Sharapov, L. Bertalot, S. Conroy, L. C. Ingesson, T. Johnson, K. D. Lawson, S. Popovichev, and EFDA-JET Workprogramme Contributors, Nucl. Fusion **42**, 999 (2002).
[4] A. Murari, M. Angelone, G. Bonheure *et al.*, Rev. Sci. Instrum., these proceedings.
[5] E. V. D. van Loef, P. Dorenbos, C. W. E. van Eijk, K. W. Krämer, and H. U. Güdel, Nucl. Instrum. Methods Phys. Res. A **486**, 254 (2002).
[6] M. Tardocchi, L. I. Proverbio, G. Gorini, G. Grosso, M. Locatelli, I. N. Chugonov, D. B. Gin, A. E. Shevelev, A. Murari, V. G. Kiptily, B. Syme, A. M. Fernandes, R. C. Pereira, and J. Sousa, Rev. Sci. Instrum. **79**, 10E524 (2008).
[7] R. C. Pereira, J. Sousa, A. M. Fernandes, F. Patrício, B. Carvalho, A. Neto, C. A. F. Varandas, G. Gorini, M. Tardocchi, D. Gin, and A. Shevelev, Fusion Eng. Des. **83**, 341 (2008).
[8] M.-L. Mayoral, P. U. Lamalle, D. Van Eester, E. A. Lerche, P. Beaumont, E. De La Luna, P. De Vries, C. Gowers, R. Felton, J. Harling, V. Kiptily, K. Lawson, M. Laxåback, P. Lomas, M. J. Mantsinen, F. Meo, J.-M. Noterdaeme, I. Nunes, G. Piazza, M. Santala, and JET-EFDA Contributors, Nucl. Fusion **46**, S550 (2006).
[9] E. Lerche, D. Van Eester, T. Johnson *et al.*, Proceedings of the 37th EPS Conference on Plasma Physics and Controlled Fusion, Dublin, Ireland, 21–25 June 2010.

Paper VIII

High Resolution Gamma Ray Spectroscopy at MHz Counting Rates with $LaBr_3$ Scintillators

M. Nocente, M. Tardocchi, A. Olariu, S. Olariu, I.N. Chugunov, A. Fernandes, D.B. Gin, G. Grosso, V.G. Kiptily, A. Neto, R. C. Pereira, A.E. Shevelev, M. Silva, J. Sousa and G. Gorini

***Abstract*– High resolution γ-ray spectroscopy measurements at MHz counting rates were carried out at nuclear accelerators, combining a $LaBr_3$(Ce) detector with dedicated hardware and software solutions based on digitization and post-mortem analysis. Spectra were reconstructed at counting rates up to 4 MHz, with little or no degradation of the energy resolution. The reported results represent a step forward towards the final goal of γ-ray spectroscopy measurements on a burning plasma device.**

***Index Terms* - Gamma-ray spectroscopy, high rate, $LaBr_3$ scintillators, fusion plasmas**

I. Introduction

UNDERSTANDING and controlling the behavior of a burning plasma is the ultimate scientific step towards the goal of using nuclear fusion as an energy source. A burning plasma is primarily a source of neutrons that, besides carrying most of the energy released in fusion reactions, provide diagnostic information on the reactants energy distribution, as demonstrated with measurements in present day tokamaks [1-6]. Although weaker, the role of γ-ray emission is also emerging for fusion plasma diagnosis [7]. γ-rays, emitted by reactions between fast ions and impurities, carry information on the energy distribution of supra-thermal particles [8] and their interaction with plasma instabilities [9]. Of special relevance are reactions in deuterium-tritium plasmas involving α particles, such as $^9Be(\alpha, n\gamma)^{12}C$, given their role for α particle studies in next generation tokamaks [10,11].

From the instrumental point of view, several developments are necessary to meet the challenging requirements imposed by γ-ray measurements for fast ion studies in a burning plasma environment. The capability to follow evolutions of the α particle energy distribution on the magneto-hydro-dynamic instability time scale, of the order of 1 ms or less, is mandatory. This in turn demands measurements of the γ-ray emission spectrum at MHz counting rates. As information on energetic ions reside in the broadening of characteristic γ-ray emission peaks or in the ratio of peaks produced by de-excitation of states from the same emitting nucleus [7,12,13], high energy resolution is also necessary.

In recent years, a new scintillator, $LaBr_3$(Ce), has emerged and has been used mainly for fundamental and applied nuclear physics studies [14]. Lanthanum bromide is fast (see pulse shape in Fig. 1), efficient and features high energy resolution, making the detector a good candidate for γ-ray spectroscopy at MHz counting rates in tokamak plasmas.

In this paper γ-ray spectroscopy measurements in the MHz range are presented. The measurements were carried out at nuclear accelerators, where counting rates from few kHz to several MHz were achieved. The adopted hardware and software solutions based on digitization of the measured signals and post-mortem analysis are illustrated. The reconstructed spectra are discussed in view of requirements for γ-ray spectroscopy measurements in burning plasma experiments. Prospects for further developments are finally addressed.

II. Experimental Setup and Data Processing

High rate gamma ray spectroscopy measurements were performed at the Tandem Van der Graaf (TVG) accelerator of the National Institute for Physics and Nuclear Engineering "Horia Hulubei" in Magurele (Romania) [15].

TABLE I. CHARACTERISTIC γ-RAY EMISSION PEAKS FROM $p+^{27}Al$ REACTIONS RECORDED DURING EXPERIMENTS AT THE TANDEM VAN DER GRAAF ACCELERATOR

Energy (keV)	Emitting nucleus
781 keV	^{27}Si
843 keV	^{27}Al
957 keV	^{27}Si
1014 keV	^{27}Al
1368 keV	^{24}Mg
1720 keV	^{27}Al
2210 keV	^{27}Al
2754 keV	^{24}Mg
2981 keV	^{27}Al

Manuscript received XXX. This work was supported by EURATOM. The views and opinions expressed herein do not necessarily reflect those of the European Commission.

M. Nocente, M. Tardocchi, G. Grosso and G. Gorini are with Istituto di Fisica del Plasma, EURATOM-ENEA-CNR Association, Via Cozzi 53, 20125, Milano, Italy (e-mail: massimo.nocente@mib.infn.it).

M. Nocente, M. Silva and G. Gorini are with Dipartimento di Fisica "G. Occhialini", Università degli Studi di Milano Bicocca, Piazza della Scienza 3, 20126, Milano, Italy

A. Olariu and S. Olariu are with National Institute for Physics and Nuclear Engineering "Horia Hulubei", EURATOM-MEdC Association, 30 Reactorului Street, Magurele, Romania

I.N. Chugunov, D.B. Gin, A.E. Shevelev are with A.F. Ioffe Physico-Technical Institute, 194021, St. Petersburg, Russian Federation

A. Fernandes, A. Neto. R. C. Pereira, J. Sousa are with Instituto Superior Técnico, Centro de Fusão Nuclear, Associação EURATOM/IST, 1049-001, Lisboa, Portugal

V.G. Kiptily is with Culham Centre for Fusion Energy, Culham Science Centre, OX14 3DB, Abingdon, United Kingdom

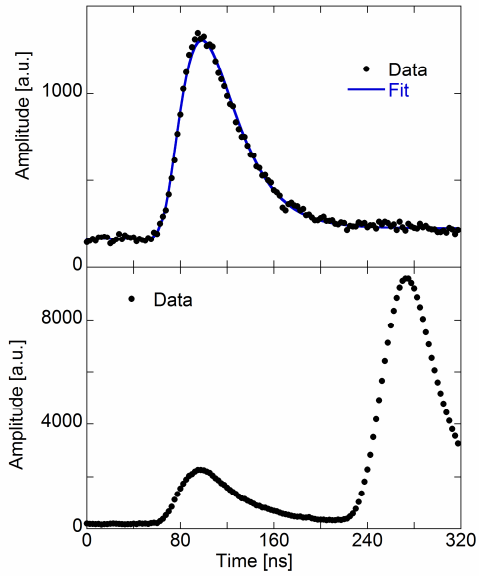

Fig. 1. Example of a digitized pulse from the $LaBr_3$(Ce) detector without (top) and with (bottom) pile up recorded during measurements at the Tandem Van der Graaf accelerator. The solid line in the top figure is a fit to digitized data with equation (1) of reference [18].

A beam of protons was accelerated to 10 MeV and interacted with an aluminum target through the reactions ^{27}Al(p, nγ)^{27}Si and ^{27}Al(p, αγ)^{24}Mg, producing characteristic γ-ray peaks from excited states of ^{27}Si and ^{24}Mg. ^{27}Si, generated in the ^{27}Al(p, nγ)^{27}Si reaction, is an unstable isotope that undergoes a β^+ decay to ^{27}Al with a half life of about 4s. This process provided an extra source of γ radiation, due to de-excitation of ^{27}Al states fed in the β^+ decay of ^{27}Si. ^{27}Al excited states could also be populated after inelastic proton scattering on aluminum. Table I summarizes the observed γ-ray peak energies and the associated emitting isotope

A 3"x6" $LaBr_3$(Ce) detector was coupled to a Hamamatsu Photo Multiplier Tube (PMT) designed to allow for operations at MHz counting rate [16] and was placed close to the reaction target. The distance was chosen in order to achieve the desired counting rate. The latter was also varied by changing the proton current of the TVG accelerator.

A data acquisition system based on the ATCA platform with a sampling rate of 400 MSample/s (MSPS) and a nominal 14-bit resolution [17] was used for the measurements. The signal coming from the PMT, fed at a voltage V_{HV}=800 V, was amplified by a fast, non-shaping pre-amplifier and digitized. The acquisition board was operated in the so called "segmented mode". A threshold is set on the signal coming from the detector. When a pulse exceeds the preset threshold, a segment consisting of 128 points is stored. The first 32 points contain samplings of the baseline level before the trigger condition occurs. The remaining 96 points are devoted to the pulse itself. A time stamp is associated to each segment for time resolved analysis of the collected data [18].

The γ-ray emission spectrum was reconstructed from the digitized data using an algorithm based on pulse fitting [18] and allowed for measurements at low counting rates *r*. At higher counting rates, say *r* > 100 kHz, superposition of more than one pulse within an acquisition segment (pile up) had to be taken into account (Fig. 1). Segments affected by pile up were discarded by a pile up rejection (PUR) routine. The latter is based on a chi-square like variable, χ^2_L, defined as

$$\chi^2_L = \sum_{i=1}^{128} (M_i - E_i)^2 \qquad (1)$$

where M_i represents the measured i-th sample within a segment and E_i the expected i-th value from a fit to data of the whole segment using equation (1) of reference [18].

A pile up event is identified when χ^2_L exceeds a preset tolerance level. This was determined from a test-run with ^{137}Cs and ^{60}Co calibration sources only, before the actual measurements at the TVG accelerator. Fig. 2 shows the distribution of the χ^2_L variable as obtained from the test-run. Most of the segments have χ^2_L values between 10^2 and 10^3 and correspond to well fitted events. In some cases, small systematic effects not accounted for by the adopted fit equation, such as a non flat baseline level after a pulse from the $LaBr_3$ crystal, result in higher χ^2_L values between 10^3 and about 10^4. These are represented by a tail in the χ^2_L distribution. Events with χ^2_L exceeding 10^4 are instead those affected by pile up. As Fig. 2 displays, most of pile up events have χ^2_L values much greater than the tolerance level, that lies around 10^4. This implies that the number of events classified as pile up is only slightly affected by the exact value of the tolerance, which makes the PUR method based on the χ^2_L variable insensitive to additional noise on the signal that might occur at high counting rates. A tolerance value of 8000 was chosen for the experiments at the TVG accelerator.

.

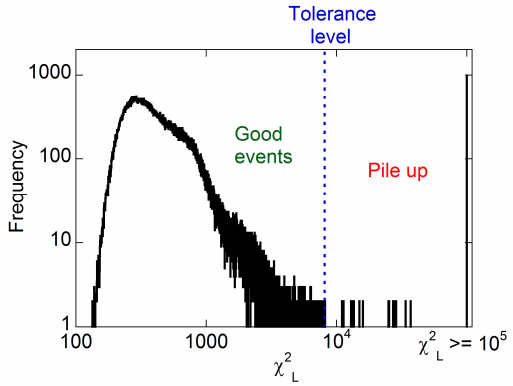

Fig. 2. Distribution of the χ^2_L variable obtained from a test-run with ^{137}Cs and ^{60}Co calibration sources. The column on the right represents acquisition segments with $\chi^2_L \geq 10^5$. The vertical dashed line indicates the chosen tolerance level that discriminates between segments without (left) and with (right) pile up.

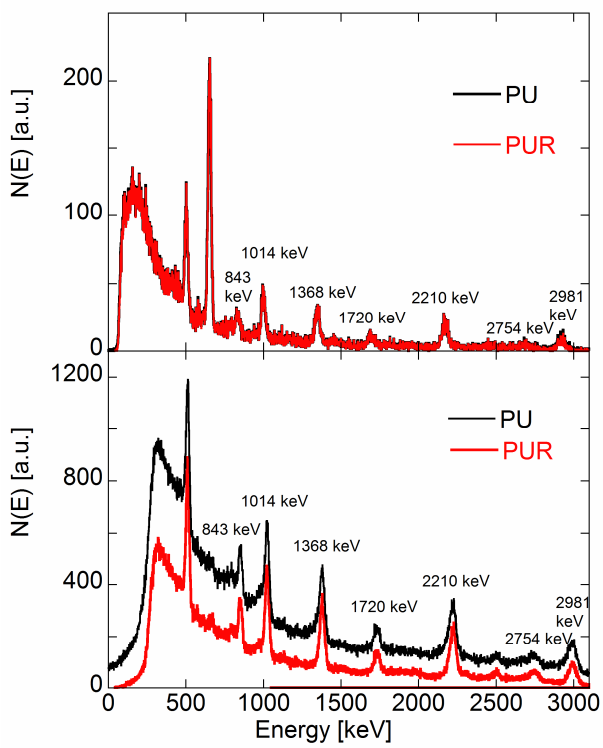

Fig. 3. (color online) γ-ray emission spectrum measured at the "Horia Hulubei" TVG accelerator at 80 kHz (top) and 2.6 MHz (bottom) counting rates. The red curve is the spectrum obtained with PUR as described in the text. The spectrum obtained without PUR is also shown (black line). The E_γ=662 keV peak from a ^{137}Cs calibration source is visible in the measurement at 80 kHz. The sharp peak at E_γ=511 keV originates from background radiation.

III. RESULTS

Fig. 3. shows the spectrum measured at the TVG accelerator for counting rates of 80 kHz and 2.6 MHz. The same energy calibration was applied to both spectra and was derived from the test-run with calibration sources only. All peaks listed in Table I can be clearly distinguished, but for peaks at E_γ=781 and 957 keV, that barely emerge from the background. The mean position of the peaks is also unchanged between measurements at 80 kHz and 2.6 MHz, showing that no appreciable variations of the PMT gain occurred, as expected. At 80 kHz there is almost no difference between spectra reconstructed with and without the PUR routine, due to the limited probability of recording pile up events at this counting rate. As the counting rate is increased toward the MHz range, pile up affects a significant fraction of the recorded events. This is shown by the 2.6 MHz spectrum of Fig. 3, where the fraction of segments affected by pile up amounts to 51.9 % of the total. When pile up is of relevance, the effect of the PUR routine is to improve both the signal to background ratio of γ-ray emission peaks and their energy resolution, with reduction of the instrumental peak broadening by fractions of percent. The effect of the PUR routine on the energy resolution was found to be more and more pronounced as the counting rate was progressively increased.

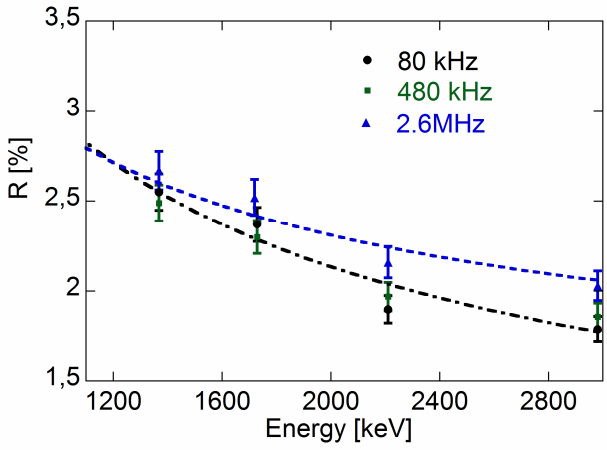

Fig. 4. (color online) Energy resolution of γ-ray emission peaks at different energies determined from measurements at the TVG accelerator. The three set of points show results at different counting rates. The dashed lines are the fit to measured data with equation (2) (see text).

Figure 4 shows the energy resolution of γ-ray emission peaks at different energies determined from measurements at the TVG accelerator. Results are shown at three different counting rates, from 80 kHz to 2.6 MHz. The data points can be fitted by the following equation [19]

$$R = A + B/\sqrt{E} \qquad (2)$$

where R indicates the energy resolution and A, B are fit parameters that depend on the counting rate. If we focus on the energy resolution at E_γ=3 MeV we note that there is almost no difference between the value obtained for r=80 kHz and 480 kHz; R is only slightly worse at r=2.6 MHz, raising to 2% from the value 1.8% obtained at r=80 kHz. This result demonstrates high resolution γ-ray spectroscopy at MHz counting rates with $LaBr_3$(Ce) scintillators.

Experiments at even higher counting rates were also performed, as shown in Fig. 5, where the γ-ray emission spectrum recorded at r=4.4 MHz is displayed. At this counting rate, the spectrum is partially degraded. γ-ray peaks at $E_\gamma < 2$ MeV are significantly broader than in Fig. 3. For $E_\gamma > 2$ MeV, characteristic reaction peaks are no more distinguished. The PUR routine (Fig. 5, red curve) improves the peak energy resolution for $E_\gamma < 2$ MeV, but fails to recover the spectrum at higher energies. The reason is that, at this counting rate, deterioration of the measured spectrum due to gain shifts of the PMT dominated over that due to pile up.

The same measurement was repeated by feeding the PMT at V_{HV}=700 V. In this way, the ratio between the mean photoelectric current running between the PMT dynodes and that flowing in the PMT voltage divider was lowered, which reduces gain variations [16]. The resulting spectrum is shown in Fig. 5, bottom part. All γ-ray peaks observed at lower counting rates are distinguished, particularly when adopting the PUR routine, that ameliorates the spectrum both at a quantitative and qualitative level. A small price is however paid in terms of energy resolution, which equals 2.4 % at

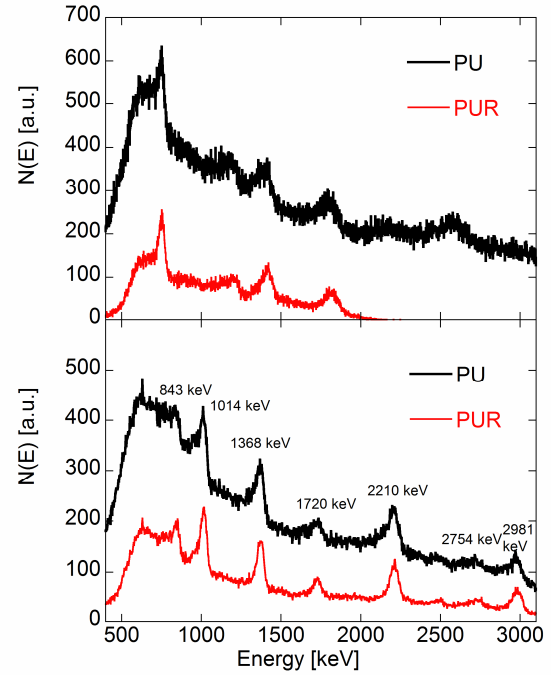

Fig. 5. (color online) γ-ray emission spectrum measured at the "Horia Hulubei" TVG accelerator at 4.4 MHz counting rate. The top figure shows the spectrum obtained when feeding the PMT with V_{HV}=800 V. The measurement at V_{HV}=700 V is shown in the bottom. Spectra processed without (black line) and with (red line) the PUR routine are shown in both cases.

E_γ= 3 MeV, due to the smaller pulse height at V_{HV}=700 V relative to V_{HV}=800 V for γ-rays of same energy.

IV. DISCUSSION

A key parameter for γ-ray spectroscopy measurements on a burning plasma device is the counting level under a certain emission peak, for example E_γ=4.44 MeV from the $^9Be(\alpha,n\gamma)^{12}C$ reaction. In fact, the counting rate carries combined information on the density and energy distribution of the reactants [7], while its temporal changes can be used to study instabilities driven by α particles and fast ions in general [9]. At low rates, say r < 100 kHz, the counting rate is readily given by the number of trigger events per unit time. As the rate is increased, however, more than one event can occur within an acquisition segment due to pile up and the trigger based method is no more correct. The measured fraction f of pile up events can be used to evaluate the counting rate instead.

For a non paralyzable system, the (rate dependent) fraction f of pile up events can be calculated as [19]:

$$f = 1 - e^{-r\tau} \qquad (3)$$

where τ is the detector dead time. This relation can be used to determine r, once f and τ are known.

The system dead time τ=265.5 ns was extracted from the test-run with calibration sources only. The counting rates

TABLE II. COMPARISON BETWEEN THE COUNTING RATE DETERMINED FROM THE FRACTION OF PILE UP EVENTS (EQ. 3) AND THE EXPECTED RATE OBTAINED FROM A MEASUREMENT IN "OSCILLOSCOPE MODE" (SEE TEXT)

F	r from Eq. (3)	Expected r
2.13 %	81 kHz	80 kHz
12.4 %	499 kHz	480 kHz
51.9 %	2.76 MHz	2.60 MHz

determined from equation (3) are reported in Table II and are compared with those expected. The latter were calculated from measurements in "oscilloscope mode". In this mode, the acquisition board operates as an oscilloscope that continuously digitizes the cable signal with a sampling frequency of 400 MSPS, without any energy threshold. The resulting digitized trace can be used to determine the expected rate by eye counting the number of events occurred in a given time interval. The calculated r values in Table II agree with those expected with an error less than 7%, that is adequate for applications of γ-ray spectroscopy to burning plasma studies.

As shown with the results of Fig. 5, PMT gain shifts are primarily responsible for degradation of the measured γ-ray emission spectrum at high rates. Gain shifts depend on the average current running between the PMT dynodes [16], which is in turn proportional to the average deposited γ-ray energy $<E_\gamma>$. The latter is given by

$$< E_\gamma >= \int_0^{+\infty} E_\gamma \cdot N(E_\gamma) \cdot dE_\gamma \Big/ \int_0^{+\infty} N(E_\gamma) \cdot dE_\gamma \qquad (4)$$

where $N(E_\gamma)$ is the number of counts per keV in a given channel of the γ-ray energy spectrum. Using the measured spectra, a value $<E_\gamma>\approx$1.36 MeV was calculated for experiments at the TVG accelerator. This value might have been underestimated by up to about 30%, due to the presence of a lower level discrimination threshold between E_γ=100 keV and E_γ=300 keV in the recorded γ-ray spectra (see Fig. 3). $<E_\gamma>\approx$1.36 MeV can be compared to $<E_\gamma>\approx$3.56 MeV for the interaction of 4.44 MeV γ-rays with the $LaBr_3$(Ce) crystal, as calculated from a simulation of the crystal response function with the MCNP code. The ratio 3.56 /1.36≈2.6 can thus be used to extract an equivalent counting rate r_{eq} at E_γ=4.44 MeV from that of a measurement at the TVG accelerator. r_{eq} represents the counting rate of an experiment with E_γ=4.44 MeV γ-rays that would produce the same average current load between the PMT dynodes as a measurement at a counting rate r at the TVG accelerator. It is found that r=2.6 MHz corresponds to $r_{eq} \geq 1$ MHz. This result is of direct relevance for α particle observations with γ-ray spectroscopy on a burning plasma device, as it demonstrates the capability of the system to perform γ-ray spectroscopy measurements of the $^9Be(\alpha,n\gamma)^{12}C$ reaction in the MHz range with no significant degradation of the energy resolution.

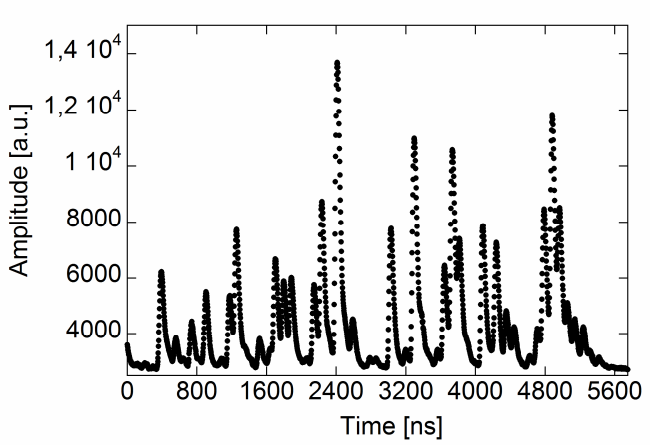

Fig. 6. Time trace from a measurement at a counting rate of about 10 MHz performed at the TVG accelerator. Almost all events are effected by pile up.

All the measurements presented in this paper were obtained by segmenting the incoming signal and reconstructing the γ-ray emission spectrum by pulse fitting and pile up rejection. Besides gain drifts, than can be partially compensated by lowering V_{HV}, at very high counting rates pile up rejection can be too limiting. Eq. (3) reveals that more than 90% of the events are affected by pile up at $r > 8.7$ MHz. This is shown for instance in Figure 6, where the time trace obtained by operating the acquisition system in "oscilloscope mode" during a measurement at the TVG accelerator for $r \approx 10$ MHz is presented.

At very high counting rates, signal processing techniques designed to recover - rather than reject - pile up events are to be preferred. Pile up recovery algorithm can also be useful at lower rates in the MHz range, especially if higher statistics is required to track changes in the γ-ray emission spectrum on time scales faster than 1 ms in a burning plasma experiment. One possibility is to employ a technique based on the trapezoidal filter [20], which was implemented in Ref. [21]. This technique has the advantage of being less time consuming than fitting from a computational point of view and is more suitable for real time applications. The drawback of the trapezoidal filter based technique is however the energy resolution that, according to the values reported in Ref. [21] for similar experiments, is slightly worse than that obtained in this paper. A more detailed comparison between the two solutions for high rate γ-ray spectroscopy applications on a burning plasma experiment will be the subject of future studies

V. CONCLUSIONS

High resolution γ-ray spectroscopy measurements at MHz counting rates were carried out at nuclear accelerators, combining a $LaBr_3$(Ce) detector with dedicated hardware and software solutions based on digitization and post-mortem analysis. The reconstructed spectra demonstrate γ-ray spectroscopy in the MHz range without significant degradation of the energy resolution up to 2.6 MHz (R=2.0 % at E_γ= 3 MeV). Measurements at higher counting rates up to 4.4 MHz were also performed, accepting a modest broadening of the energy resolution (0.4% increase at E_γ=3 MeV). The detected fraction of pile up events was used to obtain information on the true counting rate in the MHz range. The reported results represent a step forward towards the final goal of γ-ray spectroscopy measurements on a burning plasma device and provide a basis for further future hardware and software developments.

REFERENCES

[1] J. Källne et al., Phys. Rev. Lett. vol. 85, 2000, p.1246
[2] M. Nocente, G. Gorini, J. Källne and M. Tardocchi, Nucl. Fus. vol. 51, 2011, p. 063011
[3] F. Ognissanto, G. Gorini, J. Källne, L. Ballabio, M. Nocente, M. Tardocchi, Nucl. Instrum. Meth. B, vol. 269, p. 786
[4] C. Hellesen et al., Nucl. Fus. vol. 50, 2010, p. 084006
[5] M. Gatu Johnson et al., Nucl. Fus. vol. 50, 2010, p. 045005
[6] M. Gatu Johnson et al., Rev. Sci. Intrum. vol. 81, 2010, 10D336
[7] M. Tardocchi et al., Phys. Rev. Lett. vol. 107, 2011, p. 205002
[8] M. Nocente et al., "High Resolution gamma-ray spectroscopy measurements of the fast ion energy distribution in JET ^{4}He plasmas" submitted for publication to Nucl. Fus.
[9] M. Nocente et al., "Gamma-Ray Spectroscopy Measurements of Confined Fast Ions on ASDEX Upgrade", submitted for publication to Nucl. Fus.
[10] V.G. Kiptily et al., Phys. Rev. Lett. vol. 93, 2004, p. 115001
[11] V.G. Kiptily, F.E. Cecil, S.S. Medley, Plasma Phys. Control. Fusion, vol. 48, 2006, p. R59
[12] I. Proverbio, M. Nocente, V.G. Kiptily, M. Tardocchi, G. Gorini, Rev. Sci. Instrum. vol. 81, 2010, p. 10D320
[13] M. Tardocchi et al., "Production and diagnosis of energetic particles in FAST", accepted for publication on Nucl. Fus.
[14] E.V.D. van Loef, P. Dorenbos, C.W.E. van Eijk, K.W. Krämer, H.U. Güdel, Nucl. Instrum. Meth. A, vol. 486, 2002, p. 254
[15] S. Dobrescu, D.V. Mosu, D. Moisa, S. Papureanu, Proceedings of the 20th International Conference on Application of Accelerators in Research and Industry vol. 1099, 2009, p. 51
[16] M. Tardocchi et al., Rev. Sci. Instrum. vol. 79, 2008, 10E524
[17] R.C. Pereira et al., Fusion. Eng. Des. vol. 83, 2008, p. 341
[18] M. Nocente et al., Rev. Sci. Instrum. vol. 81, 2010, 10D321
[19] G.F. Knoll, "Radiation Detection and Measurement", 3rd edition, Wiley, 2000
[20] V.T. Jordanov and G.F. Knoll, Nucl. Instrum. Meth. A, vol. 345, 1994, p. 337
[21] R.C. Pereira et al, IEEE Trans. Nucl. Sci. vol. 58, 2011, p. 1531

Paper IX

Gamma-ray spectroscopy measurements of fast ions on ASDEX Upgrade

M. Nocente[1,2*], M. Garcia-Munoz[3], G. Gorini[1,2], M. Tardocchi[2], A. Weller[3], S. Akaslompolo[4], R. Bilato[3], V. Bobkov[3], C. Cazzaniga[1], B. Geiger[3], G. Grosso[2], A. Herrmann[3], V. Kiptily[5], M. Maraschek[3], R. McDermott[3], J.M. Noterdaeme[3], Y. Podoba[3], G. Tardini[3] and the ASDEX Upgrade Team

[1]Dipartimento di Fisica "G. Occhialini", Università degli Studi di Milano-Bicocca, Piazza della Scienza 3, 20126, Milano, Italy

[2] Istituto di Fisica del Plasma "Piero Caldirola," Associazione EURATOM-ENEA-CNR, via Cozzi 53, 20125, Milan, Italy

[3] Max-Planck-Institut für Plasmaphysik, EURATOM Association. Boltzmannstraße 2, D-85748 Garching, Germany

[4] Department of Applied Physics, Aalto University School of Science, Association Euratom-Tekes, P.O.Box 14100, FI-00076, Finland

[5]JET-EFDA, Culham Science Centre, Abingdon OX14 3DB, United Kingdom

[*] Corresponding author. Electronic mail: massimo.nocente@mib.infn.it

Abstract

Evidence of γ-ray emission from fast ions in ASDEX Upgrade (AUG) is presented. The plasma scenarios developed for the experiments involve deuteron or proton acceleration. The observed γ-ray emission level induced by energetic protons is used to determine an effective tail temperature of the proton distribution function that can be compared with Neutral Particle Analyzer measurements. More generally the measured emission rate is used to assess the confinement of protons with energies < 400 keV in discharges affected by Toroidal Alfvén Eigenmode instabilities. The derived information on confined ions is combined with observations made with the AUG Fast Ion Loss Detector.

PACS codes: 29.30.Kv, 52.25.Os, 52.70.La, 52.55.Pi

1. Introduction

Gamma-Ray Spectroscopy is being proposed as a diagnostic of confined α-particles in ITER [1] and used in present-day experiments as a tool to study fast ion physics [2]. In JET, ions in the MeV range produced by Ion Cyclotron Resonance Heating (ICRH) are well confined thanks to the large plasma size and high plasma currents. The recent installation of high resolution spectrometers has enhanced the quality of the γ-ray emission measurements and contributed to the development of nuclear physics based methods and models for the understanding of plasma physics [3,4]. ASDEX Upgrade (AUG) [5] is somewhat smaller than JET in terms of plasma volume and current; however it is well equipped with fast ion diagnostics. These have provided experimental results on the interaction between fast ions and MHD modes, e.g. with the characterization of losses induced by Neoclassical Tearing Modes, Toroidal Alfvén Eigenmodes (TAE) and Alfvén cascades [6,7]. The unique possibility to combine information from different diagnostics makes AUG an interesting machine also for γ-ray spectroscopy observations.

The emission of γ-rays from the plasma can be induced on AUG either by fast protons or by fast deuterons interacting with other plasma ions. ICRH at power levels up to 5 MW is available and can in principle be used to push the ions up in energy until they are no longer confined by the available plasma current. This paper reports on a series of experiments performed in order to explore the production and confinement of fast ions in AUG using γ-ray spectroscopy in combination with other diagnostics. The paper is organized as follows. Details on the designed scenarios for γ-ray spectroscopy observations on AUG are given in Section 2. Section 3 summarizes the experimental results by comparing observations with γ-ray spectroscopy, Neutral Particle Analyzer (NPA), Fast Ion Loss Detector (FILD) and Mirnov coils. Finally the γ-ray measurements are discussed in more detail in Section 4.

2. Plasma scenarios for γ-ray emission

On AUG fast deuterons can induce γ-ray emission through interaction with ^{14}N impurities. Nitrogen gas is commonly injected into AUG plasmas for divertor cooling; it also has a beneficial effect on energy confinement [8,9]. Several γ-ray emission peaks may be observed with different intensities and characteristic energies in the range 3 MeV < E_γ < 7 MeV (Table I). The latter depend on which particle is produced in the reaction exit channel (mainly α-particles or protons) and on the excited level of the

γ-ray emitting nucleus that is populated. In all cases cross section data available in the literature [10] show a substantial increase for $E_d > 0.4$ MeV, that can be regarded as an effective threshold deuteron energy for γ-ray emission induced by fast deuterons on ^{14}N.

Energetic protons can induce γ-ray emission on AUG through capture reactions on either boron or bulk deuterons (Table I). In capture reactions, the γ ray does not result from de-excitation of a heavy nucleus in a two step process (such as ^{12}C in the $^{14}N(d,\alpha\gamma)^{12}C$ reaction), but is instead the product of a fusion reaction (as for $d(p,\gamma)^3He$). Boron is present in the plasma as impurity after machine boronization, which is periodically performed to decrease tungsten accumulation in the plasma core [8]. Deuterium is the major constituent of the bulk plasma. The expected γ-ray peak energies are E_γ=5.5 MeV for the $d(p,\gamma)^3He$ reactions and 9 MeV<E_γ<12 MeV for reactions with boron as target. The main drawback of capture reactions is that the cross section is typically 2 to 3 orders of magnitude lower than that for two step reactions at same energies, with values in the micro-barn range for proton energies of some hundreds of keV (figure 1). On the other hand fast protons are expected to be more easily confined than fast deuterons. Full orbit simulations with the GOURDON code [11] for a typical AUG plasma equilibrium with B_T=2.5 T and I_P=1 MA show that the deuteron and proton energies at which first orbit losses become significant are $E_d \approx 0.8$ MeV and $E_p \approx 1.5$ MeV, respectively. The acceleration of protons or deuterons requires different heating schemes. As deuterium is the main bulk plasma component, energetic deuterons were created through ICRH tuned to second cyclotron harmonic by exploiting acceleration due to finite Larmor radius effects [12]. The required energetic ion seed was provided by neutral beam injection (energy E_d=62 keV) orthogonal to the magnetic field. Fast protons were instead generated through minority (H)D ICRH heating scheme. Here the ICRH power was coupled to hydrogen ions; these are usually present in AUG deuterium plasmas at a concentration level approaching 5%.

In both scenarios, the plasma bulk density had to be kept as low as possible to facilitate the development of tails in the hundreds keV region. This was particularly challenging for the fast deuteron scenario, where the use of NBI heating determined a density rise, a feature commonly observed in tokamak plasmas. A low density would require a low plasma current but this is in conflict with the need to confine energetic deuterons. Therefore, a trade-off had to be sought for experimentally. Lower densities were more easily achieved in discharges run immediately after machine boronization, thanks to reduced recycling.

A $LaBr_3$(Ce) scintillator designed for high rate operation [13] was used for the observation of γ-rays in discharges with fast protons and deuterons. The detector was placed at a distance of 12 m from the plasma centre, behind a 2 m thick concrete wall. The line of observation was defined by a hole in the

concrete wall with a diameter of 8.5 cm, looking through one of the diagnostic ports. A set of polyethylene, lithium and cadmium attenuators was used to reduce neutron induced background on the scintillator, which was found to be significant particularly for discharges with neutral beam injection. Neutron induced background was also the main source of recorded events in the γ-ray energy region E_γ < 3 MeV, which forced to put the detector behind the concrete wall. The background event rate was about 20 times lower in the region E_γ > 3 MeV.

3. Results

3.1. Results from the fast deuteron scenario

Several discharges were performed in order to accelerate deuterons by relying on 2nd harmonic ICRH on a perpendicular neutral beam injection, but no γ-ray emission was observed. In all discharges, NPA showed that the fast deuteron energy distribution exceeded the 62 keV NBI injection energy during the superimposed RF heating phase, demonstrating that synergetic NBI+RF heating was indeed taking place. Mirnov coils measurements revealed high frequency MHD activity of the Alfvén type only for few hundred milliseconds in one of the discharges. Few fast ion losses induced by MHD activity were correspondingly observed. A key parameter was found to be the electron density, expressed by its core line integrated value n_e. In most of the discharges n_e was above $6 \cdot 10^{19}$ m^{-2}, independently of whether the discharge was performed close to boronization or not.

The few observed signatures of fast ion induced MHD activity mentioned above were detected for short time intervals when $n_e < 6 \cdot 10^{19}$ m^{-2}. In these cases, however, magnetic islands also appeared that made the plasma unstable and ultimately led to a disruption.

3.2. Results from the fast proton scenario

Two identical discharges (#26615 and #26616) designed for minority heating of protons in (H)D plasmas were performed with I_P=1.0 MA and B_T=2.5 T. Core electron cyclotron resonance heating (ECRH) was used to raise the electron temperature thus decreasing the electron drag on energetic ions. In both discharges n_e fell in the range $5\text{-}6 \cdot 10^{19}$ m^{-2}. ICRH was applied from 1 s at a total power level of 5 MW for about 1.5 s, with resonance in the plasma centre. A 100 ms NBI blip was used at t=2 s for diagnostic purposes.

A signature of γ-ray emission from p+^{11}B and p+^{10}B reactions was observed in the measured pulse height spectrum. Figure 2 shows the number N_γ of detected events in the pulse height region 9-12

MeV as function of the absolute neutron emission Y_n as measured by a combination of neutron yield monitors and activation foils for AUG discharges with different neutron emission levels. A linear scaling between $N_\gamma = b \cdot Y_n$ with $b = 1.53 \cdot 10^{-13}$ is found for most discharges (Figure 2a). An exception is a set of discharges in which protons were accelerated, where an excess of N_γ events was found. This can be ascribed to the contribution from proton capture on boron. A more clear manifestation of γ-ray emission from fast protons was provided by the observation of the E_γ=5.5 MeV peak due to the $d(p,\gamma)^3He$ reaction (figure 3). The peak stands out of the background level in a statistically meaningful way. Figure 4 (a) shows the measured $d(p,\gamma)^3He$ emission peak. Superimposed to the data is a simulated spectral shape obtained by adding a constant background to the result of a Monte Carlo simulation using the MCNP code (providing the spectrum of energies deposited in the detection crystal) folded with the instrumental energy resolution ΔW_I and the expected kinetic broadening ΔW_K that results from the relative ion motion as predicted in reference [14] and first observed in reference [15] (see below). The simulation describes well the observed features of the peak within the available statistics. The time resolved count rate under the E_γ=5.5 MeV peak, after background subtraction, is shown in figure 4 (b). It is averaged for the two discharges with proton acceleration. The count rate increases with time during radiofrequency heating, with an average value $M_\gamma = 33 \pm 6$ counts/s between 1 and 2 s. This value can be used to estimate the temperature of fast protons in the plasma on the basis of a model calculation of the relation between the plasma γ-ray emissivity and the γ-ray flux yielding the observed detector count rate. To this end the viewing geometry of the diagnostics was modeled in terms of an effective plasma volume V emitting γ-rays within the detector solid angle $\Omega = A/d^2$ where A is the detector area exposed to the γ-ray flux and d its distance from the plasma core. The model assumes isotropic γ-ray emission. The expected signal count rate is then determined from the known full energy peak efficiency η and is $M_\gamma = \eta S_\gamma V \Omega$, S_γ being the γ-ray emissivity. The latter was calculated for a range of proton tail temperatures T_p. A value of T_p=100 keV provides the best match to the measured rate. We estimate an accuracy of ± 50 keV in T_p. This rather large confidence interval results from an estimated error of a factor 2 in the flux calculation, due to neglecting detailed photon transport and systematic uncertainties in the hydrogen concentration value. NPA was also used to measure the tail temperature of fast protons and indicated a temperature of about 70 keV averaged for the two discharges (figure 5). When combined with γ-ray spectroscopy observations, a T_p value lying in the range 70-100 keV is inferred. With these values, one can estimate the expected kinematic broadening (FWHM) ΔW_K of the γ-ray emission peak due to motion of the reacting ions using equation (5) of reference [14]. The result is $\Delta W_K \approx$ 105-140 keV that was folded with the instrumental broadening $\Delta W_I \approx 100$ keV at E_γ=5.5 MeV to give the simulated peak shape shown in Figure 4(a). The proton tail temperature could also, alternatively, be derived from the observed γ-ray peak broadening alone, by fitting the measured spectrum for several values of ΔW_K and derive the corresponding T_p

according to the model of reference [14], as done in previous works [2]. However, the limited statistics of the measurement and the fact that $\Delta W_I \approx \Delta W_K$ would not significantly improve the T_p assessment based on the observed absolute measured rate.

The two plasma discharges with strong proton acceleration were quite rich in terms of fast ion driven MHD activity. Figure 6a shows the frequency spectrogram for shot #26615 detected with Mirnov coils [16] between 1 and 3 seconds (the spectrogram for shot #26616 is very similar and is not shown). Frequencies due to Toroidal Alfvén Eigenmodes (TAE) driven by energetic protons appear in the range 100-250 kHz, from 1.11 s. The toroidal mode numbers, obtained by measurements of the phase shifts among coils displaced at different toroidal locations, are n=3-6 between 1 and 2 s; TAEs with lower toroidal numbers were also excited after the NBI blip at 2 s. A complex loss pattern in phase space was correspondingly detected with FILD [17] (figure 6b). Prompt losses with pitch angles in the range 70-75° and Larmor radii between 80-100 mm were observed at t=1.06 s, i.e. in coincidence with ICRH and 50 ms before MHD was detected on the magnetic coils. These are interpreted as first orbit losses of ions with energies > 1.5 MeV that were produced by ICRH on unconfined trajectories. At later instants, few ms after the appearance of TAEs in the magnetics, a second bright spot corresponding to energies in the range 550-800 keV was observed, soon extending to higher energies up to about 2 MeV and lasting until the end of the heating phase. TAEs also significantly enhanced losses in the pitch angle/Larmor radius region corresponding to protons accelerated by ICRH on unconfined orbits observed at t=1.06 s. No losses of protons with energies < 400 keV were observed throughout the discharges.

4. Discussion

The observed γ-ray reactivity from the $d(p,\gamma)^3He$ reaction can be interpreted as follows. For protons that are much faster than the target deuterons, the reactivity Y_γ is given by

$$Y_\gamma = \int y_\gamma(E_p) dE_p \qquad (1)$$

where the integrand $y_\gamma(E_p)=f(E_p)v\sigma(E_p)$ is the differential reactivity and expresses the γ-ray emission intensity as function of the proton energy E_p [4]. Here f represents the proton energy distribution, v its velocity and σ the reaction cross section. The latter was parameterized here as [18,19]

$$\sigma(E_p) = \frac{S(E_p)}{E_p} \exp(-\beta_G / \sqrt{E_p}) \quad (2)$$

where $S(E_p)$ is the astrophysical factor and β_G the Gamow constant. Cross section data of the $d(p,\gamma)^3He$ reaction in the proton energy range 10 keV-2 MeV can be described (figure 1, solid line) with equation (2) by expressing $S(E_p)$ as a fourth order polynomial [20,21]

$$S(E_p) = A_0 + A_1 \cdot E_p + A_2 \cdot E_p^2 + A_3 \cdot E_p^3 + A_4 \cdot E_p^4 \quad (3)$$

with best fit parameter values as given in Table 2.

The cross section parameterization is used to calculate the differential reactivity $y_\gamma(E_p)$ for several tail temperatures of the fast proton energy distribution (figure 7). For tail temperatures in the range 70-100 keV, most of γ-ray emission involves protons with $E_p < 400$ keV, with a peak energy (the so called "Gamow peak energy" E_{Gp}) between 120 keV and 180 keV. This result, combined with the observation that the γ-ray emission rate increases with time even though TAE fluctuations appear in the magnetic traces, suggests that protons with $E_p < 400$ keV are well confined and not significantly affected by TAEs. This is also in agreement with the lack of losses for $E_p < 400$ keV observed with the FILD.

Further insight is obtained by calculating resonance curves in phase space between fast protons with their turning points at the radial location of the magnetic axis and TAEs with toroidal mode numbers n=3-6 as observed between 1 and 2 s with Mirnov coils. A necessary (but not sufficient) condition for particle-mode resonance is that the relation $n\omega_\phi - p\omega_\theta - \omega \approx 0$ is satisfied. Here ω and n are the measured frequency and toroidal number of the mode, ω_ϕ and ω_θ the toroidal precession and poloidal transit frequency of the resonating ion, p the bounce harmonic [22]. Figure 8 shows contour plots of the function $\log(1/|n\omega_\phi - p\omega_\theta - \omega|)$ for n=3-6 and p=-3 to 3 in the (E,z) plane (which is equivalent to the (E,p_φ) plane for ICRH ions with turning points at the radial location of the magnetic axis [7]; p_φ indicates the toroidal component of the canonical angular momentum). The curves were obtained from the results on ω_ϕ and ω_θ calculated with the GOURDON code [11] using the magnetic equilibrium at t=1.5 s. Two observations can be made. The first is that virtually all energies may resonate with the observed TAEs, as was found in another AUG discharge with different I_p and B_T values [7]. This also explains why losses in a quite wide energy range were observed on the FILD. The second observation is that protons in the energy range $E_p < 400$ keV can resonate with the TAEs only through negative bounce harmonics. The latter, combined with the observed monotonic γ-ray emission rate, suggests that mode resonances involving negative bounce harmonics do not significantly affect fast ion confinement on AUG, in agreement with the absence of losses for $E_p < 400$ keV as detected by the FILD. As a final consideration, it would be highly desirable to have a better overlap between the region where losses were observed and that responsible for γ-ray emission in future experiments on AUG. This can be done by increasing the Gamow peak energy. A simplified analytic derivation, in

which the energy dependence of the astrophysical factor S(E) is neglected, shows that E_{Gp} scales as $T_p^{2/3}$ [18]. A Gamow peak energy of about 400 keV would of course provide almost complete overlapping but is beyond what can be reasonably achieved on AUG with the present machine parameters and power levels. More realistically one could try to reduce the electron density down to 3-4·10^{19} m^{-2} by fast current ramp up; combined with improvements of at least 10% in the RF coupling, this would yield proton tail temperatures $T_p \approx 150$ keV, based on Stix scaling of the tail temperature on n_e and RF power [12]. As shown in figure 6, the Gamow peak energy is E_{Gp}=280 keV at T_p=150 keV and about 40% of the γ-ray reactivity is due to protons with E_p > 400 keV. Furthermore the γ-ray reactivity scales roughly as T_p in the range T_p=50-200 keV meaning that improvements in measurement statistics are to be expected, possibly allowing for quantitative comparison with diagnostic information on lost protons from the FILD.

5. Conclusion

First measurements of γ-ray emission due to fast ions in ASDEX Upgrade were performed. Emission from proton capture reactions on boron and deuterium was observed in two (H)D discharges with radiofrequency heating in the minority acceleration scheme. The observed count rate was used to infer the values of the fast proton tail temperature. A value in the range 70-100 keV is compatible with both γ-ray and NPA observations. TAE fluctuations were observed with Mirnov coils throughout the heating phase and associated proton losses were detected with the FILD. The observed emission rate, combined with calculations of the γ-ray differential reactivity and particle-mode resonance curves in phase space, revealed that resonances with negative values of the bounce harmonics did not significantly affect fast ion confinement (E_p < 400 keV). Future γ-ray spectroscopy measurements of confined protons in AUG should be aimed at raising the proton tail temperature up to 150 keV and above, where the improved measurement statistics would allow for even better comparison with diagnostic information on lost protons from the FILD.

6. Acknowledgment

This work was supported by EURATOM and carried out within the framework of the European Fusion Development Agreement. The views and opinions expressed herein do not necessarily reflect those of the European Commission. The computing resources of CSC - IT centre for science were used in the data-analysis.

References

[1] Kiptily V G, Cecil F E and Medley S S, *Plasma Phys. Control. Fusion* **48 (**2006) R59

[2] Kiptily V G *et al., Nucl. Fusion* **42** (2002) 999

[3] Tardocchi M *et al.* , "Spectral broadening of characteristic γ–ray emission peaks from $^{12}C(^{3}He,p\gamma)^{14}N$ reactions in fusion plasmas", accepted for publication on *Phys. Rev. Letters*

[4] Proverbio I, Nocente M, Kiptily V G, Tardocchi M and Gorini G, *Rev. Sci. Instrum.* **81** (2010) 10D320

[5] Zohm H *et al., Nucl. Fusion* **49** (2009) 104009

[6] Garcia-Munoz M *et al.*, *Phys. Rev. Letters* **104** (2010) 185002

[7] Garcia-Munoz M *et al., Nucl. Fusion* **49** (2009) 085014

[8] Gruber O *et al., Nucl. Fusion* **49** (2009) 11501

[9] Tardini G *et al*., "Core transport and pedestal characteristics of nitrogen seeded H-mode discharges in ASDEX Upgrade", *Proc. 37th EPS Conference on Plasma Physics* (2010), P1.1097

[10] Pellegrino S, Beck L and Trouslard P, *Nucl. Instrum. Meth. B* (2004) 140-144

[11] Gourdon C, "Programme Optimise de Calculs Numeriques dans les Configurations Magnetiques", *Centre d'etudes nucleaires de Fontenay aux Roses* (1970)

[12] Stix T H, "Waves in Plasmas", *Ed. Springer* (1992)

[13] Nocente M *et al., Rev. Sci. Instrum* **81** (2010) 10D321

[14] Cecil F E and Newman D E, *Nucl. Instrum. Methods* **221** (1984) 449

[15] Newman D E and Cecil F E, *Nucl. Instrum. Methods* **227** (1984) 339

[16] Zohm H *et al., Plasma Phys. Control. Fusion* **37** (1995) A313

[17] Garcia-Munoz M, Fahrbach H U and Zohm H, *Rev. Sci. Instrum.* **80** (2009) 053503

[18] Gamov G, *Z. Phys*. **51** (1928) 204

[19] Burbidge E M *et al., Rev. Mod. Phys*. **29** (1957) 547

[20] Bosch H S and Hale G M., *Nucl. Fusion* **32** (1992) 611

[21] Nocente M, Gorini G, Källne J and Tardocchi M, *Nucl. Fusion* **50** (2010) 055001

[22] Heidbrink W W, *Phys. Plasmas* **15** (2008) 055501

List of figures

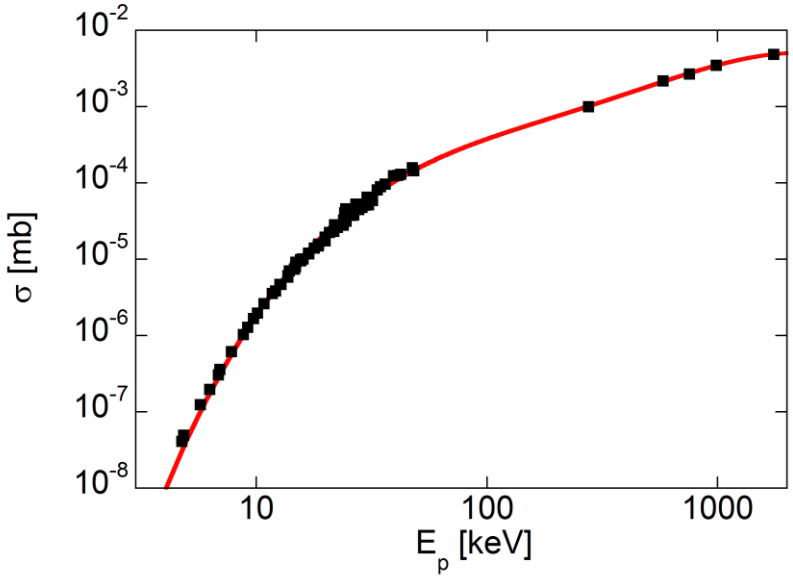

Figure 1. Cross section of the d(p,γ)^{3}He reaction as a function of the proton energy in the lab system. Data points are taken from the EXFOR database[1]. The solid line is the best fit to the data using eq. 2.

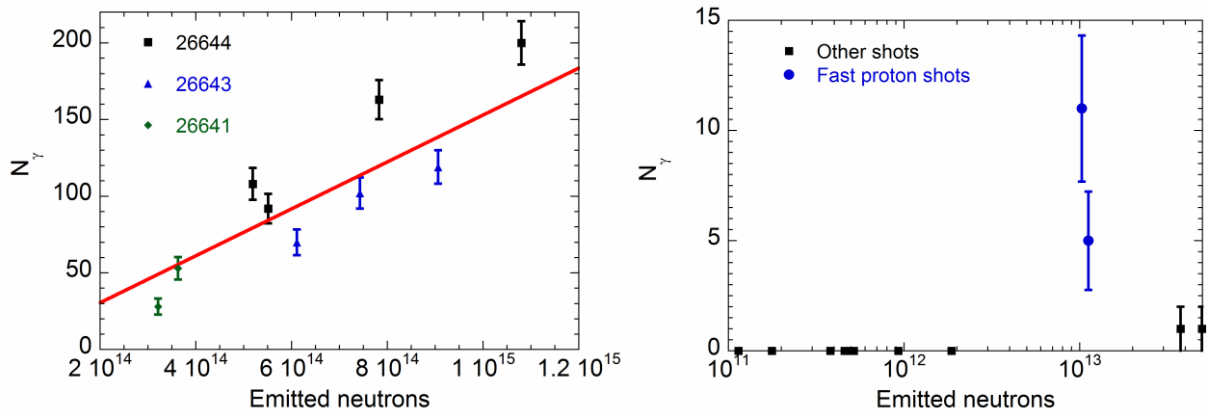

(a) (b)

Figure 2. (a) Measured counts in the energy region 9-12 MeV for several AUG discharges and time windows as function of the number of neutrons emitted by the plasma in the same time window. (b) Same as (a), but for discharges with a lower neutron yield. The two discharges in which fast protons were accelerated clearly deviate from the general trend.

[1] http://www-nds.iaea.org/exfor

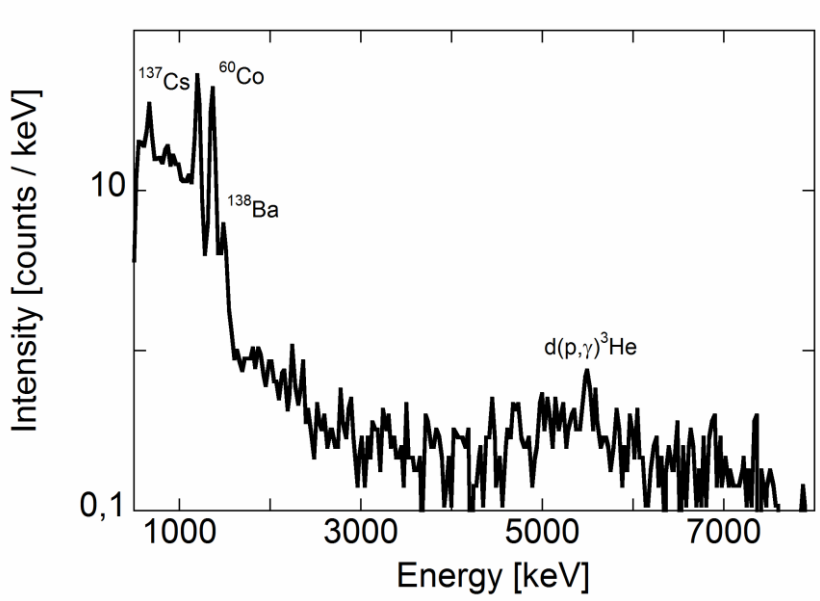

Figure 3. Sum of γ-ray spectra for discharges #26615 and #26616 integrated for 1 s during ICRH. Peaks at low energies are due to energy calibration sources (^{137}Cs and ^{60}Co) or to the detector intrinsic radioactivity (^{138}Ba). At high energies, the E_γ=5.5 MeV peak from the d(p,γ)^{3}He reaction is visible above the background level.

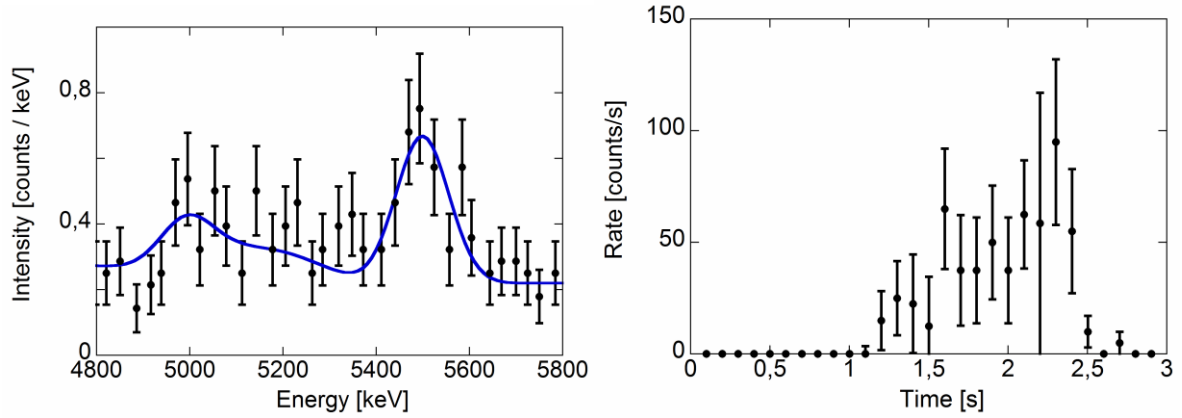

(a) (b)

Figure 4. (a) MCNP simulation (full line) of the E_γ=5.5 MeV peak from the d(p,γ)^{3}He reaction superimposed to data from Figure 3 in the energy range of interest. (b) Time resolved count rate in the E_γ=5.5 MeV peak energy range, averaged between the two discharges.

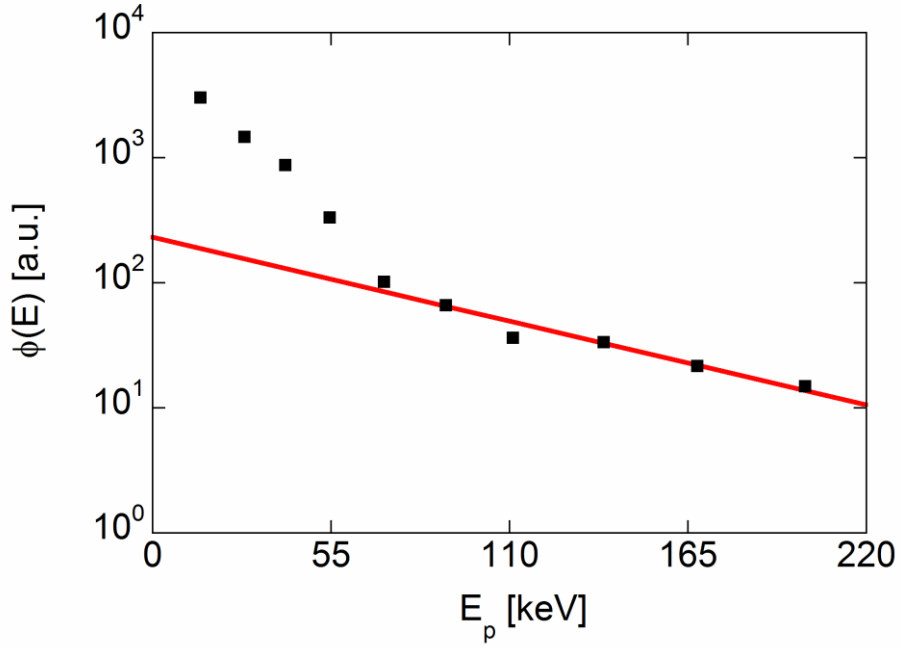

Figure 5. Average energy distribution of fast protons accelerated by ICRH for discharges #26615-26616 as measured by Neutral Particle Analyzer. The solid curve is a fit to the high energy tail of the distribution and indicates a temperature of about 70 keV.

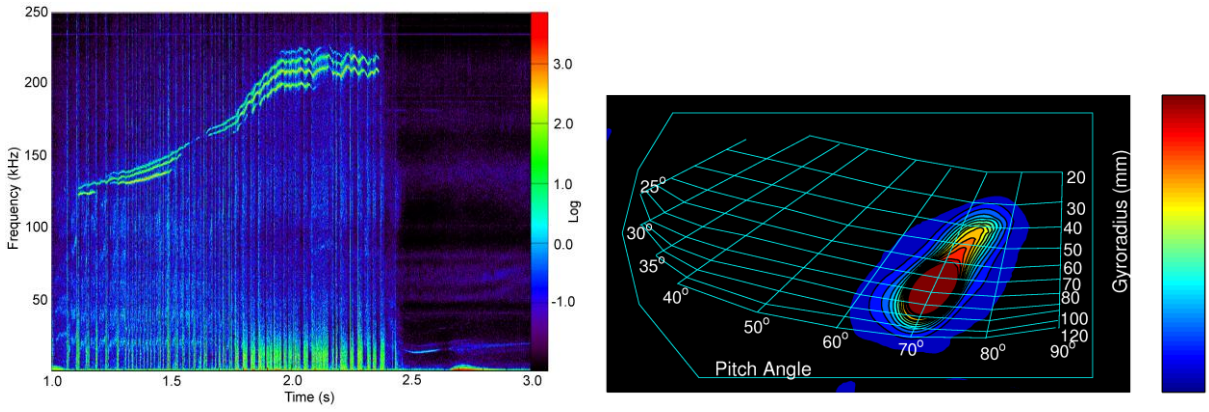

(a) (b)

Figure 6. (a) Frequency spectrogram from Mirnov coils showing characteristic frequencies of TAEs driven by fast protons and (b) data from the fast ion loss detector at 1.5 s for discharge # 26615.

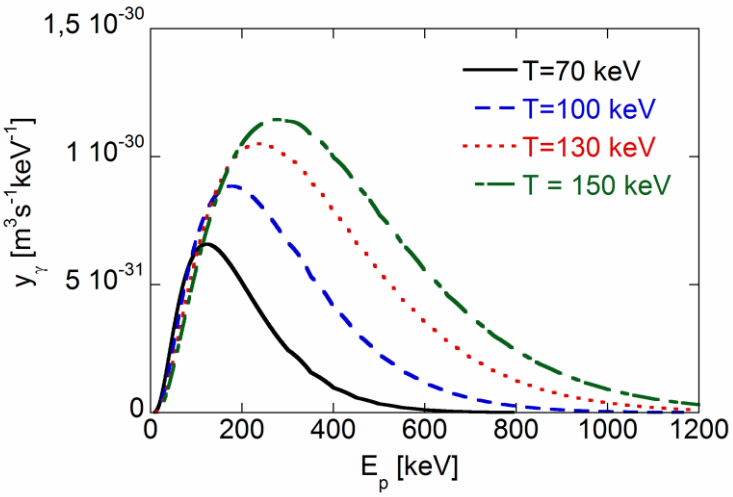

Figure. 7 Differential reactivity of the d(p,γ)^{3}He reaction calculated for different tail temperatures as function of proton energy.

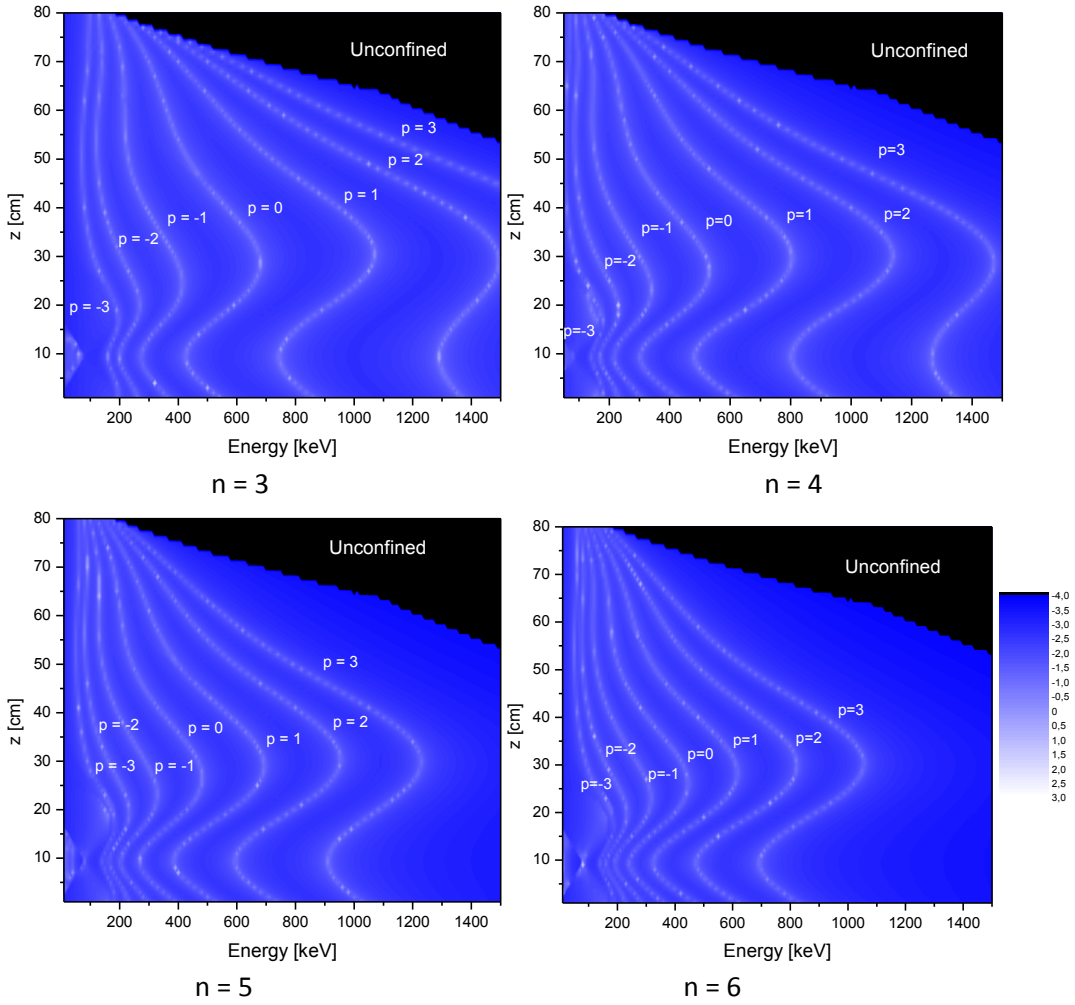

Figure 8. Calculated resonances in phase space between protons having their turning points on the magnetic axis and TAEs with toroidal mode numbers *n* = 3 to 6. Only curves for bounce harmonics p= -3 to 3 are shown.

List of tables

Table 1. Reaction of interest for γ-ray emission studies on AUG

Reactions induced by fast deuterons	Reactions induced by fast protons
$^{14}N(d,p\gamma)^{15}N$ (5 MeV < E_γ < 7 MeV)	$^{11}B(p,\gamma)^{12}C$ (9 MeV < E_γ < 12 MeV) $^{10}B(p,\gamma)^{11}C$
$^{14}N(d,\alpha\gamma)^{12}C$ (3 MeV < E_γ < 5 MeV)	$d(p,\gamma)^{3}He$ (E_γ = 5.5 MeV)

Table 2. Gamow constant and fit parameters for the astrophysical factor $S(E_p)$. E_p is expressed in MeV

Parameter	Value
β_G	1.07
A_0	8.09E-4
A_1	1.92E-3
A_2	1.21E-2
A_3	-5.26E-3
A_4	6.52E-4